

	Document Nr. FR.DLR.WindVal.270717	Issue: V1.1	Date: 27.07.2017	Page: 1/146	
	Doc. Title: WindVal Final Report				

<u>Doc.-Nr.:</u>	FR.DLR.WindVal.27072017												
<u>Doc.-Title:</u>	WindVal Final Report FR Joint DLR-ESA-NASA Wind Validation for Aeolus												
<u>Contract Number</u>	ESA 4000114053/15/NL/FF/gp												
<u>Number of pages:</u>	146 pages + 39 pages Data acquisition Report (Annex B)												
<u>Prepared by:</u>	<table style="width: 100%; border: none;"> <tr> <td style="width: 50%;">Oliver Reitebuch</td> <td style="width: 50%;">Deutsches Zentrum für</td> </tr> <tr> <td>Christian Lemmerz</td> <td>Luft- und Raumfahrt DLR e. V.</td> </tr> <tr> <td>Oliver Lux</td> <td>Oberpfaffenhofen</td> </tr> <tr> <td>Uwe Marksteiner</td> <td>Germany</td> </tr> <tr> <td>Benjamin Witschas</td> <td></td> </tr> <tr> <td>Ryan R. Neely III</td> <td>National Centre for Atmospheric Science NCAS, University Leeds, UK</td> </tr> </table>	Oliver Reitebuch	Deutsches Zentrum für	Christian Lemmerz	Luft- und Raumfahrt DLR e. V.	Oliver Lux	Oberpfaffenhofen	Uwe Marksteiner	Germany	Benjamin Witschas		Ryan R. Neely III	National Centre for Atmospheric Science NCAS, University Leeds, UK
Oliver Reitebuch	Deutsches Zentrum für												
Christian Lemmerz	Luft- und Raumfahrt DLR e. V.												
Oliver Lux	Oberpfaffenhofen												
Uwe Marksteiner	Germany												
Benjamin Witschas													
Ryan R. Neely III	National Centre for Atmospheric Science NCAS, University Leeds, UK												

	Document Nr. FR.DLR.WindVal.270717	Issue: V1.1	Date: 27.07.2017	Page: 2/146	
	Doc. Title: WindVal Final Report				

0 Document Change Log

Issue.	Date	New pages	Modified pages (after introducing new pages)	Observations	Name
V1.0	19.05.2017	1 - 134	--	draft prepared by Reitebuch, Lemmerz, Marksteiner, Lux, and Witschas	Reitebuch
V1.1	27.07.2017	Ch. 5.5: 20-25 Ch. 5.7: 27-28	all	major revisions after review by Thomas Kanitz, Dirk Schüttemeyer, and Anne-Grete Straume (ESA) with comments on June 1 and 21, 2017, and from Final Meeting on May 30, 2017 by Reitebuch, Witschas, Lemmerz, Marksteiner and Lux Input from Ryan Neely (University Leeds) in Ch. 5.5 included	Reitebuch

	Document Nr. FR.DLR.WindVal.270717	Issue: V1.1	Date: 27.07.2017	Page: 3/146	
	Doc. Title: WindVal Final Report				

1 Table of Contents

0	Document Change Log	2
1	Table of Contents	3
2	Introduction and Purpose of Document.....	5
3	Acronyms and Abbreviations	6
4	Objectives of the WindVal 2015 campaign	8
5	Overview of instrumentation and flights	11
5.1	Payload of the DLR Falcon aircraft.....	11
5.2	Payload of the NASA DC-8.....	11
5.3	Flight Tracks during airborne campaign 2015	15
5.4	Coordination with NASA DC-8	18
5.5	Greenland Summit Station	19
5.5.1	Observations during May 22, 2015.....	20
5.5.2	Instrument Details and Processing.....	22
5.6	Satellite underpasses.....	26
5.7	Data processing and availability	27
6	The 2- μ m Doppler wind lidar	29
6.1	Instrument description.....	29
6.2	Measurement procedure and wind retrieval	31
6.2.1	Line-of-sight wind speed.....	31
6.2.2	Horizontal wind speed and direction.....	32
6.3	2- μ m Wind Lidar performance during WindVal 2015.....	34
6.4	Discussion of results	37
6.4.1	15 May 2015 – Cyclone/Jet stream flight	37
6.4.2	21 May 2015 – Greenland – Summit station	42
6.4.3	25 May 2015 – Jet stream flight.....	44
6.5	Statistical comparison to dropsonde data.....	46
6.6	Summary.....	47
7	A2D operation and performance	49
7.1	Introduction	49
7.2	Description of main A2D modifications and performance assessment before the campaign	49
7.3	Operational procedures and constraints.....	51
7.4	A2D performance overview.....	56
7.5	Summary of A2D performance during WindVal 2015.....	60

	Document Nr. FR.DLR.WindVal.270717	Issue: V1.1	Date: 27.07.2017	Page: 4/146	
	Doc. Title: WindVal Final Report				

8	Airborne response calibrations.....	62
8.1	Introduction	62
8.2	Flight tracks and A2D operation.....	62
8.3	A2D performance and quality control.....	66
8.4	Mie response calibration	70
8.5	Rayleigh response calibration.....	81
8.6	Summary.....	89
8.7	Recommendations	90
9	A2D wind measurements and comparison with 2- μ m winds	91
9.1	Overview of flights and wind measurements	91
9.2	Rayleigh and Mie wind retrieval	93
9.2.1	Rayleigh wind retrieval.....	94
9.2.2	Mie wind retrieval	94
9.3	Wind processing exemplarily shown for the flight on 19/05/2015.....	95
9.3.1	Flight leg and attitude data	96
9.3.2	Range correction and bin size scaling of the intensity distribution	97
9.3.3	Quality control	98
9.3.4	Raw wind profiles.....	101
9.3.5	Cloud and ground mask for Rayleigh winds	103
9.3.6	Rayleigh background subtraction and Mie SNR mask	105
9.3.7	Zero wind correction (ZWC).....	108
9.3.8	Statistical comparison with 2- μ m winds.....	109
9.4	Results from selected flights	115
9.4.1	Rayleigh wind results from 25/05/2015 – broad data coverage	115
9.4.2	Mie winds from 28/05/2015 – Influence of Rayleigh background subtraction	119
9.4.3	Increased Mie standard deviation compared to the campaign in 2009.....	125
9.5	Statistical comparison of all wind measurement scenes	127
9.5.1	Statistical comparison of Rayleigh winds with 2- μ m winds	127
9.5.2	Statistical comparison of Mie winds with 2- μ m winds.....	131
9.6	Summary.....	132
9.7	Recommendations and open points	133
10	Summary and recommendations.....	135
11	References	140
12	Appendix A: Additional plots from selected wind measurements.....	142
13	Appendix B: Data Acquisition Report	146

	Document Nr. FR.DLR.WindVal.270717	Issue: V1.1	Date: 27.07.2017	Page: 5/146	
	Doc. Title: WindVal Final Report				

2 Introduction and Purpose of Document

This Final Report (FR) discusses the results obtained during the joint DLR-ESA-NASA wind validation campaign (WindVal) in preparation of the ADM-Aeolus validation. It covers tasks in response to the Statement of Work (SoW) from ESA with reference EOP-SM/2722/DS-ds from 16 March 2015 with title "Technical Assistance for the Deployment of the ALADIN Airborne Demonstrator (A2D) lidar during the 2015 ESA/NASA Joint Wind Validation (WindVal) Campaign" (ESA 2015, Contract Number ESA 4000114053/15/NL/FF/gp). The FR was prepared by Oliver Reitebuch, Christian Lemmerz, Oliver Lux, Uwe Marksteiner, Benjamin Witschas (all DLR Oberpfaffenhofen, Germany) and Ryan Neely II (University Leeds, UK).

This FR is output from WP 300 from DLR's proposal to ESA's SoW as Deliverable Item D5. It is based on the Campaign Implementation Plan CIP (DLR 2016a), the Data Acquisition Report DAR (DLR 2015c) and the results presented at three Progress Meetings PMs (DLR 2015c, 2016b, 2016c) and the Final Meeting FM (DLR 2017b). The DAR (DLR 2015c) contains a detailed description of the campaigns dataset and is attached to the Final Report as Annex A.

	Document Nr. FR.DLR.WindVal.270717	Issue: V1.1	Date: 27.07.2017	Page: 6/146	
	Doc. Title: WindVal Final Report				

3 Acronyms and Abbreviations

A2D	Aladin Airborne Demonstrator
a/c	aircraft
ACCD	Accumulation Charge-Coupled Device
ADM	Atmospheric Dynamics Mission
ALADIN	Atmospheric LAsEr Doppler Instrument
ATM	ATMosphere
Cal	Calibration
CC	Cavity Control
CI	Confidence Interval
CIP	Campaign Implementation Plan
CIOUSR	Cloud Out of Useful Spectral Range
CoG	Centre of Gravity
CP	Crosspoint
DAR	Data Acquisition Report
DBS	Doppler Beam Swinging
DCO	Detection Chain Offset
DEM	Digital Elevation Model
DSA	Downhill Simplex Algorithm
DWL	Doppler Wind Lidar
EMC	Electro-Magnetic Compatibility
EOM	Electro Optical Modulator
E2S	End-to-End Simulator
EMR	non-linearity error of the Mie response calibration curve
FL	Flight Level
FM	Final Meeting
FR	Final Report
FWHM	Full Width Half Maximum
GR	Ground Return
GrOUSR	Ground Out of Useful Spectral Range
HU	Heterodyne Unit
ICECAPS	Integrated Characterization of Energy, Clouds, Atmospheric State and Precipitation at Summit
INT	INTernal reference
IOCV	In Orbit Commissioning and Validation
IR	Infrared

	Document Nr. FR.DLR.WindVal.270717	Issue: V1.1	Date: 27.07.2017	Page: 7/146	
	Doc. Title: WindVal Final Report				

IRC	Instrument Response Calibration
IRS	Inertial Reference System
MAD	Median Absolute Deviation
MODIS	MODerate resolution Imaging Spectroradiometer
MOUSR	Mie Out of Useful Spectral Range
MPL	Micro-Pulse Lidar
MSP	Mie SPectrometer
N. B.	Nota Bene
netCDF	Network Common Data Format
OBA	Optical Bench Assembly
PM	Progress Meeting
PPI	Plan Position Indicator
QC	Quality Control
RH	Relative Humidity
RHI	Range Height Indicator
RL	Reference Laser
rms	root-mean-square
RSP	Rayleigh SPectrometer
SD	Standard Deviation
SL	Seed Laser
SNR	Signal to Noise Ratio
STD	Standard Deviation
TIm	Telescope Image
TOBS	Tripod Obscuration
UV	UltraViolet
UTC	Universal Time Coordinated
UV	Ultraviolet
VAD	Velocity Azimuth Display
Val	Validation
WM	Wavelength Meter
wrt.	with respect to
ZWC	Zero Wind Correction

	Document Nr. FR.DLR.WindVal.270717	Issue: V1.1	Date: 27.07.2017	Page: 8/146	
	Doc. Title: WindVal Final Report				

4 Objectives of the WindVal 2015 campaign

The last airborne campaign with the ALADIN airborne demonstrator was performed in 2009. Results are summarized in the Final Report (DLR 2012a), in TN 5.2 (DLR 2012b), in the PhD thesis by Marksteiner (2013) and Master thesis by Manninen (2012) and the paper by Li et al. (2010) for the sea surface reflectance measurements. The objectives for this campaign in 2015 were derived from results, experience and lessons learnt from this last airborne campaign in 2009 and were presented and discussed at different Mission Advisory Group Meetings in 2013-2014. In addition the objectives of ESA SoW (chapter 1.4.2) were fully implemented.

The main objectives of the campaign as discussed in the CIP (DLR 2015b) with highest priority are:

1. Confirm and document the technical performance of the ALADIN Airborne Demonstrator (A2D) lidar and its suitability for the foreseen calibration/validation of ADM-Aeolus.
2. Extend existing datasets on response calibrations over favourable areas for Aeolus calibrations, e.g. ice or land with high surface albedo in nadir-pointing mode.
3. Extend existing datasets on Rayleigh and Mie wind observations. This shall include measurements in highly variable atmospheric conditions (vert./hor.) w.r.t. wind and clouds
4. Rehearsal for airborne Cal/Val activity after launch with focus on
 - a. Test Aeolus satellite measurement-track predictions and airborne flight planning
 - b. Enhance and test capabilities for quick-look data processing
 - c. Coordination with other aircrafts and ground validation sites
 - d. Demonstrate complementarities and synergies between different measurement techniques utilized aboard the same platform, from co-located platforms and on-ground during the campaign.
 - e. Demonstrate the performance and adequacy of the A2D data processing chain for the foreseen Aeolus CAL/VAL campaigns
 - f. Provide feedback on measurement strategies and procedures of data collection for future campaigns
 - g. Extend lessons learnt from previous campaigns
5. Perform at least one flight under the satellite track of TDS-1 to achieve co-located satellite measurements of wind vectors with airborne wind lidars.

The following objectives were targeted with lower priority on a best-effort basis:

6. Extend existing datasets on Rayleigh and Mie wind observations for variable aerosol conditions, e.g. low to high backscatter and different depolarization's characteristics from the aerosol.
7. Extend existing datasets on response calibration during less favourable conditions (cloud contamination or strongly varying ground albedo conditions, PBL snow drift conditions).
8. Demonstrate the ADM-Aeolus capabilities in resolving the vertical structure of the atmosphere and compare measurements to output from numerical weather prediction models.
9. Perform satellite underpasses for CALIPSO, ASCAT, or other existing satellite sensors of interest.

Two tables summarize the objectives and an assessment of the achievement. The achievements are substantiated in the following chapters and the summary in more detail. All major objectives no. 1-5 were achieved; from the secondary objectives no. 6 and 7 could be not achieved due to the prevailing weather conditions during the campaign. These objectives were implemented for the WindVal II campaign in September-October 2016 and could be achieved during this period.

	Document Nr. FR.DLR.WindVal.270717	Issue: V1.1	Date: 27.07.2017	Page: 9/146	
	Doc. Title: WindVal Final Report				

Table 4-1: Main objectives of the WindVAL campaign and its assessment of achievement.

No.	Objective	Remark	Achievement
1	Confirm A2D performance for Cal/Val	all flights incl. test flight, 47.5 flight hours (see results and summary chapter)	✓
2	Extend Response Calibrations	5 response calibrations over ice (May 16) + 2 over sea ice (May 23) compared to 2 calibrations in 2009	✓
3	Wind observations in variable atmospheric conditions	all flights with clear and cloudy conditions, strong wind gradients for Jet Stream flights (May 15, 25) and Tip Jet flight (May 19)	✓
4	Rehearsal	campaign implementation with coordinated flights of 2 aircrafts, ground sites and satellite underpasses; rehearsal for A2D operation and QL-processing on-site	✓
4a	Aeolus sat track predictions	similar to other satellite underpass flights exercises, Aeolus-like track on May 13, 19, 28.	✓
4b	Quick-Lock processing	Falcon in-situ (up to 1 d), 2- μ m DWL (1-2 days), A2D (1-2 days for QC, signal intensity; calibration analysis, 3-4 d for selected wind retrievals) data processing on-site in Iceland	✓
4c	Coordination with other a/c and ground sites	coordinated flights with DC-8, Greenland summit station, and transfer flights over Netherlands (Cabauw), UK (windprofiler); no flight to ALOMAR (Norway) due to weather	✓
4d	Show complementarities of different sensors	4 wind lidars on 2 aircrafts, dropsondes and ground-site instrumentation	✓
4e	A2D data processing chain	A2D data was conditioned for use in L1B-L2B-chain	✓
4f	Provide feedback for Cal/Val campaigns	campaign on-site experience, data analysis and recommendations	✓
4g	Extend lessons learnt	campaign on-site experience, data analysis and recommendations	✓
5	TDS-1 Satellite underpass	flight on May 13 achieved, but satellite instrument was not operating	✓

Table 4-2: Secondary Objectives of the WindVAL campaign and its assessment of achievement.

No.	Objective	Remark	Achievement
6	A2D observations of aerosol	low amount of aerosol during all flights; no long-range transport (e.g. biomass burning)	-
7	Response Calibration during less favourable conditions	all response calibrations during no/low cloud conditions and over ice (but not over land)	-
8	Resolve vertical structures and compare to NWP analysis	comparison to ECWMF analysis was performed for flight on May 15 and 25 as case study and statistically for all flights (DLR 2016b)	✓
9	Satellite underpass of CALIPSO, ASCAT and others	Metop-B (ASCAT) underpass on May 28, CALIPSO on May 11, 16, 19, and 25.	✓

	Document Nr. FR.DLR.WindVal.270717	Issue: V1.1	Date: 27.07.2017	Page: 11/146	
	Doc. Title: WindVal Final Report				

5 Overview of instrumentation and flights

The following section describes shortly the airborne and ground based instrumentation as well as the achieved satellite underpasses. More details about data content and format is contained in the DAR (DLR 2016a).

5.1 Payload of the DLR Falcon aircraft

The payload of the DLR Falcon aircraft consisted of the A2D (Reitebuch et al. 2009, Paffrath et al. 2009) and the 2- μ m Doppler wind lidar (DWL, Weissmann et al. 2005, Witschas et al. 2017). The A2D and the 2- μ m DWL were pointing in the same line-of-sight (LOS) direction to the right side of the aircraft (in flight direction) with a nadir angle of 20°.

The nominal operation of the 2- μ m DWL was the measurement of the LOS wind and conical step-stare scans (21 LOS directions, 20° off-nadir angle) were performed in order to measure the horizontal wind vector during flight. Different off-nadir angles of both instruments, e.g. 0-3° were achieved by rolling the aircraft while flying curves (May 16 and 23, 2015). The vertical sampling of the A2D was set such, that the ground layers are sampled with highest vertical resolution (2.1 μ s, 315 m range). The highest vertical resolution is chosen for A2D for ground return layers to minimize atmospheric contribution in range gate and to enhance chance to capture ground return in range-gate overlap region.

The 2- μ m DWL measures time series of raw signal with a sampling rate of 500 MHz, which corresponds to a range resolution of 0.3 m for each emitted laser shot with a repetition rate of 500 Hz. This amounts to rather high raw-data rates of up to 60 GByte/hour depending on maximum range. The data was processed on-ground to range-gates of 100 m resolution and temporal resolution of 1 s (500 shots).

Standard meteorological parameters (pressure, horizontal wind vector, vertical wind speed, temperature, humidity (relative humidity, mixing ratio)) were measured by in-situ sensors inside the Falcon nose-boom with a temporal resolution of up to 100 Hz and processed with resolution of 1 Hz. Thus vertical profile data are available for ascent and descent and flight-level data from cruising altitude.

The performance and results of the 2- μ m DWL and the A2D are discussed in detail in the subsequent chapters of the Final Report.

5.2 Payload of the NASA DC-8

The NASA DC-8 was equipped with the 2- μ m DWL DAWN (Doppler Aerosol Wind) from NASA (Langley), the 355-nm DWL TWiLiTE from NASA (Goddard) and a Yankee dropsonde unit. The 2- μ m DWL from NASA is equipped with a single, conical wedge-scanner, which allows pointing with fixed 30.1 ° off-nadir angle (Kavaya et al. 2014). The control of the scanner allows step-stare pointing in forward direction (not full 360°) with a difference in azimuthal position of 22.5° and a maximum number of 5 LOS directions. The DAWN laser transmitted 100 mJ/pulse (nominal 250 mJ/pulse) with a repetition rate of 5 Hz (nominal 10 Hz) and uses a 15 cm telescope, compared to the DLR 2- μ m DWL with 1-2 mJ/pulse, a repetition rate of 500 Hz, and a 10.8 cm telescope. The DAWN laser operated only with 1 amplifier due to stability issues, which resulted in lower pulse energy and repetition rate. A 4 s duration for signal acquisition is used for each LOS direction and a total of 25 s is needed for all 5 directions. The DAWN data are processed to 156 m range-gate lengths (non-overlapping).

The DLR 2- μ m DWL is equipped with a double wedge-scanner, which allows also vertical pointing, and full 360° scanning capability. The Figure-of-Merit FOM for comparison of coherent wind lidars (energy*aperture* \sqrt PRF) is a factor of 13 higher for DAWN compared to the DLR 2- μ m DWL. After the campaign a signal loss in the receiver part of DAWN was encountered, which could result in a degradation of 20 dB for

	Document Nr. FR.DLR.WindVal.270717	Issue: V1.1	Date: 27.07.2017	Page: 12/146	
	Doc. Title: WindVal Final Report				

the DAWN performance (see PM1 presentation by D. Emmitt (DLR 2015c)). The main properties of the 4 different wind lidars A2D, DLR 2- μ m DWL, DAWN and TWiLiTE are summarized in **Table 5-1** and **Table 5-2**.

The direct-detection wind lidar TWiLiTE from NASA-GSFC (<http://twilite.gsfc.nasa.gov/>) is a direct detection wind lidar at 355 nm using the double-edge technique for the molecular return (Gentry et al. 2014). It is equipped with a conical, step-stare, holographical scanner with an off-nadir angle of 45 ° and thus measures LOS winds and horizontal wind vector. A LOS wind is obtained within 30 s averaging per LOS and 192 s for a full conical scan with 6 LOS directions at 45° azimuthal difference (except 0°/180°). The laser transmits 200 pulses per second with 25 mJ/pulse. In combination with the larger telescope, this leads to a factor of 5 higher power-aperture product for TWiLiTE compared to the A2D (this factor does not include any optical efficiencies or transmission losses, which are different for TWiLiTE and A2D). TWiLiTE operates autonomously and was deployed on the ER-2, WB-57 and the Global Hawk before. The optical receiver for TWiLiTE uses a Fabry-Perot Interferometer FPI for the detection of the Doppler shift of the molecular return with slightly different FPI parameters (FWHM, FSR) than the A2D or ALADIN. A photomultiplier tube PMT is used as a detector. The FPI calibration is performed by varying the FPI distance, in contrast to A2D and ALADIN where the laser frequency is tuned. A FPI calibration scan is performed every 15 minutes during flight. A significant FPI frequency drift was observed during WindVAL due to thermal drifts, which are caused by the DC-8 operating environment. Procedures to correct for FPI drifts have to be developed. The laser frequency is monitored via an additional FPI locking channel with different FWHM than used for the atmospheric signal. 6 PMT's (photomultiplier tubes) are used for both FPI filters as high (90%), medium (9%) and low (1%) intensity channels. A 7th PMT is used as a pure backscatter channel without transmitting the signal through the FPI. A 1s temporal and 21 m vertical resolution is obtained for the raw data, which is processed to 30 s and 100 m resolution for the LOS product.

A number of 101 dropsondes from Yankee Environmental Systems (<http://www.yesinc.com/news/research.html>) were deployed during the campaign. The dropsondes measure pressure, horizontal wind vector, temperature, and relative humidity and can be deployed every 4 s. 17 dropsondes provided no data, so a total of 84 dropsondes are available from flights on May 11, 13, 15, 16, 17, 19, 21, 23, 24, and 25, 2015 (Version December 2015). The dropsondes do not have a parachute as the NCAR AVAPS dropsondes (AVAPS: Airborne Vertical Atmospheric Profiling System). Thus different descent modes (wobbling, spiral) with different fall speeds (10-15 minutes, 5-6 minutes) could be observed. This results in different quality and noise on the wind speed of the dropsondes with oscillations of the wind speed and direction (but not temperature and humidity). Averaging over 20 points corresponding to 45 m significantly reduced the oscillations on the dropsonde wind speed and direction. SWA recommended using the hydrostatic height as altitude assignment. It was discovered that this height has significant less data points, than the GPS altitude; both are referenced to MSL (mean sea level), and show only a mean altitude difference of 9 m. Thus it is recommended to use GPS altitude.

A number of 126 single profiles of the DAWN lidar data are provided from 15, 16, 21, 23, 25 May 2015; the complete DAWN data set is not available yet. The quality of the DAWN data was assessed by SWA through comparisons with the dropsonde (DLR 2016c) with a mean bias of below 0.2 m/s (except 23 May: 1.2 m/s) and root mean square errors (RMSE) of 2 m/s to 4 m/s (except 23 May: 5.3 m/s).

No data was received from the TWiLiTE lidar due to problems in the calibration of the FPI, which was caused by the unfavourable temperature environment for the lidar within the DC-8 aircraft not in a temperature controlled hangar. This would cause a significant effort for analysis of the TWiLiTE data, which was not foreseen.

Table 5-1: Main specifications and products from the 2 different direct-detection wind lidars.

Parameter	DLR A2D	NASA TWiLiTE
Wavelength	354.89 nm	354.7 nm
Laser energy	50-60 mJ	25 mJ
Pulse repetition rate	50 Hz	200 Hz
Pulse length	20 ns (FWHM)	15 ns (FWHM)
Telescope diameter	20 cm	32 cm (eff.)
Vertical resolution	300 m – 2.4 km	100 m (21 m raw data)
Temporal averaging raw data (horizontal)	20 laser shots = 0.4 s	200 laser shots = 1 s
Temporal averaging product (horizontal)	14 s (+4 s data gap)	30 s for each LOS 192 s for 6 LOS scan
Horizontal resolution @ 200 m/s=720 km/h = 12 km/min.	3.6 km (18 s)	6.0 km for LOS 38 km wind vector
Scanning capabilities	No, fixed 20° off nadir	Yes, step-stare conical scan with 45 ° off nadir
Precision (random error)	1.5 m/s Mie wind 2.5 m/s Rayleigh wind	2 m/s

Table 5-2: Main specifications and products from the 2 different coherent-detection wind lidars.

Parameter	DLR 2- μ m DWL	NASA 2- μ m DAWN
Wavelength	2022.54 nm	2053.472 nm
Laser energy	1-2 mJ	100 mJ (nominal 250 mJ)
Pulse repetition rate	500 Hz	5 Hz (nominal 10 Hz)
Pulse length	400-500 ns (FWHM)	180 ns
Telescope diameter	10.8 cm	15 cm
Vertical resolution	100 m	156 m (78 m with 50% overlap)
Temporal averaging raw data (horizontal)	single shot = 2 ms	single shot = 200 ms
Temporal averaging product (horizontal)	1 s per LOS (500 shots), 42 s scan (21 LOS)	4 s per LOS (20 shots) 25 s per scan; 5 LOS
Horizontal resolution @ 200 m/s=720 km/h = 12 km/min.	0.2 km LOS, 8.4 km scan	0.8 km LOS 5 km scan
Scanning capabilities	Yes, double wedge, conical scan, fixed LOS and vertical	Yes, single wedge, conical scan, only fixed 30.12° off nadir with 5 LOS in forward direction
Precision (random error)	< 1 m/s wind speed	< 1 m/s wind speed

5.3 Flight Tracks during airborne campaign 2015

The flight tracks from the airborne campaign 2015 are shown in **Figure 5-1** and **Figure 5-2**. The duration and time of flight is summarized in **Table 5-3**. A total of 47.5 flight hours was performed on the Falcon aircraft including the test flight. The flight track, data sets and results from the test flight are reported in DLR (2015a).

Table 5-3: List of all flights from the airborne campaign WindVal in 2015 with the following IATA codes: OBF: Oberpfaffenhofen, PIK: Glasgow Prestwick, KEF: Keflavik, SFJ: Kangerlussuaq.

Date	Time (UTC)	route	Objective
30.04.	12:51 – 15:47	OBF-OBF	Test flight
11.05.	08:12 - 10:46	OBF-PIK	Transfer 1
	12:29 - 14:49	PIK-KEF	Transfer 2
13.05.	10:56 - 13:39	KEF-KEF	TDS-1 underpass
15.05.	16:02 - 20:11	KEF-KEF	Jet Stream
16.05.	13:54 -17:19	KEF-SFJ	Ice Calibration
	18:12 - 21:12	SFJ-KEF	Ice Calibration
19.05.	11:58 - 15:54	KEF-KEF	Greenland Tip Jet Aeolus Track
21.05.	22:28 - 02:25	KEF-KEF	Greenland Summit
23.05.	16:54 - 21:09	KEF-KEF	Sea ice calibration
25.05.	14:04 – 17:20	KEF-KEF	Jet Stream
28.05.	10:23 - 13:24	KEF-KEF	ASCAT underpass Aeolus Track
29.05.	10:08 - 12:39	KEF-PIK	Transfer 1
	13:54 - 15:54	PIK-OBF	Transfer 2

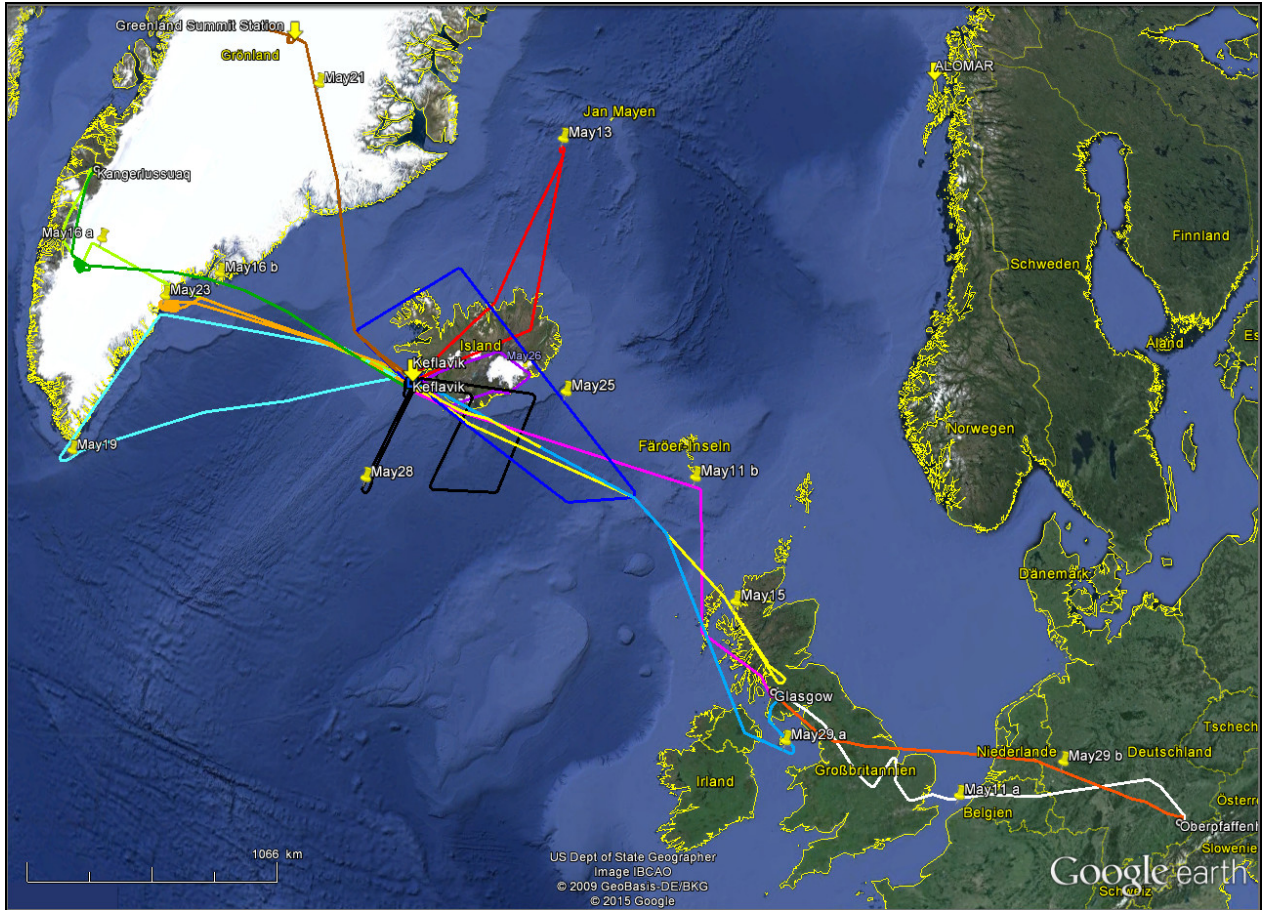


Figure 5-1: Map with flight tracks of the Falcon aircraft during the WindVal campaign in 2015 from May 11 to 29 (w/o test flight on April 30); deployment in Iceland from May 11 to May 29; each colour represents a single flight; transfer from OBF to Keflavik on May 11 (white, magenta flight) via Prestwick; transfer flight from Keflavik to OP on May 29 (blue, orange flight) via Prestwick.

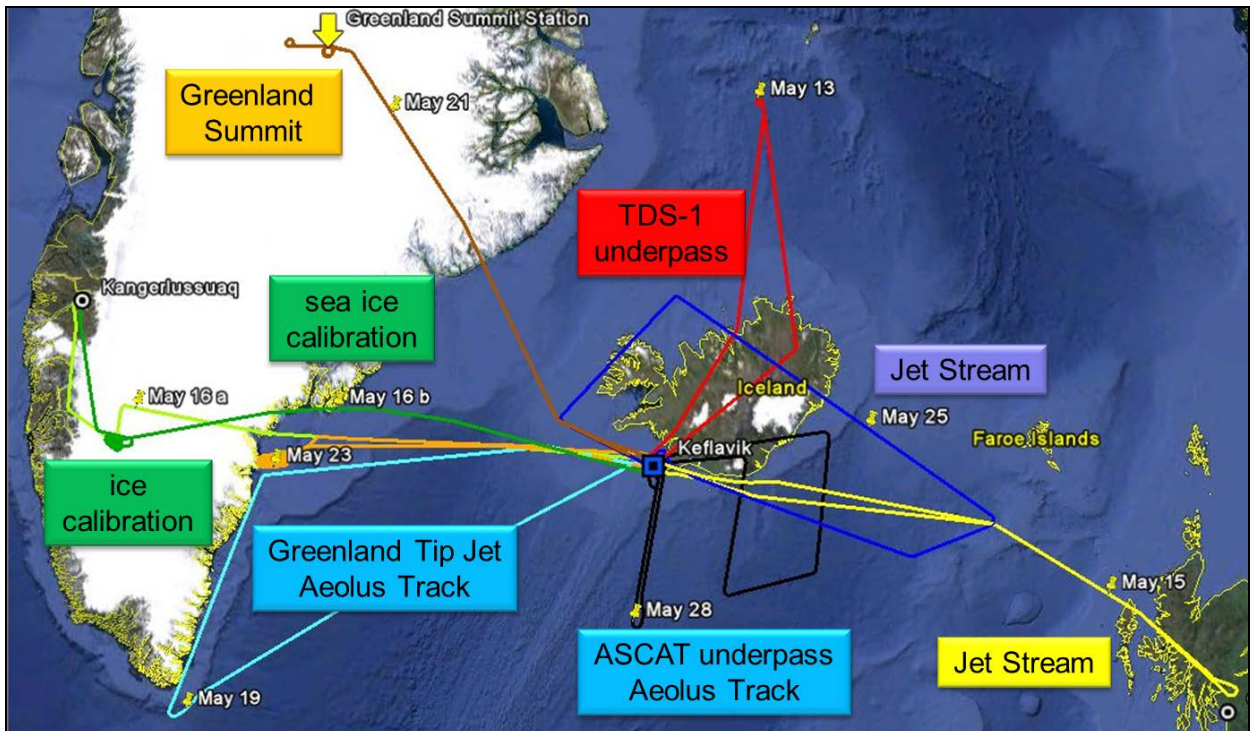


Figure 5-2: Map with flight tracks of the Falcon aircraft from Keflavik from May 13 to May 28 with the corresponding objectives of the flight.

5.4 Coordination with NASA DC-8

The NASA DC-8 aircraft transferred to Iceland from California on May 9 and back on May 28, 2015. The DLR Falcon aircraft and the NASA DC-8 aircraft performed coordinated flights, except for the Greenland Summit flight on May 21 and the ASCAT underpass on May 28 with only the Falcon aircraft. Due to the extended duration and range of the DC-8 compared to the Falcon, the DC-8 could extend the flight tracks after the Falcon had to fly back to Keflavik. A total number of 51 flight hours (excluding transfer flights) were performed by the DC-8. The flight tracks of the DC-8 are shown in **Figure 5-3**. The DC-8 was flying mainly behind the Falcon in a distance of several km. For the calibration flights on May 16 and May 23 the DC-8 was flying in the vicinity of the circles of the Falcon.

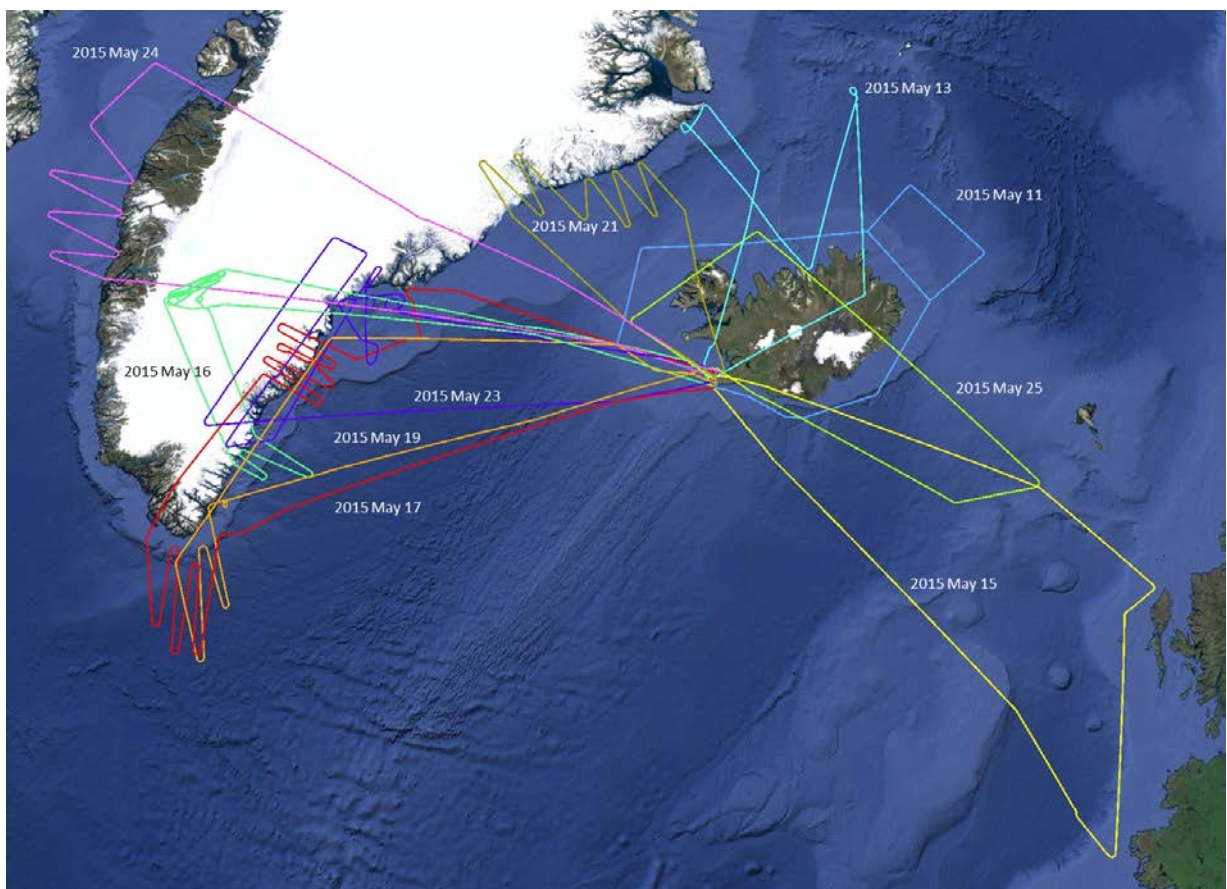


Figure 5-3: Map with flight tracks of the NASA DC-8 aircraft from Keflavik from May 11 to May 28 (courtesy D. Emmitt) with a total of 51 hours.

	Document Nr. FR.DLR.WindVal.270717	Issue: V1.1	Date: 27.07.2017	Page: 19/146	
	Doc. Title: WindVal Final Report				

5.5 Greenland Summit Station

The Greenland Summit Station (72.58°N, 38.48 W, 3216 m ASL) releases 2 radiosondes per day and is equipped with an aerosol lidar from the MPL (micro-pulse lidar) network from U.S. Department of Energy's Atmospheric Radiation Measurement (ARM) Climate Research Facility (contact Ryan Neely at the University Leeds and Ralf Bennartz at the University of Vanderbilt, see Shupe et al. 2013). In conjunction with the ongoing measurements, the NCAS (National Centre for Atmospheric Science) Atmospheric Measurement Facility (AMF) Doppler Aerosol lidar (Halo Photonics) collected data continuously at Summit, Greenland from May 1, 2015 to June 27, 2015 (contact Ryan Neely, University Leeds).

During the deployment, the Doppler lidar made scans specifically scheduled to observe the aerosol layers lowest to the ground and the horizontal wind speed with respect to blowing snow conditions. The scan parameters were following a set pattern of measuring vertical wind and depolarization profiles for 30 minutes followed by an 8 point PPI at 0 degrees, a 8 point PPI at 30 degrees, a 8 point PPI at 70 degrees, a RHI scan from East to West (i.e. from 90 degrees to 270 degrees), a RHI scan from North to South (i.e. from 0 degrees to 180 degrees) and a standard 3 point DBS wind profile at 70 degrees (PPI: Plan Position Indicator, RHI: Range Height Indicator, DBS: Doppler Beam Swinging). This provides 3D wind observations at several different heights and a detailed look at the boundary layer every 30 minutes.

The instrument operated continuously throughout the period with varying success. During periods of low clouds (<5km) and deep layers blowing snow at the surface (also referred to as diamond dust) excellent vertical observations of backscatter and wind were obtained. **Figure 5-4** shows an example of such a period. During periods of clear sky and low blowing snow, the low aerosol loading and relatively weak signal of the NCAS Halo Photonics Streamline lidar hindered accurate wind profiles (even with ~10 min integration periods). In addition, wind profiles derived from 8 point PPI scans showed no marked improvement over the manufacturer's default 3-point DBS wind profile.

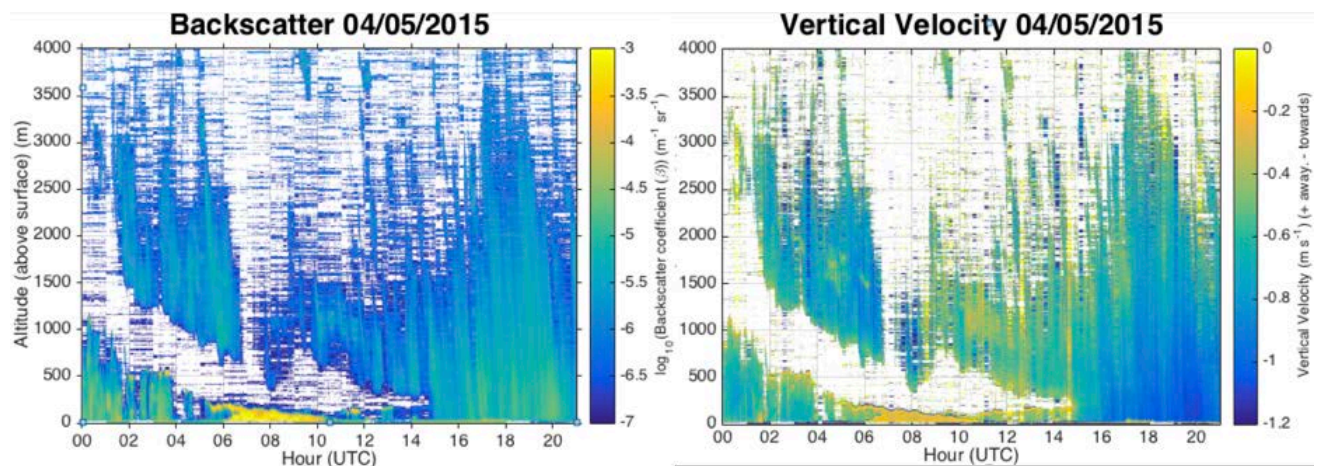


Figure 5-4: Backscatter and wind velocities profiles collected from vertical stare scans collected in 30 minute segments (separated by windprofile and other scans) over 24-hour period from May 4, 2015.

5.5.1 Observations during May 22, 2015

During the flyover of Summit of the DLR Falcon aircraft on midnight May 22, 2015 the ground-based lidar collected 14-minute average 3-point wind profiles (each individual wind profile took 1/3 of the total average time) at 60 degrees in elevation. The averaging period of the DBS profiles during the flyover was increased from the typical scan averaging periods being utilised at Summit due to the extremely clear conditions. Observations from the Summit MPL in **Figure 5-5** during the day of the flyover provide clear evidence of the extremely low amounts of aerosol scatter over Summit during and after the flyover.

The DBS profile was followed by a 4 point PPI (spaced equally at 90 degree intervals from true N). Each ray of the PPI was averaged for 2.5 minutes. These scans did not result in any good data during the flyover due to the lack of aerosol (**Figure 5-6, Figure 5-7**). Both scans were repeated every 30 minutes. The long averaging periods were needed due to the extremely clear conditions during the overpass. The mean wind speed and direction profiles are derived from the matrix inversion of three line-of-sight Doppler wind profiles (using the HALO Photonics internal algorithm). The pointing angles for the three measurements were: 1) elevation=90°, azimuth=310°, 2) elevation=60°, azimuth = 0, 3) elevation = 60°, azimuth = 0°.

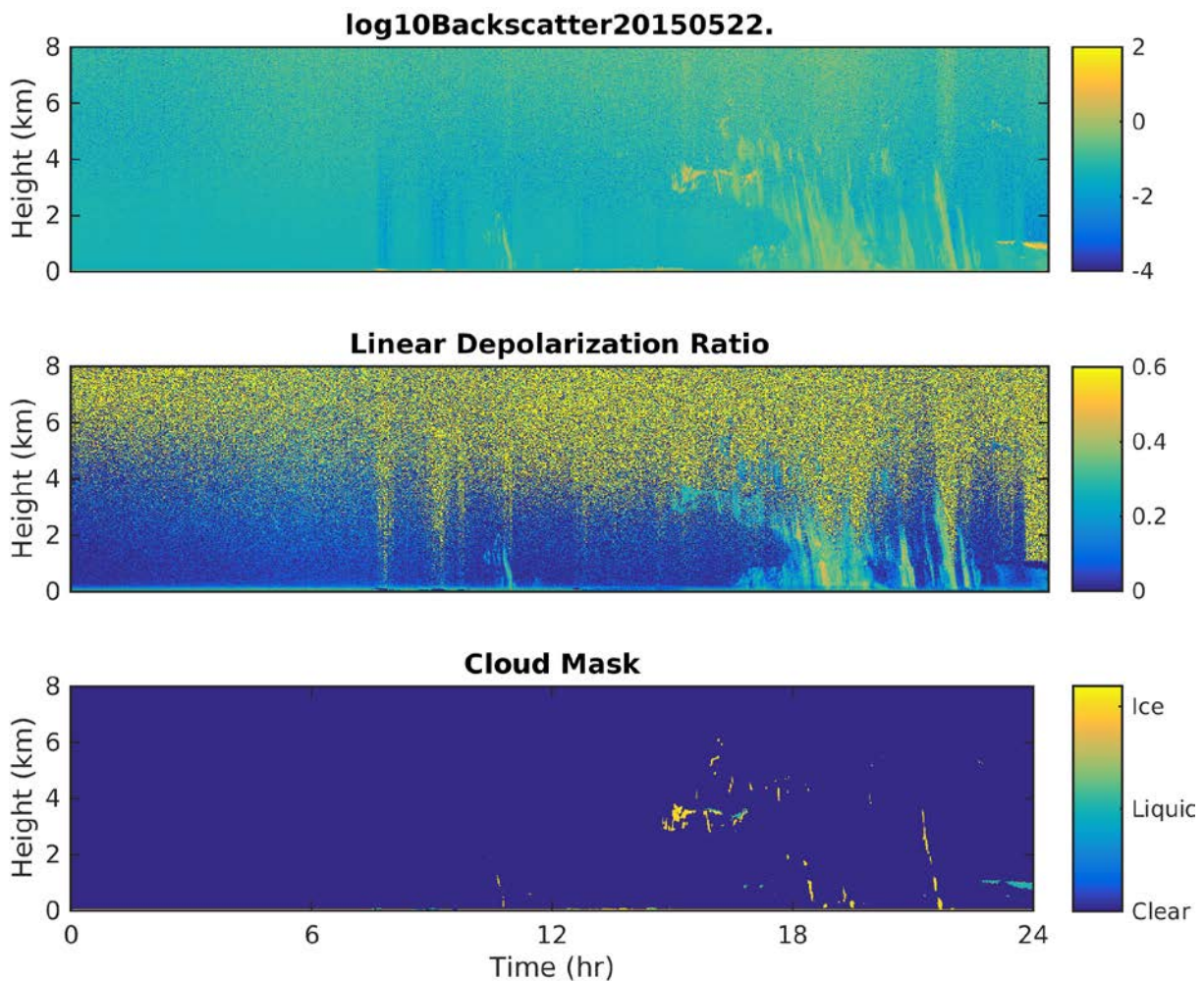


Figure 5-5: MPL observations from May 22nd, 2015. Observations from the beginning of the day show extremely low backscatter and low depolarisation values that are characteristic of clear air conditions

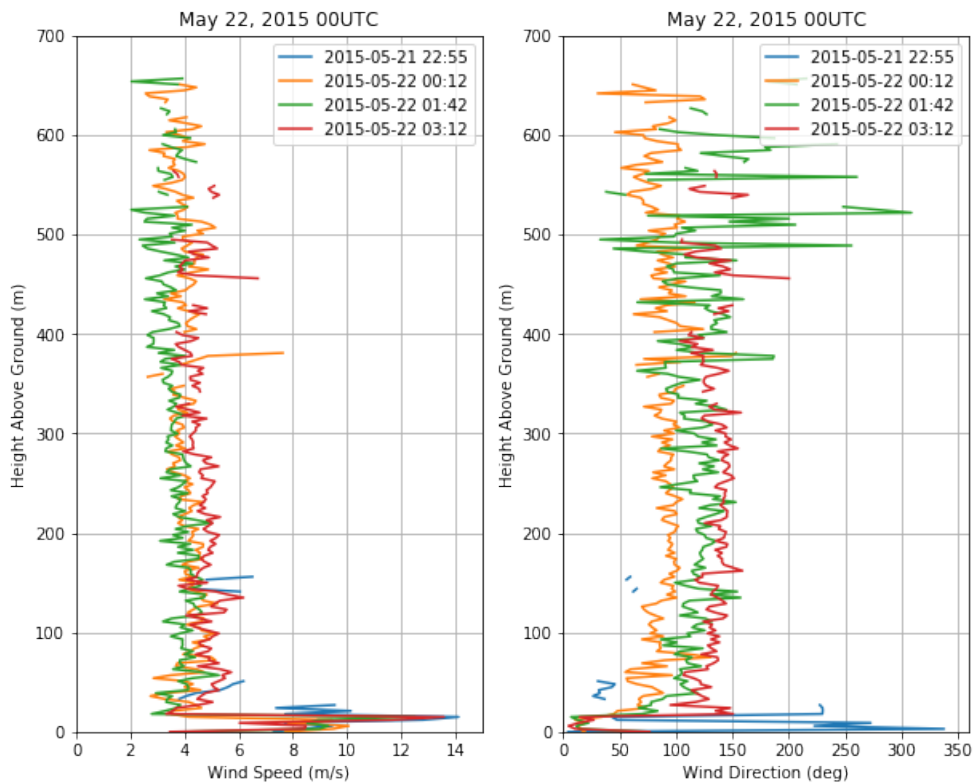


Figure 5-6: DBS wind profiles collected before, during and after the flyover. The relatively short and poor-quality profiles are due to the low SNR in clear conditions.

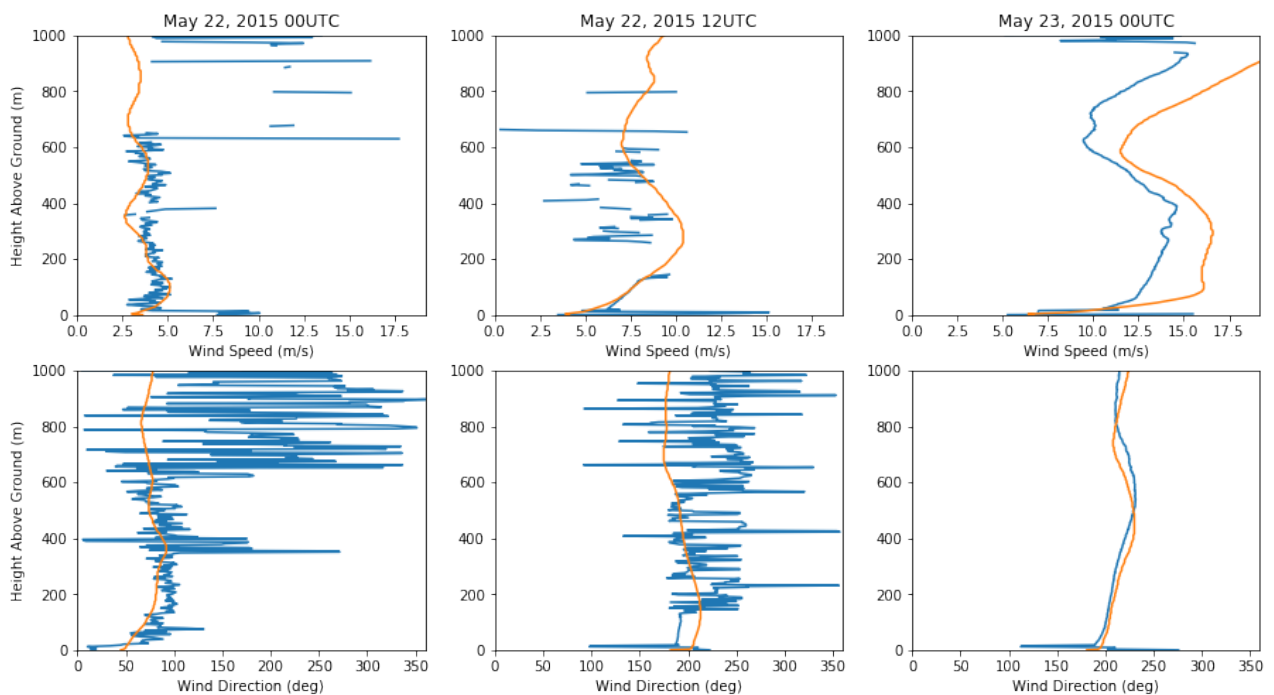


Figure 5-7: Comparison of the vertical profiles of wind speed and direction from HALO Doppler lidar and radiosondes at launched on 00UTC May 22, 2015, 12UTC May 22, 2015, and 00UTC May 23, 2015.

5.5.2 Instrument Details and Processing

The NCAS Doppler Aerosol Lidar is a 1.55 μm eye-safe (Class 1M) scanning micro-pulsed LiDAR providing profiles of the co- and cross-polarized aerosol backscatter coefficient (β) in units of $\text{m}^{-1}\text{sr}^{-1}$ and line-of-sight radial velocity in ms^{-1} at user specified azimuth and elevation angles. These values are calculated by the proprietary software provided with the lidar by HALO. In addition, a 3-point scanning algorithm is supplied by HALO for automated vertical wind profile measurement. Using this method, vertical profiles of wind speed and direction can be obtained at a minimum of once every two minutes given high enough aerosol loading. The lidar specifications are summarized in **Table 5-4** and at <https://www.ncas.ac.uk/index.php/en/data-products/campaign-products/251-amf-main-category/amf-doppler-lidar/1093-doppler-lidar-overview>

The precision of the horizontal wind vector from the HALO Photonics Doppler Wind Lidar was assessed by a 1-year comparison (2012-2013) with a radar wind profiler at 482 MHz and the Vaisala RS92 radiosonde at DWD Lindenberg observatory (Päschke et al. 2015). The root-mean square error RMSE of the comparison was 0.6 to 0.9 m/s for horizontal wind speed and 5-10° for direction with negligible systematic differences of 0.06 m/s.

Table 5-4: Main specifications of the NCAS Wind Lidar.

Parameter	NCAS Doppler Wind Lidar
Wavelength	1.55 μm
Pulse repetition rate	15 kHz
Vertical resolution	18 m
Temporal averaging raw data (horizontal)	15 000 laser shots = 1 s
Scanning capabilities	Hemispheric scanning
Precision (RMSE) horizontal wind vector	0.6 m/s – 0.9 m/s 5° – 10°

Data File Descriptions

As per NCAS AMF protocol, upon completion of the deployment the data was processed by the NCAS AMF Instrument Scientist. The processing included application of quality controls, transformation of the raw instrument files into netCDF and archival of the data on to the Centre for Environmental Data Analysis (CEDA) archive (in process). Data is provided to ESA and CEDA in netCDF format and follows the AMF protocol for file naming and structure. Each data files contain no more than 24 hours' worth of data. Detailed information about the data format may be found at <https://www.ncas.ac.uk/index.php/en/the-facility-amf/251-amf-main-category/amf-doppler-lidar/1126-doppler-aerosol-lidar-data>.

The full wind lidar data were provided on a hard-disc (August 2016 version, 568 GByte, including CF compliant netCDF and equivalent Matlab formatted files used internally by the NCAS Instrument Scientist). Ancillary observations from the MPL and radiosondes made during the deployment of the Doppler lidar were also provided. The complete Summit data archive (including the Doppler wind lidar observations) may be accessed at <ftp1.esrl.noaa.gov/psd3/arctic/summit/>

	Document Nr. FR.DLR.WindVal.270717	Issue: V1.1	Date: 27.07.2017	Page: 23/146	
	Doc. Title: WindVal Final Report				

Observations

During the deployment, the following scan types were made (name in parentheses corresponds to the top-level directory name of the data): 1) Wind Profiles (WP), 2) PPIs (ppi), 3) RHIs (rhi) 4) Vertical Stare ('fix_co' and 'fix_cr') and 5) 4 user specified patterns ('user 1', 'user 2', 'user 3', 'user 4') which changed over the deployment depending on the science question being addressed.

For all line-of-sight data (designated by LoS in the file name) collected, the observations separated into files that contain the backscatter ('beta') and files containing the radial velocity ('rv'). The individual data files follow the naming convention 'Scan_Type_18_YYYYMMDD_HHMMSSLoS_Variable.nc'. The derived WP data files are just labelled with a simple 'YYYYMMDD.nc'.

Processing of Raw Data and Quality Control:

After the campaign, all collected data were parsed into daily and hourly CF compliant netCDF files and organised by scan type. No data averaging was applied over and above that performed at the time of measurement by the instrument. All data was inspected by the NCAS AMF Instrument Scientist for spatial and temporal consistency as well as quality following the NCAS AMF protocols outlined here:

<https://www.ncas.ac.uk/en/251-amf-main-category/amf-doppler-lidar/1126-doppler-aerosol-lidar-data>.

Notably this included fixing of the data's time step due to an error in the time server at Summit Station.

In summary, the quality control includes processing of the data with a semi-automated quality script that examines every voxel of data and designates a code integer value to the 'qc_flag' variable array within the data file. The quality control codes are as follows:

- 1: Scientifically valid data.
- 2: Data values outside system measurement range.
- 3: Data quality compromised due to low operational temperature (<-15C).
- 4: Data quality compromised due to high operational temperature (>40C).
- 5: Data quality compromised due to system failure.
- 6: Periods where data is good but range/SNR is compromised (due to low cloud or fog episodes for example).

The limits used to create these flags are given by HALO as part of the instrument's specifications. The details of the quality control flags are embedded in the global attributes of each netCDF data file for reference. Missing data is handled separately and a -9e33 place holder value is used to designate this within each variable's array. As part of the processing of the raw data and creation of the Level 2 data files, the specific metadata for the instrument, sampling period, averaging, campaign information and details of the NCAS AMF Instrument Scientist and software used to process the observations are all embedded within the global attributes of the netCDF data file.

Ancillary Data Details:

Since the spring of 2010, the NSF-funded ICECAPS (Integrated Characterization of Energy, Clouds, Atmospheric State and Precipitation at Summit) project has operated a suite of instruments at Summit Camp. Notably, this includes launching twice a day radiosondes (operationally ingested into the GTS system) and a MPL (micro-pulse lidar) from U.S. Department of Energy's Atmospheric Radiation Measurement (ARM) Climate Research Facility (See below). Other instruments include a vertical pointing Doppler 35 GHz cloud radar, two microwave radiometers and a polar-atmospheric emitted radiance interferometer (full details are discussed in Shupe et al. 2013). Quick-time plots of observations and details of data access from the majority of the instruments up to previous day may be found at: <https://www.esrl.noaa.gov/psd/arctic/observatories/summit/>.

The MPL is a 532-nm wavelength system that provides near zenith (2°–4° off zenith) profiles of backscatter and depolarization with a 5-s time resolution and 15-m vertical resolution. The raw data has been processed into daily netCDF files with file names that follow the DOE ARM format (smtmpl-pol1turnX1.c1.YYYYMMDD.HHMMSS.cdf). Processing of the MPL data includes correcting systematic

changes in the depolarization values due to the impact of temperature changes on the system's receiver and removing signal induced noise. For more information on this instrument see: https://www.arm.gov/publications/tech_reports/handbooks/mpl_handbook.pdf. In addition to the standard product, a simple cloud mask is also derived from the observations to distinguish between predominantly clear conditions and liquid and ice clouds.

The radiosondes launched at Summit during the NCAS Doppler Aerosol Lidar deployment were Vaisala Radiosonde RS92-SGP with code correlating GPS wind finding. The raw Vaisala data format is processed by the ICECAPS project into netCDF files (smtsondewnpnX1.b1.YYYYMMDD.HHMMSS.cdf) which contain the raw observations as well as derived thermodynamic variables.

An example of typical observations made by the MPL and radiosondes are given in **Figure 5-8** and **Figure 5-9**. Process and quality controlled observations from the radiosondes and MPL during the deployment of the NCAS Doppler wind lidar have been provided as part of the Doppler wind lidar's database.

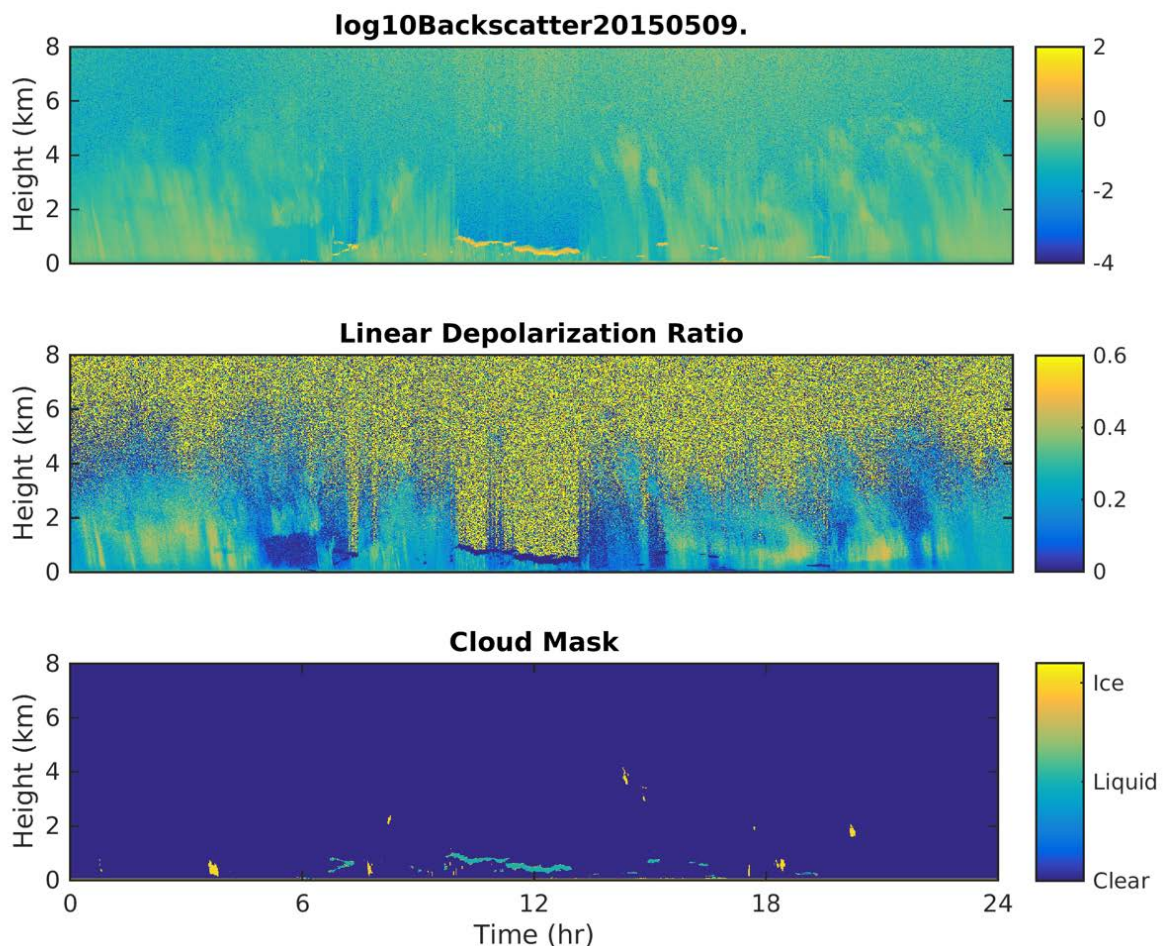


Figure 5-8: MPL Observations from May 9th, 2015 under a typical 24-hour period at Summit with both ice precipitation and periods of low-level mixed phase

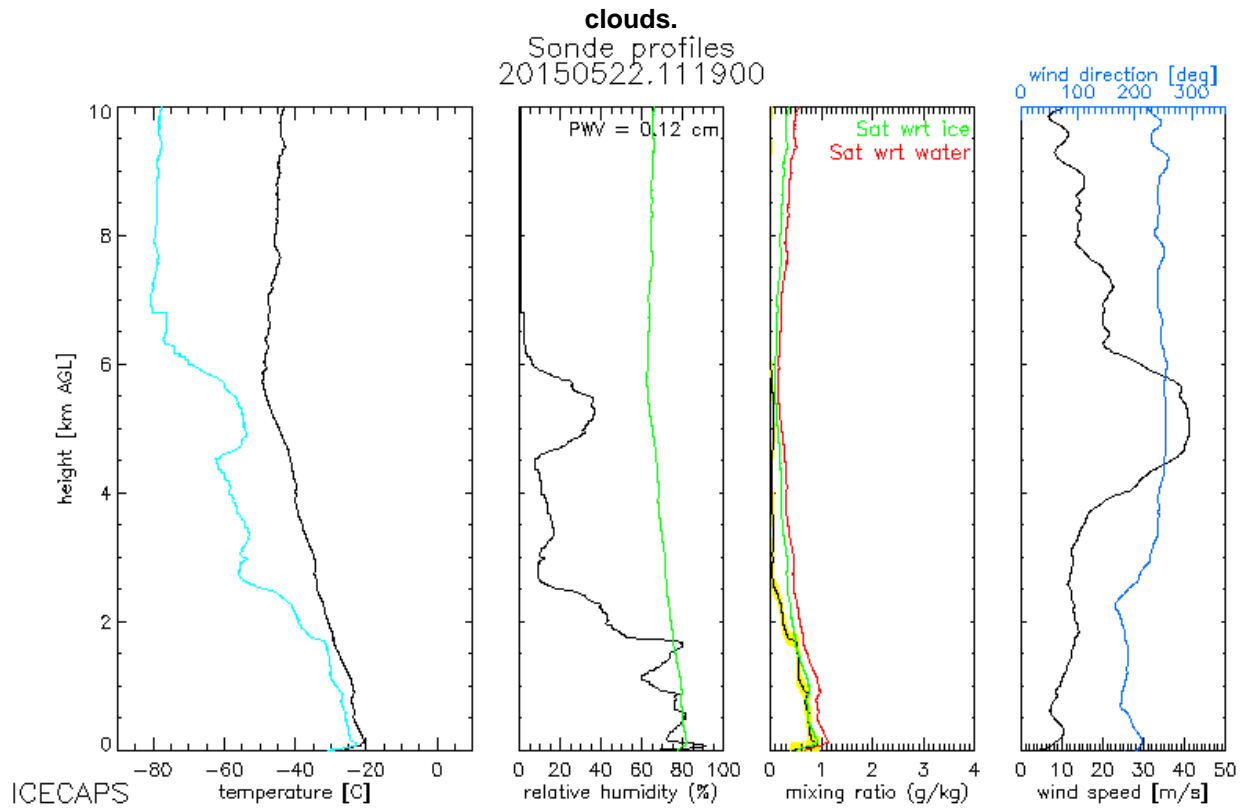


Figure 5-9: Observations and derived values from the 12 UTC radiosonde launched on May 22, 2015.

	Document Nr. FR.DLR.WindVal.270717	Issue: V1.1	Date: 27.07.2017	Page: 26/146	
	Doc. Title: WindVal Final Report				

5.6 Satellite underpasses

The planned underpasses with the following satellite instruments were achieved.

- CALIPSO lidar from NASA providing attenuated backscatter, cloud and aerosol location (16 days repeat cycle, 233 orbits): no direct underpass performed with Falcon aircraft, but CALIPSO passes were in the vicinity of the Falcon flight tracks on May 11, 16, 19, and 25.
- Scatterometer ASCAT on Metop A and Metop B from EUMETSAT providing sea surface winds at 10 m with two swaths of 500 km width on each side of the satellite ground track (29 day repeat cycle); an underpass was performed on May 28; some passes were in the vicinity of the Falcon flight tracks on May 15, 16, and 19.
- Rotational Fan-Beam scatterometer on HY2A with a 6:00 Local Time of Ascending Node (LTAN) and a 1800 km wide nadir swath: no underpass was performed
- TechDemoSat 1 (TDS-1) with GNSS reflection technique to derive sea-surface winds; a direct underpass was performed on May 13, but the GNSS instrument was not operating during the underpass time.
- ALADIN lidar from ESA (7 day repeat cycle, 109 orbits); similar flight tracks than ALADIN were flown on May 13, 19 and 28.

The satellite track predictions were obtained from:

<http://www-angler.larc.nasa.gov/predict/> and

<http://www.n2yo.com/>

The publically available CALIPSO track predictions are not accurate enough for flight track planning. Thus the correct predictions were provided by NASA LaRC (via SWA). A specific DLR tool was prepared during the campaign to visualize the satellite tracks for the specific days and regions from the CALIPSO tracks and the information provided on the n2yo-Website. It should be noted here that this website provides numerous satellite track predictions, but is maintained by amateur astronomers. An ESA website for satellite track predictions was not available during the campaign in 2015, but is considered as necessary for Aeolus Cal/Val activities (N.B. Track prediction tools from ESA were available in early 2017 for the preparation of the Cal/Val Workshop 2017 and tested by DLR.)

Trial runs were performed with predicted Aeolus tracks (geographical location and time) provided by ESTEC (Thomas Kanitz) on May 13 (north of Iceland), May 19 (along Greenland Coast) and May 28 (south of Iceland). It is expected that actual track predictions for Aeolus will be available daily from ESA after launch. In addition to track predictions the actual instrument settings for ALADIN, e.g. calibration or wind mode, vertical sampling, on-board pulse accumulation should be provided. It should be also considered for ALADIN to place most of the vertical range-gates below the aircraft flight level (e.g. 11 km, and 2 range-gates above) to enhance the vertical collocation. It is expected that the ALADIN time of overpasses are around 5-7 UTC and 19-21 UTC in the North-Atlantic Region; thus it was only considered to collocate with the evening overpass during the WindVal Campaign.

The TechDemoSat 1 mission was launched in July 2014, and has the capability to derive sea-surface winds by use of an enhanced GPS receiver to monitor reflected signals to determine the ocean roughness. This is equivalent to the 10 m sea-surface wind speed (equivalent to sea surface winds from scatterometer). The satellite track predictions for TDS-1 were available on the n2yo-Website. It was encountered during the campaign the GPS receiver instrument is not switched on all the time due to power constraints. Thus, in addition to the track predictions, the specific operating times for the instruments should be provided by ESA in the future for potential TDS-1 or Aeolus validation.

	Document Nr. FR.DLR.WindVal.270717	Issue: V1.1	Date: 27.07.2017	Page: 27/146	
	Doc. Title: WindVal Final Report				

5.7 Data processing and availability

This chapter discusses the the timeline for processing of the different data sources from the instrument on-board the DLR Falcon aircraft during and after campaign (**Table 5-5**). Data in that context does not only cover data products with a specific data format, but also data provided within figures, which are shown on quicklook data meetings during the campaign and at progress meetings. The times provided in **Table 5-5** are taking into account both the experiences made during WindVal I and II in 2015 and 2016, respectively.

During the WindVal I campaign (and also during WindVAL II) weekly data-quicklook meetings were organized, where Falcon in-situ, 2- μ m DWL and A2D data were presented in form of quicklook plots. In general, the analysis of Falcon in-situ data is performed on-site at the campaign by a dedicated person of DLR Flight Experiment facility and data (plots, and TXT-files) are typically provided 1 day after each flight. This data is also used as input to the A2D processing (see chapter ch. 9.3.1). Both the aircraft cabin housekeeping data (HK) and the wavemeter frequency measurements from the A2D are immediately available after the flight, because no post-processing is applied.

The 2- μ m DWL data, which consists of a large data volume (\approx 200 GByte / flight) is first copied two times to external hard-discs and then processed to LOS winds (Level 1) and to horizontal wind vectors (level 2) within 1-2 days after each flight. Thus, first 2- μ m DWL wind data is available during the campaign after 1-2 days, except for flights with anomalies, which need adaptation of the processing algorithms. The preliminary 2- μ m DWL data product files are available 1-2 months after the campaign, and about 6 months for the final product (as TXT files or netCDF).

The A2D processing capabilities could be largely improved compared to the 2009 airborne campaign, where first LOS wind and calibration results were available 1 year after the campaign. In contrast, A2D data were already provided during the WindVal I campaign in 2015 for selected wind scenes and selected calibrations. This was further improved for the WindVal II campaign in 2016, where Rayleigh and Mie LOS winds and related calibration output was available for more scenes already during the campaign. The A2D processing starts with assessing the quality of the data wrt. outliers and verifying the signal intensities. Also, the data from each flight needs to be separated according to the specific instrument operation modes (e.g. wind mode, MOUSR, calibration, imaging mode, non-valid data due to laser and spectrometer warm-up anomalies), which is considered then as "consolidated raw data". This is performed within 1-2 days after each flight. The calibration mode data is processed to obtain response curves and their corresponding fit parameters also within 1-2 days for each calibration. If calibration mode data is available, then the A2D wind mode data can be processed to LOS winds. This was performed for some selected scenes already during the WindVal I campaign. For WindVal II first LOS wind profiles from the A2D were analysed during the campaign and a comparison to the 2- μ m DWL was already presented less than 1 month after the end of the campaign for 1 selected flight.

Reprocessing of the data (Falcon, A2D, 2- μ m DWL) is only considered in case of major algorithm and processor improvements due to identified algorithm and software errors or as a result of an improvement in the retrieval algorithms. It was necessary to re-process the A2D Level 1 LOS winds and the A2D winds for the L1B processor once. Also, other data types from the campaign (e.g. NASA DC-8 dropsondes, or NASA DAWN data) were reprocessed once. As the reprocessing is not scheduled in the processing schemes of the data, the availability of the reprocessed data mainly depends on the time, when the need for reprocessing was identified.

Both the 2- μ m DWL and A2D data processing on-site during the campaign require a dedicated person for data analysis in addition to the 3 persons for operating both instruments. The latency times discussed in **Table 5-5** are based on the assumption that the persons for the data analysis are fully available after the campaign for that task. The full dataset from a campaign should be available as a final data product in a specific format about 12 months after the end of the campaign. This is a typical period for data availability of instrument products on a database obtained during large field campaigns.

Table 5-5: Data availability from DLR Falcon aircraft

Availability	Time after each flight during campaign	Time after end of campaign for preliminary data product	Time after end of campaign for final data in final format
Falcon in-situ	1 day	1-2 weeks	
Aircraft cabin HK	1 day	no post-processing	
Wavemeter A2D	1 day	no post-processing	
2- μ m DWL	1-2 days	1-2 months	6 months
A2D wind mode	1-2 days for signal intensity and QC relevant parameters (e.g. DCO) for wind mode 3-4 days for selected wind scenes for LOS wind (in case calibration mode data is available)	3-6 months for Rayleigh and Mie LOS winds for selected wind scenes; this period was 9 months for WindVal	6-12 months for Rayleigh and Mie LOS winds for all wind scene; this period was 14 months for WindVal
A2D calibration mode	1-2 days for signal intensity, QC relevant parameters (e.g. DCO) and response curves and fit parameters for each calibration	1-3 months for assessment of all calibrations, this period was 6 months for WindVal	
A2D as input to L1B	not available	6-9 months for selected flight scenes, this period was 16 months for WindVal	

6 The 2- μm Doppler wind lidar

This chapter discusses the performance and results of DLR's 2- μm Doppler wind lidar (DWL) measurements carried out in the framework of the WindVal campaign in 2015 conducted from Keflavik, Iceland. Though the key instrument on-board DLR's Falcon aircraft was the A2D as it is similar to the ADM-Aeolus satellite instrument ALADIN, the 2- μm DWL represented a reliable reference system providing accurate measurements of the three-dimensional wind vector needed for comparison and useful for later ADM-Aeolus instrument calibration and validation.

First the instrumental setup of the 2- μm DWL is explained (Section 6.1), followed by a description of the data retrieval algorithm (Section 6.2). Further details about the instrument and the retrieval algorithm can be found in a recent publication by Witschas et al. (2017). After that, the performance of the 2- μm DWL during the WindVal campaign is discussed (Section 6.3) and a few measurement examples are given in Section 6.4.

6.1 Instrument description

A schematic block diagram of the DWL system is shown in **Figure 6.1**. The transceiver was developed and built by CLR Photonics (today Lockheed Martin Coherent Technologies), the double-wedge scanner system and the data acquisition unit were developed at DLR.

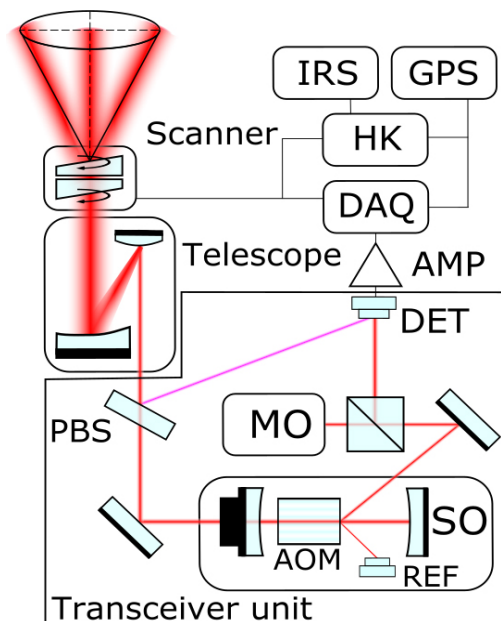


Figure 6.1: Simplified sketch of DLR's coherent DWL system indicating the transceiver unit including master oscillator (MO), slave oscillator (SO), acousto-optical modulator (AOM), reference pulse detector (REF), polarizing beam splitter (PBS) and detector (DET). The acquisition chain including signal amplifier (AMP), data acquisition unit (DAQ), housekeeping data acquisition unit (HK), global positioning system (GPS), inertial reference system (IRS) as well as the beam expanding telescope and the double wedge scanner are shown.

The transceiver unit comprises a continuous-wave master oscillator (MO) which is used as an injection seeder for the slave oscillator (SO) and additionally as local oscillator for the coherent heterodyne detection. The MO is a diode-pumped Tm:LuAG laser characterized by single-frequency operation and a low bandwidth providing high heterodyne efficiency. A part of the MO radiation is coupled into the SO via an acousto-optic modulator (AOM) which is shifting the original MO-frequency by 100 MHz, and thus, permitting determination of the magnitude and sign of the frequency difference between MO and SO which is later needed for wind measurements.

	Document Nr. FR.DLR.WindVal.270717	Issue: V1.1	Date: 27.07.2017	Page: 30/146	
	Doc. Title: WindVal Final Report				

The SO is based on a two-side pumped Tm:LuAG crystal and produces laser pulses with a wavelength of 2022.54 nm (vacuum), a pulse energy of 1-2 mJ, a pulse length of 400 ns (~120 m) at a pulse repetition rate of 500 Hz, leading to an average transmitted laser power of 0.5-1.0 W. The laser wavelength of 2022.54 nm allows for an eye-safe operation in an atmospheric window with low absorption of water vapor enabling wind measurements up to a range of 12 km. Furthermore, the pulse repetition rate of 500 Hz provides the possibility of signal accumulation which reduces speckle noise. In addition, the laser beam has a nearly Gaussian shape in the spatial, temporal and spectral domain, which reduces the uncertainty of the Doppler estimates. To ensure resonance between the SO cavity length and the MO radiation, the SO-cavity length is controlled by the ramp and fire technique, where the resonance signal is monitored by the reference detector (REF).

After the SO, the laser beam is expanded to a diameter of about 10 cm by means of a telescope after it was passing a polarizing beam splitter (PBS). The expanded laser beam then enters an optical double-wedge scanner which enables to steer the laser beam to any position within a cone angle of 30°. The scanner itself is composed of two anti-reflection coated rotating silicon wedges, especially doped to be transparent for the 2022.54 nm wavelength. The wedge angle is 6.0° and the index of refraction is 3.452 (at 2022.54 nm), respectively. The actual wedge positions for the desired beam direction are set by two stepper motors working with a micro-stepping driver that is controlled by the housekeeping computer (HK).

Once traveling through the atmosphere, a small portion of the emitted laser pulse partly scatters on aerosols and cloud particles back to the lidar system, where it is received with the same telescope that was used for emission. The backscattered light is reflected on the PBS and directed to the optical signal detector (DET), where it is mixed with a portion of the MO laser. After pre-amplification directly at the detector, the analog detector signal is additionally amplified by a custom-made 500 MHz amplifier (AMP). In particular, the internal reference pulse is attenuated by 9 dB and the atmospheric signal is amplified by 24 dB such that they reach a comparable signal level before digitization. Now, the time-resolved detector signal resulting from each single laser shot is sampled with 500 MHz and 8 bit resolution (Agilent U1064A, Acqiris DC241) before it is stored to a solid-state drive connected to a dedicated computer (ADLINK, ePCIS-6400x) (DAQ). This procedure leads to a data rate of about 15 MByte/s (54 GByte/h) and gives maximum flexibility for post-processing.

In order to achieve a high timing accuracy for the data processing, all measured quantities (time-resolved laser pulse signal, scanner position, aircraft position, speed and attitude angles) are stored with an accurate time stamp generated by a custom made GPS controlled oscillator. In particular, a 10 MHz signal of an oven controlled crystal oscillator is fed into a timer/counter module (National instruments, Ni-PXI-6608). Here, the signal is divided by 100 in order to reach a 100 kHz clock signal which is synchronized by the pulse-per-second signal provided by the GPS module (Septentrio, PolaRx2), which is additionally used to measure the aircraft position and speed. The latter one is important as the aircraft speed (~200 m/s) is the main contributor to the measured Doppler shift (i.e. larger than the expected horizontal wind speed) and thus, has to be considered in order to retrieve the actual wind speed reliably. The 100 kHz time stamp is also sent to the DAQ computer where it is acquired (NI PXI-6602) and stored together with each single laser pulse.

Additionally to the aircraft speed, the aircraft attitude has to be measured and considered for the wind retrieval. For that reason, roll, pitch and yaw angles are measured with an inertial reference system (IRS, Honeywell LASEREF YG 1779) whose data including time stamp is also stored on the HK-computer. The velocity and the actual position of the aircraft are obtained by GPS. The accuracy of the horizontal velocity measured with the GPS receiver is specified to be 1.5 mm/s. The main parameters of the DWL are summarized in **Table 6-1**.

Table 6-1: Overview of the 2- μ m wind lidar system parameters.

Laser		
	Laser active medium	Tm:LuAG
	Wavelength (vacuum)	2022.54 nm
	Repetition rate	500 Hz
	Energy/pulse	1-2 mJ
	Output power	0.5-1 W
	Pulse length (FWHM)	~400 ns (~120 m)
	Frequency offset	100 \pm 2 MHz
Transceiver		
	Telescope type	Off-axis
	Telescope diameter	0.11 m
Scanner		
	Type	Double wedge
	Wedge angle	6°
	Maximum displacement	30°
Detector		
	Type	InGaAs PIN photo diode
Data acquisition		
	Type	Single shot
	Sample frequency	500 MHz
	Resolution	8 bit

6.2 Measurement procedure and wind retrieval

During the WindVAL campaign, the DWL was mainly operated in scanning mode aiming to measure vertical profiles of the three-dimensional wind vector. Alternatively, the system can measure with a fixed line-of-sight (LOS) e.g. in order to measure vertical wind speed by pointing the laser in nadir direction or measuring with the same geometry as the A2D instrument (20° off-nadir). While operating in scanning mode, a conical step-and-stare scan (VAD-technique) around the vertical axes with a nadir angle of 20° is performed. 21 LOS wind velocities are measured per one scanner revolution and used to retrieve the three-dimensional wind vector as described in section 6.2.2. Considering 1 s averaging time for each LOS measurement (21 s), 21 s for the scanner motion between each measurement position, and an aircraft speed of about 200 m/s, the spatial resolution along flight track of the horizontal wind speed data is about 8.4 km. Operating in fixed LOS mode, the laser beam is intentionally pointed to a user-defined direction. Considering 1 s averaging time, the horizontal resolution for the retrieved LOS wind profiles is about 200 m.

6.2.1 Line-of-sight wind speed

LOS winds are retrieved from the detector raw signal, which itself is stored for each single laser pulse with a sampling rate of 500 MHz, 8 bit resolution and a duration of $t = 97.8 \mu\text{s}$. This leads to an overall sampling range of $r = c \cdot t / 2 = 14.659 \text{ km}$ which is sufficient as the distance to ground is always lower considering a maximum flight altitude of 12 km and maximum off-nadir angles of 30°. A schematic overview of the LOS wind processing steps is given in **Figure 6.2**.

	Document Nr. FR.DLR.WindVal.270717	Issue: V1.1	Date: 27.07.2017	Page: 32/146	
	Doc. Title: WindVal Final Report				

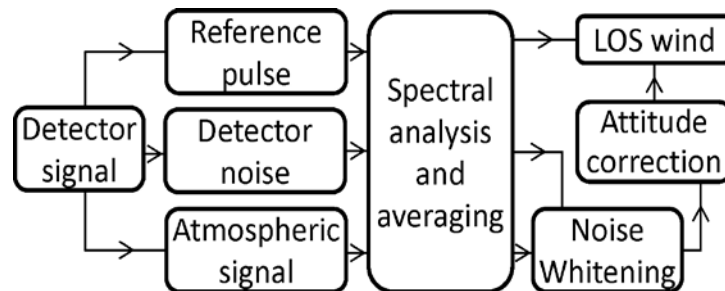


Figure 6.2: Schematic overview of the LOS wind processing procedure

The single-shot data storage enables to exclude bad pulses and to correct the laser frequency variations from pulse to pulse before accumulation (e.g. all valid laser pulses within 1 s). In order to do so, the power spectrum of the reference pulse signal, which is the beat signal of the local oscillator (MO) and the emitted laser pulse, is calculated and analysed regarding its frequency. If the beat frequency differs by more than 10% of the nominal AOM-frequency of 100 MHz, or if the laser pulse built-up time is less than 3.5 μs (about 2.6 μs is usual), the laser pulse is not considered for accumulation. Moreover, before accumulating respective reference pulse spectra, they are frequency shifted to a defined reference value of e.g. 100 MHz in order to correct for pulse to pulse frequency variations and thus to avoid spectral broadening in the accumulation process. The applied frequency shift is afterwards equally applied to the atmospheric signal power spectra. The part of the detector raw signal containing the atmospheric return is divided in segments that lead to 100 m range-gates in the vertical by considering the actual laser beam pointing angle, the aircraft altitude and attitude and the reference pulse timing. After that, the power spectrum is calculated for each range-gate and laser pulse, is frequency shifted according to the reference pulse frequency shift and subsequently accumulated. The detector signal at the end of the record (after ground return) is used to analyse the detector noise characteristics which is especially important in the weak signal regime (Frehlich et al. (1997)). Consequently, each power spectrum for each single range-gate is divided by the respective noise spectrum for correction purposes. In a next step, the resulting power spectra are corrected for the actual LOS direction which is derived as explicitly described by Chouza et al. (2016a), and for the aircraft speed projected onto LOS direction which is derived from the ground speed measured by the GPS module and the actual laser pointing direction. The remaining frequency shift Δf between reference pulse and atmospheric signal is proportional to the wind speed v according to $\Delta f = (2f_0 v)/c$, where f_0 is the laser frequency, c is the velocity of light and $\lambda_0 = c/f_0 = 2022.54 \text{ nm}$ the laser wavelength. Using this relation, the actual LOS wind speed v is calculated. For instance a wind velocity of $v = 1 \text{ m/s}$ leads to a frequency shift of $\Delta f = 2/\lambda_0 = 0.9889 \text{ MHz}$. The backscattered signal close to "hard targets" as for example ground or clouds is usually not considered for wind retrieval as the backscattered laser pulse and its frequency chirp may distort the wind retrieval.

As shown in recent publications by Witschas et al., (2017) and Chouza et al. (2016a), the bias of LOS winds is less than **0.05 m/s** and the statistical uncertainty is about **0.2 m/s**.

In order to get the actual vertical wind speed or rather the three-dimensional wind vector from respective LOS wind measurements, further processing steps are needed as discussed in the following.

6.2.2 Horizontal wind speed and direction

In order to measure the horizontal wind speed and direction with the DWL, a conical step-and-stare scan of the laser beam around the vertical axes with an off-nadir angle of 20° is performed with 21 LOS measurements per one scanner revolution of 360° . Various LOS or rather radial velocities at different azimuth angles are derived and analysed, leading to the mean wind vector in the measurement volume. As summarized by Smalikho (2003), there are several techniques of wind vector estimation from DWL data. For the 2- μm DWL, two different retrieval algorithms are applied.

The commonly used algorithm for 2- μm DWL data processing (inversion) derives the LOS velocity for each of the 21 scanner positions during one scan (Weissmann et al. (2005)). Afterwards, the 21 LOS velocities are grouped in three 120° sectors. Thus, seven different wind vectors ($21/3$) are calculated for each scan.

	Document Nr. FR.DLR.WindVal.270717	Issue: V1.1	Date: 27.07.2017	Page: 33/146	
	Doc. Title: WindVal Final Report				

Afterwards, the seven vectors are averaged. LOS values that do not agree with the resulting wind vector (deviation larger than 1 m/s) are eliminated and a new wind vector is calculated by using the remaining LOS velocities. Finally, an averaged wind vector is reported as valid, if a minimum number of wind vectors (default 4) were obtained from the inversion results of one scan. Hence, the inversion algorithm gives a good possibility for quality controlling, as “bad” LOS estimates can be excluded. On the other hand, an alternative algorithm based on the maximum function of accumulated spectra (Witschas et al. (2017)) is used in regions of low SNR. All spectra of one conical scan are accumulated after they were shifted to different hypothetical winds. If the hypothetical wind matches the real wind, the accumulated spectra show an intensity maximum. Using this approach, no estimates of single LOS winds are needed and reliable winds can be retrieved for lower SNR levels compared to the inversion algorithm. However, as the inversion algorithm gives the better quality control, it is decided to use wind estimates of the accumulation algorithm only in cases where the inversion algorithm gives no wind data. As a final step a median filter is applied to each range bin. The neighbouring range bins in a box of N by N range bins (default N=5) is investigated. The range bin is considered as valid, if a fraction (default value is 20 %) of all horizontal wind speed values surrounding this range bin is within a certain range of wind speeds (default is ± 4 m/s). In order to additionally increase the accuracy of 2- μ m DWL winds, the ground return is used to determine the exact installation position of the lidar with respect to the aircraft (see also Chouza et al. (2016a)). As the installation position is shown to stay constant during one campaign, a flight scene of about 15 minutes with ground visibility in flat terrain is enough (and needed) to correct all measurements acquired during on campaign.

Based on dropsonde comparisons performed during the A-TREC campaign in 2003 (Weissmann et al. (2005)), the systematic (bias) and statistical (standard deviation) uncertainty of horizontal wind speeds derived from the 2- μ m DWL have been estimated to be **(0.0 \pm 1.2) m/s** (by applying the inversion algorithm).

The 2- μ m DWL data are provided for wind vector profiles (Level 2; filename *_L2.txt) from conical scans and as LOS wind profiles from conical scans and in case of non-scanning mode (Level 1, filename *_L1.txt). For the Level 2 wind vector profiles only altitude levels from aerosol backscatter are reported. No level 2 wind vector profiles are derived from high SNR targets as clouds or ground. Cloud backscatter is not reported in the Level 2 product, because the cloud backscatter is often not uniform within 1 scan, e.g. clouds are present only for some LOS pointing directions. In contrast the information for aerosol, clouds and ground LOS winds is obtained in the Level 1 product.

The 2- μ m DWL does allow a precise determination of ground-return range and cloud-top range, due to the sampling of the backscatter signal with 500 MHz corresponding to 0.3 m, which is much higher than the resolution of the 2- μ m data product for LOS winds and horizontal wind vector with 100 m. This allows to precisely identifying the location of the ground-return and cloud-top within the A2D or ALADIN range bins. This was applied for ground returns by Weiler (2017) and could be used for studying representativeness issues for Mie winds for A2D (see section 9.4.2) and ALADIN.

It is also worth mentioning that the times provided in the Level 1 and Level 2 files are based on GPS time, which is not corrected for leap seconds. Thus, the following correction needs to be applied to obtain time in UTC (before 1 July 2015): UTC = GPS -16 s. Further information about the 2- μ m Wind Lidar data product can be found in the data acquisition report (DLR 2016a) and in Witschas et al. (2017).

6.3 2- μ m Wind Lidar performance during WindVal 2015

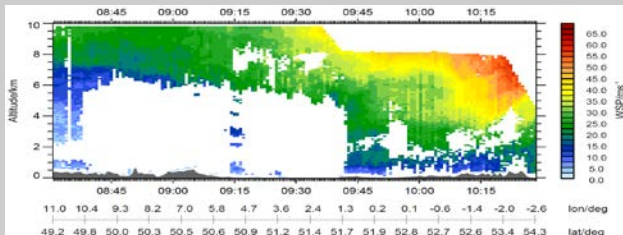
During the WindVal 2015 campaign, the 2- μ m DWL was working reliably during all flights. On the two flights performed on 19 May and 21 May, a failure in the GPS module occurred which led to missing GPS information at certain LOS measurements every 4 minutes. For that reason a wind measurement is missing every 4 minutes at these flights. In very few cases, the new accumulation algorithm was able to retrieve wind only from a few valid LOS measurements during on VAD-scan. However this is rare. Anyway, the overall wind information is also available on these flights and data gaps could be interpolated if necessary. The GPS failure was not reproducible and did not occur again since then. Furthermore, on 25 May, the lidar data acquisition computer crashed at 16:31 UT (50 minutes before landing) and had to be rebooted. As the timestamps of the lidar data after that software crash do not agree with the time stamps of the HK-computer, the wind processing cannot be performed adequately and no wind data is available for this period. A software crash did not happen again since then. An overview of the flights performed during the campaign and the corresponding lidar cross sections of the horizontal wind is given in **Table 6-2**.

After take-off, the system was switched-on immediately and was operational about 10 to 15 minutes. Considering the usual climbing rate of the Falcon aircraft, reliable lidar data are available from an altitude of about 5 km. As the lidar has to be completely shut-down before landing, and as the shut-down time is also approximately 10 minutes, lidar data is available down to altitudes of about 5 km to 3 km (see also the overview plots in **Table 6-2**).

As the 2- μ m DWL is based on coherent heterodyning detection, the data coverage of the measurements depends on the aerosol load and the cloud coverage as thick clouds cannot be penetrated by the laser beam. Thus, flight planning was performed accordingly. In particular, it was tried to fly through areas with high relative humidity RH (~60% to 80%) but without opaque clouds. This RH criteria is one among several criterias; for post-launch validation the aircraft flight tracks need to be aligned to the satellite track independent of the RH or cloudiness. The RH and cloudiness was used from ECWMF forecast products in the day-to-day flight planning. Measurements during previous campaigns have demonstrated that these conditions are optimal for the coverage of 2- μ m DWL measurements. Most likely, the water vapor itself or welling aerosols represent adequate scatterer for the 2- μ m wavelength. As can be seen from the lidar cross sections, the coverage was remarkably high for all flights (60% and larger). The highest wind speeds measured during the campaign reached up to 70 m/s.

An overview of the performed flights including 2- μ m DWL wind measurements is given in **Table 6-2**. A more detailed discussion about particular flights is given in Section 6.4.

Table 6-2: Overview of flight and 2- μ m wind lidar measurements of the horizontal wind speed (WSP, colour coded) performed during WindVal 2015. The white areas in the lidar cross sections in the rightmost panel indicate areas with the valid data due to low SNR.

Date	Time TO/Ldg. (UTC)	Route	Objective	2- μ m wind
30.04.	12:51 – 15:47	OBF-OBF	Test flight	2- μ m DWL data of the test flight is also available (see e.g. presentation by O. Reitebuch at PM 2).
11.05.	08:12 - 10:46	OBF-PIK	Transfer 1	



	12:29 - 14:49	PIK-KEF	Transfer 2	
13.05.	10:56 - 13:39	KEF-KEF	TDS-1 underpass	
15.05.	16:02 - 20:11	KEF-KEF	Jet Stream	
16.05.	13:54 - 17:19	KEF-SFJ	Ice Calibration	
	18:12 - 21:12	SFJ-KEF	Ice Calibration	
19.05.	11:58 - 15:54	KEF-KEF	Greenland Tip Jet Aeolus Track	



21.05.	22:28 - 02:25	KEF-KEF	Greenland Summit	
23.05.	16:54 - 21:09	KEF-KEF	Sea ice calibration	
25.05.	14:04 - 17:20	KEF-KEF	Jet Stream	
28.05.	10:23 - 13:24	KEF-KEF	ASCAT underpass Aeolus Track	
29.05.	10:08 - 12:39	KEF-PIK	Transfer 1	
	13:54 - 15:54	PIK-OBF	Transfer 2	

6.4 Discussion of results

In order to demonstrate the quality and the usefulness of 2- μm DWL wind measurements for both A2D and weather model comparison and validation, a few exemplary cases are discussed in the following. The objectives of the flights on May 15 and 25, 2015 were mainly related to campaign Objective #3 (Table 4-1) and to objective #4c and #4d for the flight on May 21, 2015.

6.4.1 15 May 2015 – Cyclone/Jet stream flight

On 15 May 2015, a pronounced low-pressure system was located south-west of Iceland leading to a jet stream with wind speeds of up to 80 m/s blowing between Iceland and Scotland with south-westerly directions. The associated strong wind gradients and the wide wind speed range provided ideal conditions for a measurement flight in order to validate the A2D performance over a wide wind speed range. Furthermore, such a synoptic situation is an interesting case in order to validate the ECMWF forecast skill for strong jet-stream winds.

The ECMWF forecast of the geopotential height (m) and the horizontal wind (m/s) at 300 hPa for 15 May 2015, 18:00 UTC are shown in Figure 6.3 (left). Additionally, MSG SEVIRI HRV image from 15 May 2015, 18:00 UTC is shown in Figure 6.3 (right).

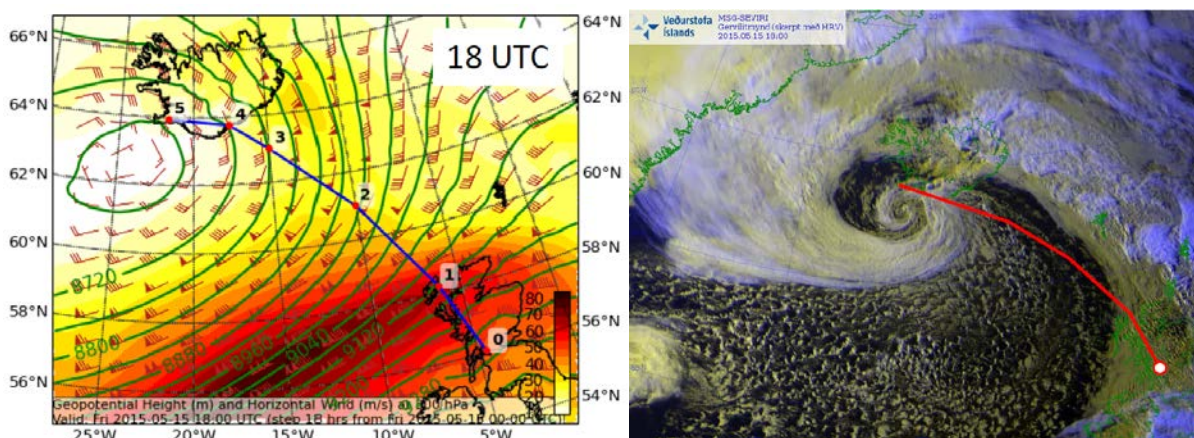


Figure 6.3: (left): ECMWF forecast of geopotential height (m) and horizontal wind (m/s) at 300 hPa for Friday 15 May 2015, 18:00 UTC. (right): MSG Seviri HRV image from 15 May 2015, 18:00 UTC (produced by the Icelandic Met Service).

As both lidar instruments cannot penetrate opaque clouds, it was planned to fly eastwards from Keflavik airport and then southwest in order to cross the jet-stream. The turning point above Scotland was set according to the Falcon flight duration limit of about 4 hours. The flown flight track is shown in Figure 6.4.

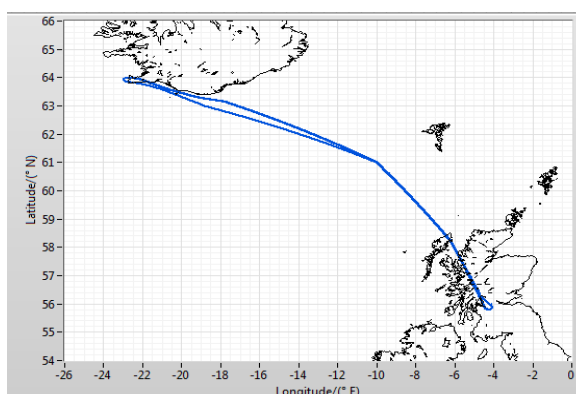


Figure 6.4: Flight track flown on 15 May 2015 from 16:02 to 20:11 UTC.

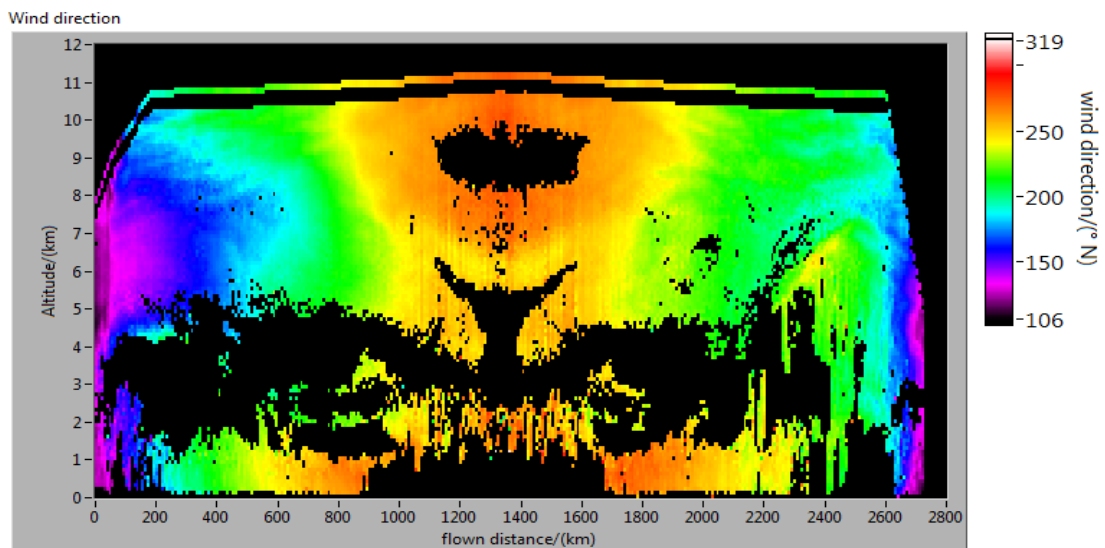
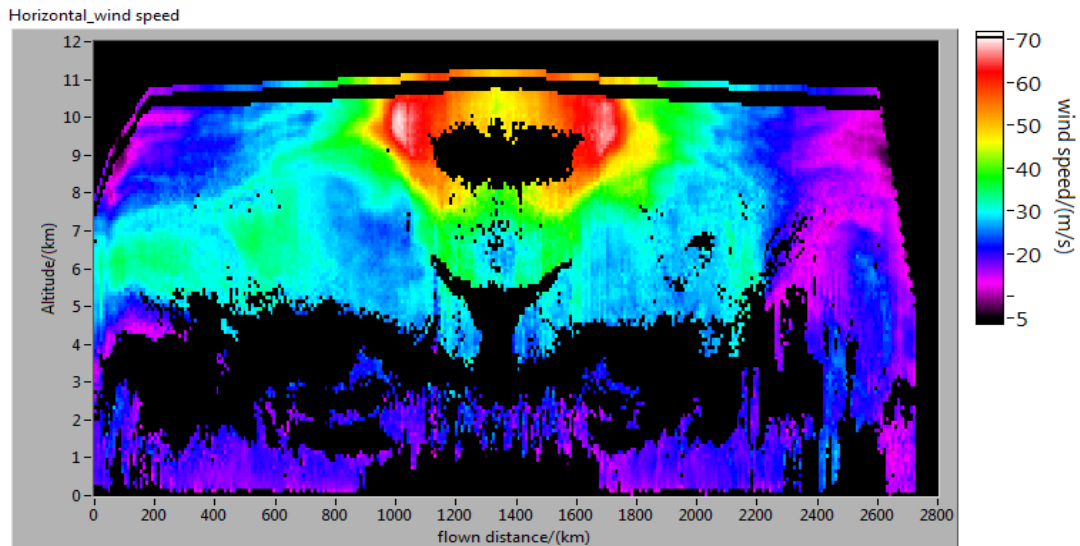
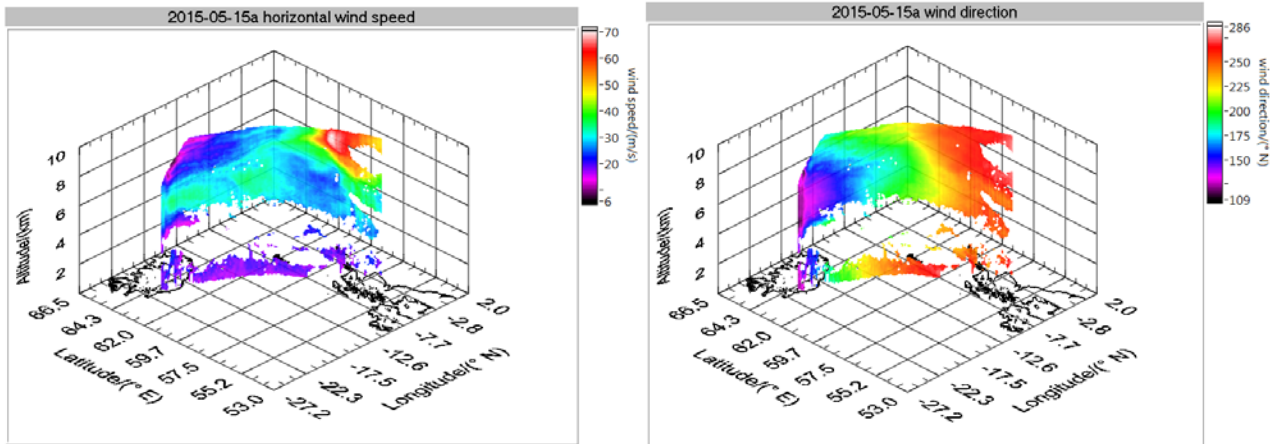


Figure 6.5: Horizontal wind speed (top, left) and wind direction (top, right) on 15 May 2015 in 3-D in order to relate the measurements to the geographical location (only the first half of the flight is visible due to overlapping with the return-leg). Additionally, the entire lidar measurements (outbound flight leg and return flight leg) are displayed in the bottom panels. The wind information measured in-situ by the aircraft is indicated by the coloured line at flight level.

	Document Nr. FR.DLR.WindVal.270717	Issue: V1.1	Date: 27.07.2017	Page: 39/146	
	Doc. Title: WindVal Final Report				

The 2- μm DWL was operated in scanning mode and was working reliably without any failures during the entire flight. Thus, the 3-D wind vector (wind speed and wind direction) is available along the entire flight track as shown in **Figure 6.5**. The top panels show the wind speed (left) and wind direction (right) in 3-D in order to relate the measurements to the geographical location (only the first half of the flight is visible due to overlapping with the return-leg). Additionally, the entire lidar measurements (outbound flight leg and return flight leg) are displayed in the bottom panels.

From the 3-D display it can be seen that the jet-stream was blowing north-west of Scotland as forecasted by the ECMWF model. The highest measured wind speeds reached values above 70 m/s. Also the wind direction was accordingly forecasted. Westward the jet-stream the wind was blowing from east and south whereas it was blowing from south-west in the vicinity of the jet. Thus, from the measured wind direction it can be seen that the flight was performed across the cyclone.

In the bottom panels of **Figure 6.5**, lidar measurements are shown for the entire flight. The turning point above Scotland is at about 1300 km and the entire flight distance was about 2700 km. The thin line between 10.8 km and 11.2 km additionally indicates the in-situ wind measurements performed by the nose-boom 5-hole probe. Comparing the in-situ measurements of wind speed and wind direction with the 2- μm DWL measurements at the range-gate closest to the aircraft it can be seen that they are in great accordance (not quantified in detail). Furthermore it can be seen that the coverage of the measurements is remarkably high (~ 80%) though they are depending on laser light backscattered on aerosols. Only in the vicinity of the jet-stream and above the boundary layer, the air was too clear to derive wind from the lidar data.

In addition to the Falcon in-situ measurements, dropsonde measurements are available from the NASA-DC-8 aircraft flying close to Falcon. First comparisons performed by E. Kendall (L2 progress meeting Nr. 38) show likewise great accordance (see **Figure 6.6**). Slight discrepancies are caused by temporal and spatial differences between lidar and dropsonde measurements.

The 2- μm DWL measurements shown above have recently been used for first scientific case studies. A comparison of the 2- μm DWL wind measurements with ECMWF data showed quite large deviations in the edges of the jet-stream. In particular, the wind speeds were underestimated by up to 9.2 m/s which corresponds to 13.5%. This situation is displayed in **Figure 6.7**, showing the ECMWF wind speed (WSP_{ECMWF}) interpolated to the 2- μm measurement grid, the 2- μm DWL wind speed (WSP_{Lidar}), their difference ($WSP_{ECMWF} - WSP_{Lidar}$) and the normalized difference ($(WSP_{ECMWF} - WSP_{Lidar}) / WSP_{Lidar}$). The figure is taken from the presentation given by A. Schäfler on 22. September 2015 (Auswertung_WindVAL.pptx). For this comparison, the ECMWF data (T1279L137) was downloaded from the Meteorological Archival and Retrieval System (MARS) and spatially interpolated to a 0.15°/0.15° grid by means of MARS software. After that, the data was bi-linearly interpolated to the lidar profile position from the surrounding grid points. The interpolation in z-direction (altitude) was performed linearly. In addition, the ECMWF model data was temporally interpolated in order to get model data for every hour. Therefore the analysis from 00, 06, 12 and 18 UTC and additionally the short term forecast from 00, and 12 UTC is used. Finally, the model was linearly interpolated to the flight time.

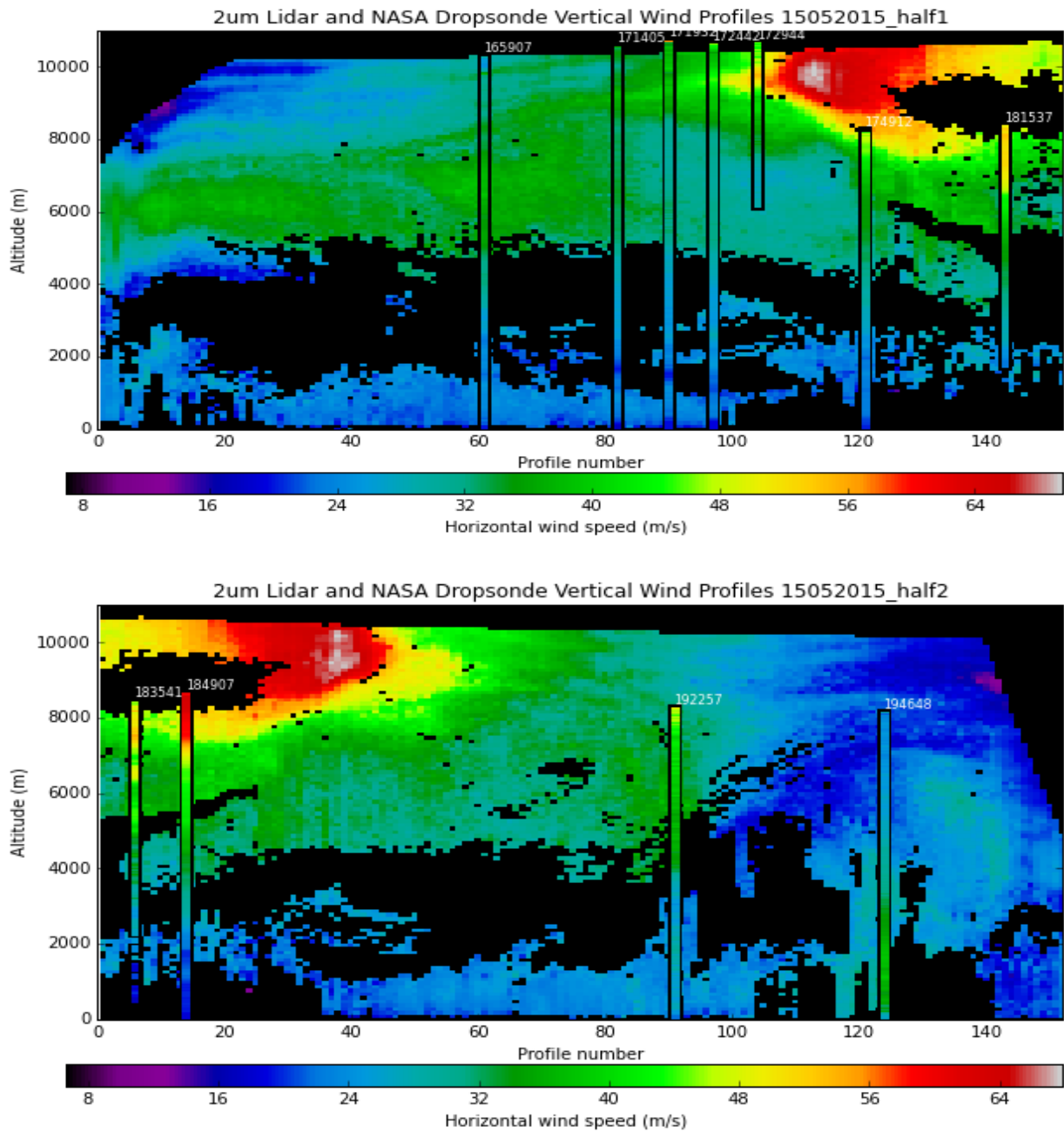


Figure 6.6: 2- μm DWL wind speed measurements of the outbound flight-leg (left) and the return flight-leg (right) as shown in Figure 6.5. Wind speed data available from the NASA-DC-8 aircraft are overlaid. Courtesy E. Kendall (presented at L2 progress meeting Nr. 38).

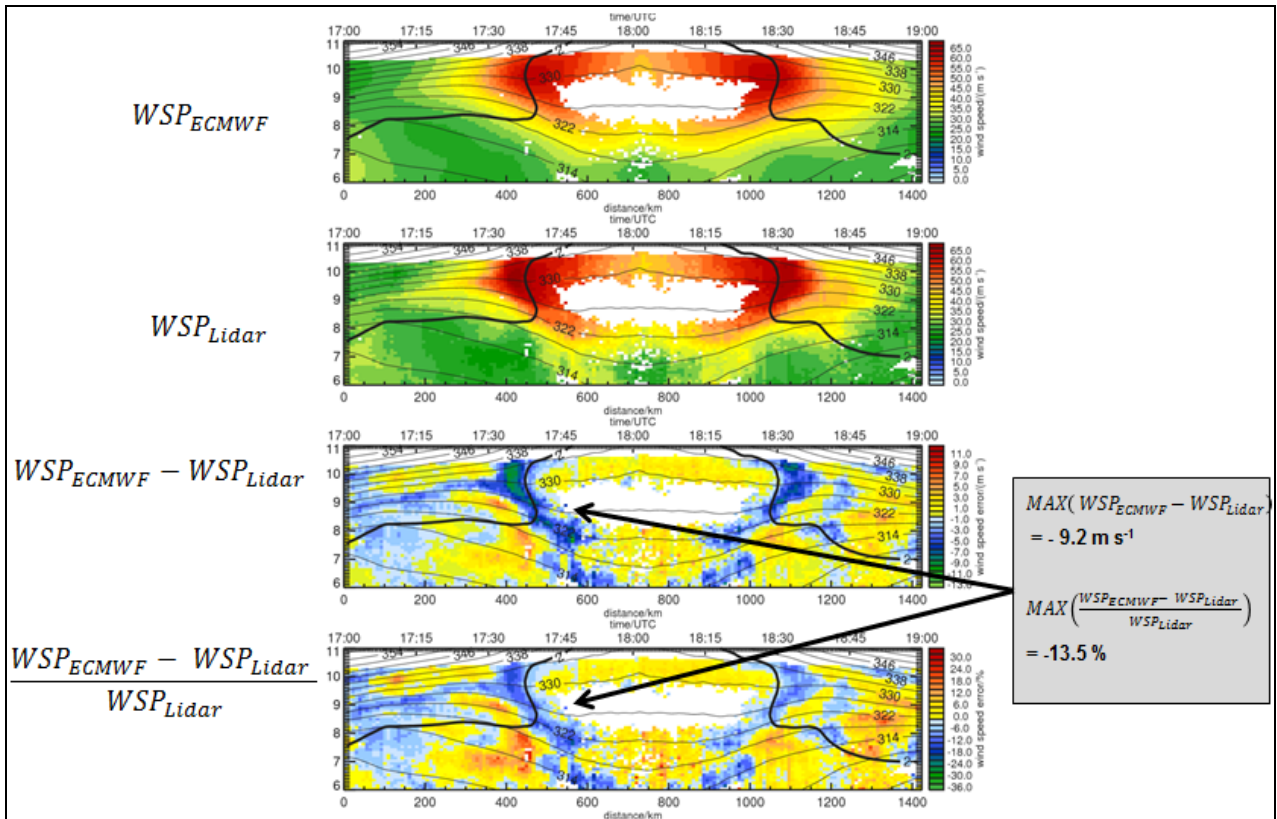


Figure 6.7: Horizontal wind speed from ECMWF (WSP_{ECMWF}) and from the 2- μ m DWL (WSP_{Lidar}) on 15 May 2015. The corresponding differences of both data sets are shown below. The thick black line indicates a potential vorticity of 2 PVU and isentropic lines with equal potential temperature are marked in grey. Courtesy by A. Schäfler.

In order to verify if the interpolation procedures explained above led to these remarkable differences, modified 4D-Var interpolations of ECMWF data have been performed and used for additional comparisons (M. Rennie at L2B/C PM 38) leading to similar results. Thus, these 2- μ m DWL wind measurements are a good example of how important accurate wind measurements are in order to improve numerical weather prediction and that the 2- μ m DWL provides the data needed for that purpose.

Though there is a remarkable representativeness error of ECMWF data at the edge of the jet stream it has to be mentioned that the overall wind field is represented rather well (see Figure 6.7).

6.4.2 21 May 2015 – Greenland – Summit station

Among others, one objective of the WindVal campaign was to perform measurements with the Falcon aircraft in coordination with other aircrafts (NASA DC-8) and ground sites (DLR 2015b). For that reason, on 21 May 2015 a research flight was planned above Summit Station in Greenland (72.58 °N, 38.48 °W, 3216 m asl.). The Greenland Summit Station releases 2 radiosondes per day and is equipped with an aerosol lidar from the MPL (micro-pulse lidar) network (contact Ralf Bennartz, University of Vanderbilt, Wisconsin, Shupe et al. (2013)). In addition to that, the NCAS (National Centre for Atmospheric Science) Atmospheric Measurement Facility (AMF) Doppler Aerosol lidar (Halo Photonics) collected data continuously at Summit, Greenland from May 1, 2015 to June 27, 2015. The instrument operated continuously throughout the period with varying success.

As shown in **Figure 6.10**, the cloud coverage on 21 May, or rather the night between 21 May and 22 May was promising for lidar measurements. The flight path was more or less directly heading from Keflavik to Summit station. Above Summit station, the Falcon aircraft did a few circles in order to gather data available for comparison.

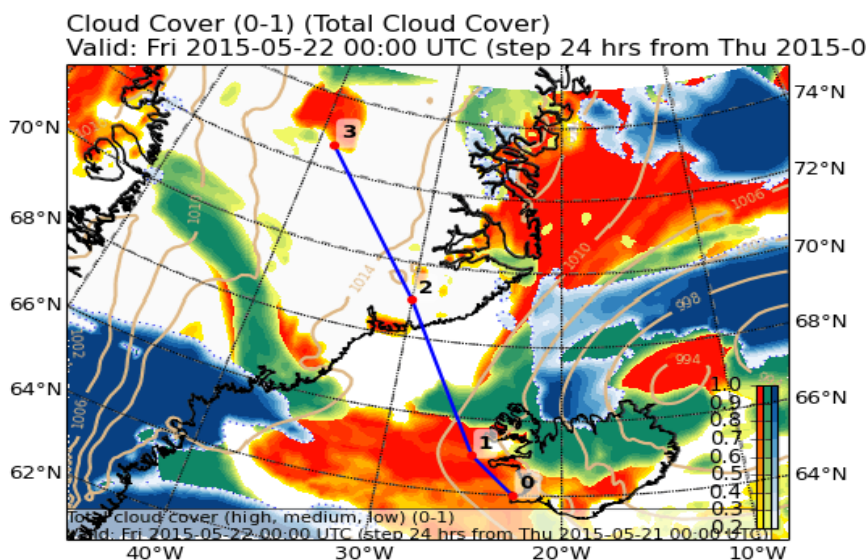
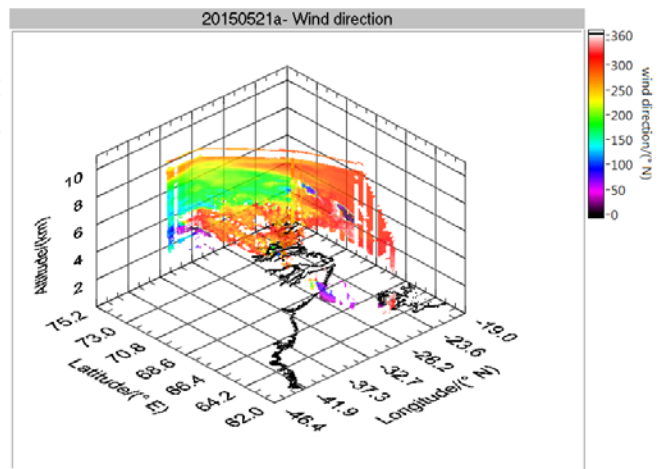
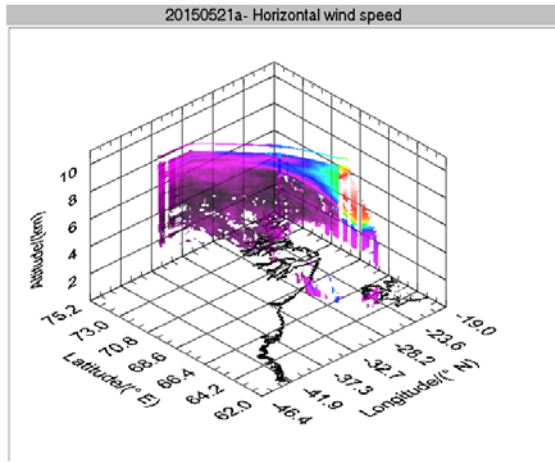


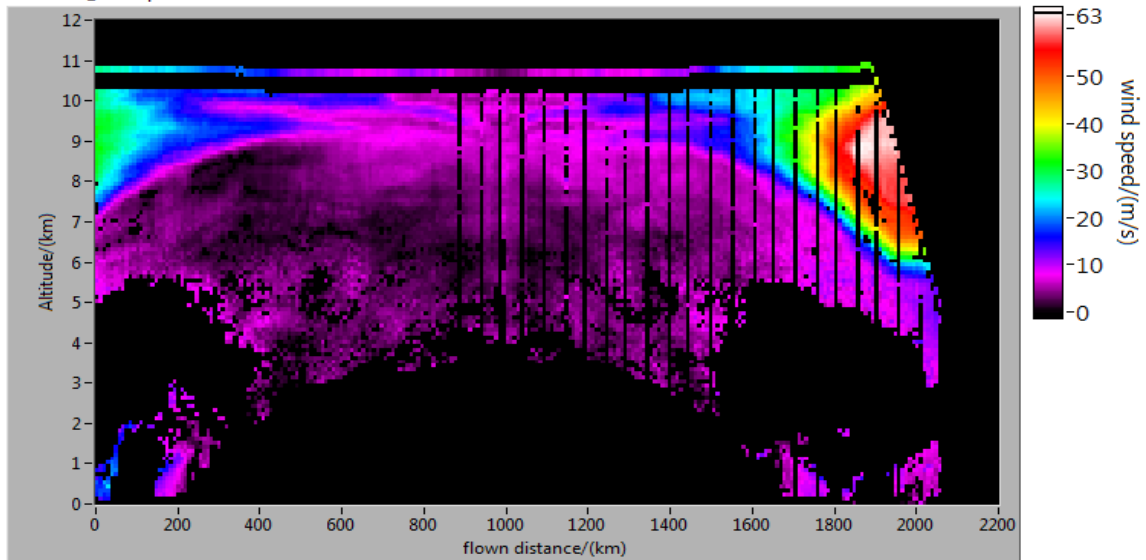
Figure 6.8: ECMWF forecast of total cloud cover for Friday 22 May 2015, 00:00 UTC. Cloud cover goes from 0 to 1 for low-level clouds (yellow, 0; red, 1), mid-level clouds (dark green, 0; light green, 1) and high-level clouds (blue, 0; white, 1).

The 2- μ m DWL wind speed and wind direction data are shown in **Figure 6.9**. The in-situ measured wind speed of the Falcon nose-boom is additionally indicated by the color-coded line at flight level. It can be seen that there was a jet-stream prominent above Iceland with wind speeds up to 63 m/s. Above Greenland itself, the wind speed was rather low between 10 m/s and 15 m/s. However, as can be seen from the wind direction plot in, **Figure 6.9** bottom, there was a directional wind shear above Greenland. The wind was blowing from the north at altitudes of 7 km and above, and was blowing from South between 4 km and 7 km.

It has to be mentioned that the stripes in the lidar data are due to failures in the GPS module mentioned earlier (see also section 6.3). These failures prevented reliable data retrieval for certain VAD scans.



Horizontal_wind speed



Horizontal_wind speed

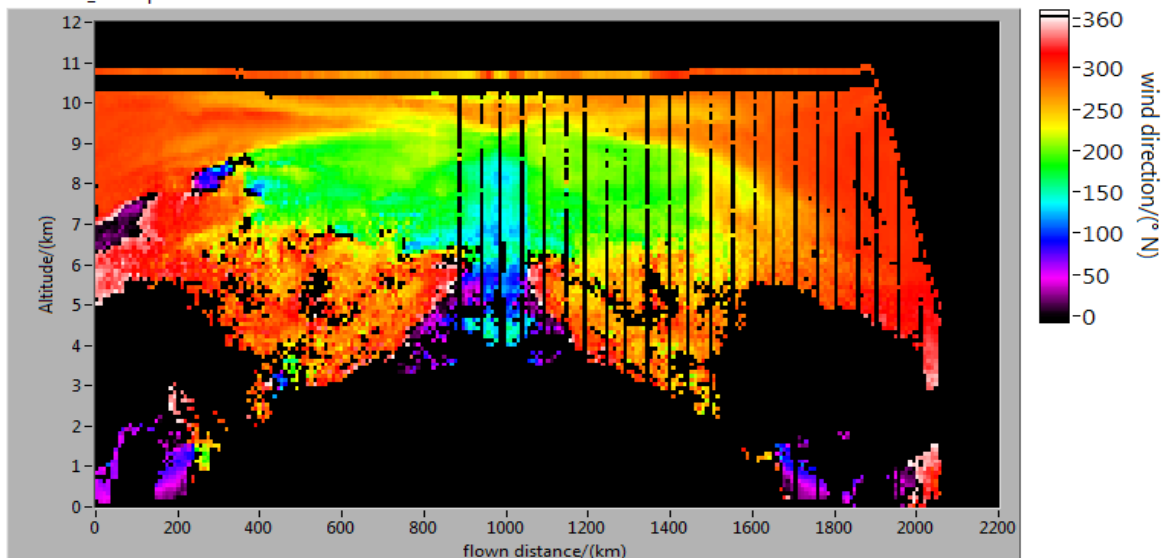


Figure 6.9: Horizontal wind speed (top) and wind direction (bottom) measured with the 2- μ m wind lidar on 21 May 2015 on the way to Summit Station, Greenland. The wind information measured in-situ by the aircraft is indicated by the coloured line at flight level.

6.4.3 25 May 2015 – Jet stream flight

On 25 May, the jet-stream was again getting close to Iceland providing good conditions for measurements in heterogeneous scenes with strong wind shear. As can be seen from the total cloud cover forecast (**Figure 6.10**, bottom), the flight track was planned (and conducted) such that high-level clouds were avoided but still crossing the jet-stream two times.

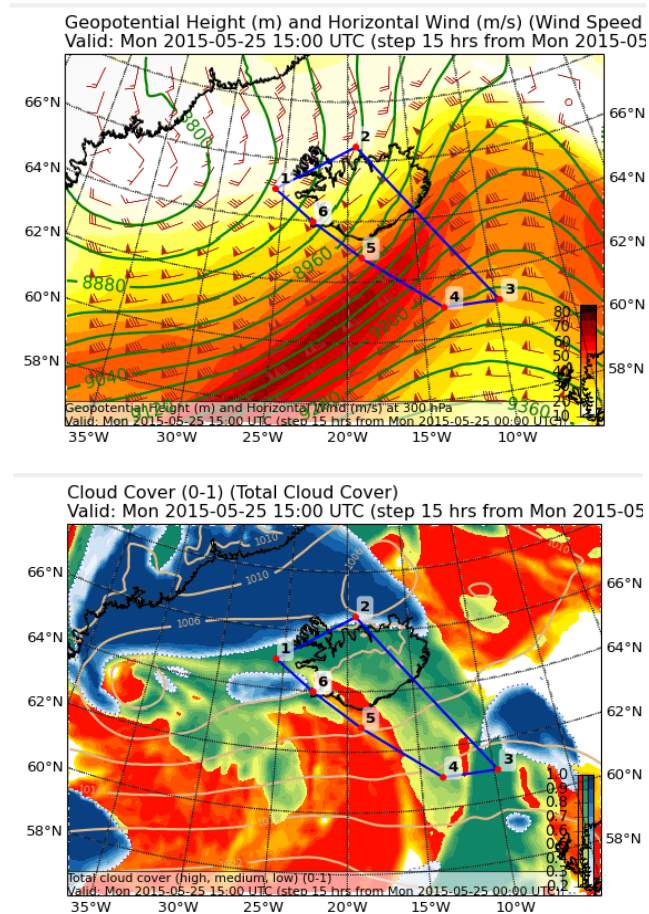
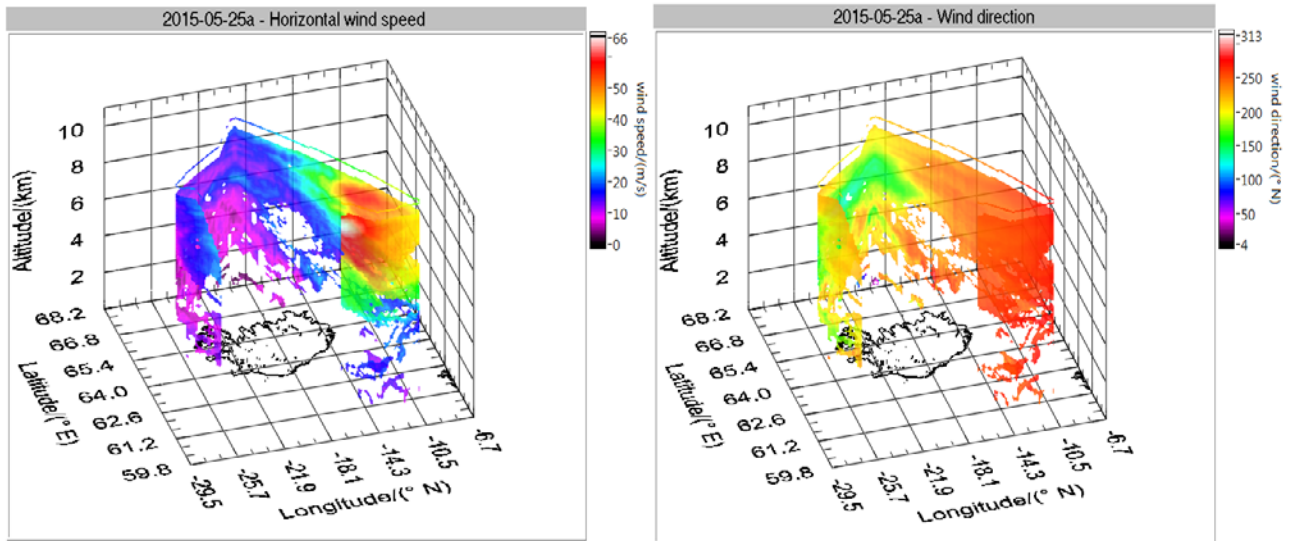
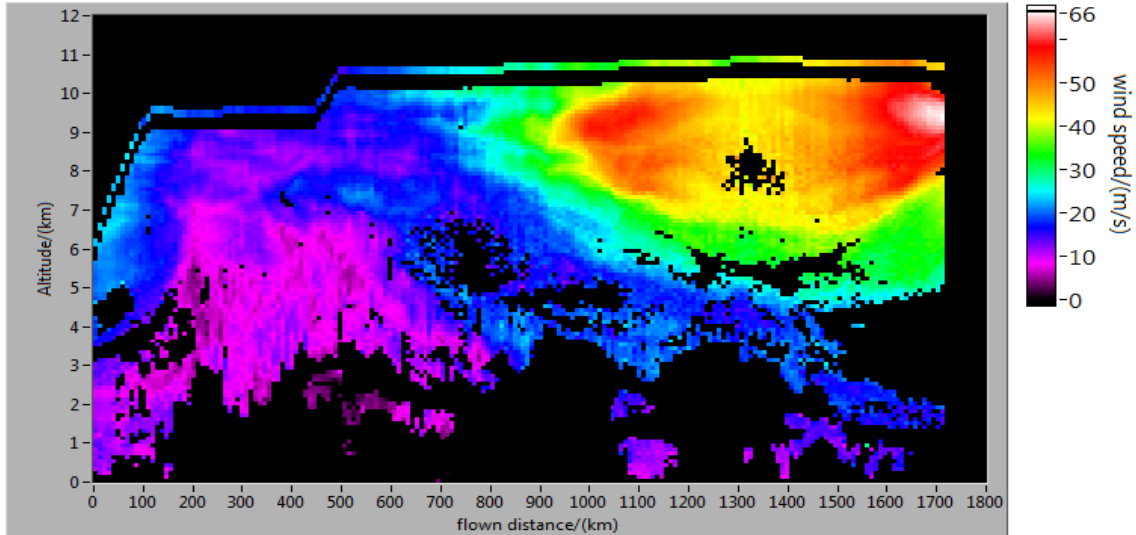


Figure 6.10: ECMWF forecast of geopotential height (m) and horizontal wind (m/s) at 300 hPa (top) and total cloud cover (bottom) for Monday 25 May 2015, 15:00 UTC. Cloud cover goes from 0 to 1 for low-level clouds (yellow, 0; red, 1), mid-level clouds (dark green, 0; light green, 1) and high-level clouds (blue, 0; white, 1).

The corresponding lidar measurements are shown in **Figure 6.11**. As forecasted, the jet-stream was crossed two times west and south of Iceland. The maximum measured wind speeds reached up to 66 m/s. The wind direction was measured to be blowing from south west (as forecasted). Closer to the centre of the Cyclone (above Iceland), the wind was accordingly blowing from the south. Due to a crash of the data acquisition software, no 2- μ m DWL data is available for the last flight segment (see also section 6.3).



Horizontal_wind speed



Horizontal_wind speed

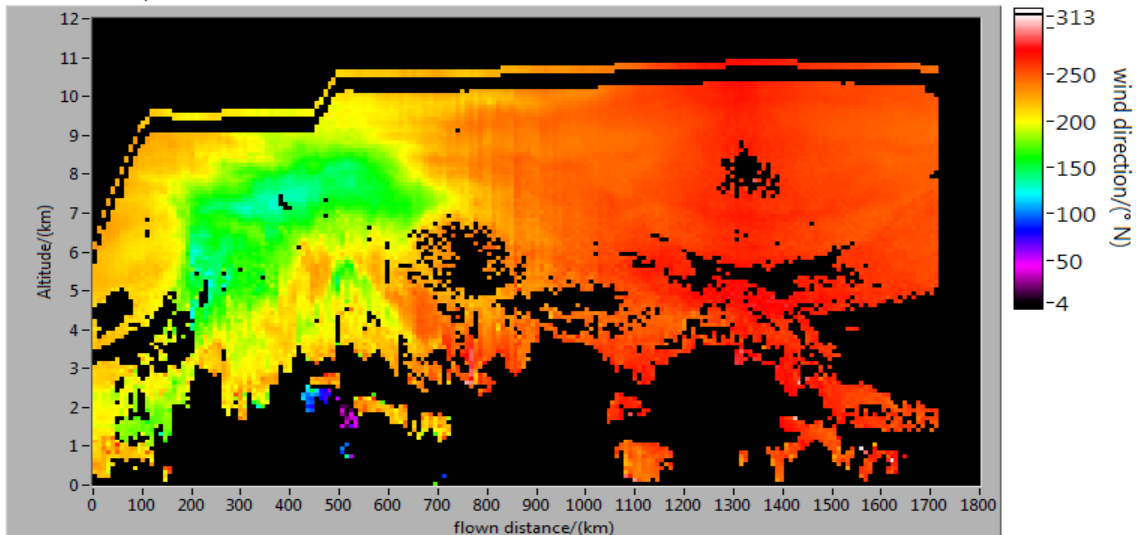


Figure 6.11: Horizontal wind speed (top) and wind direction (bottom) measured with the 2- μ m wind lidar on 25 May 2015.

	Document Nr. FR.DLR.WindVal.270717	Issue: V1.1	Date: 27.07.2017	Page: 46/146	
	Doc. Title: WindVal Final Report				

6.5 Statistical comparison to dropsonde data

During the WindVal Campaign, ten collocated flights of the Falcon and the DC-8 aircraft were performed (May 11, 13, 15, 16, 17, 19, 21, 23, 24, 25). As the DC-8 launched dropsondes from Yankee Environmental Systems during these flights, dropsonde data of horizontal wind and direction are available for comparison with the 2- μ m DWL data. Details about the various quantities measured by the dropsondes and the available data product can be found in the data acquisition report (DLR 2016a). The DC-8 aircraft was flying mainly behind the Falcon aircraft with a separation of 1-2 nautical miles (1.8-3.7 km, corresponding to 9-18 s with a ground speed of 200 m/s) during coordinated flight legs. In addition the DC-8 was also dropping sondes on non-coordinated flight legs, which were not used for the comparison.

Before comparing to the lidar data, the dropsonde data was vertically averaged to 100 m as this is the vertical resolution of the lidar measurements. Furthermore, only dropsonde measurements with a temporal difference of less than 3 minutes, and a spatial difference of less than 5 km to the lidar measurements (spatio-temporal difference criteria wrt. release of dropsonde in the aircraft) were used for comparison resulting in a total of 15 sondes (13 May 2017: 11:50:52, 12:28:58, 12:40:48; 15 May 2017: 16:59:53, 17:14:28, 17:20:00, 17:25:05, 17:30:12; 19 May 2017: 13:24:23, 13:36:25, 13:48:06, 13:59:53, 14:11:17; 25 May 2017: 16:22:19, 16:28:38). The collocation requirement was chosen such, that only dropsondes are compared on coordinated flight legs. Another rationale for the collocation requirement is the correspondence of spatial difference and horizontal averaging length for the horizontal wind vector, which is 8.4 km for the 2- μ m DWL (for 200 m/s ground speed).

Single measurements that differ by more than 5 m/s or 25° are identified as gross outliers and are not considered for the statistical comparison. For all measurements ($n = 953$), 15 values and thus 1.5 % are identified as gross outliers. Thus, $n = 938$ measurements are used for the statistical comparison.

The lidar data versus dropsonde data is plotted in **Figure 6.12**. The wind speed for all data points ranges from about 2 m/s to 65 m/s. It is obvious that both data sets are in great accordance over the entire wind speed range. In particular, a line fit to the data set leads to a slope of **1.01** and an intercept of **-0.20 m/s**.

The bias of the 2- μ m DWL wind speed $v_{2\mu}$ and the dropsonde v_{DS} is calculated according to be

$$bias = \frac{1}{n} \sum_{i=1}^n (v_{2\mu_i} - v_{DS_i}) = -0.03 \text{ m/s}$$

The standard deviation σ is calculated to be

$$\sigma = \sqrt{\frac{1}{n-1} \sum_{i=1}^n [(v_{2\mu_i} - v_{DS_i}) - bias]^2} = 1.46 \text{ m/s}$$

Here, the standard deviation is composed of three contributors, namely the random error of 2- μ m DWL measurements, the random error of dropsonde measurements (~ 0.5 m/s) and the representativity error as both measurements are performed in a partly different volume. The representativeness error is difficult to determine for single cases. It's determination was discussed in Weissmann et al. (2005) with an rms-value of 0.5 m/s according to the empirical formula of Frehlich and Sharman (2004).

By comparing the data set in different altitude ranges (0 km to 3 km (red) and 3 km to 12 km (blue)) it can be seen, that the accordance is slightly better for higher altitudes. In particular, at the lower range (0 km to 3 km), a line fit yields a slope of **0.97** and an intercept of **0.15 m/s**, whereas at higher altitudes (3 km to 12 km), the line fit yields a slope of **1.00** and an intercept of **-0.04 m/s**. The statistical comparison of the derived wind direction (not shown) leads to a standard deviation of **5.2°** and a bias of **0.3°** and thus additionally confirms the reliable wind measurements of the 2- μ m DWL and the dropsondes, respectively.

It is worth mentioning that similar comparisons to dropsonde measurements have been performed for previous campaigns. For instance during the A-TREC campaign (Weissmann et al., 2005), Väisälä RD93 dropsondes were launched from the Falcon aircraft. Altogether $n = 740$ measurement points could be used for comparison leading to a wind speed and wind direction bias of **0.00 m/s** and a standard deviation of **1.2 m/s (3.6°)**, respectively (inversion algorithm). During the SALTRACE campaign (June/July 2013, Barbados), a set of 34 Väisälä RD93 dropsondes, operated in conjunction with the NCAR AVAPS system were launched from the Falcon aircraft. 2- μ m DWL profiles with 1 min. time difference to the dropsonde were used for comparison while the dropsonde measurements were vertically averaged to match the DWL vertical

resolution. Altogether, $n = 1329$ measurement points could be used for comparison leading to a wind speed and direction bias of **0.08 m/s (0.5°)** and a standard deviation of **0.92 m/s (10°)** (Chouza et al. (2016a)).

Thus, the bias values smaller than **0.1 m/s** are comparable for all three data sets and demonstrate the reliability of 2- μm DWL measurements. The same is true for the standard deviation which is lower than 1.5 m/s for all three data sets. The highest standard deviation of 1.46 m/s was obtained for the WindVal campaign. One reason for that might be the different dropsondes (Yankees) used in that campaign compared to the previous ones (Väisälä RD93). However, also different thresholds for the comparisons or different synoptical situations could explain the small differences in the derived standard deviation.

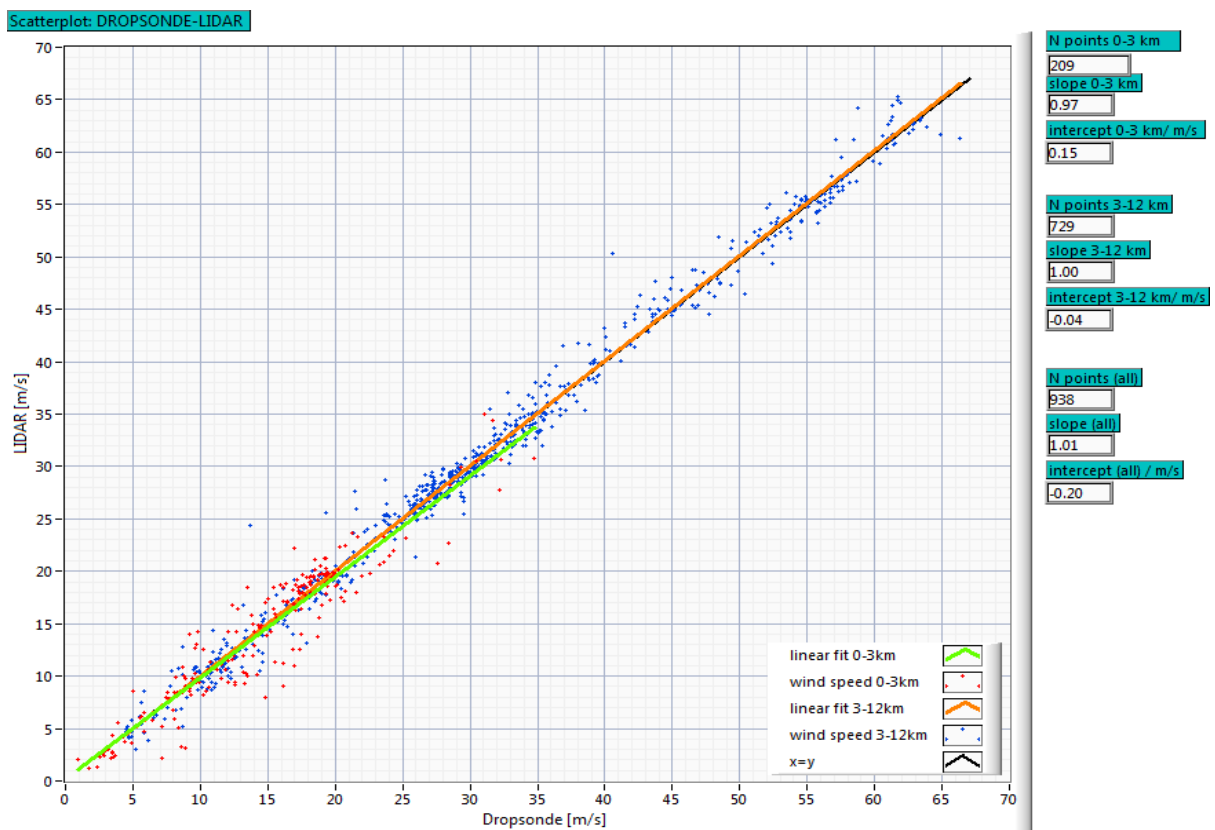


Figure 6.12: Horizontal wind speed from lidar measurements versus horizontal wind speed measured by dropsondes for different altitude ranges (0 km to 3 km, 3 km to 12 km).

6.6 Summary

DLR's 2- μm DWL is introduced and shown to be a reference system for ADM-Aeolus calibration and validation activities. The instrument and the retrieval procedures are discussed and the systematic and statistical uncertainties of 2- μm DWL measurements are determined. In particular it is shown that the bias of single LOS measurements is less than 0.05 m/s and the corresponding standard deviation is about 0.2 m/s (section 6.2.1). Based on earlier campaigns, the standard deviation for the horizontal wind speed measurements compared to dropsonde measurements was determined to be (0.0 ± 1.2) m/s (2003) and (0.08 ± 0.92) m/s (2013) - (section 6.2.2). Thus, the actual uncertainty of 2- μm DWL measurements is smaller than these values and can be estimated to be in the order of 1 m/s.

A statistical comparison of 2- μm DWL data to wind speed measured by the NASA DC-8 dropsondes yields a standard deviation of 1.46 m/s and a bias of -0.03 m/s. The corresponding values for the wind direction are 5.2° and 0.3°, respectively. This comparison further accentuates the reliability of 2- μm DWL measurements.

	Document Nr. FR.DLR.WindVal.270717	Issue: V1.1	Date: 27.07.2017	Page: 48/146	
	Doc. Title: WindVal Final Report				

In addition to that, the system performance during the WindVal campaign 2015 is illustrated. It is shown that the system worked without any remarkable failures. At two flights on 19 May 2015 and 21 May 2015, data gaps in the GPS module data prevented reliable data retrieval for a few VAD scans and thus led to a few data gaps and on 25 May, the data lidar data acquisition software crashed on thus, 2- μ m DWL wind data is not available for the end of the flight.

Though the 2- μ m DWL is based on coherent detection and thus depending on light backscattered on aerosols, the data coverage during the WindVal campaign was remarkably high (60% - 80%). This is due to the fact that the flights were planned in areas with little opaque cloud coverage but a high relative humidity (60% - 80%) whenever this was possible. This helped to increase the 2- μ m DWL coverage and should be performed similarly for following cal/val campaigns.

The usefulness and relevance of 2- μ m DWL data for ADM-Aeolus validation is additionally demonstrated by means of 3 research flights. A first scientific case study shows that the ECMWF underestimates the wind speed in the edges of the jet-stream of up to 13.5 %.

	Document Nr. FR.DLR.WindVal.270717	Issue: V1.1	Date: 27.07.2017	Page: 49/146	
	Doc. Title: WindVal Final Report				

7 A2D operation and performance

7.1 Introduction

This chapter summarizes the A2D technical and operational issues related to the WindVal campaign in 2015. An overview of applied modifications and system performance results before the campaign will be given, followed by a description of the operational procedures and constraints during the campaign. The performance will be discussed for all the flights.

7.2 Description of main A2D modifications and performance assessment before the campaign

As preparation for the campaign the electro optic modulator (EOM) inside the A2D front optics (AFRO) was replaced and re-aligned after greyed crystals had been observed within the receiver optics examination of the A2D noise study. On the laser side a complete realignment of the infrared (IR) and ultraviolet (UV) chain was performed. The third harmonic generation crystal and a dichroic mirror were replaced because of damaged coatings. Two Shack-Hartmann wavefront sensors were procured to allow alignment optimisation w.r.t. beam parameters in the IR and UV path. The comparison to the beam parameter measurements according to the caustic method of ISO 11146 showed a good agreement within 10% for the achieved M^2 beam quality and divergence results in the UV. With the caustic method full divergence angles were measured to be 75 μrad and 68 μrad (4σ , 86.5% enc. energy) for x and y with respective M^2 of 1.5 and 1.4 at 58 mJ pulse energy. All these activities were performed in a laser laboratory at DLR under a laminar flow-box.

The growing demands for airworthiness certification in the recent years were the major driver for necessary A2D modifications. The main activities in this context were.

- Integration of a laser cockpit – switch
- New cooling concept for laser and receiver optical bench assembly (OBA)
- Re-built with focus on high integration of some electronics to meet volume constraints
- Re-arrangement of electronic components within the hardware racks including partly new harness
- EMC test of new electronics
- Update of mechanical, electrical and eye-safety airworthiness documentation and re – certification of the A2D for the DLR-Falcon

For eye safety reasons a cockpit – switch had to be implemented giving the pilots the ability to turn off the laser emission in case of approaching aircraft and at altitudes below 5 km. The formally used heat sink for the laser cooler was not certified any more. Instead of a recertification it was decided to replace both heatsink and cooler by the new laser cooler for the A2D2G laser system of the 2nd generation currently under development. This is a liquid to air cooler using the cabin air as a heat sink. To leave margin within the operational temperature range inside the cabin the laser temperature was raised by two degrees to 18 °C. This in turn required a delta alignment and parameter adaptation on the laser system as well as a check of the spectral overlap between reference and power laser. Also the OBA was integrated in the liquid cooling loop after the laser and thus its thermalisation had to be tested. A new wavemeter (WM, HighFinesse WSU-2) has been procured and integrated in the airborne system layout. A test in the DLR pressure chamber confirmed the high accuracy in the UV and the reliable performance of the new wavelength correction based on an internal pressure and temperature sensor within the airborne operational range. As a back-up a HeNe – laser is integrated in the A2D and used as a calibration reference for the WM. It demonstrated no pressure dependency in output frequency within the accuracy of the WM during the tests in the pressure chamber. The achieved WM signal levels in flight allowed acquiring subsequent single pulse measurements. Software adaptations were implemented combining the wavemeter and ambient sensor measurements with the BRC of the receiver for synchronisation.

	Document Nr. FR.DLR.WindVal.270717	Issue: V1.1	Date: 27.07.2017	Page: 50/146	
	Doc. Title: WindVal Final Report				

Before the test flight the system was set-up in the container at DLR, where system tests and the alignment procedure were performed. Also the final inspection for airworthiness was conducted.

After integration into the aircraft ground tests and alignment optimisations of the lidar signal were performed prior to the test flight. For that, the emission path is aligned at low laser energy with the telescope and receiver optical axis as a coarse alignment with the help of a retro-reflector and target positions on the mirrors after the telescope and at the OBA input window. The fine alignment is performed at full power with clear sky atmospheric signal in imaging mode on ground, using a mirror beneath the Falcon lidar window to redirect the lidar path upward as shown in **Figure 7-1** left. With a removed internal reference fiber, an EOM setting that blocks the overlap region and with a laser frequency set to MOUSR fringe position the Rayleigh illuminated telescope image (TIm) for the far field is centered on the Mie ACCD. The center of gravity (COG) locking coordinates for the co-alignment loop are adapted such that the emission direction is steered to get an even illumination across the TIm aperture. This state is maintained while scanning the angles of the two mirrors in front of the OBA window for signal strength and Rayleigh spot position optimization. A typical signal scene of this alignment step is shown in **Figure 7-1** right. A final alignment is performed in lidar mode at cross-point frequency, finding the co-alignment coordinates for the strongest signal with balanced Rayleigh channel ratios along the far field range-gates. IRCs in lidar mode for different COG positions help selecting the preferred COG position for nominal operation based on the least gradient in the intercept profile outside the overlap region.

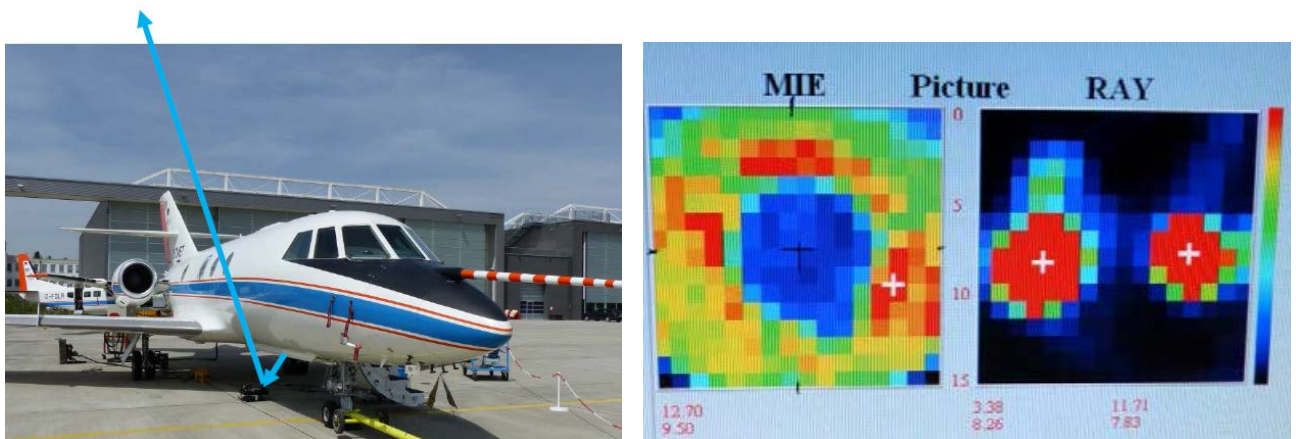


Figure 7-1: (left) DLR Falcon on the DLR apron during alignment and ground measurements. (right) Imaging mode Mie and Rayleigh signals at MOUSR frequency from atmospheric return.

The IRC results and the information gained from the pressure test with the A2D in 2008 allow calculating receiver temperature settings for optimized co-registration of Mie and Rayleigh spectrometer in the flight cabin pressure environment.

A test flight dedicated to system checks on April 30th 2015 showed good performance as summarized in (DLR 2015a) and (DLR 2012b). The main points of verification were:

- Performance of the system cooling equipment
- Laser performance in frequency stability and output power
- Performance of the re-worked receiver acquisition trigger electronics
- Receiver temperature settings for spectral co-registration in flight
- Transmit-receive path alignment
- Laser eye safety operation procedures
- Performance of auxiliary equipment (ambient data recording, wavemeter and heterodyne unit)
- Operational procedures

	Document Nr. FR.DLR.WindVal.270717	Issue: V1.1	Date: 27.07.2017	Page: 51/146	
	Doc. Title: WindVal Final Report				

During this flight the data acquisition of the 2- μ m lidar was partly used for a relative IR pulse-to-pulse frequency stability measurement of the heterodyne unit (HU). Comparison with simultaneously recorded wavemeter UV - data demonstrated its high accuracy with a frequency stability measurement over 700 shots resulting in a std. dev. of 3.4 MHz, whereas the heterodyne measurement provided 1.2 MHz, i.e. 3.6 MHz converted to UV. Thus the continuously recording WM gives the opportunity to monitor the laser based frequency drift and correct their influence on the receiver data on measurement level.

Also all other points of verification were successfully tested and the A2D could be declared fit for campaign operation.

7.3 Operational procedures and constraints

As the A2D is installed in the Falcon together with the 2- μ m DWL, only one operator seat is available for each system. For acceleration of procedures and flexibility in case of operational difficulties usually the two scientific crew members are trained in both lidar systems. **Figure 7-2** gives an impression of the cabin with the installed equipment.



Figure 7-2: The Falcon cabin with A2D and 2- μ m Doppler wind lidars installed.

During a normal flight day the system is switched on 2.5 h – 3 h prior to take-off for system checks and thermalisation of the spectrometers. This is first to have time for solving possible problems and second to accelerate the time to reach working temperature after take-off. Also the number of pulses (P) accumulated per measurement (usually P=20) and the range-gate settings are prepared optimized for the mission and altitude profile of the flight. For further details regarding the A2D system layout and user settings please refer to (DLR 2010).

Usually 1 h before take-off the system is switched off and the Falcon leaves the hangar for refuelling. The available time during these preparation activities is too short and another switch-on for thermalisation is only performed in case of a delayed departure.

The inflight start-up procedure for the A2D is as follows:

- Switch-on of system shortly after take-off
- Computer time synchronization with GPS
- Start temperature stabilization of spectrometers
- Laser pump-diodes on, if water-cooling is o.k.
- Reference laser head (RLH) on and frequency-lock
- Laser power measurement
- WM on, WM calibration and start recording
- Start acquisition and laser house-keeping data-link
- Open Falcon lidar window and receiver
- Laser beam steering and start of co-alignment loop, after optimizing contrast and averaging settings
- Frequency tuning to Rayleigh spectrometer (RSP) cross-point and Mie spectrometer (MSP) center
- Switch to RSP thermal fine control



Figure 7-3: Falcon during take-off at Keflavik airport

The **thermalisation** time of the spectrometers allows wind measurements to start around 45 min. after take-off. This time is already minimized by switching to the slower thermal fine control of the RSP after the set temperature is reached as shown in **Figure 7-4** at 9:00 UTC (take-off during this first transfer flight to Glasgow-Prestwick on May 11th, 2015 was 8:12 UTC). As a result of the A2D noise study, the fine control was implemented to eliminate the temperature control influence on the RSP measurement.

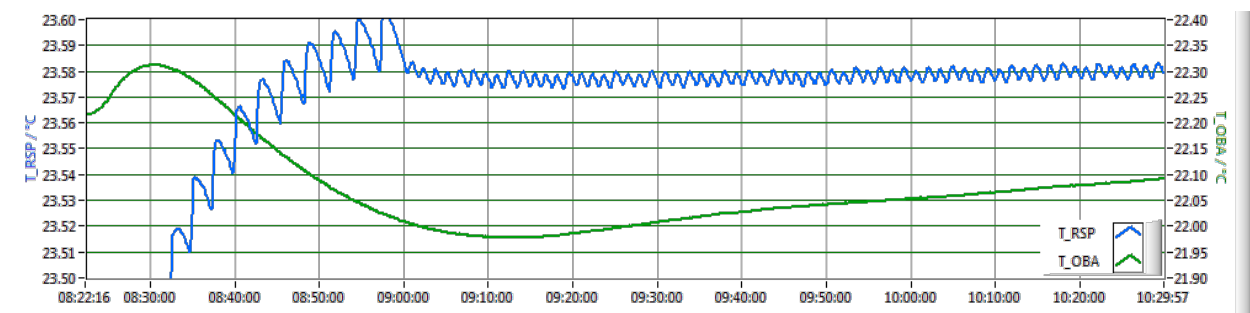


Figure 7-4: Temperature of Mie spectrometer (T_OBA) and Rayleigh spectrometer over time (UTC) during flight.

As also the **cabin pressure** influences both spectrometers and the laser, it is kept constant at the minimum to avoid pressure changes by the aircraft air conditioning system. The pressure then depends on the flight level (FL) and is at 780 hPa in FL 360 (36000 ft above MSL). To allow post processing corrections and for data quality control sensors in the cabin record temperatures, pressure and humidity synchronized with the wind measurements. A typical example of pressure and temperature data from a flight on May 29th is shown in **Figure 7-5** and proves the high pressure stability to within 0.5 hPa.

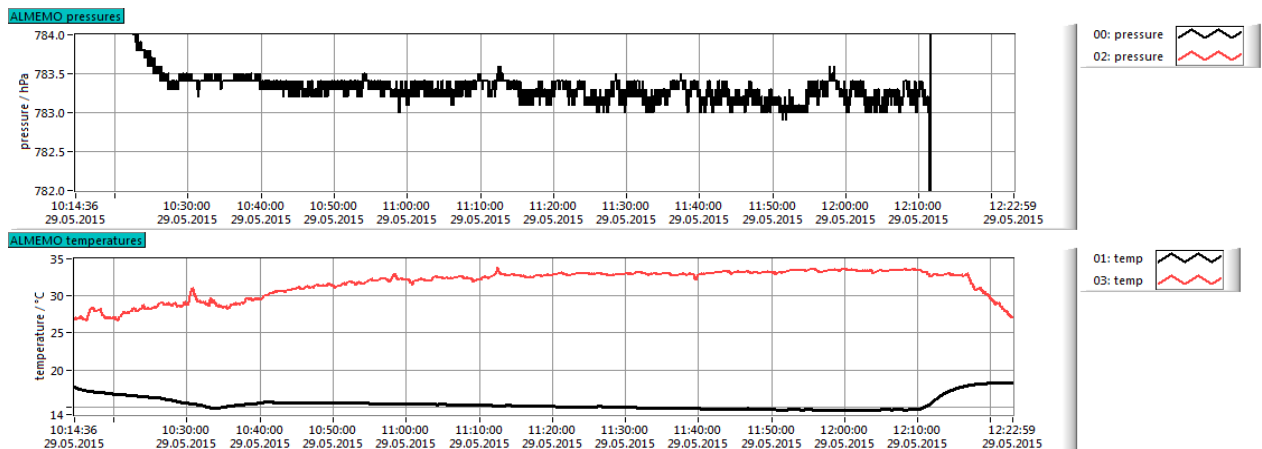


Figure 7-5: Temperature and pressure recording inside the Falcon cabin during a flight of May 29th, 2015 (Time in UTC). The red temperature follows the liquid-to-air cooler fan outlet and the black is installed on the lower optical bench close to the laser and the lidar window.

The **co-alignment loop** is based on the image of the UV-camera which is a sample of the column integrated return signal forming a spot on the sensors and is acquired with 4 Hz. Consequently 4 COG values are calculated per second and recorded as housekeeping data. The user sets the low and high intensity limits as contrast range for the UV-camera and consequently for the COG algorithm and the averaging for the co-alignment control. This is done such that the lower limit is well above the electronic and optic noise floor (e.g. multiple scattering in presence of clouds close below the aircraft) and the control is based on the difference between the reference position (determined by the A2D alignment procedure) and an average of 16 COG coordinates acquired within 4 s. The response time of this loop thus allows compensating slow variations as introduced by thermally induced drifts of the emission or reception path mirrors. However, in case clouds especially cirrus clouds are very close below the aircraft, or in case the Falcon is flying in clouds, the multiple scattering returns lead to a blurred spot inappropriate for a reliable COG determination. The co-alignment loop is then temporarily switched off manually to avoid its diverging from the reference position and the wind measurements are unreliable even if there is lidar return from below the clouds.

For performing wind measurements, the **laser frequency setting** is chosen at the RSP crosspoint. Based on the optimized temperature setting for flight, at this frequency also the Mie fringe is centered within the USR such that pixels 7 and 8 are equal in intensity for the internal reference (7=8 frequency setting). Lidar mode signals of this nominal setting are shown in two visualization options of the online data available in flight in **Figure 7-6**. The online lidar data is displayed on observation basis (average of measurements), but it is possible to scroll through individual measurements within a selected observation. As the data processing is not part of the A2D operation software suite, wind, aerosol data and time series of backscatter cannot be displayed during flight. However, aerosol layers may be identified in the Mie channel raw data as a fringe signal above the Rayleigh TIm background as shown in **Figure 7-6**.

In order to increase the SNR of the aerosol signal it is necessary to remove the Rayleigh background on the Mie channel forming the range-gate integrated version of the TIm as shown in **Figure 7-1** (right). Therefore the laser frequency is occasionally set to the **MOUSR** frequency w.r.t. the Fizeau 1 – 3 times per flight, preferably with ground visibility. Because there is a difference in illumination of the field stop between the internal reference signal delivered through a multimode fiber and the free path atmospheric signal, the MOUSR (and 7=8) frequency would be a few MHz different when optimized for the ground return layer. During WindVal 2015 also MOUSR settings were tested for the ground layer (GrOUSR) and for the cloud layer (ClOUSR) in case there was no ground visibility. This approach was tested during WindVal 2015 for the first time, but the MOUSR approach was kept as baseline for processing of most Mie winds, while some flights were processed with GrOUSR (see Table 9-8).

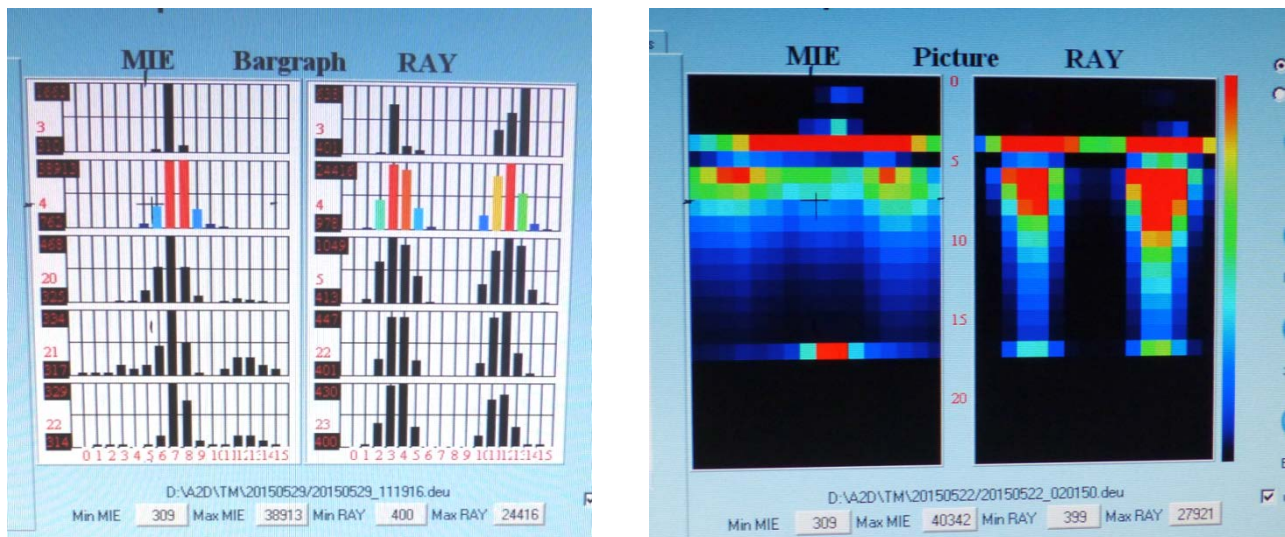


Figure 7-6: A2D raw data of one observation at the Rayleigh cross point frequency setting (7=8 for Mie internal reference pixel intensities) as shown in the online display. (left) Mie and Rayleigh data for selected layers (layer 4 shows the internal reference signal) and for the range-gate overview (right). More distant range-gates are towards the lower part with the ground signal falling into range-gate 17 for the case on the right side.

During WindVal 2015, several instrument **calibrations** were performed in flight. For doing that the aircraft is rolled to the right by 20° to point the A2D in nadir thus minimizing wind speed influence on the LOS. While flying circles an instrument response calibration (IRC) is performed in 25 min. The wind at FL lets the circling aircraft drift along as visible in the calibration regions of the flight paths from May 16th and May 23rd. The different frequency settings and the frequency steps of the calibration ramp are clearly visible in the wavemeter recording example shown in **Figure 7-8**

At stable frequency settings as well as during calibration ramps, every few minutes there are spikes visible. They originate from a reset of the ramp-fire laser cavity control electronics. This occurs whenever the slow cavity length drift compensation reaches the travel limit of the piezo. The reset causes an absolute frequency jump associated with the non-linearity of the piezo ramp. This happens around every five minutes shortly after turning on the laser and only once or twice per hour when the laser is thermalised. There are no unseeded shots. Jump and following relaxation to the set point are a matter of seconds. As the frequency steps during calibration act like a thermal drift these jumps occur more frequently, but usually during the 4 s inactive time of the acquisition cycle while the frequency step is performed (for the A2D the acquisition is on for 14 s and off for 4 s due to the earlier burst mode operation principle) The residual frequency difference to the commanded frequency is the reason for the various jumps and slope variations visible in Figure 8-8 of section 8.3. As the thermal drift compensation is a common feature for injection seeding cavity control techniques and also a piezo transducer is used for cavity length change in the ALADIN lasers, similar occasional jumps might be observed in orbit, especially during calibration and temperature change situations. At around 16:35 UTC the laser frequency was not stable which could be compensated by increasing the injected seed laser (SL) power. The data gap around 17:00 UTC is due to the WM calibration with the HeNe signal. This is usually performed automatically every 10 min. but was set to manual for not disturbing the data recording during the calibrations.

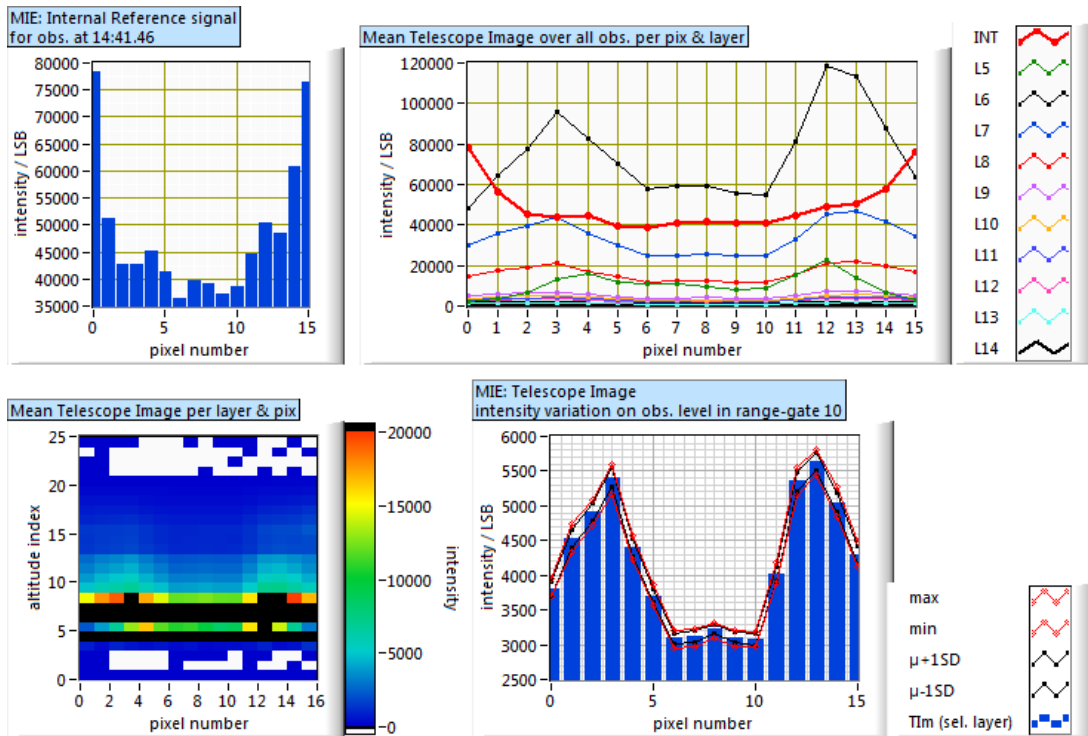


Figure 7-7: Example of the layer averaged TIm acquisition during MOUSR for Rayleigh background correction on the Mie aerosol signal. (Upper left) Internal reference layer, (upper right) intensity profile for different layers, (lower left) corresponding lidar mode display of the Mie channel and (lower right) raw signal and intensity profile for a selected range-gate.

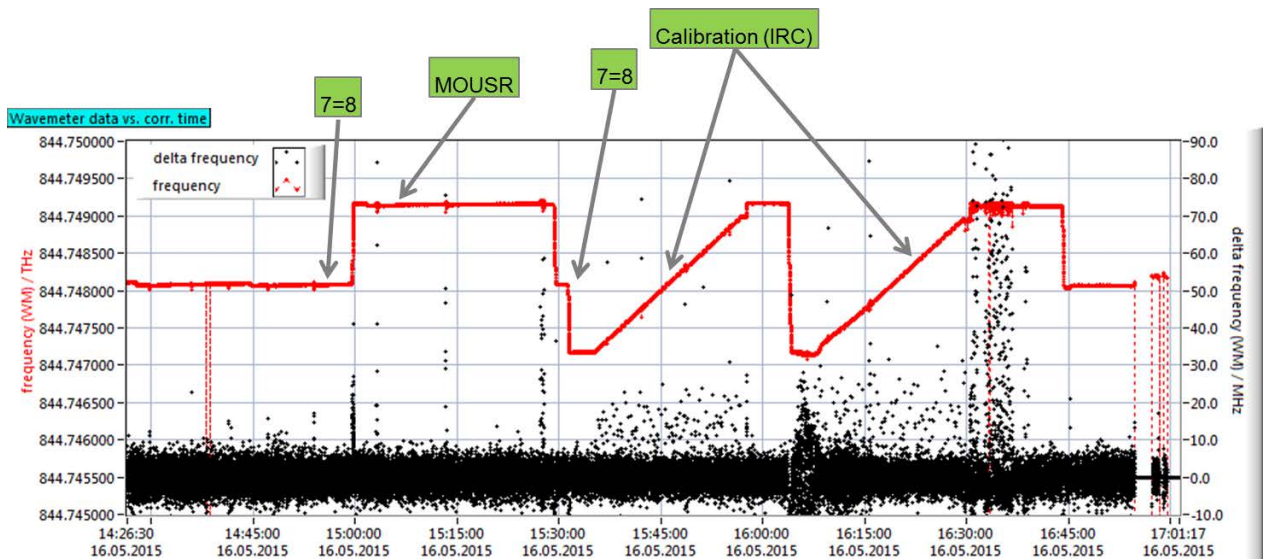


Figure 7-8: Wavemeter frequency recording (red) and subsequent data delta frequency (black) from the calibration flight on May 16th, showing typical frequency settings (Time in UTC).

	Document Nr. FR.DLR.WindVal.270717	Issue: V1.1	Date: 27.07.2017	Page: 56/146	
	Doc. Title: WindVal Final Report				

The signal for the receiver trigger electronics and the associated signals from the laser cavity control input are regularly monitored with a hand-held two channel 200 MHz oscilloscope. The timing of this trigger signal is important for the ranging accuracy and to minimize the range-gate overlap effect, especially for maintaining a pure internal reference signal without atmospheric contribution. The pulse-to-pulse stability of this trigger can't be measured as a statistical result with this oscilloscope, but it is intrinsically connected to the laser frequency stability through the CC ramp-delay-fire scheme. Thus it can be concluded that the timing stability is within requirements as long as the frequency stability monitored with the WM is. Timing fluctuations on a level above a few 100 ns are recognized as changes in the signal strength in the layers next to the internal reference layer 4 and can thus be detected and excluded for analysis by the QC algorithm.

Operational commands and monitoring of the system performance throughout the flight impose a tight action sequence on the crew owed to the complexity of the system. A regular observation of laser frequency, co-alignment loop and lidar data acquisition is necessary for detecting malfunctions quickly and starting mitigation measures on short notice. Given the thermalisation time at begin of the flight and the necessity to change the cabin pressure conditioning when leaving FL for decent leads to a remaining approximately 2.5 h to 3 h measurement time for wind data operation per 4 h flight duration. Although in principle the pilots could switch off the laser emission in case of an closely below approaching aircraft for eye safety reasons, this was not necessary in the low frequented airspaces of operation around Iceland during WindVal 2015 and fortunately didn't lead to significant data gaps during the flights.

7.4 A2D performance overview

Due to various technical or software reasons interruptions of the A2D data stream occurred in almost every flight. However, as fixes or workaround solutions could be quickly executed in most cases by the operators on-board the aircraft, the data base produced for analysis is not limited significantly. Thus, the A2D can only be operated with highly experienced personal on-board the aircraft, which is different for the 2- μ m DWL which only needs a trained person in case of nominal operation (N.B. due to technical problems with the 2- μ m DWL during WindVal II in 2016 also a highly experienced person was needed on-board in 2016). This is also thanks to the recording of auxiliary data with the WM and the ambient sensor suite, because it allows automatic data quality control and selection. An overview of limitations that possibly affect the analysis and comments with performance indication are given in **Table 7-1** for all the flights of WindVal 2015. For example on May 15 the fuse of the reference laser (RL) electronics made a frequency locking of the SL impossible. Consequently also the laser frequency tuning e.g. to the CP could not be commanded. Connecting an unused voltage output, that was formally foreseen for frequency tuning of the RL to the SL tuning input, re-activating the associated software parts and testing the voltage with the oscilloscope, finally allowed to manually tune the voltage to a laser frequency at the CP. As this could be verified thanks to the absolute frequency knowledge from the WM, it took less than half of the flight to identify and solve the issue. The laser power is usually measured at start and at end of the flight, after leaving the measurement FL.

Apart from the mostly short interruptions the overall performance was reliably satisfying and improved compared to the 2009 AC03 campaign results. Up to approximately 16 h A2D measurements are available including special data like imaging mode, and airborne calibrations.

One of the most important parameters affecting the data quality is the **laser frequency stability**. An example of a frequency stability characterization performed during the test flight of April 30th 2015 is shown in **Figure 7-9**, where an absolute UV frequency measurement with the WM (WSU-2) was recorded in parallel to a relative IR frequency stability heterodyne measurement. Focusing on the region between the red lines, an analysis of the standard deviation over 700 shots (representative for one observation period) results in 1.2 MHz for the relative IR frequency stability (measured with the HU) and 2.4 MHz for the frequency stability in the UV (measured with the WM based on 40 ms averages per data point). With the assumption that there are no RL drifts, the UV frequency stability is deduced from the IR stability by applying a factor of 3 giving 3.6 MHz.

	Document Nr. FR.DLR.WindVal.270717	Issue: V1.1	Date: 27.07.2017	Page: 57/146	
	Doc. Title: WindVal Final Report				

Table 7-1: Overview of the system performance limitations and operation for the flights during WindVal 2015.

Flight Date	Mission	A2D operation	Limitations	Comments
May 11 a/b	Transfer to Iceland, refuel in Prestwick	Nominal	a: 5 min interruption from crashed co-alignment loop (COG). Slight icing on lidar window.	Laser 2.8 W at start, 2.6 W before landing for refuel. Automatic reboot problem after refueling.
May 13	TDS-1 underpass	Nominal	Interruptions from jammed acq. during first half of the flight. Higher timing jitter for 2 nd half. WM data gap 5 min.	Detection electronics (DEU) unstable trigger. Original trigger scheme set for 2 nd half. WM-notebook power interruption. Cloudy 2 nd half. Laser 2.9 - 2.7 W.
May 15	Jet-stream flight Scotland	Nominal (Wind measurements available for flight back from Scotland)	2 nd half of the flight needs to be analyzed using WM-frequency measurement. Interruptions from Cavity control (CC) - error and DEU. WM recording interruptions.	Broken fuse of RL stabilization unit. Manual frequency stabilization during second half of the flight using WM-observations
May 16 a/b	Calibration over Greenland ice	Nominal and Imaging 2 Calibrations (IRC) a, 1 IRC b	a: laser frequency instability sporadic during start of 2 nd IRC. b: 10 min missing Laser HK at end	Alignment verification in imaging mode Laser 2.9 W. SL fiber splitter by-passed in Kangerlussuaq. Receiver background 2 min.
May 19	Greenland Tip-Jet/Aeolus-track	Nominal and Imaging	Data gaps in last third of flight back to Iceland due to jammed acq. and in-flight alignment activities	Laser 2.9 W FM4 realignment after hitting it on the way back to Iceland
May 21	Greenland summit	Imaging Nominal, 0° and nominal over summit	Wind data gap first 30 min. due to imaging mode for alignment verification. 3 min. gap (COG jammed)	Laser 2.8 W COG variation alignment checked confirmed original setting
May 23	Sea-ice calibration	Nominal 2 Calibrations (IRC)	Data gap 20 min. on way to sea-ice (CC- and DEU error). 2 min. COG-gap @1 st IRC. Turns start 1.5 min after start of 2 nd IRC.	Laser 2.9 W GrOUSR and ClOUSR tested on way back to Iceland.
May 25	Jet-stream south of Iceland	Nominal	Declined frequency stability (RL-SL locking instability) especially during northern leg. sporadic frequency jumps and slow drifts during rest of flight. 3 min. COG-gap	Laser 2.9 W
May 28	ASCAT underpass/Aeolus-track	Nominal	WM-data gap 4 min. due to software crash. Sporadic turbulence and clouds	Laser 2.7 W
May 29 a/b	Transfer to Oberpfaffenhofen, refuel in Prestwick	Nominal	a: Frequency slow drifts b: Sporadic frequency jumps and slow drifts	Laser 2.9 W

As the WM measurement from the test flight on April 30th, 2015 was based on an average over 40 ms or $n=2$ pulses (due to a drift in the fiber coupling causing signal loss by the end of this flight), the frequency stability from pulse to pulse is deduced by applying the factor $\sqrt{n} = \sqrt{2}$ to the 2.4 MHz, giving a 3.4 MHz result for the WM. This compares well with the heterodyne result and proves that the WSU-2 provides a continuous monitoring with accuracy appropriate for post processing correction. As the HU data acquisition is done with the 2- μ m lidar electronics instead of 2- μ m operation, heterodyne measurements are not possible to be recorded on a regular basis and for long time periods. The standard deviation over 700 shots is monitored constantly with the statistics tool of the WM software during flight. Usually the signals levels allow single-pulse measurements without need for averaging. Observed frequency stabilities are typically around 3.5 MHz which is below the specification of 4 MHz for the A2D (as compared to the 7 MHz for Aeolus). Since the frequency stability is connected to the receiver trigger timing stability provided by the laser CC – electronics as described in section 7.3, the WM monitoring is also a measure for the timing monitoring where the 3.5 MHz frequency stability correspond to 100 ns timing stability (both rms).

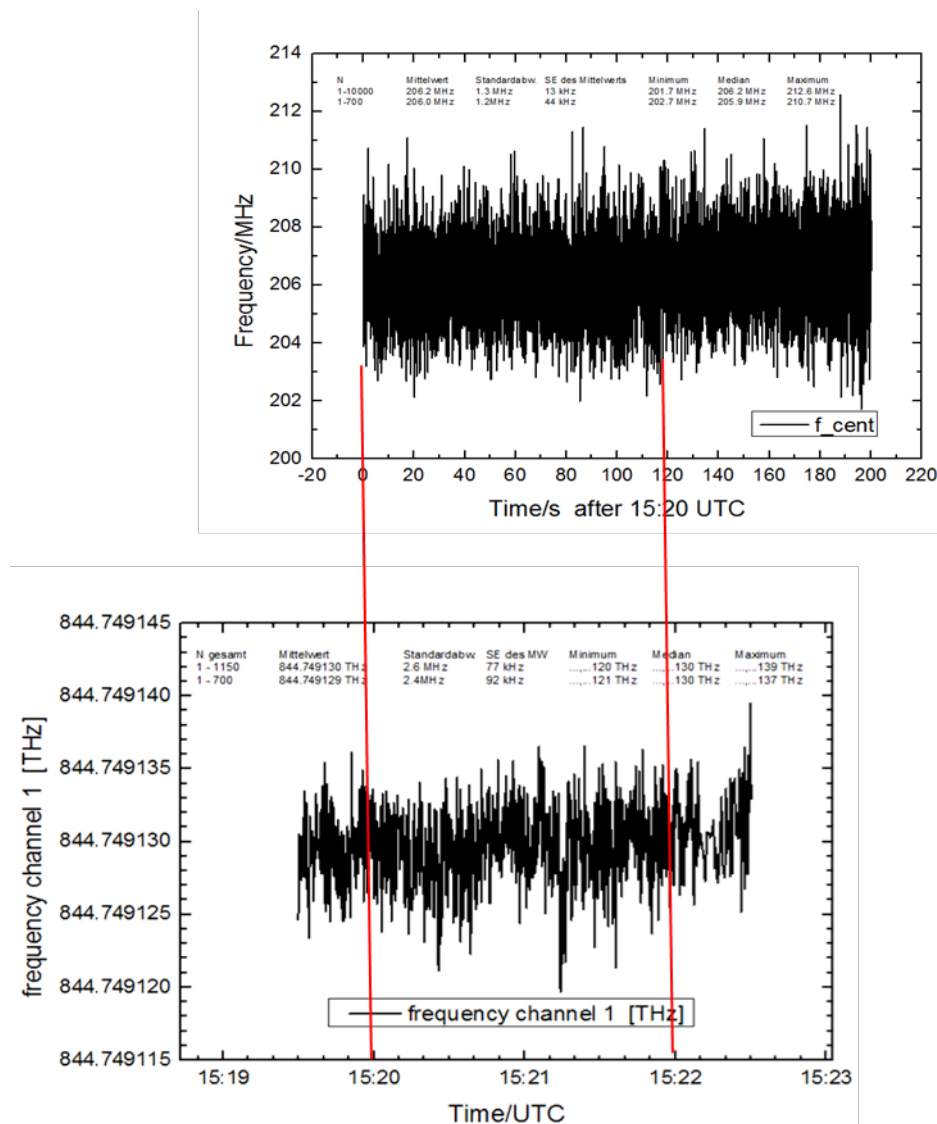


Figure 7-9: Relative IR frequency measurement from the heterodyne unit (top) and parallel WM measurement of the absolute UV frequency (bottom) from the test flight on April 30th, 2015. The time between the red lines was used for a comparing analysis (see text).

Another important parameter for wind data quality is the **alignment stability**. This is managed by the co-alignment control loop by steering the emission path in order to keep the COG of a sample of the received light at the user set reference position on the dedicated UV-camera inside the AFRO. As housekeeping data the COG values are constantly recorded with 4 Hz, but it is also possible to save the raw images of the UV-camera within the user set contrast range. This is done occasionally and processed on ground for a detailed analysis of the signal intensity and as monitoring for significant beam divergence changes. Typical examples of the relevant part of UV-camera raw images with its vertical and horizontal cross-sections are shown in **Figure 7-10**. It can be seen that the SNR in both images is well suitable for the COG detection and the intensity from the sea ice return (right) dominates the column integrated signal, giving an almost double maximum value.

As the spot on the camera is formed in the focal plane of the optics before, the pixels (pix) correspond to an angle in free space with a conversion factor of $13.0 \mu\text{rad}/\text{pix}$ for the horizontal axis and $6.75 \mu\text{rad}/\text{pix}$ for the interlaced vertical axis (DLR 2014). Thus when fitting a Gaussian profile to the cross-sections one obtains a

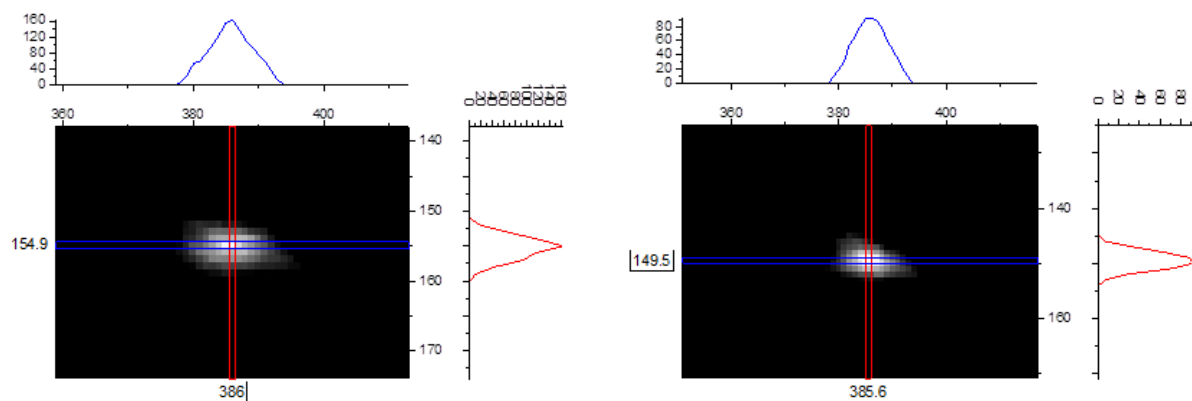


Figure 7-10: UV-camera raw images showing two samples from the column integrated lidar return and their cross sections through the spot. The left image was recorded on May 23rd during the sea ice calibration and the right image during a flight on May 25th 2015 with clouds in 4 km (around 7 km below the aircraft). Picture axes are the horizontal and vertical pixel number and the intensity is grey-scale. The profiles in the two axes show the intensity values in LSB within the contrast limits.

measure for the **laser beam divergence**, especially in case of the far field dominated UV-camera signal like in the shown examples. Applying the conversion values to the fitted beam width parameter, a free space beam divergence of around $90 \mu\text{rad}$ (4σ , 86.5% enc. energy) is obtained. This is in line with the divergence results from measurements in the laboratory after the campaign which provided $89 \mu\text{rad}$ in both axes. This proves a small degradation of the laser divergence compared to the laboratory measurement prior to installation of the A2D in the Falcon before the campaign.

The alignment stability on shorter scale is analyzed based on the recorded COG values like shown as example of the flight on May 25th, 2015 in **Figure 7-11**. It can be seen that the mean of the COG value for both axes is constant over time. This demonstrates that the active co-alignment loop effectively compensates thermal drifts of the laser emission and optical receive path. However, the variations due to the vibrations inside the aircraft affect the alignment stability on short scale, even on observation scale of 14 s. Although the change in COG position from observation to observation are only in the order of $3 \mu\text{rad}$ in both axes (using the conversion factors above), these 3% variations w.r.t. the field of view ($100 \mu\text{rad}$ in the atmosphere) are the main reason for the wind speed differences obtained on these short time scales. A possibly alignment performance degrading effect can be caused by clouds close below the aircraft up to around 2 km. The then higher return coming from the overlap region in the near field could result in a spot with a different shape and thus COG compared to a cloud free spot. As the loop constantly corrects for the COG position, this effect would not necessarily be visible in the COG data, but the resulting misalignment

between emit and receive path could lead to an error in the wind data. When flying in clouds or close above multiple scattering effects can also distort the spot resulting in a wrong COG determination. To prevent both effects from influencing the system performance, these types of cloudy measurement conditions are tried to be avoided already during the flight planning and also in flight, by changing FL (e.g. well above or below cirrus clouds). Overall the alignment stability performance was similar to that of the AC03 campaign in 2009.

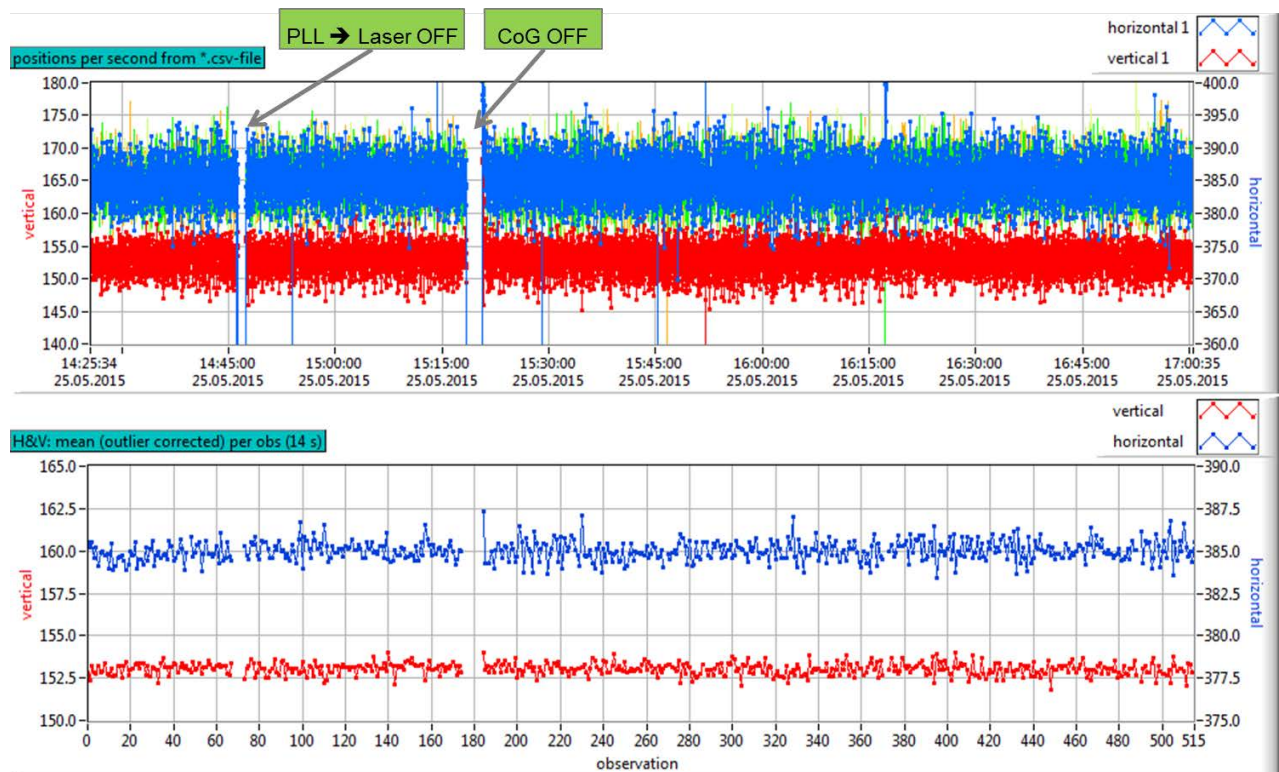


Figure 7-11: Vertical and horizontal COG-values (pix-position) of the co-alignment loop from May 25th, 2015 on raw data level (first of 4 data points per second) on top and on observation averaged level below (time in UTC).

7.5 Summary of A2D performance during WindVal 2015

It can be concluded that the overall performance of the A2D was well suitable for accomplishing the mission goals. Despite various technical issues requiring special attention throughout the campaign, valuable data was obtained during every flight leading to more than 20 h of wind and calibration data. Next to the intensive preparation activities this was also achieved thanks to an A2D optimized flight planning which takes into account specific operational constraints. An appropriate thermal preparation time prior to take-off (2.5 h – 3 h) reduces the in-flight spectrometer thermalisation to around 45 min. With the constraint to stop lidar operation shortly after leaving the cruising altitude for landing, this leaves about 2.5 h – 3 h measurement time for a 4 h flight. Flying in or close (< 2 km) above clouds, especially cirrus clouds is tried to be avoided during flight and considered already in flight planning to avoid an accuracy degrading influence on the co-alignment loop. The performance of the system was comparable to that during the previous campaign in 2009 and the implemented technical, software and operational improvements increased the high quality data output per flight hour.

Both reliability and stability of A2D are proven by the presented instrument housekeeping data and by the results of the comparison to the 2- μ m lidar wind data in this report. Compensation of the spectrometer signals based on various available AUX information like cabin pressure, co-alignment or frequency stability data, is possible but usually not necessary to be performed, thanks to the intrinsic stability of the system

	Document Nr. FR.DLR.WindVal.270717	Issue: V1.1	Date: 27.07.2017	Page: 61/146	
	Doc. Title: WindVal Final Report				

which is achievable with well managed operation. The operation of the A2D on-board the aircraft needs a highly experienced operator in for nominal operation and reactions to instrument anomalys.

The summary information of the A2D performance as provided in **Table 7-1** is in principle already available after landing of the aircraft. This information was provided to ESA in form of flight reports for each flight, which were released about 1 day after each flight (or earlier) during WindVal II in 2016.

To maintain and further increase the A2D performance and reliability a number of actions were realized after the campaign:

- The A2D reference laser was re-aligned and a broken cable for a temperature sensor was repaired to regain the RL-SL locking instability that occurred sporadically towards the end of the campaign.
- The power supply of the A2D control computer, which turned out to be the reason for unreliable boot behavior during the campaign, was repaired.
- A permanent shielding was developed and certified for use in flight that now better protects the relay mirror of the A2D telescope from being misaligned (see May 19th).
- The A2D keyboard drawer was repositioned (and recertified) for a more user friendly system operation.
- A Go-Pro video camera was purchased, which can be mounted above the A2D output window to provide additional information about the cloud and ground conditions within the A2D field of view.

Both the observed performance during WindVal 2015 and the continuous detailed operational and architectural system optimizations show the readiness of the A2D for being deployed in future campaigns related to wind measurements, especially in the context of calibration and validation activities for the Aeolus mission.

8 Airborne response calibrations

8.1 Introduction

This chapter discusses the five airborne response calibrations (also named Instrument Response Calibration (IRC) performed by the A2D in the Mie and Rayleigh channel during the WindVal campaign in 2015. The main statistical parameters are derived and the calibrations are compared among each other applying a recently developed method.

For a more detailed explanation of A2D response calibrations in general and airborne response calibrations performed during campaign in the past years please refer to (DLR 2010) and ch. 3 and 4 in (DLR 2012b).

8.2 Flight tracks and A2D operation

During the campaign in Iceland in 2009 only two airborne calibrations have been performed above the Greenland ice shield (**Figure 8-1**, left). After having analysed both, it was neither possible to tell which of the two calibrations is of better quality nor what exactly caused the difference between them. In addition, from only two calibrations one could not derive an estimation of the general performance of A2D airborne calibrations, i.e. the expectable spread of their characteristics. Consequently, it was a main objective of the WindVal campaign in 2015 to obtain more airborne calibrations. The flight tracks of the five calibrations are depicted in **Figure 8-1**, right, three located again above the Greenland ice shield and two performed over sea ice for the first time.

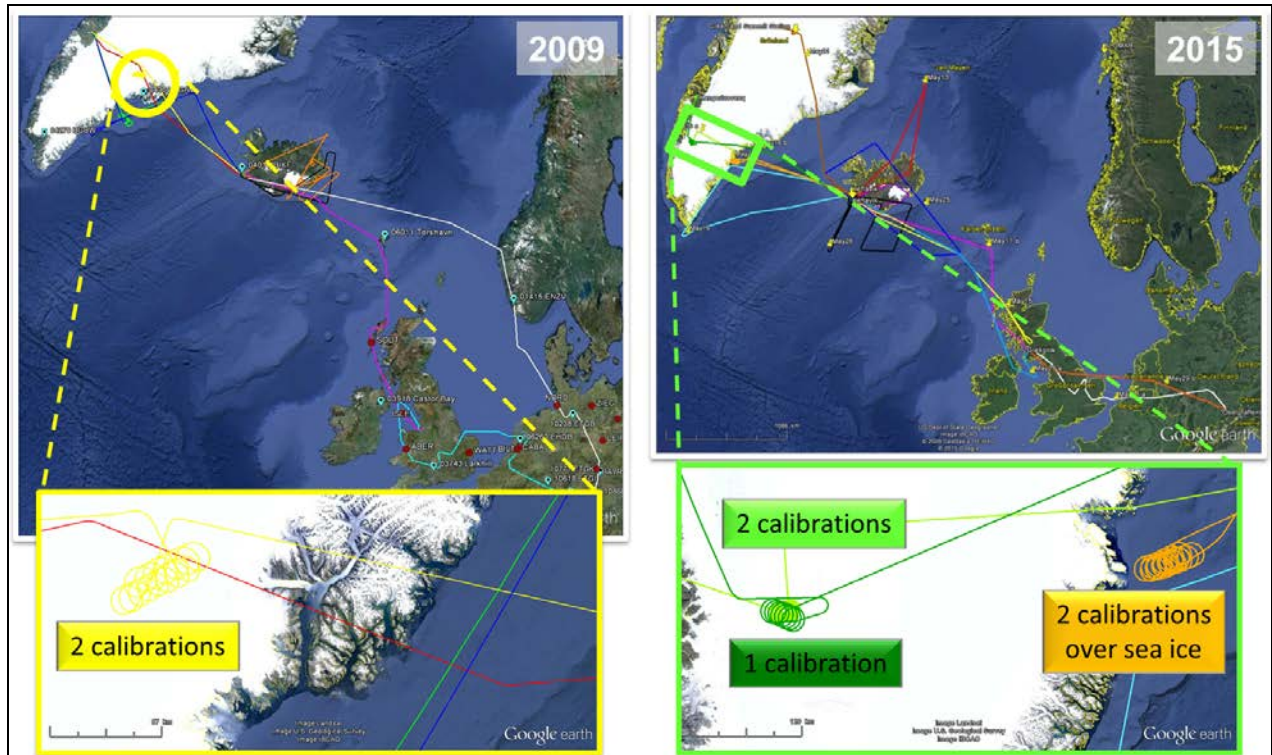


Figure 8-1: Flight tracks of the Falcon aircraft during two calibrations (yellow, left) on September 21st in 2009 and five calibrations in 2015 (right) on May 16th (light green for flight from Keflavik to Kangerlussuaq and dark green for the return flight) and on May 25th (orange).

Figure 8-2 visualizes the range-gate settings during the seven airborne calibrations. The 0 km on the y-axis corresponds to the flight level of the Falcon, i.e. the location of the instrument. The black bar marking the first 315 m takes into account the fact, that the laser pulse is in average emitted in the middle of range-gate #4, which is also used for the Internal Reference. The atmospheric range-gates #5 - #24 follow in alternating green colors. The measurement grid of calibration #7 extended up to 12 km away from the instrument. As the grids of the other calibrations had a shorter range, the gap from 9 km and 10.5 km, respectively, was filled in black in **Figure 8-2**. The locations of range-gates #6, #10 and #15 are marked with grey boxes for each calibration. Due to the range-gate overlap effect on the ACCD the ground return signals are mostly spread over two range-gates marked by orange boxes, additionally distinguishing between the major (dark orange) and the minor contributor (light orange). Considering that the A2D is operated in a nadir viewing direction during the response calibration, the distance from the instrument found for the ground returns equals also the flight height above the ground return, for example about 7 km for the calibrations #3 and #4 over the Greenland iceshield and more than 10 km for the calibrations #6 and #7 over the sea ice.

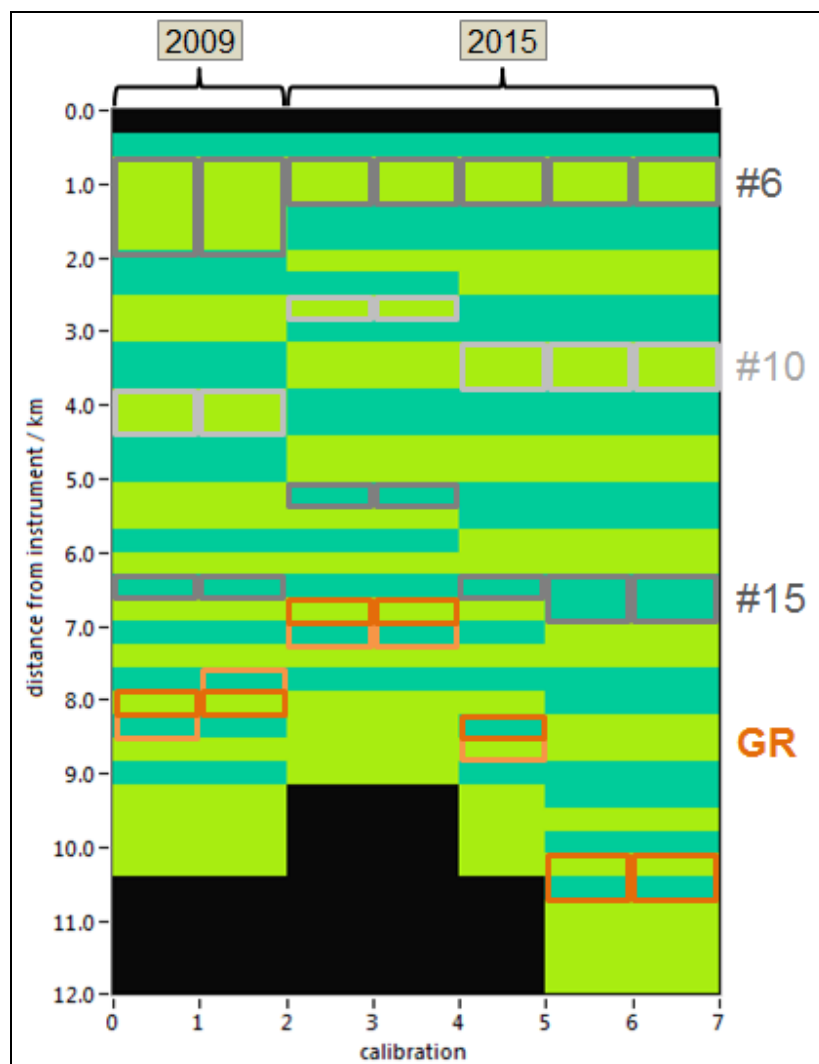


Figure 8-2: Range-gate thicknesses along the LOS for all seven airborne calibrations available from 2009 and 2015. The measurement grid starts at the top of range-gate #5 about 315 m below the Falcon flight altitude. The black bar at the top depicts half the size of the Internal Reference range-gate #4, the black region at the bottom lies below the last A2D range-gate #24. Main and secondary ground return bins (GR) are marked in dark and light orange, respectively.

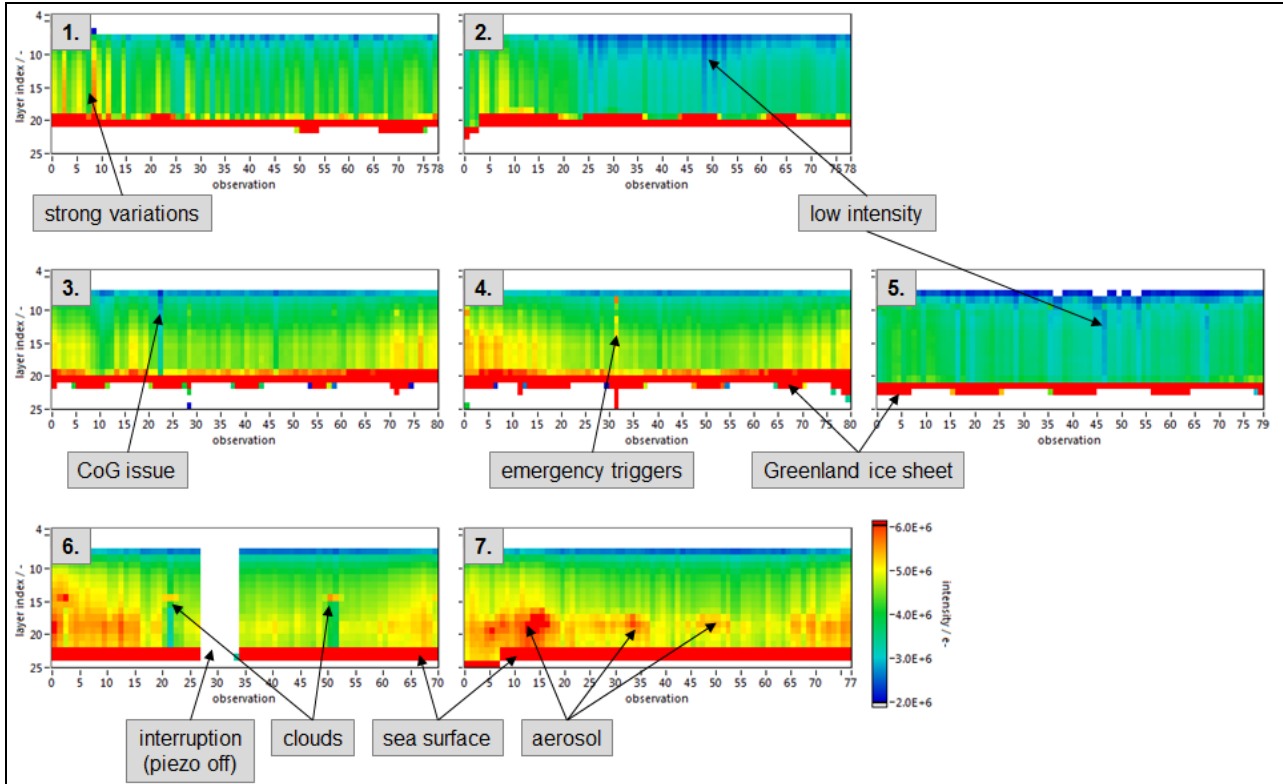


Figure 8-3: Comparison of intensities in electrons on the Rayleigh channel measured during the seven calibrations (#1 and #2 from 2009, #3 - #7 from 2015) including several leading and trailing observations. Intensities are summed over 16 pixels, range corrected and scaled to bins size as well as to the number of measurements.

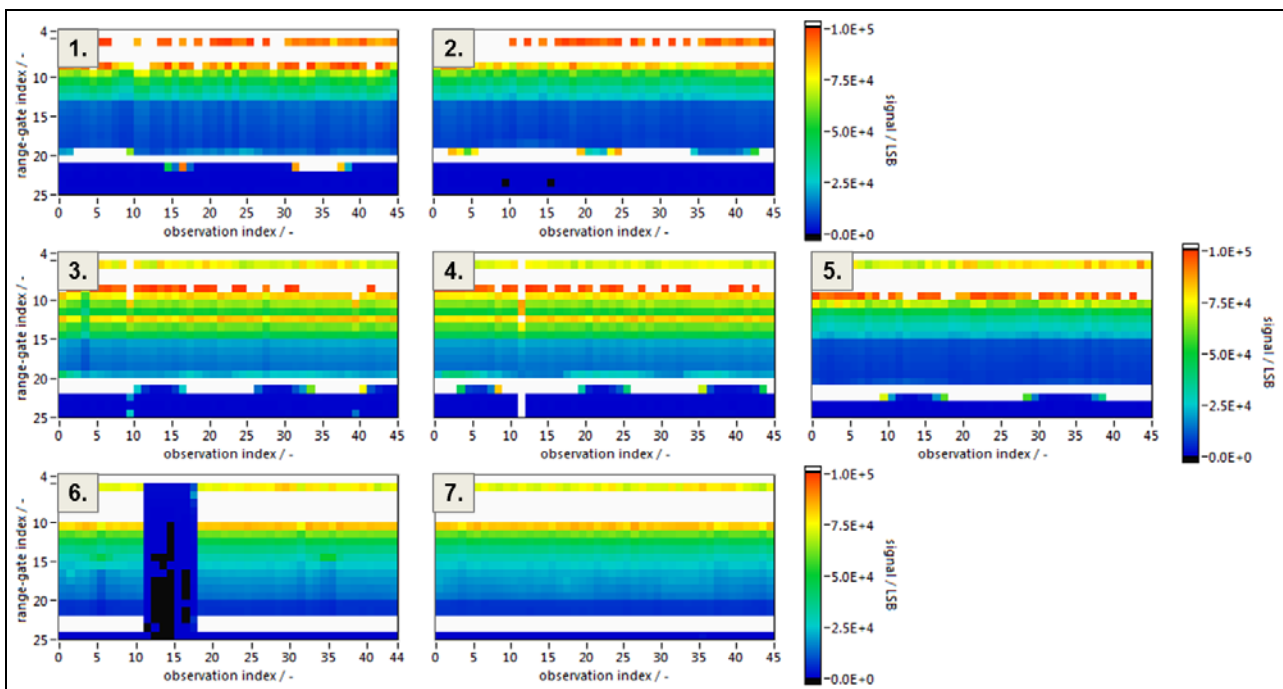


Figure 8-4: Comparison of intensities on the Mie channel measured during the seven calibrations. The 45 observations shown for each calibration and used for the analysis correspond to a frequency interval of 1100 MHz.

	Document Nr. FR.DLR.WindVal.270717	Issue: V1.1	Date: 27.07.2017	Page: 65/146	
	Doc. Title: WindVal Final Report				

Figure 8-2 helps to interpret the intensity plots of the Rayleigh channel in **Figure 8-3**. Range-gate or layer index #4, respectively, at the top of the graphs corresponds to flight level of the Falcon as well as to the Internal Reference signal. Below follow the intensities of the atmospheric range-gates as sum over 16 pixels, i.e. over both uncut Rayleigh channels A and B. White color in range-gates #5 and #6 indicate low signal levels, which are due to both, the telescope overlap function and the still partly closed electro-optical modulator (EOM). For different reasons white colour appears also for the Internal Reference (due to a range correction with 0 m distance from the instrument) and below the ground return (noise only). The Rayleigh intensities are range corrected by a factor of r^2 as well as scaled to the individual range-gate thicknesses and to the number of valid measurements used after for the summation to an observational signal after quality control.

The strong ground return signal distributed over two or more range-gates stands out in red for all seven calibrations. Whereas calibrations #1 - #5 were acquired over the Greenland iceshield including its altitude variations, calibrations #6 and #7 were performed over sea ice resulting in a more steady distribution of the ground signal with respect to the affected range-gates. The intensity plots in **Figure 8-3** are plotted over the for the whole A2D calibration mode, i.e. including the frequency ramp and several leading and trailing observations. A frequency interval of ± 750 MHz, as used for the actual calibration analysis, comprises only 61 observations. Thus, the ground return being in range-gate #24 at the start of calibration #7 is due to the Falcon aircraft not yet having reached its roll angle of 20° which is needed for nadir pointing. For analysis, calibration #7 has been cut to 1100 MHz (± 550 MHz around center frequency) and 1500 MHz (± 750 MHz around assumed crosspoint) intervals for the Mie and the Rayleigh, respectively. Several comments are given in **Figure 8-3** explaining further striking features in the intensity distribution. Most of the reasons are negatively affecting the quality of the corresponding response calibration, especially issues related to pointing, i.e. a variation of the center of gravity (CoG) or an interruption of the piezo control for the last mirror in the transmit path. The obviously consistent behavior of high atmospheric intensities at the start and at the end as well as a drop of intensity towards the middle is expected. It can be attributed to the changing frequency during calibration, resulting in a strongly illuminated filter A first, followed by a transition phase including the crosspoint and a strong illumination of filter B.

As for the Rayleigh channel **Figure 8-4** presents the summed intensities over all 16 pixels for the seven calibrations in the Mie channel. The intensities are again summed for all valid measurements per observation and range-gate. Unlike for the Rayleigh channel only the minimum value of the 16 pixels has been subtracted from the Mie intensities. The broadband Rayleigh background on the Mie channel, often also referred to as telescope image or MOUSR correction, has not been subtracted. This is not necessary because only the response curve of the ground return is evaluated and the Rayleigh background in these usually distant range-gates is negligibly small in comparison to the signal from the highly reflective ice surfaces. Additionally, the thickness of the remaining atmospheric column above the ground is unknown. A precise correction would require detailed knowledge of the DEM and the intersection points (which could potentially be obtained from the $2\text{-}\mu\text{m}$ power measurements) or would induce a bias otherwise. The thickness of the remaining atmospheric column was assessed within the Master's thesis at DLR by Weiler (2017). The altitude resolution of the ground return is even better than 100 m for the $2\text{-}\mu\text{m}$ lidar because it is extracted from the raw data time series with a resolution of 0.3 m. Moreover, it would be necessary to perform a MOUSR procedure in nadir pointing mode since a clear range-gate allocation would be impossible when trying to subtract a Rayleigh background that was obtained under the usual 20° off-nadir angle. At least, in this case a new approach (such as inter- or extrapolating the Rayleigh background curves) would have to be accurately investigated before being taken into account for implementation.

However, a correction via the MOUSR procedure is strongly recommended for the wind retrieval. If a qualitatively satisfying telescope image can be recorded close in time to the wind measurement, its subtraction substantially improves the number and the precision of the retrieved Mie winds (**Figure 9-29**). Regarding Aeolus a MOUSR procedure should be performed in orbit in order to verify the assumed TOBS correction array.

8.3 A2D performance and quality control

Already during operation of the laser in flight its performance is continuously checked by the operator via various software monitoring tools. The same holds for the temperature and pressure within the optical bench assembly (OBA) and the Falcon aircraft. Temperature and pressure at the Rayleigh spectrometers and the Mie spectrometer are routinely checked for plausibility before the processing of the wind or calibration data. Data from the Inertial Reference System (IRS) such as velocity, roll, pitch and yaw angle are considered in a correction for the aircraft induced LOS speed as already extensively described in (DLR 2012b), as have been most of the other quality checks and correction procedures.

Figure 8-5 shows the quality control matrices for the seven calibrations with invalid measurements marked in red. Invalidity can be attributed by non-compliance to thresholds set with respect to the co-alignment of transmit and receive path, the detection chain offset (DCO), saturation of the ACCD and laser emission time. Obviously, a significant number of measurements of the two calibrations from 2009 did not pass the DCO check. During the WindVal campaign in 2015 much less measurements had to be rejected from processing. One possible cause for DCO outliers can be a mismatch of the time between laser emission and receiver trigger (provided by the laser cavity control based on a prediction) such that a part of the actual internal reference signal falls into the DCO range-gate. The alignment of the laser oscillator and the optimization of the cavity control parameters led to a more stable trigger of the receiver during the 2015 campaign and thus less DCO outliers. Prominent features in **Figure 8-5** are visible for calibration #4, where a wrong time of laser emission affects the quality of observation #32 and for calibration #6 where the co-alignment loop failed for 7 observations.

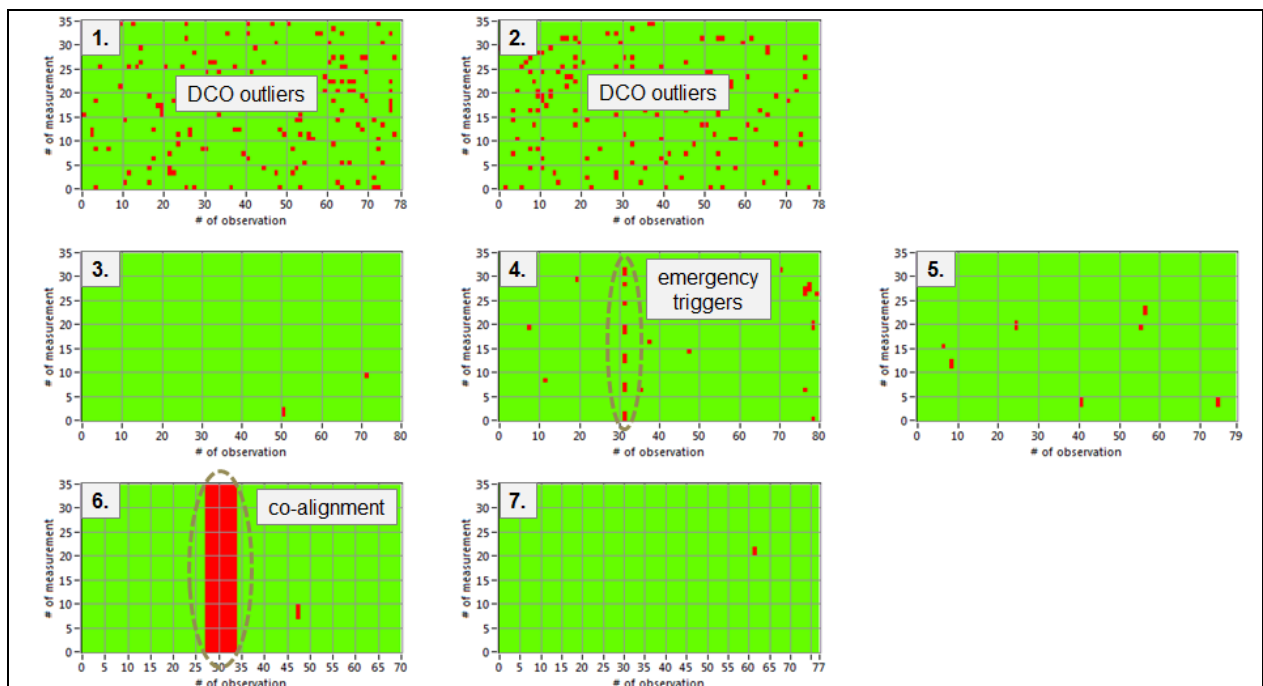


Figure 8-5: Comparison of quality control results for the seven Rayleigh response calibrations. Invalid measurements are marked in red.

The co-alignment control loop includes a UV camera that analyses a part of the atmospheric backscatter signal with respect to the position of its maximum intensity on a CCD. After the integration of the A2D into the Falcon a reference position is defined via a procedure that attempts to optimize the illumination in the far field by maximizing and balancing the Rayleigh backscatter signal in imaging mode on the Mie channel. This reference position usually changes from campaign to campaign. During subsequent calibrations and wind measurements, deviations from the reference position are recorded per second. **Figure 8-6** gives an overview of the statistics of the co-alignment during the seven calibrations. Obviously, a significant difference exists in the reference position itself between the two calibrations from 2009 and the calibrations from 2015,

with a change of 8 pixels in the vertical and 7 pixels in the horizontal axis. For the A2D it is crucial that the reference position is the same for both, a wind measurement and the calibration used to process it. Regarding the variation of the pointing, the 3rd calibration (2015-05-16 a) stands out with the highest standard deviation on both axes, i.e. 1.6 pixels compared to an average of about 1.2 in the vertical and 3.2 pixels versus 2.0 pixels in the horizontal. As depicted at the bottom of **Figure 8-6** the cause can be traced back to a few observations around 15:40 UTC. Such a behavior mostly indicates either a dense cloud close below the aircraft or a piezo malfunction. In the case of a dense cloud the strong near field illumination causes a wrong CoG. Therefore, the A2D should either fly below clouds or significantly above clouds in order to assure good quality of the wind measurement and calibration data. The lowest standard deviation on both, horizontal and vertical axis, has been reached for the last two calibrations, #6 and #7.

The removal of single measurements or even whole observations depends on the type of outlier found during quality control. Regarding the CoG outlier in calibration #3, the whole observation has been removed from the resulting wind profile and hence the statistical comparison. The data including the outlier is shown here only for the purpose of visualization. Removing this outlier will very likely push the respective SD of the pointing down to a level comparable to the other calibrations.

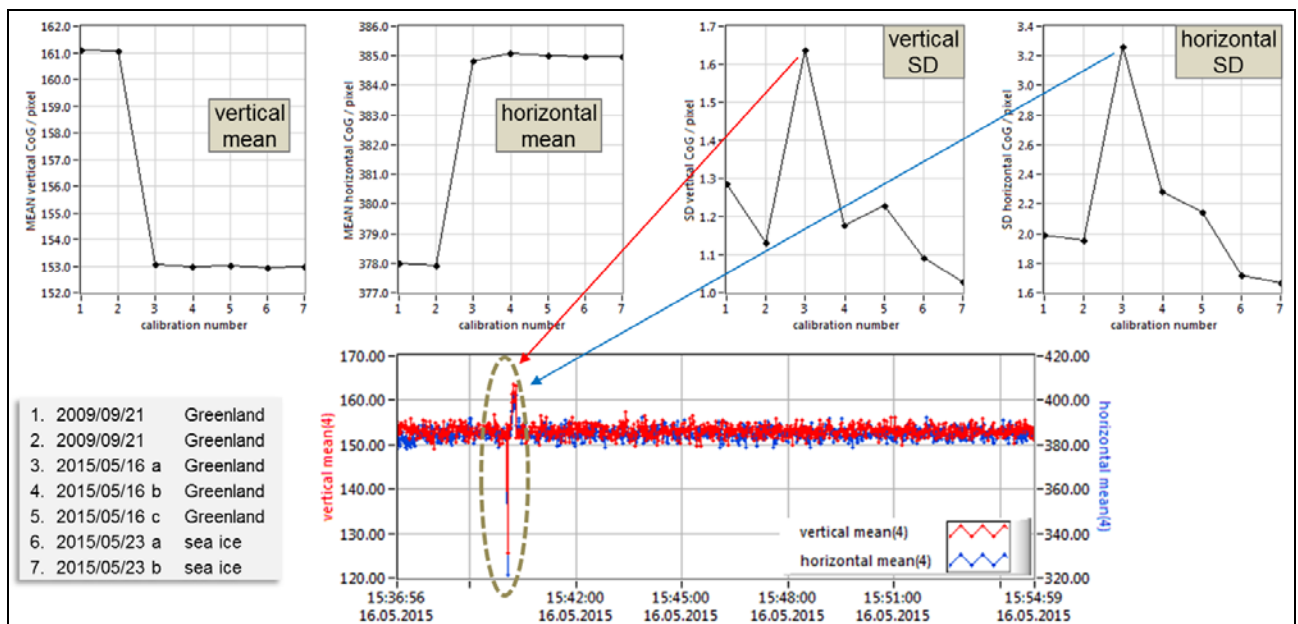


Figure 8-6: Comparison of statistics related to the co-alignment during the seven calibrations.

Unlike for the Aeolus satellite the A2D features a wavemeter which is used to accurately measure the frequency of the emitted laser pulse. Within the processing of response calibrations this ability allows for a correction of the frequencies reported in the telemetry files and, hence, for an improvement of the quality of the calibrations. **Figure 8-7** shows the frequencies measured by the wavemeter during the seven calibrations and explains prominent features. Obviously, the measured frequencies deviate from a perfect straight line that would be described by the reported frequencies. This deviation is plotted in **Figure 8-8**, showing that the real slopes of calibrations can easily differ up to $\approx 1.7\%$ ($= 25 \text{ MHz} / 1500 \text{ MHz}$) from the slopes expected from commanded frequencies, but also by more than 3% in worse cases such as calibration #2 or #4. However, since the precise frequency measurements by the wavemeter allow for correcting these deviations, none of the calibrations needs to be rejected on the basis of laser frequency drifts, at least as long as no gaps appear in the recorded frequency data, which was for instance not the case for calibration #2 (**Figure 8-8**, magenta). In order to characterize the performance of the flight lasers before launch, it would be desirable to seize the last chance and perform such an analysis of the frequency drifts of both flight lasers during the Thermal Vacuum test (TRG-11).

Table 8-1 gives a short summary of calibration related data including a coarse assessment of their impact on the quality of these calibrations. Referring to the presented parameter the best airborne calibrations tend to be #1, #3 and #4 for which frequency drifts as well as emergency triggers and CoG outliers (respective QC included at a late stage of the composition of this TN) are known and considered during processing. Also

calibrations #5 and #7 show good potential, however, only if the low intensities as well as the probable aerosol load only negligibly impact the quality of the response curve.

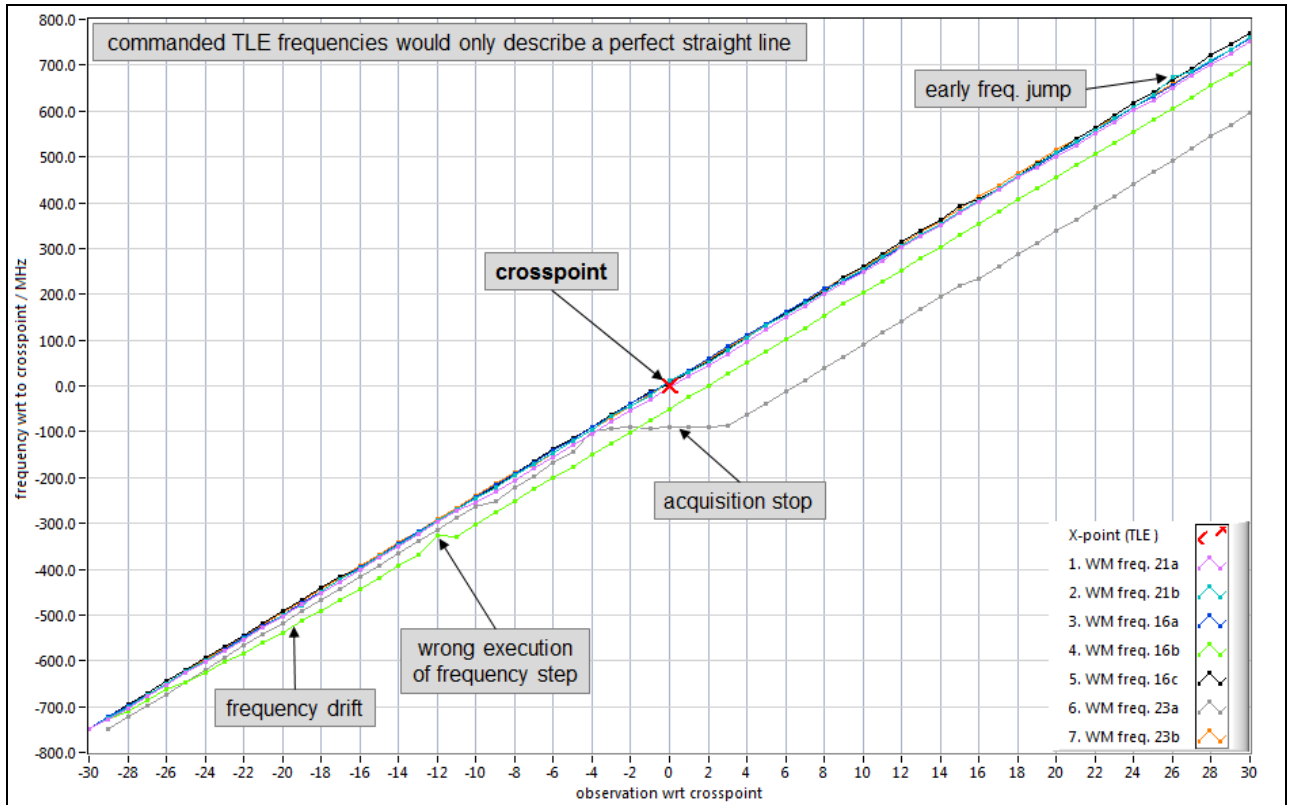


Figure 8-7: Comparison of frequencies measured by the wavemeter during the seven calibrations.

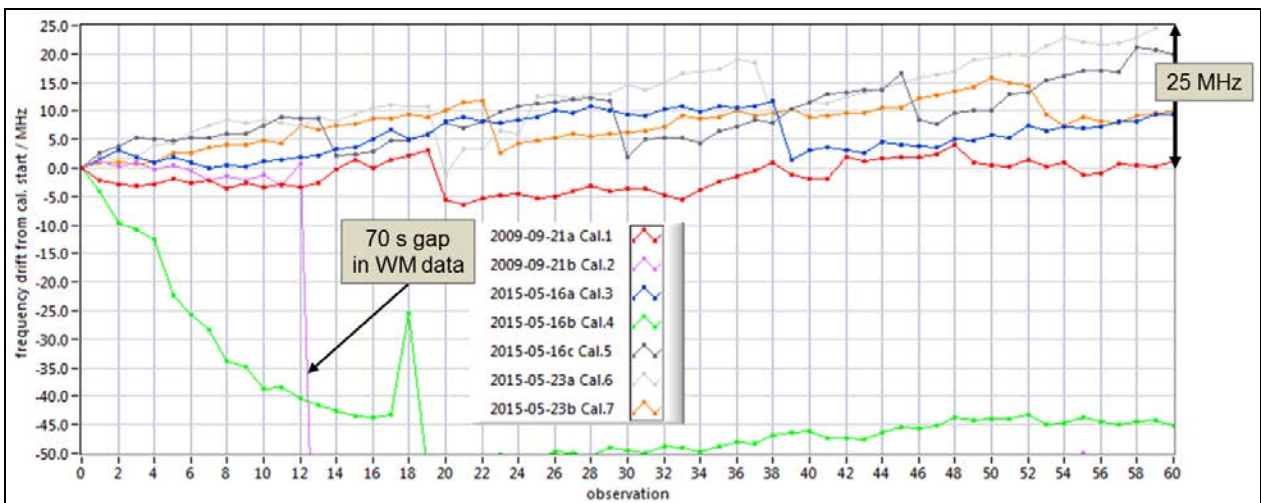


Figure 8-8: Comparison of frequency drifts derived from wavemeter measurements during the seven calibrations. 25 MHz correspond to about 4.5 m/s LOS.

It was found that the characteristics of the two response calibration curves from 2009 differ significantly from those obtained in 2015, mainly in terms of intercept and sensitivity. This is caused by different reference positions used for the co-alignment loop. Thus, calibration #1 should not be used for wind retrievals from the 2015 data set. Unlike for calibration #3, which was performed over the Greenland ice shield, the range-gate grid of calibration #7 reached down to sea surface level. This fact allows the derivation of response curves

for the whole atmospheric altitude range up to the flight level of the Falcon and renders calibration #7 the obviously best choice to process the winds of this airborne campaign. **Figure 8-31** shows the differences in Rayleigh slope and intercept along with **Figure 8-32** showing the differences between calibrations (including 2009). The y-scale of **Figure 8-28** does not allow drawing conclusions with respect to the intercept. The A2D RSP is much more sensitive to alignment changes than the A2D MSP. Thus, the differences for the Mie calibrations (**Figure 8-16, Figure 8-17**) do not seem to be significant.

The two last calibrations #6 & #7 were performed over sea ice, which is supposed to have a high albedo and should hence allow for a high quality ground return calibration curve. However, this does not seem to be the case. Consequently, the ground return response curve of calibration #3 should be used for the processing of the Mie winds of this campaign. Deeper insights into optimized usage of ground return signal for the A2D is available from a master's thesis prepared at DLR (Weiler 2017).

Table 8-1: A general comparison of calibration related data.

cal. #	date	co-alignment	intensity	frequency	quality control	remarks	ground return range-gates
1.	2009/09/21	161/378	strong variations	smallest drift	many DCO outliers	above Greenland	20 + 21
2.	2009/09/21	161/378	low intensities	70 s time gap (WM)	many DCO outliers	above Greenland	19 + 20
3.	2015/05/16	153/385 CoG issue in obs.10				above Greenland	20 + 21
4.	2015/05/16	153/385	emergency triggers	strongest drift	emergency triggers in obs.31	above Greenland	20 + 21
5.	2015/05/16	153/385	low intensities			above Greenland	21 + 22
6.	2015/05/23	153/385	clouds in \approx 4 obs			interrupted / sea ice	22 + 23
7.	2015/05/23	153/385 lowest SD	aerosol in lower range-gates			sea ice	22 + 23

In a nutshell the following steps are performed during the processing of a calibration:

1. coarse determination of Rayleigh crosspoint or Mie center frequency (\rightarrow these can differ depending on the spectral registration of the spectrometers tuned by temperature in their relative position)
2. Subtraction of DCO per measurement
3. Subtraction of background per measurement
4. Calculation of response
5. Quality control: disregard invalid observations
6. Subtraction of aircraft LOS velocity per observation
7. Summation of signal for distributed ground returns
8. Polynomial (Rayleigh) or linear (Mie) fit procedure
9. Extrapolation of fit coefficients for range-gates below ground (Rayleigh only)

	Document Nr. FR.DLR.WindVal.270717	Issue: V1.1	Date: 27.07.2017	Page: 70/146	
	Doc. Title: WindVal Final Report				

8.4 Mie response calibration

The final Mie response calibration curves including all corrections as mentioned above are presented in **Figure 8-9** for the Internal Reference and in **Figure 8-10** for the ground return. All response curves of the Internal Reference in **Figure 8-9** meet at a frequency of 0 MHz (but with different response values). This is due to the definition the center frequency at this point. It is noted that the x-axes in the following figures uses relative frequencies for a more convenient presentation of the curves. That means that the absolute frequencies measured by a wavemeter for “the same” observation can differ between calibrations. Especially the absolute frequency of the defined Mie center can differ from the absolute frequency of the defined Rayleigh crosspoint, but mostly only by a few MHz. In order to correctly determine the response curves of the ground return the signals of the range-gates as indicated in **Figure 8-2** and **Table 8-1** were summed up for all observations. This procedure can be used as a good approximation since there was only little altitudinal variation of the terrain within the A2D measurement grid during the calibration flights in 2009 and 2015 as visible in **Figure 8-3** and **Figure 8-4**. However, this simplified summation can also introduce avoidable errors due to atmospheric contamination. Therefore, a more sophisticated algorithm was developed by Weiler (2017). On measurement level it will minimize the influence of the remaining atmospheric column between the actual ground and the top of the uppermost range-gate used for the summation. This improvement will be implemented for the evaluation of the wind data from the NAWDEX campaign in 2016.

The non-linearities of the Mie response calibration curves are shown in **Figure 8-11** for the Internal Reference and in **Figure 8-12** for the ground return. Instead of a linear fit, which is currently applied within the Mie wind retrieval, the consistent shape of the non-linearities rather supports the introduction of a polynomial fit of at least 5th order as it has been done for the Rayleigh response calibration. The benefit would be a reduced standard deviation in the measured Mie wind speeds. A deviation from the linear fit by 0.1 pixel corresponds to 1.76 m/s LOS, if computed with a mean slope of 99.28 MHz/pixel (**Table 8-2**) and a conversion factor of 5.63 MHz/(m/s). It is not clear why the overall shape of the Mie non-linearities of the internal reference (**Figure 8-11**) consistently differs from those of the ground return (**Figure 8-12**). One reason could be the influence of the molecular background from the remaining atmospheric column of the ground return range-gate due to the non-correction of the ground return signal by a MOUSR procedure.

Table 8-2 presents an overview of characteristics and statistics of the Mie response calibration curves. The intercept and the slope of the linear fits are listed for the Internal Reference as well as for the ground return. The corresponding mean values, the standard deviations and the minima (green) and maxima (red) give an impression of the inherent variability of the calibrations. Obviously, the intercepts of Internal Reference and the ground return calibration curves are similarly stable with σ_{STD} of 0.10 and 0.09, however the slopes are not (σ_{STD} of 0.33 and 0.62). The fact that the average slope of the Internal Reference curves differs from that of the ground return can be explained by effects of the atmospheric path, including the disturbance by the Rayleigh background as well as by CoG variations causing different illuminations of the spectrometer and therefore different FWHM. Another interesting parameter to be monitored is the difference in intercept between the linear fits for the Internal Reference and the ground return (**Table 8-2**, right column). To convert this difference from pixels to more descriptive m/s the following equation has been used:

$$\Delta IC_{m/s} = \Delta IC_{pix} \cdot \frac{1}{2} (\text{slope}_{\text{mean,INT}} + \text{slope}_{\text{mean,GR}}) / 5.63 \text{ MHz/m/s}$$

According to **Table 8-2** the intercepts between Internal Reference and ground return differ in average by about 1.42 m/s. The difference is consistent for all calibrations from 2015 except #7. It is not clear why the latter deviates and this deviation should be considered as one among several criteria in a qualitative assessment of the calibrations. As mentioned above, the calibration mode of the A2D has been started already during the off-nadir mode and the relevant observations used for the analysis were all obtained in nadir mode. Therefore, the preceding and trailing observations can not provide an explanation either.

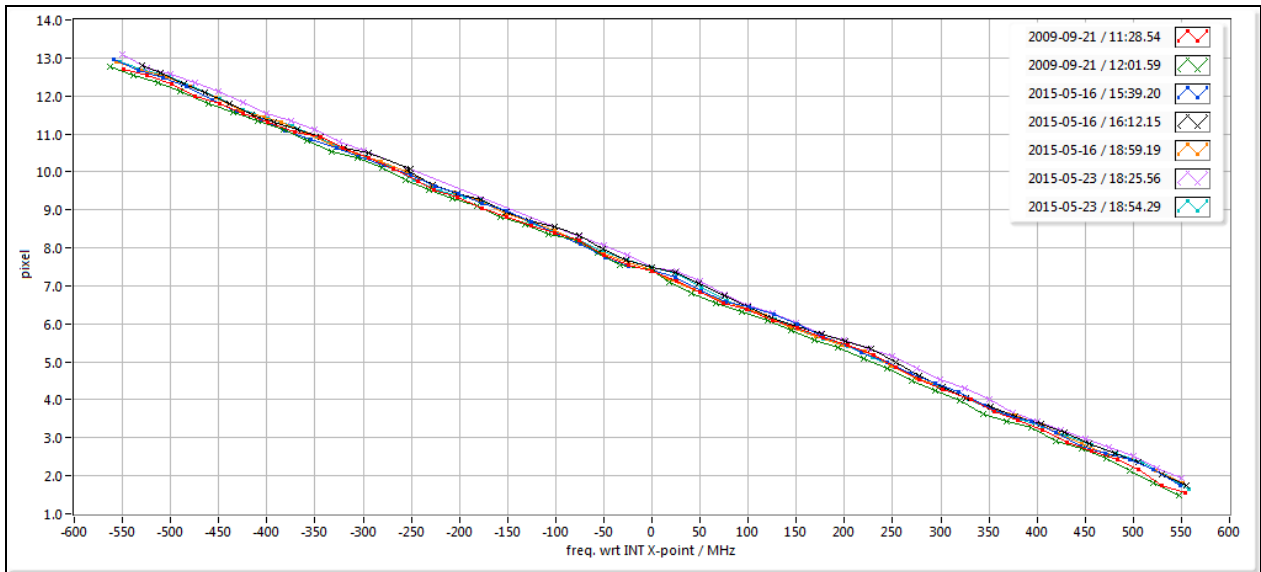


Figure 8-9: Mie response calibration curves of the Internal Reference for the seven calibrations and plotted over frequencies measured by the wavemeter.

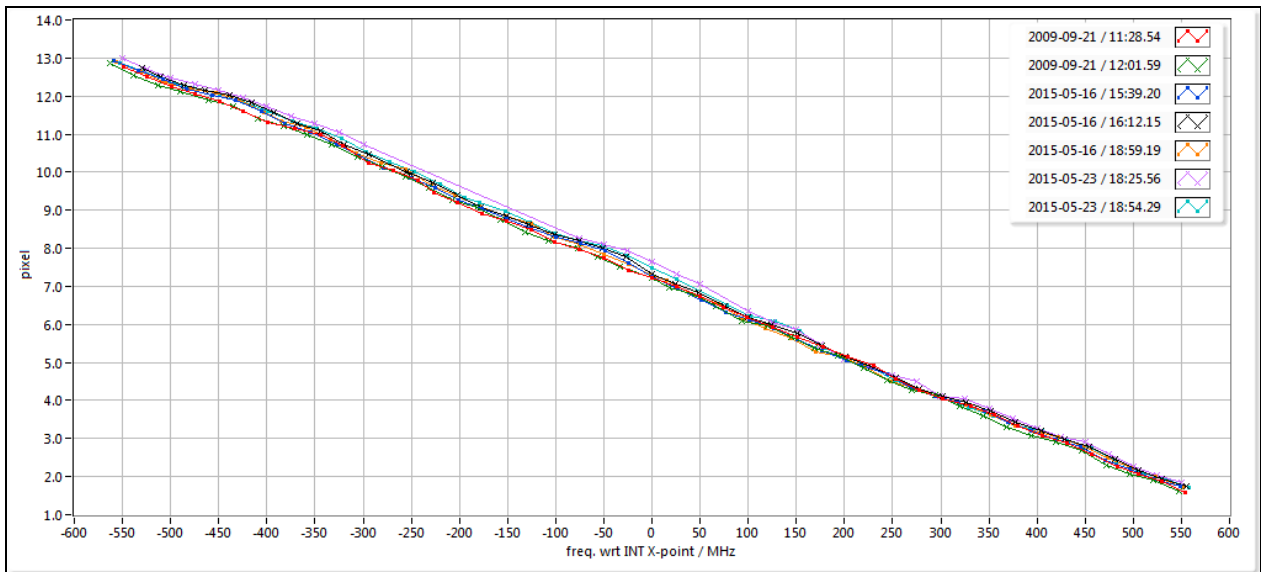


Figure 8-10: Mie response calibration curves derived from the ground return signal of the seven calibrations and plotted over frequencies measured by the wavemeter.

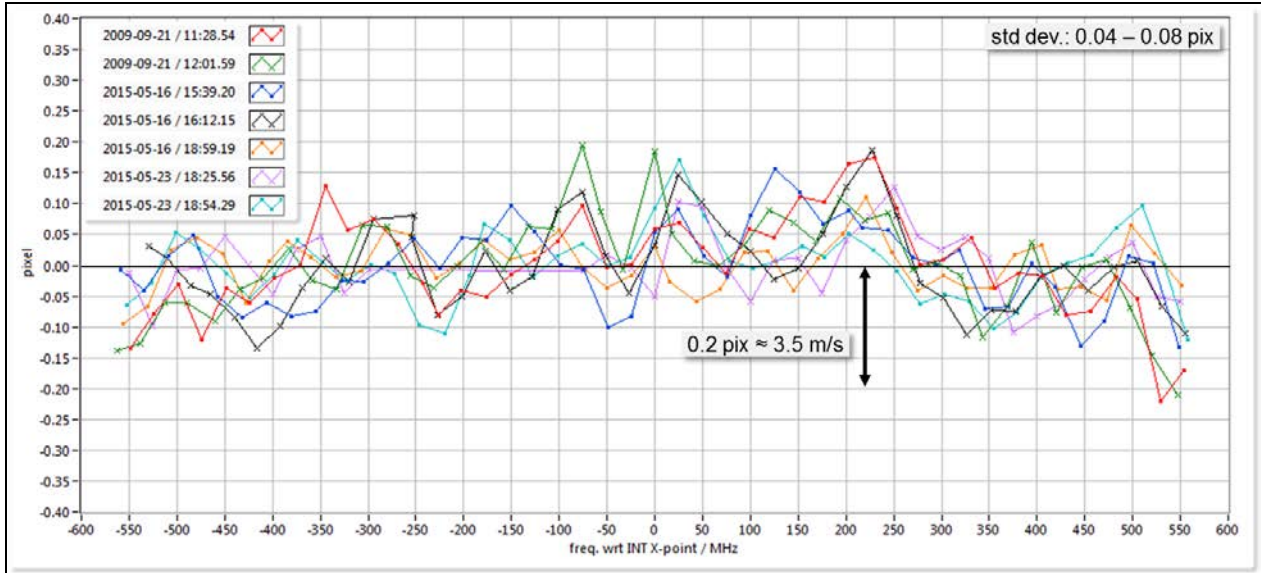


Figure 8-11: Mie non-linearities derived from the Internal Reference of the seven calibrations and plotted over frequencies measured by the wavemeter.

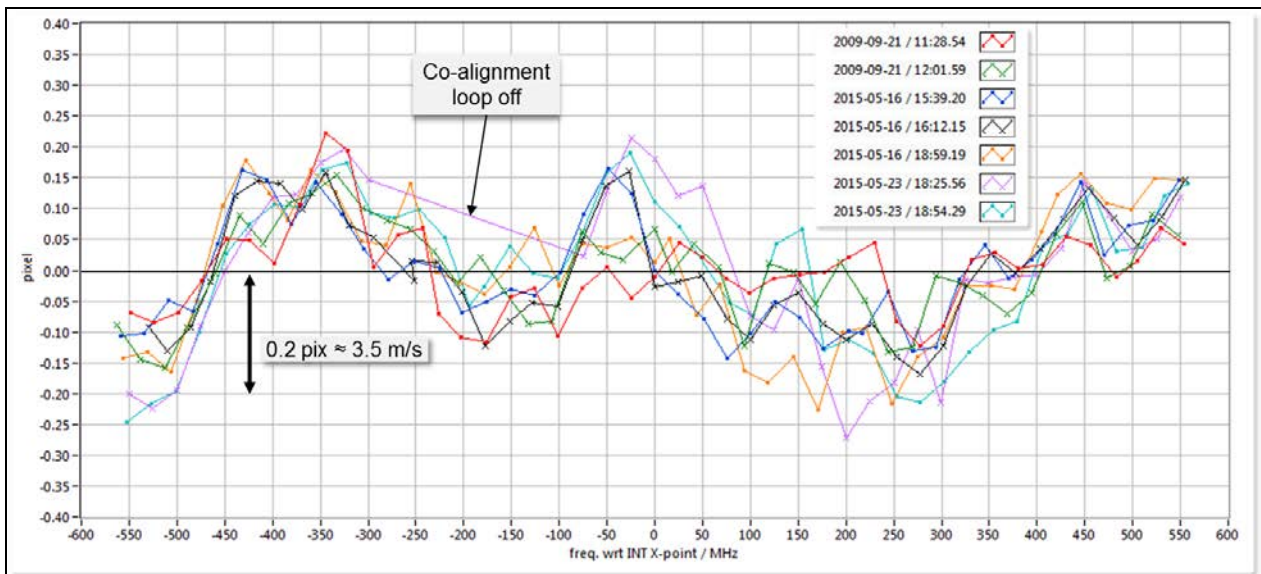


Figure 8-12: Mie non-linearities derived from the ground return signal of the seven calibrations and plotted over frequencies measured by the wavemeter.

Nevertheless, the properties of calibration #7 have been investigated more closely in **Figure 8-13 - Figure 8-15**. No obvious difference can be seen when comparing the response curves of Internal Reference and Ground return of calibration #6 (**Figure 8-13**) and #7 (**Figure 8-14**). In addition, when comparing calibration #7 to #3 (**Figure 8-15**) no remarkable difference is visible. However, calibration #3, which was obtained over the Greenland ice shield, shows a much stronger ground return signal (by about a factor of 4) than the two calibrations over sea ice. Although the response differences between Internal Reference and ground return (grey lines) show the same coarse structure for all three calibrations with preferably negative/positive values left/right of the center frequency, but calibration #6 and #7 reach higher values (≈ 0.6 pixel) in the right part compared to calibration #4 (≈ 0.4 pixel). Thus, one could also potentially assume that the $\Delta intercept$ of calibration #6 is actually very similar to the one of #7 but has been corrupted by the deleted observations (failed co-alignment) and accidentally ended up with a value close to that of calibration #3 - #5. This would support a classification of Mie ground return into two categories: calibrations over the Greenland ice shield and calibrations over sea ice.

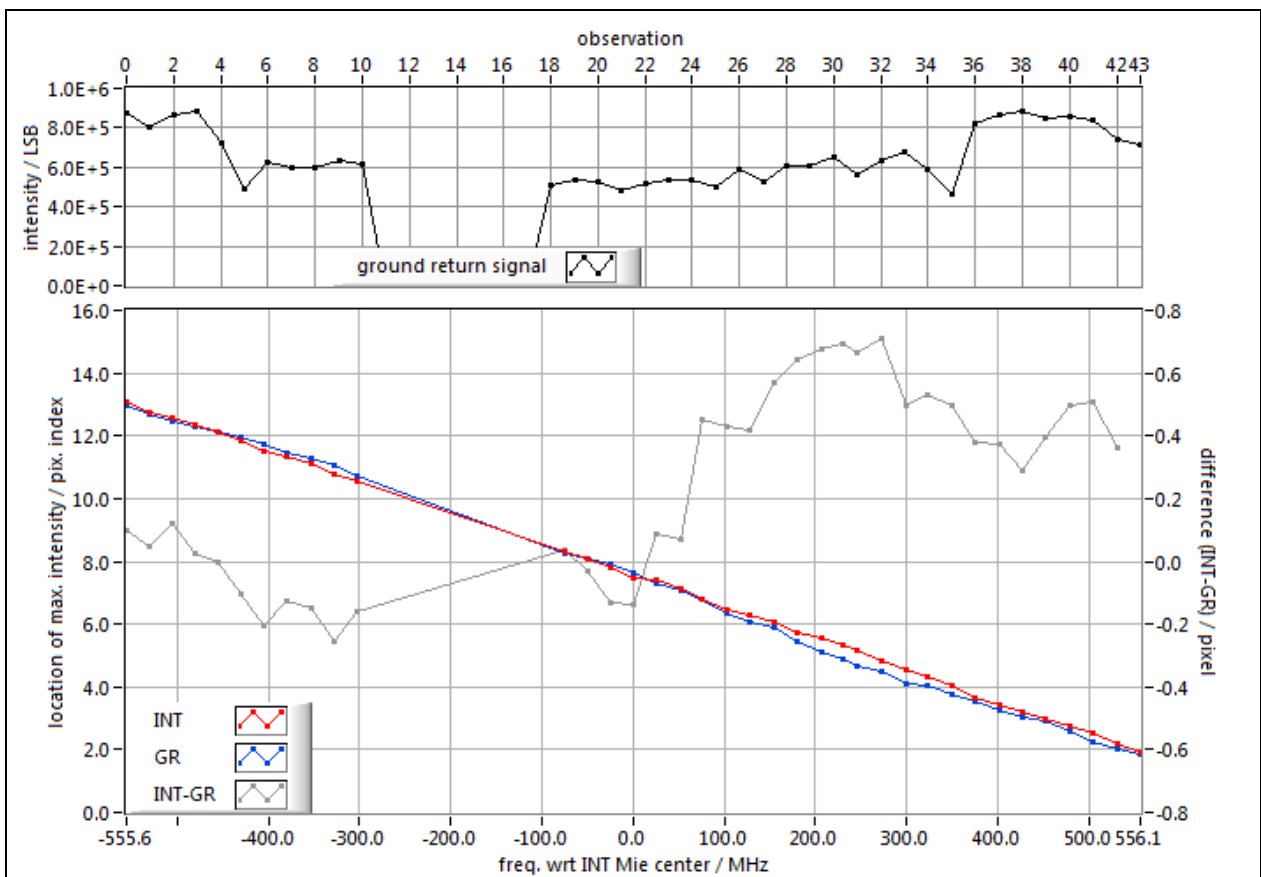


Figure 8-13: Ground return signal as the sum of intensities of range-gates #22 and #23 per observation (top) and the derived response curves of the Internal Reference and the ground return as well as their difference (INT-GR) per frequency step (bottom) for Mie calibration #6.

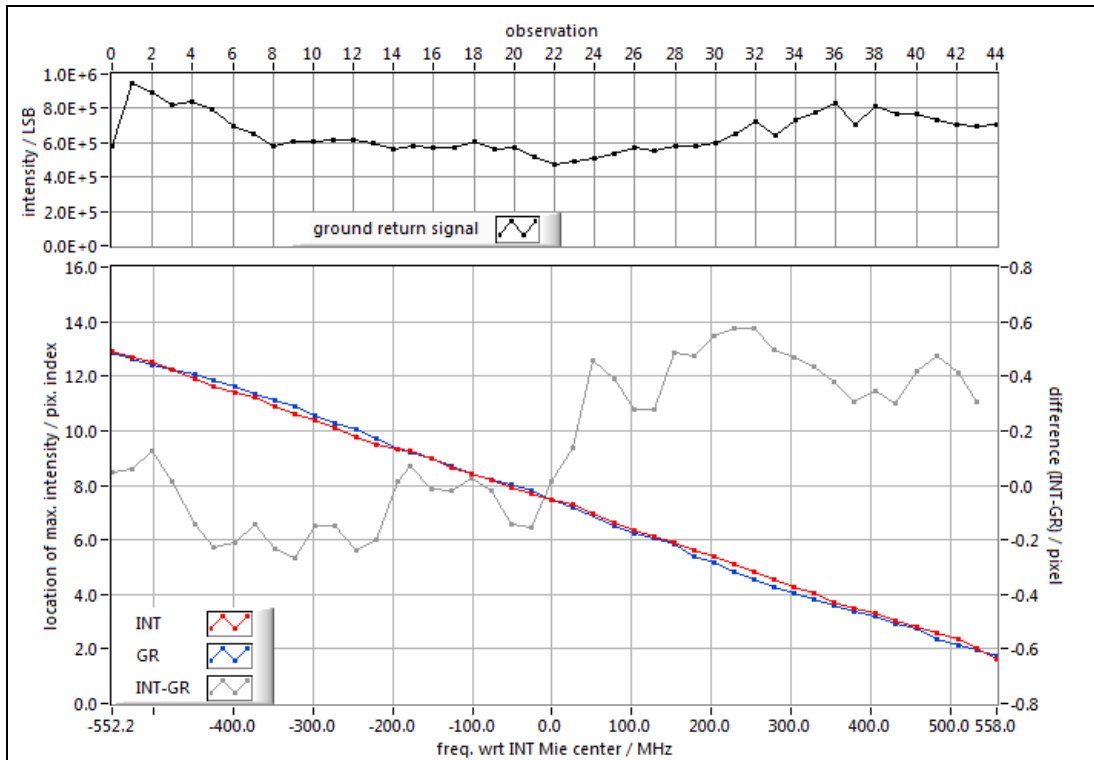


Figure 8-14: Ground return signal as the sum of intensities of range-gates #22 and #23 per observation (top) and the derived response curves of the Internal Reference and the ground return as well as their difference (INT-GR) per frequency step (bottom) for Mie calibration #7.

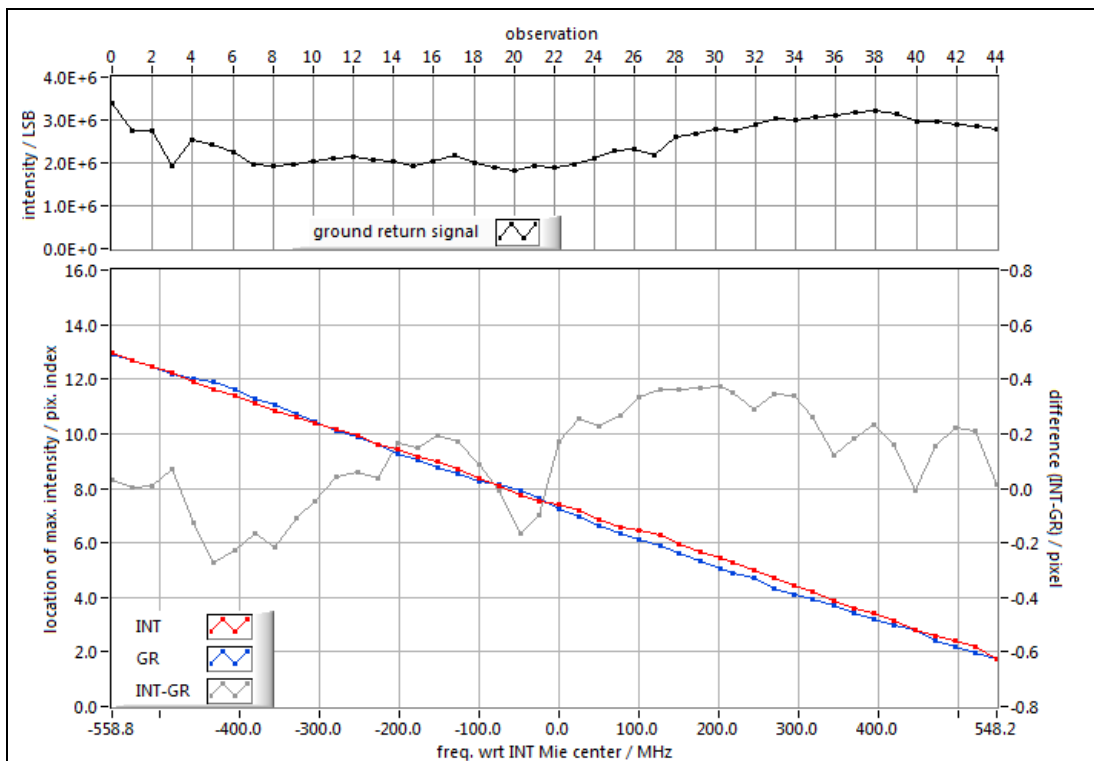


Figure 8-15: Ground return signal as the sum of intensities of range-gates #22 and #23 per observation (top) and the derived response curves of the Internal Reference and the ground return as well as their difference (INT-GR) per frequency step (bottom) for Mie calibration #3.

Table 8-2: Summary of characteristics of the Mie response calibration curves. Minimum and maximum values of each parameter are indicated in green and red, respectively.

Calibration	INTERNAL		GROUND		Δ intercept = INT-GR (pixel & m/s)
	intercept (pixel)	slope (MHz/pix)	intercept (pixel)	slope (MHz/pix)	
2009-09-21 / 11:26	7.32	-99.20	7.23	-97.70	0.09 / 1.57
2009-09-21 / 11:59	7.22	-99.00	7.17	-97.36	0.05 / 0.87
2015-05-16 / 15:36	7.37	-99.99	7.26	-96.80	0.11 / 1.91
2015-05-16 / 16:10	7.45	-99.22	7.35	-96.39	0.10 / 1.74
2015-05-16 / 18:57	7.38	-99.32	7.28	-96.53	0.10 / 1.74
2015-05-23 / 18:23	7.54	-99.09	7.45	-95.93	0.09 / 1.57
2015-05-23 / 18:52	7.40	-99.17	7.37	-96.29	0.03 / 0.52
mean	7.38	-99.28	7.30	-96.71	0.08 / 1.42
σ_{STD}	0.10	0.33	0.09	0.62	0.03 / 0.52
Δ (max - min)	0.32	0.99	0.28	1.77	0.08 / 1.39

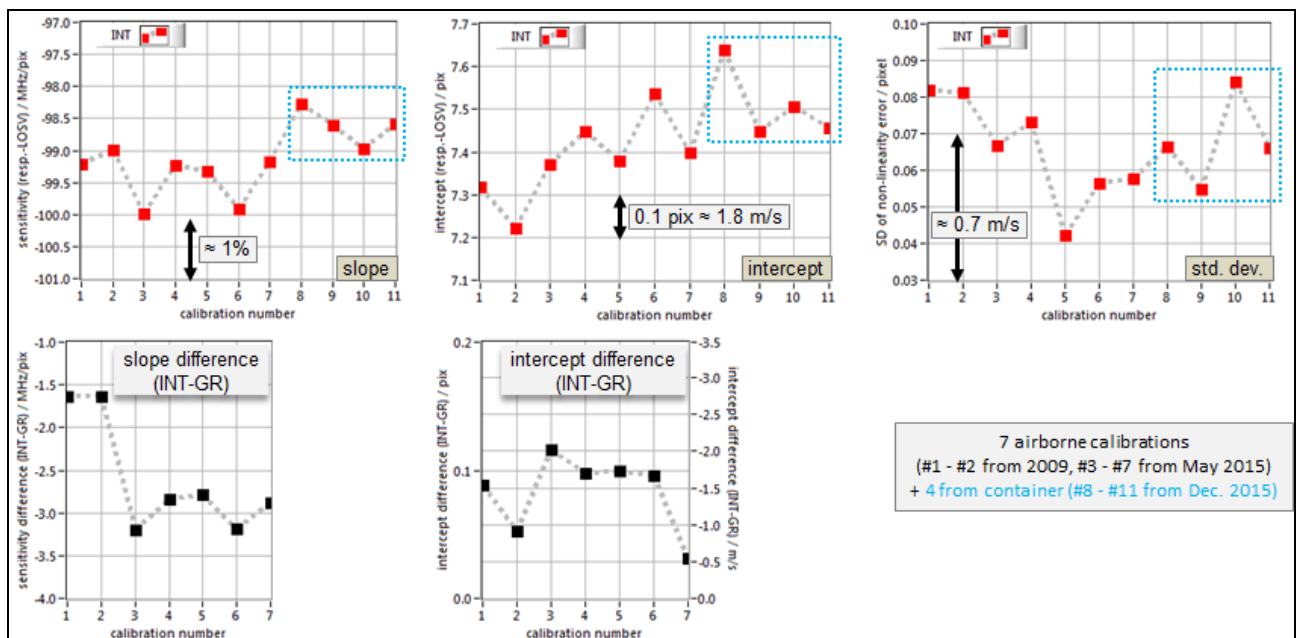


Figure 8-16: Comparison of slope, intercept and standard deviation of the non-linearity for the seven airborne as well as four ground based Mie Internal Reference response calibration curves (top, red). The differences for slope and intercept between the ground return and the Internal Reference response curves can only be derived for the airborne calibrations (bottom, black).

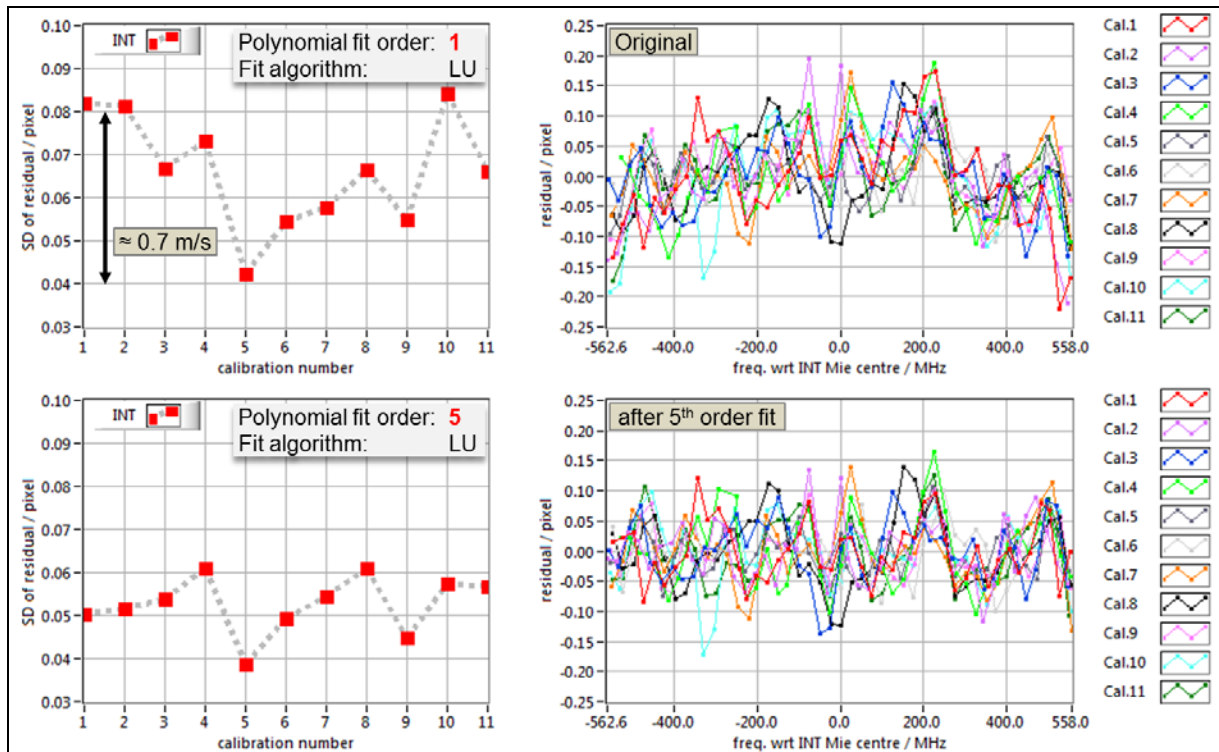


Figure 8-17: Comparison of Mie residuals derived from the Internal reference response calibration curves after subtraction of a polynomial fit of 5th order, plotted over frequencies measured by a wavemeter. The fit algorithm used the Gaussian LU (lower/upper) decomposition method.

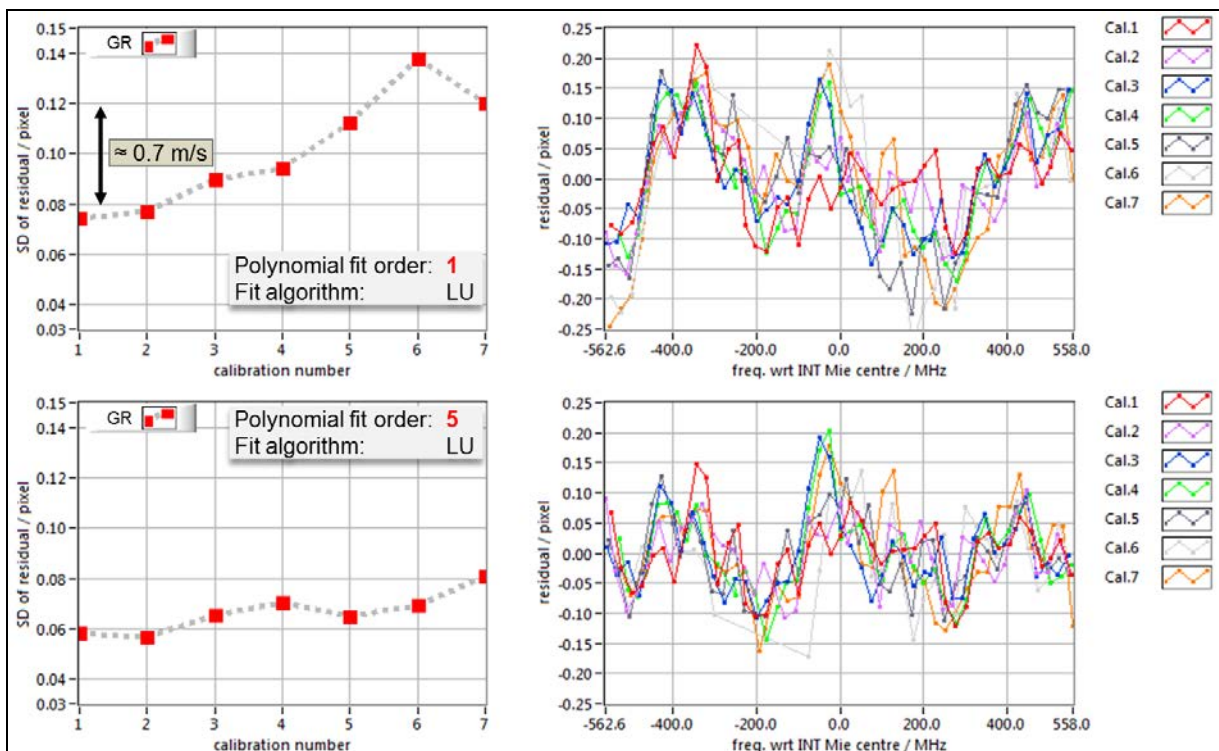


Figure 8-18: Comparison of Mie residuals derived from the ground return response calibration curves after subtraction of a polynomial fit of 5th order, plotted over frequencies measured by a wavemeter. The fit algorithm used the Gaussian LU (lower/upper) decomposition method.

A comparison in terms of slope, intercept and standard deviation of the non-linearity between airborne and ground based Internal Reference calibrations is shown in **Figure 8-16**. The four selected ground based calibrations were subsequently performed from the container at DLR in December 2015 and their characteristic match well with the airborne calibrations, consequently highlighting the good quality of the airborne calibrations in the Internal Reference in particular with respect to the standard deviation. A noticeable feature is the inconsistency of the slope differences between Internal Reference and ground return for the calibrations from 2009 compared to 2015, which might be explainable by the usage of a different reference position for the co-alignment and, thus, a different illumination of the MSP).

After the WindVal campaign the availability of now seven airborne calibrations finally allows substantiated statements regarding the behaviour of the Mie non-linearity in the A2D system. The graphs on the top of **Figure 8-17** and **Figure 8-18** give an impression of the coarse structure of the non-linearity (which is equal to the residual after a polynomial fit of 1st order, i.e. a straight line fit) of the Internal Reference and the ground return, respectively (see also **Figure 8-11** and **Figure 8-12**). On the bottom both figures show the structure of the residual after subtraction of a polynomial of 5th order. The standard deviations of the residuals plotted to the left of these four graphs decreases for all calibrations, even by up to ≈ 1 m/s for single calibrations. This confirms that the implementation of a procedure similar to what is done in the Rayleigh wind retrieval is likely to reduce the random error in the Mie winds. So far the polynomial fit is only performed here as a first test and is not yet implemented in the A2D Mie wind retrieval.

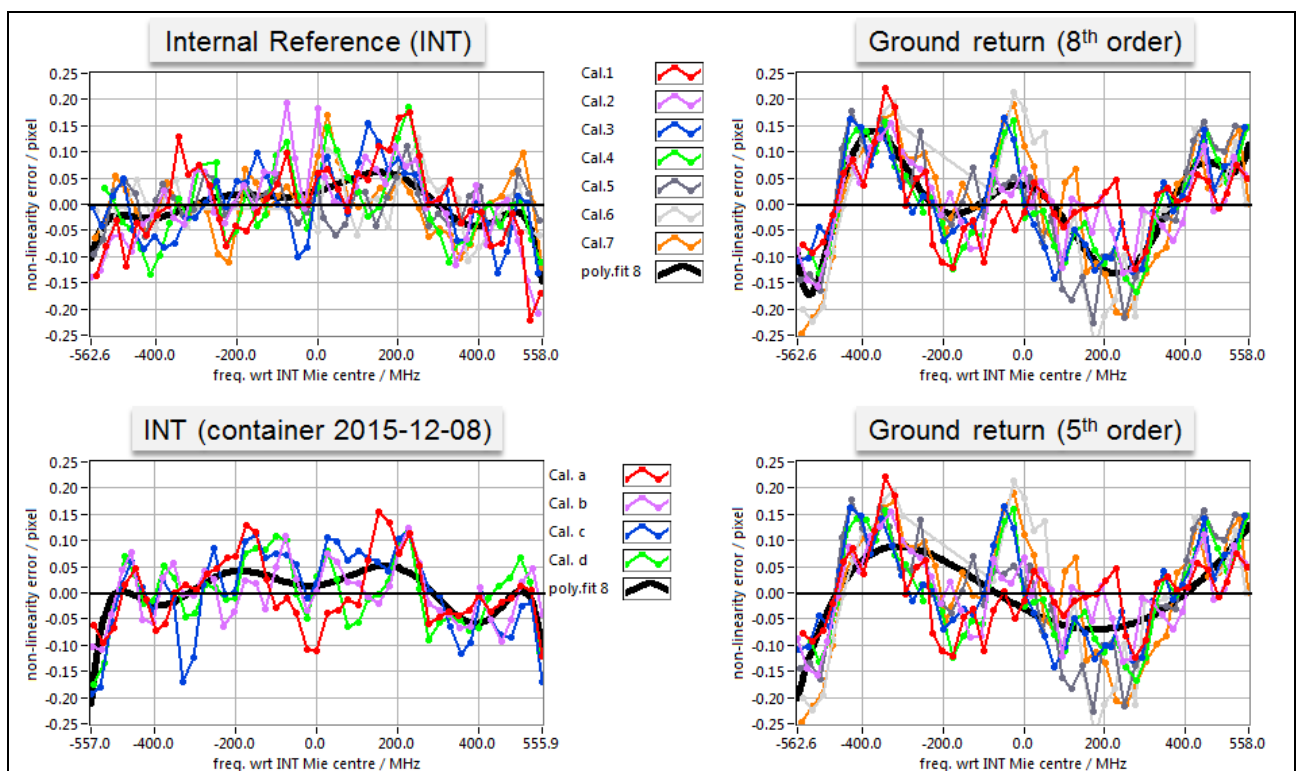


Figure 8-19: The shapes of Mie non-linearities as well as their polynomial fits of 8th order for the seven airborne calibrations for Internal Reference and ground return (top). For comparison the Internal Reference of four ground based response calibrations in 2015 (bottom left) and the polynomial fit of 5th order for the ground return (bottom right) are plotted.

Still a periodic structure is visible in the residuals after subtraction of a polynomial of 5th order, in particular for the ground return (**Figure 8-18**). Further test have shown that the accordance between non-linearity and polynomial increases with increasing fit order. As the right graphs in **Figure 8-19** show, a polynomial of 8th order traces the shape of the ground return non-linearity much better than one of 5th order. The bold black polynomials in the graphs constitute a mean polynomial considering the points of all non-linearities. For the Internal Reference of airborne and ground based calibrations the shapes of the polynomial fits of 8th order are very consistent. Regarding the available frequency interval for this scenario of roughly 1100 MHz in

conjunction with a pixel width of about 100 MHz a maximum polynomial order of 11 should be reasonable. This would potentially enable to include the modelling of the small scale pixilation effect in case this is visible at all.

In the past it was found to be disputable to reason why one calibration should be worse or better than another just by arguing with differences in intercept and slope. Thus, a new method has been developed to compare the various calibrations and to further improve the argumentation. Therefore, “virtual” wind speeds are computed not by introducing real measurements into the wind retrieval algorithm but by inserting a manually defined array of frequencies over the whole available calibration range, e.g. ± 550 MHz in uniform steps of e.g. 10 MHz. These imitate wind speed measurements from -98 m/s to +98 m/s in steps of about 1.8 m/s. Afterwards the “virtual” wind speeds derived from each calibration are mutually compared. Examples of the resulting differences in retrieved wind speed depending on the “actual” wind speed (i.e. the defined array of frequencies) are presented in **Figure 8-20** for calibration #3 - #7 (top) and #3 - #5 (bottom). The difference of the retrieved wind speeds (as the final result of the whole process using the response calibration curves) is displayed on the colour scale between ± 2 m/s, whereas the “actual” wind speed is plotted on the x-axis. The graph in **Figure 8-20** should be read as follows: Considering the conversion factor of 5.63 MHz / m/s (for LOS) a frequency offset with respect to the crosspoint of +100 MHz corresponds to a LOS wind speed of about 19 m/s. Running the wind retrieval algorithm twice, using two different calibrations but with the same input frequency of +100 MHz, will (almost everytime) result in two different wind speeds. In the case of calibration #3 and #7 (**Figure 8-20**, top, 4th row from bottom) these two wind speeds differ by roughly 1.5 m/s (orange), whereas almost no difference (green) is found between the wind speed retrieved for instance via calibration #4 and #5 (**Figure 8-20**, top, 5th row from bottom).

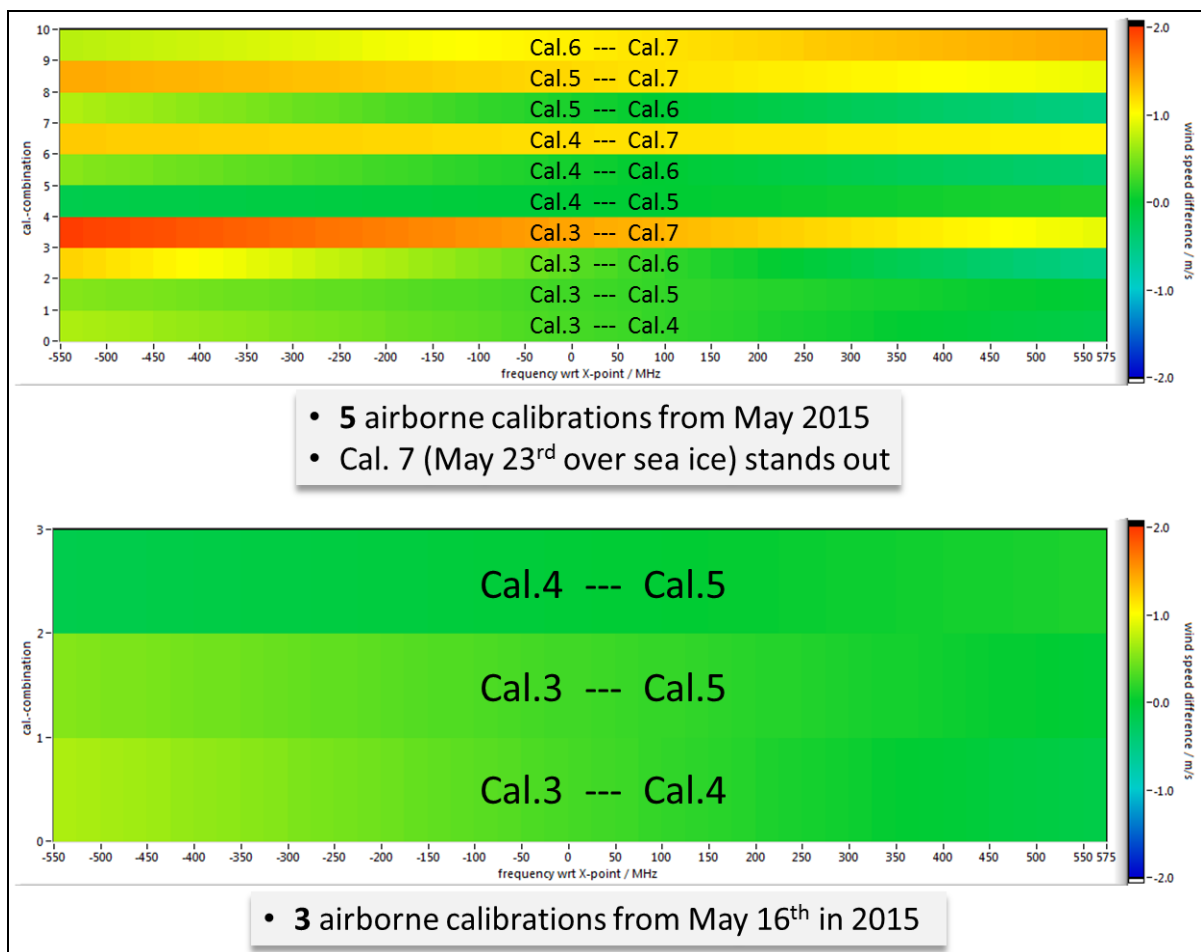


Figure 8-20: Simulated wind speed differences over a frequency range of ± 550 MHz with respect to the use of each two Mie response calibrations: for all airborne calibrations from the 2015 WindVal campaign (top) as well as for the three calibrations over the Greenland ice shield.

	Document Nr. FR.DLR.WindVal.270717	Issue: V1.1	Date: 27.07.2017	Page: 79/146	
	Doc. Title: WindVal Final Report				

Whereas by using calibrations #3, #4 or #5 in the wind retrieval one would obtain almost the same wind speeds (**Figure 8-20**, bottom) it is obvious that calibration #7 deviates from all the other calibrations (**Figure 8-20**, top). The question is, “why?” It is striking that calibration #7 also shows the lowest difference in intercept between the response curves of the Internal Reference and the ground return (**Table 8-2**). This difference is able to explain the average bias of about 1 m/s found in the simulated wind speeds (**Figure 8-19**, top). Since for the retrieval of Mie winds in general a single response curve is available only, which is derived from the ground return signal, one could assume that moving sea ice might have affected calibration #7. However, one would then also expect calibration #6 to be affected in the same way since both calibrations were performed in direct temporal sequence over the same area. For this analysis still the linear fits are used to calculate the Mie wind speeds, i.e. no polynomial fit. Future re-processings using polynomials might improve the results for calibration #7.

From **Figure 8-20** one can derive plot types as shown in **Figure 8-21**, **Figure 8-22** and **Figure 8-23**. The wind speed differences for all calibration combinations (10 in case of **Figure 8-20** top and 3 in case of **Figure 8-20** bottom) are considered per frequency step, deducing the minimum (green in **Figure 8-21** - **Figure 8-23**) and the maximum (red) absolute difference values as well as the mean (bold blue) and the standard deviation (black dotted) derived from these absolute differences. That means, the 10 absolute difference values available from **Figure 8-20** (top) at for instance 0 MHz result in single values for the absolute minimum (≈ 0.02 m/s), the absolute maximum (≈ 1.45 m/s), mean (0.64 m/s) and the standard deviation (0.45 m/s) which then became part of **Figure 8-21**. Repeating this procedure for all frequency steps and a selectable number of calibrations, results in the respective curves provided in **Figure 8-21** to **Figure 8-23**. It is noted that the above mentioned input array of frequencies is considered to be an ideal measurement and no quality control or corrections (e.g. aircraft attitude) need to be performed.

According to the comparison of all seven airborne calibrations (**Figure 8-21**) one can state that, depending on the actual wind speed measured, a mean difference (bold blue) between **0.6 – 1.0 m/s** can be expected on average when processing the **same** wind field with **two** calibrations **randomly** chosen among the seven. Whereas the range of ± 550 MHz corresponds to about ± 98 m/s, the usual LOS wind speeds measured by the A2D are rather between ± 25 m/s, being equivalent to about ± 140 MHz. Taking now into account only the 5 available airborne calibrations from the WindVal campaign in 2015, a mean difference between 0.5 – 0.7 m/s can be expected on average when processing the same wind field with 2 calibrations randomly chosen.

The uncertainty in measured wind speeds decreases even further when just looking at the three calibrations performed on May 16th (**Figure 8-20** bottom and **Figure 8-23**). Here one can expect a mean difference between 0.1 – 0.2 m/s for wind fields comprising a range of maximum ± 25 m/s. However, the meaning of the standard deviation in this case with only three members is questionable. It was decided to use calibration #3 for the processing of all Mie wind measurement scenes from the 2015 airborne campaign.

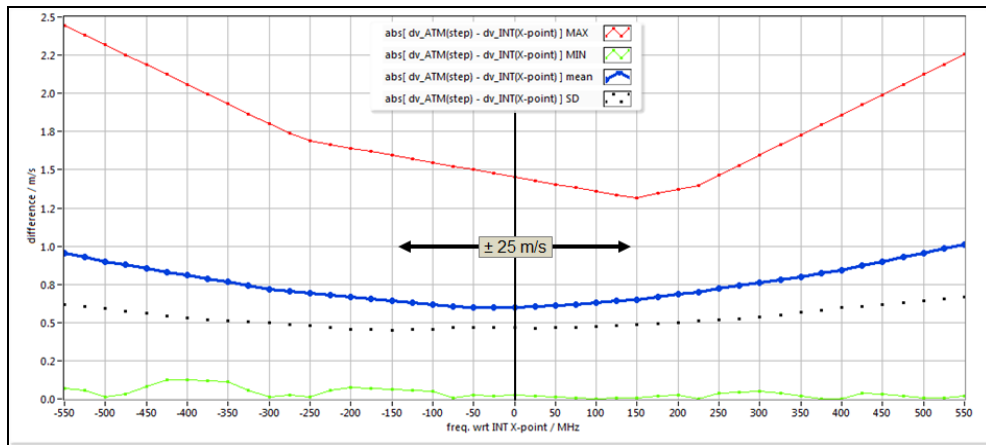


Figure 8-21: The average expectable Mie absolute wind speed differences over a range of ± 550 MHz (± 98 m/s) when using two randomly chosen response calibrations among the 7 available ones from 2009 and 2015 for wind retrieval. Maximum & minimum absolute difference values are marked in red & green, respectively, as well as the derived mean value in blue and the standard deviation in black.

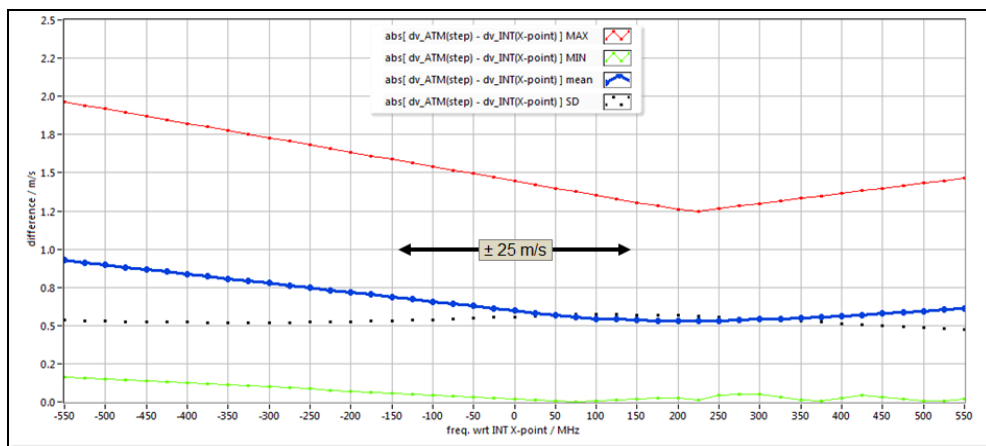


Figure 8-22: The average expectable Mie absolute wind speed differences over a range of ± 550 MHz (± 98 m/s) when using two randomly chosen response calibrations among the 5 available ones from the 2015 WindVal campaign for wind retrieval.

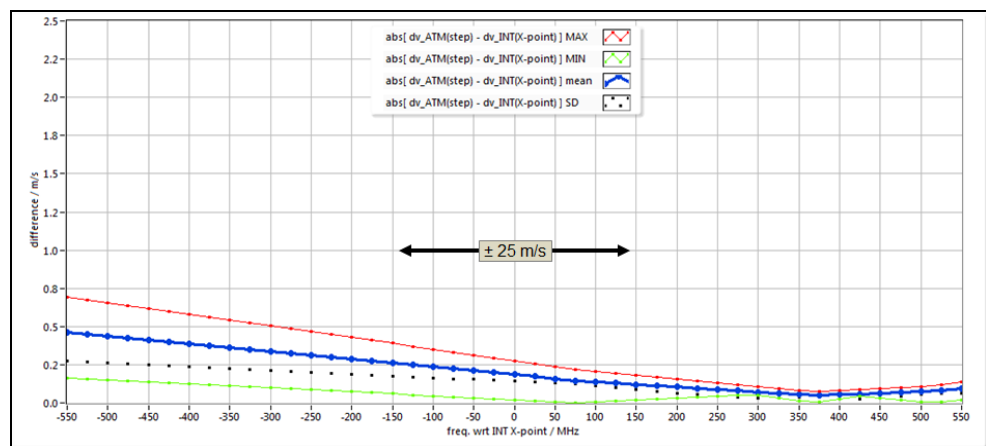


Figure 8-23: The average expectable Mie absolute wind speed differences over a range of ± 550 MHz (± 98 m/s) when using two randomly chosen response calibrations among the 3 ones available from May 16th in 2015 for wind retrieval.

8.5 Rayleigh response calibration

Pre-processing of the Rayleigh channel calibrations also comprises quality control steps as described in ch.8.3 and DLR (2012b). The resulting response curves are presented for two selected calibrations, for the first calibration from September 21st in 2009 (**Figure 8-24**) and the first one from May 16th in 2015 (**Figure 8-25**). The Internal Reference is marked by a fat dotted red line that shows a flatter slope than the curves of the atmospheric range-gates #5 - #19. Both calibrations were performed over the Greenland iceshield. The ground return signals have not been summed yet for these graphs. Instead one can see the single response curves indicated by a fat brown line (range-gate #20) and a fat dashed orange line (range-gate #21). Especially the brown curves exhibit a slope similar to the one of the Internal Reference. As can be seen from **Figure 8-2** the range-gates #22 - #24 are located below the ground.

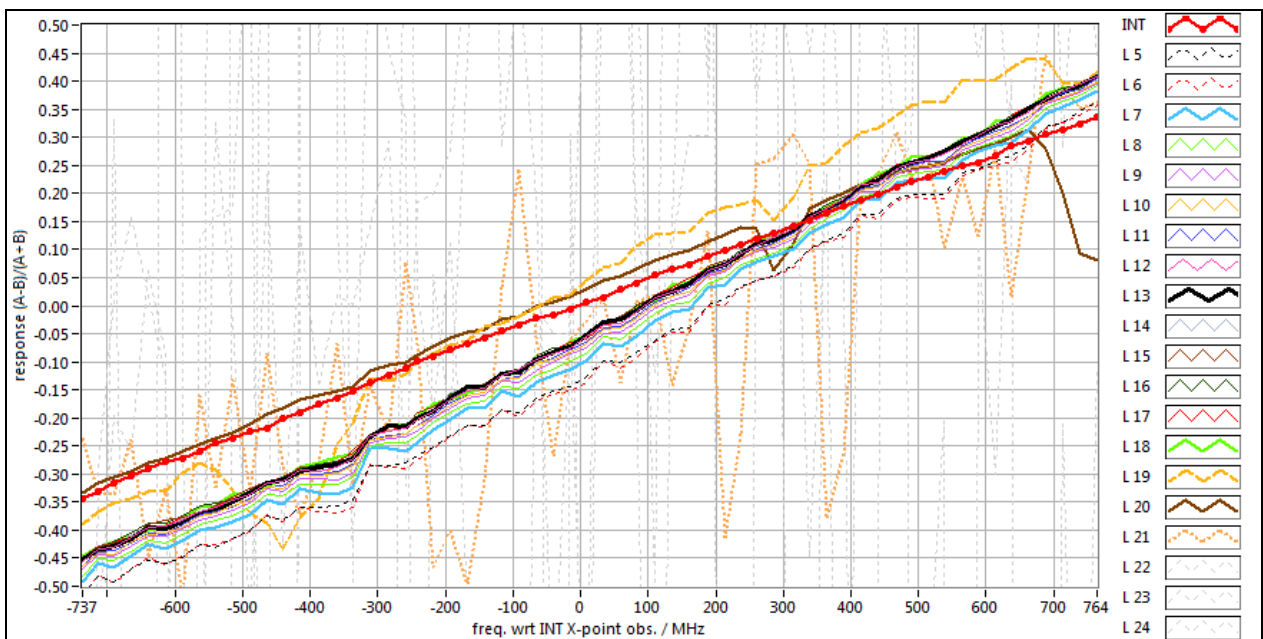


Figure 8-24: Rayleigh response curves for the first airborne calibration on September 21st in 2009.

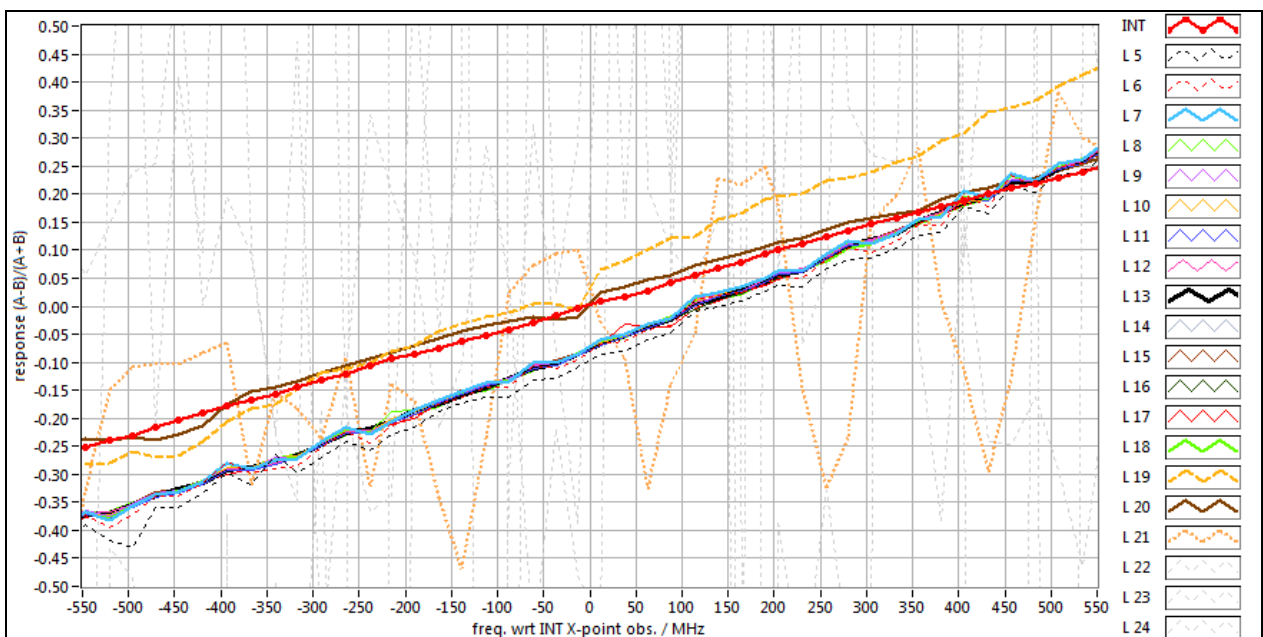


Figure 8-25: Rayleigh response curves for the first airborne calibration on May 16th in 2015.

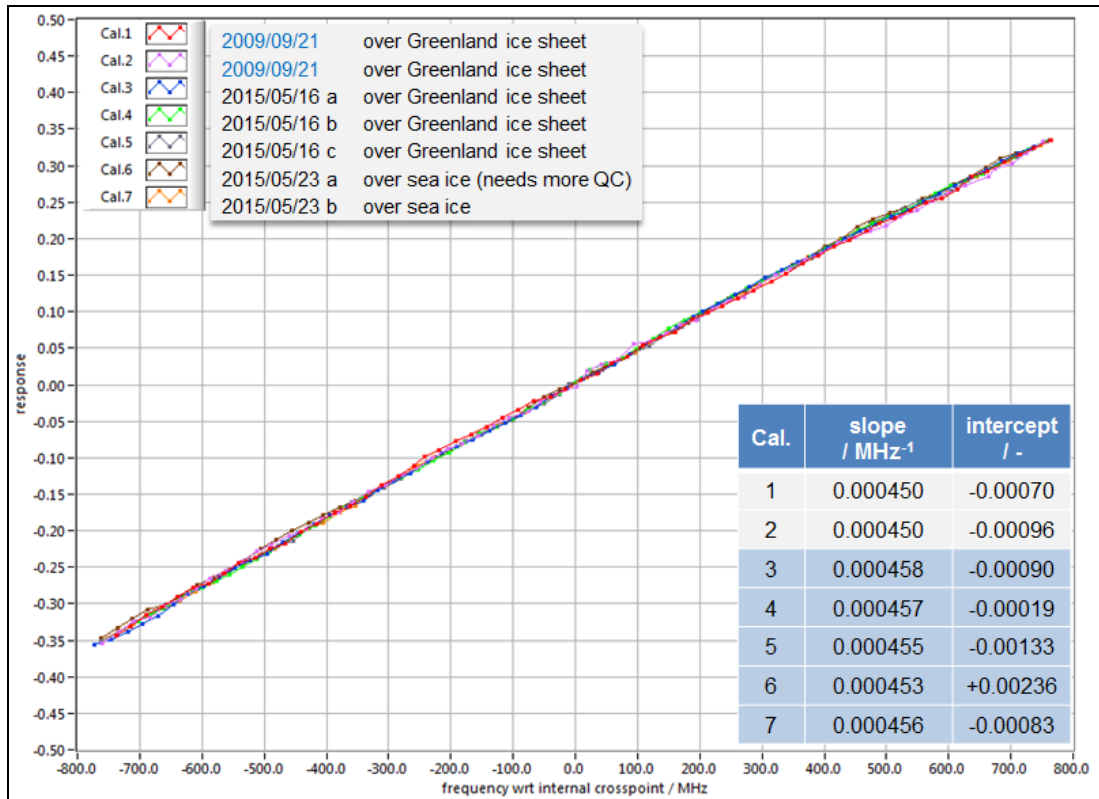


Figure 8-26: Rayleigh response curves for the Internal Reference of all seven airborne calibrations plotted over frequencies measured by the wavemeter.

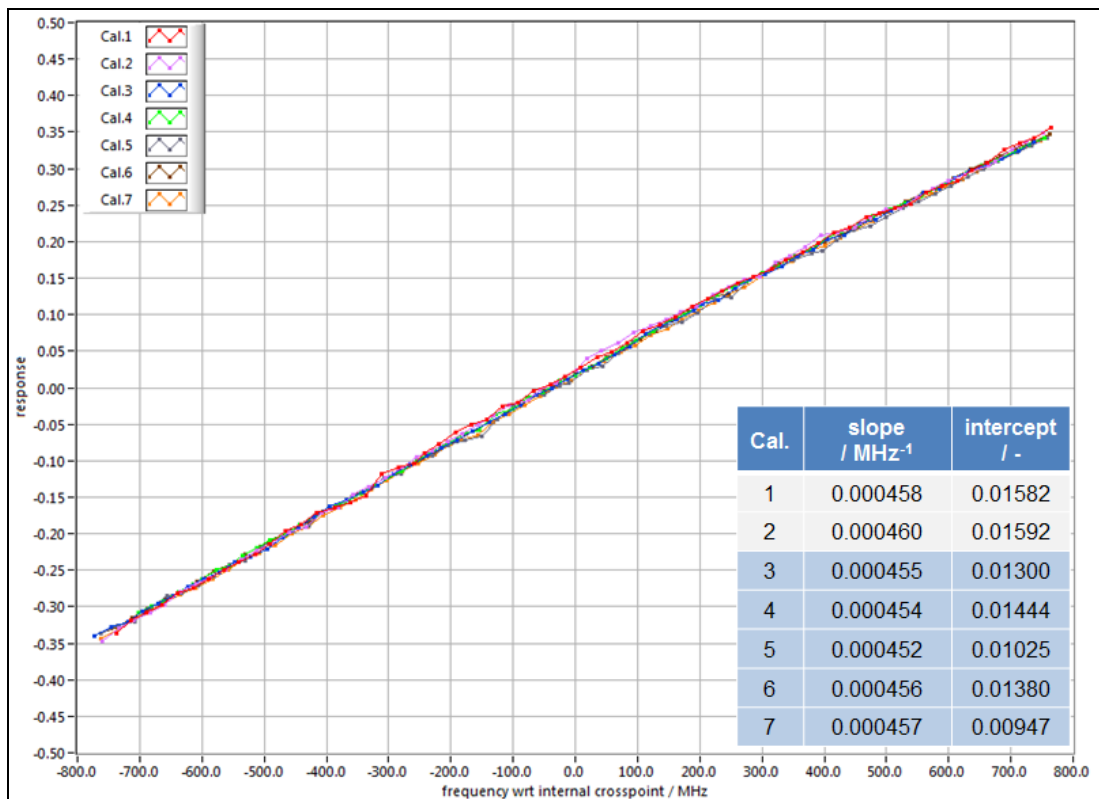


Figure 8-27: Rayleigh response curves for the ground return of all seven airborne calibrations plotted over frequencies measured by the wavemeter.

The zig-zag behavior of L19 - L21 in **Figure 8-24** and **Figure 8-25** is caused by the distribution of ground return signal over several range-gates within an observation (≈ 3 km horizontal accumulation during 14 s) in connection with range-gate overlap and instrument imperfections (shifted Rayleigh spot positions). Although hardly visible in intensity plots, L21 still contains a small share of the ground signal from time to time.

The striking difference between **Figure 8-24** and **Figure 8-25** is the spread in intercept of the atmospheric range-gates. The first and also the second calibration from 2009 show an intercept that increases from about -0.15 for range-gate #5 to about -0.05 for roughly range-gate #11. This behavior is related to the overlap effect of transmit and receive path which in turn is connected to the selected reference position (**Table 8-1**). In contrast, the corresponding intercepts in **Figure 8-25**, and in general for all the calibrations from 2015, scatter much less and show a mean intercept of about -0.07 for the atmospheric range-gates (disregarding range-gate #5 and #6).

For all seven airborne calibrations **Figure 8-26**, **Figure 8-27** and **Figure 8-28** show the response curves of the Internal Reference, the ground return and the atmospheric range-gate #17, respectively. All calibrations have been evaluated over the same frequency range of ± 750 MHz (corresponding to about ± 135 m/s) around the crosspoint and the resulting polynomials are used for the wind retrieval. Due to the high signal to noise ratio the curves for the Internal Reference are very closely spaced compared to the atmospheric response curves. Also for the ground return the response curves can hardly be distinguished. The spread in the atmospheric curves can be attributed to a low signal to noise ratio but also to the fact that the atmospheric conditions (e.g. pressure, temperature, aerosol content) were different at the time each of the calibrations was performed. Another main contributor to the differences in intercept between 2009 (**Figure 8-28** red, pink) and 2015 is the difference of the co-alignment. Additionally, the vertical thickness of range-gate #17 is only 315 m for calibration #1 - #5 but 630 m for calibrations #6 and #7. Finally, there is also a difference in the distance of the range-gates from the instrument and their altitude above sea level which might account for some of the variability in the comparison of the response curves. Hence, the center of range-gate #17 is located between 5.8 km (e.g. calibration #3 & #4) and 7.9 km (calibration #6 and #7) below the aircraft (**Figure 8-2**).

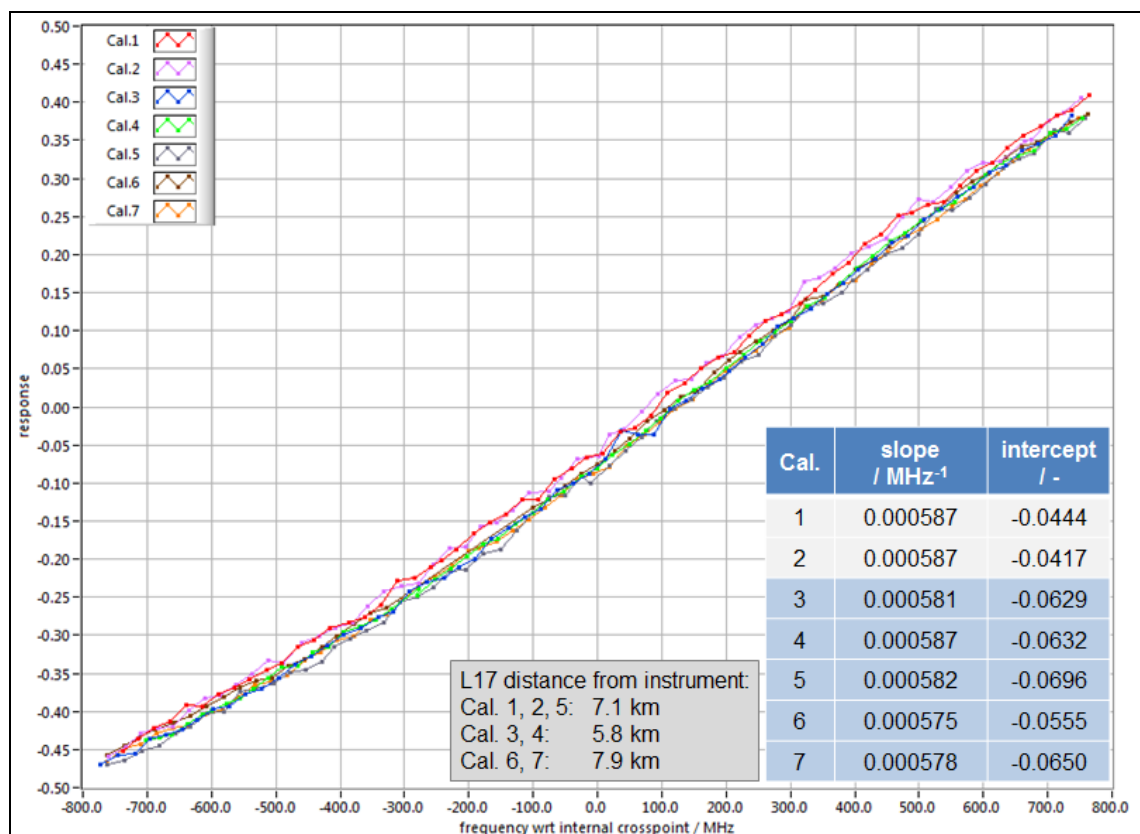


Figure 8-28: Rayleigh response curves for the atmospheric range-gate #17 of all seven airborne calibrations plotted over frequencies measured by the wavemeter.

	Document Nr. FR.DLR.WindVal.270717	Issue: V1.1	Date: 27.07.2017	Page: 84/146	
	Doc. Title: WindVal Final Report				

As for the Mie channel the non-linearities are also monitored for the Rayleigh channel. A comparison of non-linearities along with the respective polynomial fits for the Internal References of all seven airborne calibrations can be seen in **Figure 8-29**. The data is displayed over a frequency interval of roughly ± 750 MHz being equivalent to ± 133 m/s. Neglecting the non-linearity correction of the Internal Reference during the wind retrieval can introduce a systematic offset in the resulting LOS winds of up to 2 m/s depending on the applied response calibration.

The comparison of non-linearities and polynomial fits for the atmospheric range-gate #16 (INT=4) is presented in **Figure 8-30**, left. The shapes of the polynomial fits are each very similar for both, the Internal Reference and the atmospheric calibrations. Depending on the actual wind speed systematic errors of up to 6 m/s can be introduced to the resulting LOS winds if the non-linearity correction of the atmospheric range-gate is neglected during wind retrieval. For wind speeds around 0 m/s one could in that case expect a bias of around 5 m/s whereas no bias would be introduced for wind speeds of about 50 m/s or -85 m/s.

On the right side of **Figure 8-30** the standard deviation of the measured residual error around the 5th order polynomial fit is shown for all range-gates including the Internal Reference at the top at 0 km distance from the instrument. This standard deviation of these calibrations is closely related to the expectable minimum random error of the resulting wind speed measurements. The standard deviations from an analysis of four ground based calibration from December 8th in 2015 have been included as fat grey lines on the right graph in **Figure 8-30**. Since these ground based calibrations are of excellent quality this comparison proves that the A2D performed very well during the airborne calibrations of the WindVal campaign in 2015. The Internal Reference exhibits the lowest standard deviation and its values vary from 0.0013 to 0.0029 depending on the calibration. Minimum values of ≈ 0.0035 are reached for atmospheric range-gates of calibration #3, #4, #6 and #7, together with the ground based calibrations at medium distances of 5.5 km from the instrument. The spread of the curves decreases from top to bottom. Apart from the overlap region in the first 2-3 km the spread is in the order of 7 MHz which is equivalent to about 1.3 m/s. At the same time also the average SD for the biggest part of the atmospheric region (between 4 – 10 km away from the instrument) is about 7 MHz or 1.3 m/s. Starting from below 6 km the data of the calibrations performed over the Greenland iceshield become invalid whereas the two calibrations over sea ice (orange, brown) reach down to 10 km distance from the instrument. The standard deviation can be used as a quality criterion to detect single range-gates or even whole calibrations of low quality. Location and time of the A2D airborne calibrations have always been chosen with great care in order to obtain Rayleigh responses from clear atmosphere. Nevertheless degradation might occur in future, either unexpectedly or obviously, e.g. by contamination due to clouds or aerosol, where affected measurements could not be removed completely by quality control. Despite the interruption of calibration #6 due to a co-alignment error and manual intervention accompanied by a loss of 7 observations, the results in terms of Rayleigh non-linearity and standard deviation of the residual error are still fairly good after quality control.

The standard deviation on the right side of **Figure 8-30** also depends on the range-gate thickness, i.e. the integration time. Regarding the magnitude of the standard deviation the airborne calibrations could be sorted into a group with smaller (#3, #4, #6 and #7) and higher standard deviation (#1, #2 and #5), mainly visible between distances of 1.5 to 5.5 km. An increased standard deviation of calibration #1 and #2 could be explained for example by different reference positions in terms of pointing used in 2009 compared to 2015. However, this does not hold for calibration #5, which in addition shares the same sampling grid resolution as calibrations #6 and #7 for the first 14 range-gates. It is unknown why the standard deviation of calibration #5 is increased.

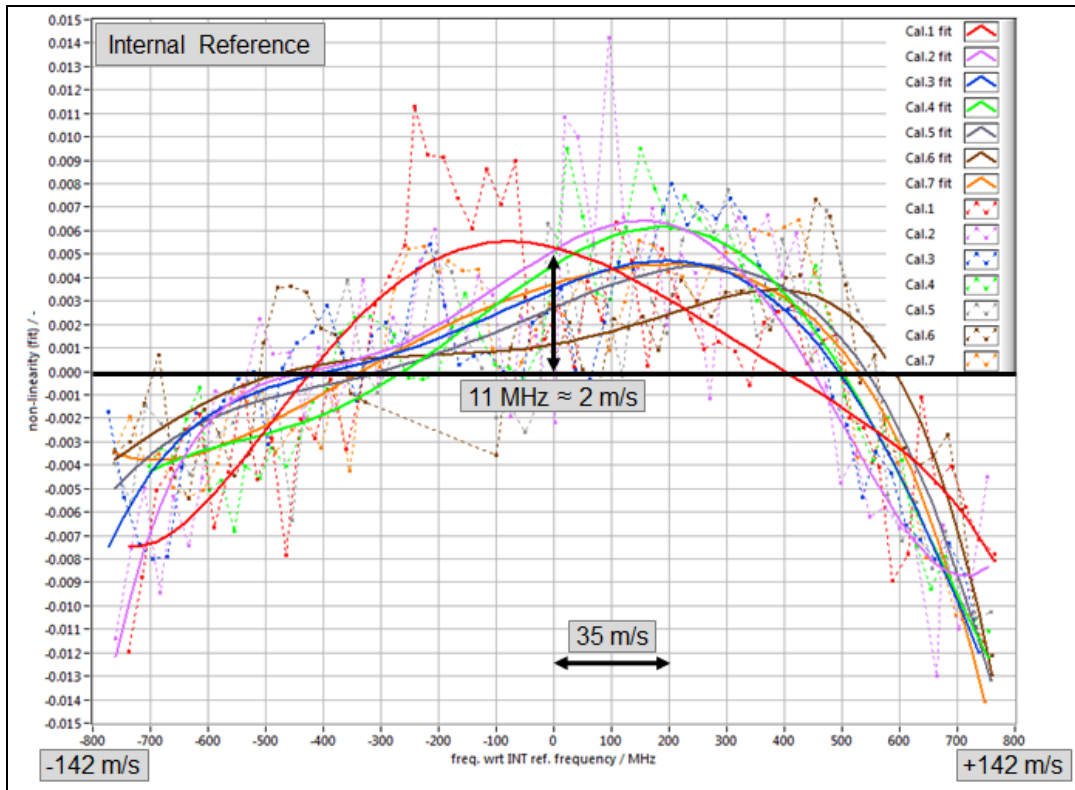


Figure 8-29: Comparison of Rayleigh non-linearities and polynomial fits of 5th order for the Internal Reference signals obtained during the seven airborne calibrations from 2009 and 2015. A frequency shift of ± 800 MHz would correspond to ± 142 m/s LOS wind speed.

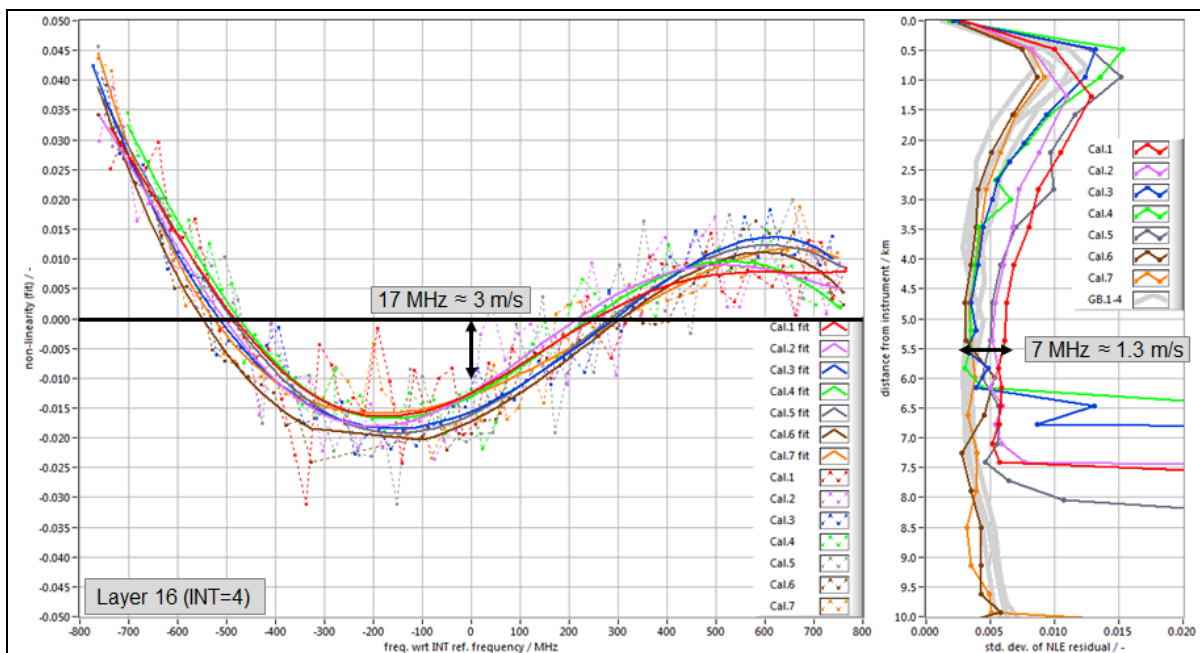


Figure 8-30: Left: Comparison of Rayleigh non-linearities and polynomial fits of 5th order for the signals of atmospheric range-gate #16 obtained during the seven airborne calibrations from 2009 and 2015. Right: The residual error of the measured responses around the polynomial fits for each range-gate and calibration. The fat grey curves refer to four ground based (GB) calibrations obtained on December 8th in 2015.

	Document Nr. FR.DLR.WindVal.270717	Issue: V1.1	Date: 27.07.2017	Page: 86/146	
	Doc. Title: WindVal Final Report				

Figure 8-31 presents intercept and slope profiles as derived from linear fits through the response calibration curves per range-gate. These parameters are usually considered for argumentations regarding the differences between two calibrations and respective wind fields. All profiles for both, slope and intercept, are plotted versus altitude with respect to the instrument. This allows a visually easier comparison of the curves shapes for example in terms of the overlap region. One can see that the atmospheric slopes vary within 3% from 0.057 %/MHz (Cal- #6 and #7 close to the ground) to 0.060 %/MHz (Cal. #2 in the overlap region) which is most likely caused by a combination of different reference positions for the co-alignment, pointing variation and atmospheric effects such as temperature differences or unperfectly removed influences of clouds and aerosols. In contrast, the slopes of the Internal References vary by only about 1.7% between 0.000450/MHz and 0.000458/MHz (see also **Figure 8-26**) which is almost equal to the spread of the ground return curves with values between 0.000452/MHz and 0.000460/MHz (**Figure 8-27**). These slope variations have to be viewed in the context of the ADM requirement of a wind speed dependent error of less than 0.7%.

The intercepts (**Figure 8-31** bottom) of the Internal Reference curves gather between -0.00133 and -0.00019 (**Figure 8-26**, disregarding calibration #6) and between 0.00947 and 0.01592 (**Figure 8-27**) for the ground return. Calibrations that were obtained at the same location and close in time exhibit very similar profile shapes, for example the slopes of calibration #6 and #7 or the intercepts of calibration #3 and #4 as well as #1 and #2. In terms of intercepts one would expect a congruent behavior also for calibration #6 and #7. However, this is not the case because 7 observations had to be deleted from the response curve of calibration #6 between -300 MHz to -100 MHz (**Figure 8-30**) resulting in a “lift” of the intercept towards positive values while keeping a more or less reasonable slope (see table in **Figure 8-28**).

Taking into account only the intercept profiles one could argue that calibration #5 (despite the same location) deviates from calibrations #3 and #4, for example due to the difference of almost 5 hours in acquisition time. However, in terms of slope profile calibration #5 agrees much more with calibration #3 than calibration #4 does. This shows that solely considering the two parameters slope and intercept is not sufficient anymore when attempting to explain such small differences between calibrations. Therefore also the additional orders of the polynomial fit have to be considered, for what the new method presented in **Figure 8-20** and **Figure 8-32** to **Figure 8-34** can be applied.

The same concept as presented for the Mie channel along with **Figure 8-20** to **Figure 8-23** applies for **Figure 8-32** to **Figure 8-34** which describe the variability inherent to the airborne Rayleigh response calibrations. The simulated wind speed differences for all combinations of the considered calibrations (10 in case of **Figure 8-33**, equivalent to **Figure 8-20** top) are taken into account per frequency step, deducing the minimum (green in **Figure 8-32** to **Figure 8-34**) and the maximum (red) difference as well as the mean (bold blue) and the standard deviation (black dotted) over the differences. According to the comparison of all seven airborne calibrations from 2015 (**Figure 8-32**) one can state that, depending on the actually measured wind speed, a mean difference (bold blue) between **1.7 – 4.0 m/s** can be expected on average when processing the **same** wind field with **two** calibrations **randomly** chosen among these seven. Whereas the range of ± 750 MHz corresponds to about ± 133 m/s, the usual LOS wind speeds measured by the A2D are rather between ± 25 m/s, being equivalent to about ± 140 MHz. Considering only the five airborne calibrations from 2015 (**Figure 8-33**) an expectable mean difference of 1.2 m/s – 1.5 m/s remains within a reasonable wind speed range of ± 25 m/s, i.e. ± 140 MHz. Finally, disregarding the inaccurate calibration #6 the mean difference goes down to 0.8 m/s to 1.1 m/s (**Figure 8-34**). However, the meaning of the standard deviation in this case with only four members is questionable. It was decided to use calibration #7 for the processing of all Rayleigh wind measurement scenes from the 2015 airborne campaign. The results presented in **Figure 8-32** to **Figure 8-34** are an example for range-gate #15. Performing the same comparison for other atmospheric range-gates yields different values which are in the same order of magnitude though. Comparisons of calibrations #3, #4, #5 and #7 (**Figure 8-34**) suggest mean differences of 2.3 m/s for range-gate #6, 1.1 m/s for range-gate #10 and 1.0 m/s for range-gate #18. The decrease with distance from the instrument strongly points towards the telescope overlap affecting the precision of the wind measurements.

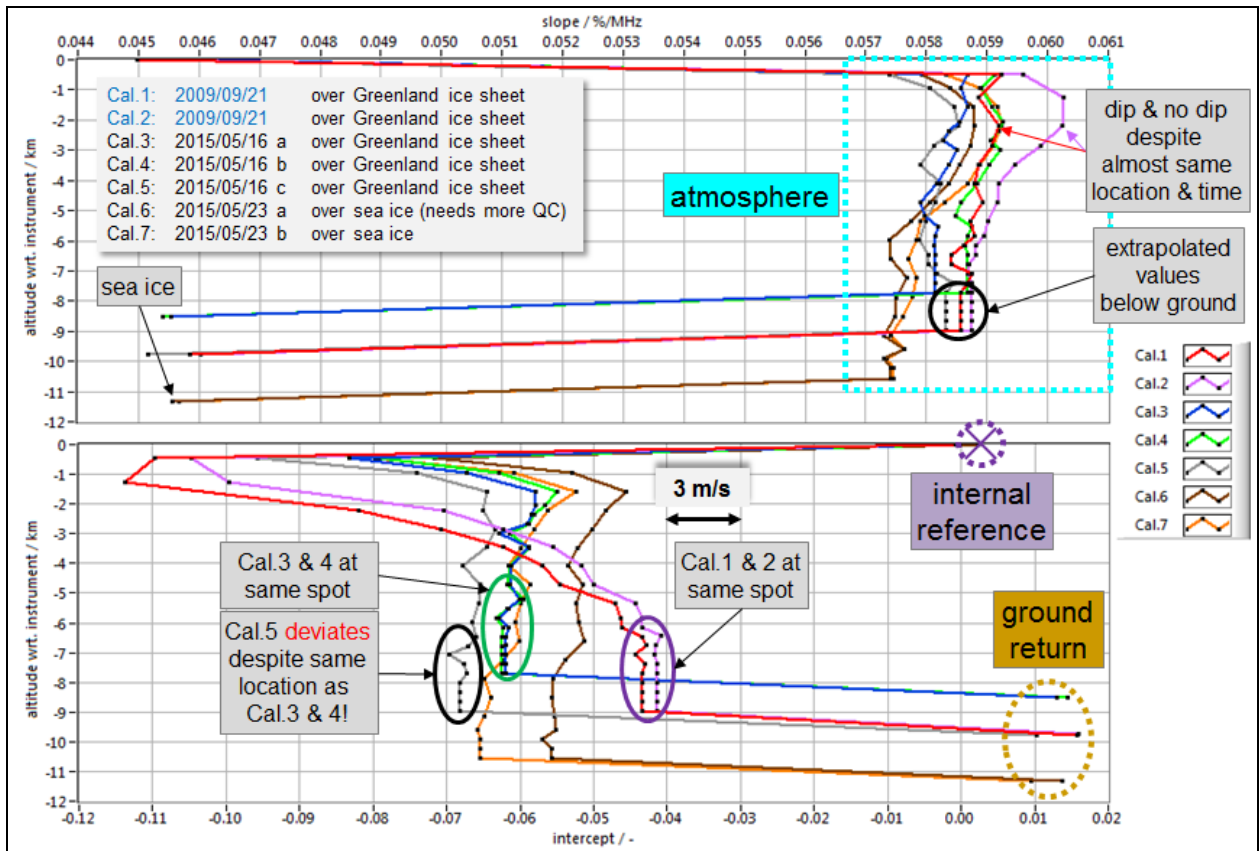


Figure 8-31: Profiles of intercept (top) and slope (bottom) for all airborne calibrations.

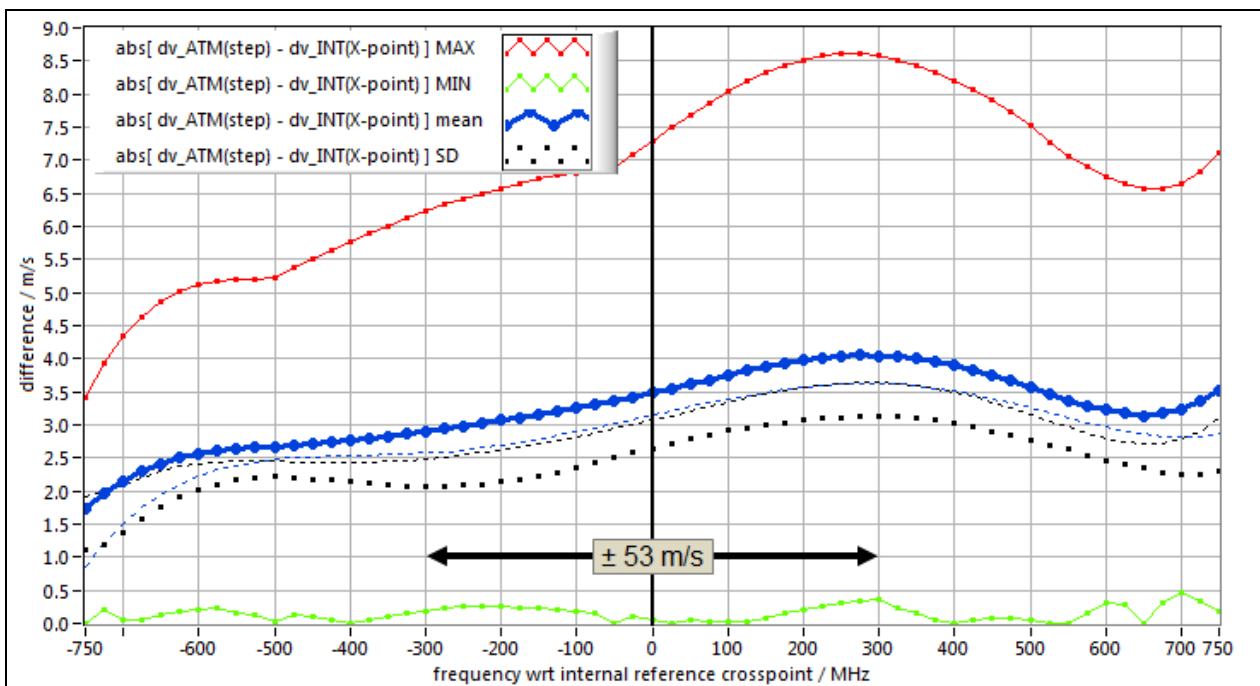


Figure 8-32: The average expectable Rayleigh wind speed differences in range-gate #15 over a range of ± 750 MHz (± 133 m/s) when using two randomly chosen response calibrations among the seven available ones from 2009 and 2015 for wind retrieval. Maximum and minimum differences are marked in red and green, respectively, as well as the mean value in blue and the standard deviation in black.

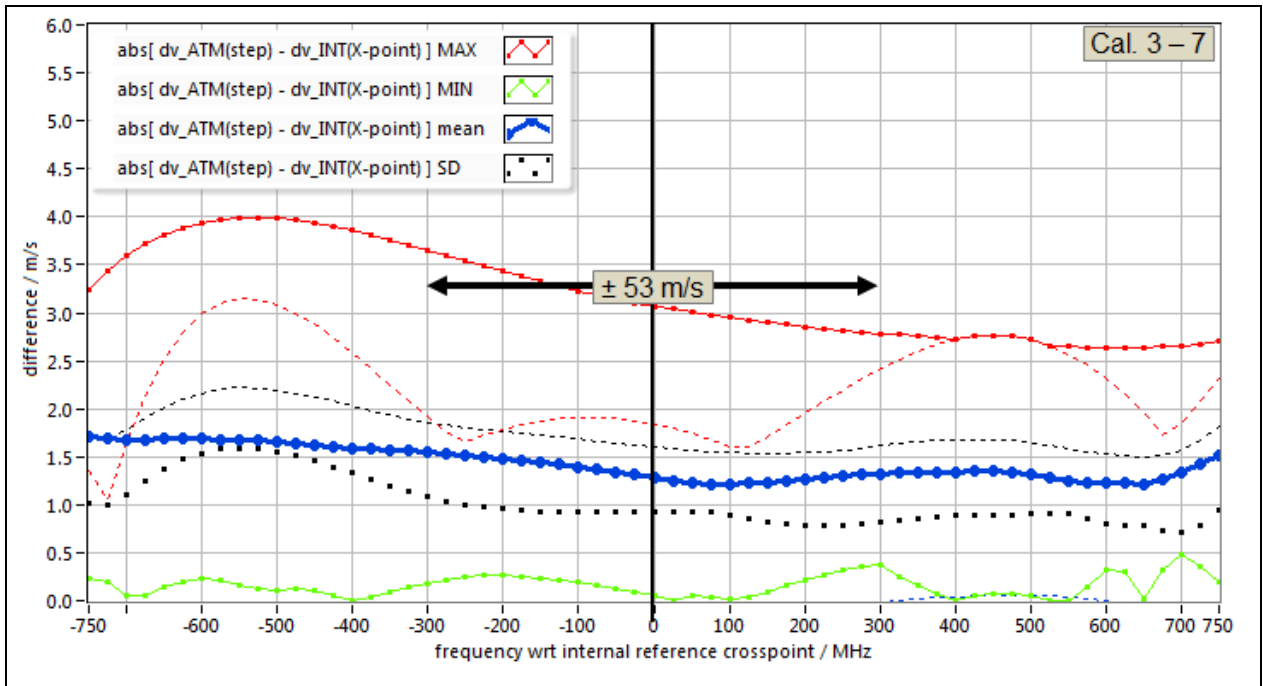


Figure 8-33: The average expectable Rayleigh wind speed differences in range-gate #15 over a range of ± 750 MHz (± 133 m/s) when using two randomly chosen response calibrations among the five available ones from the 2015 WindVal campaign for wind retrieval.

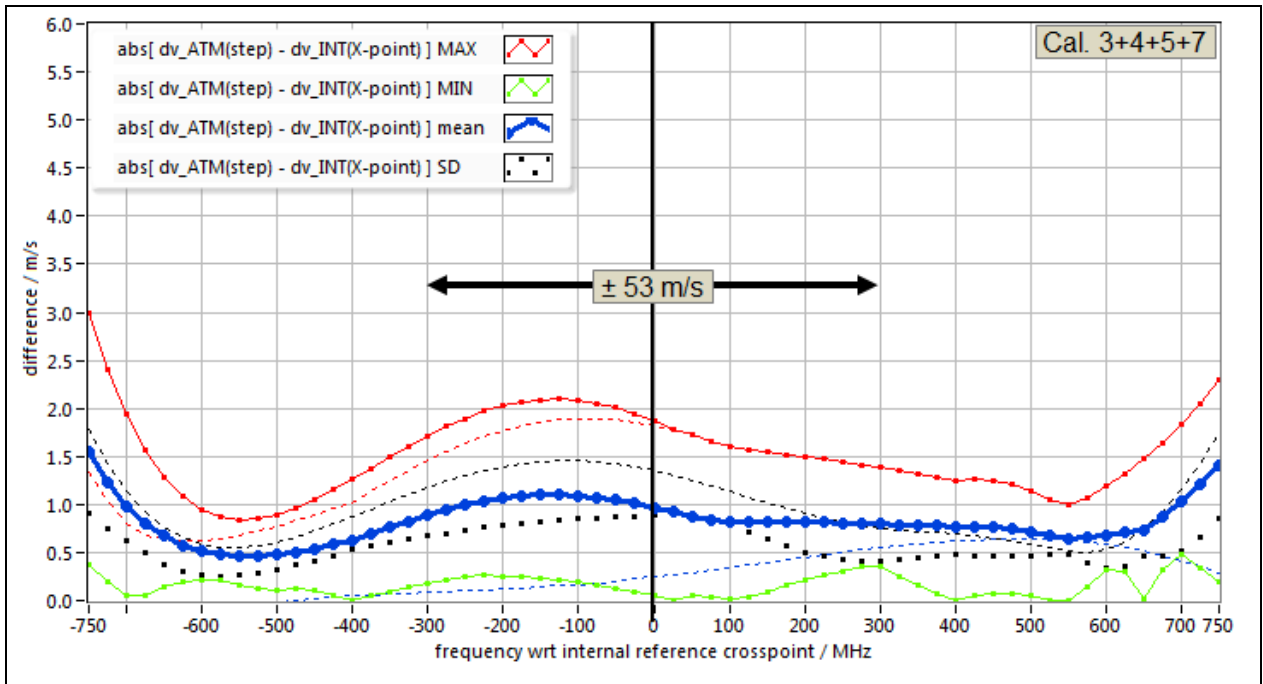


Figure 8-34: The average expectable Rayleigh wind speed differences in range-gate #15 over a range of ± 750 MHz (± 133 m/s) when using two randomly chosen response calibrations among the ones available from WindVal, except calibration #6, for wind retrieval.

	Document Nr. FR.DLR.WindVal.270717	Issue: V1.1	Date: 27.07.2017	Page: 89/146	
	Doc. Title: WindVal Final Report				

8.6 Summary

The WindVal campaign provided a large number of wind measurement scenes and five response calibrations and has in this respect been much more productive than the airborne campaign from 2009. An overview of time, location and performance of the airborne calibrations has been given with a detailed view into the parameters of the quality control process.

The WindVal campaign has largely contributed to the improvement of the A2D processor, specifically in terms of quality control. The 6th calibration, which was interrupted by a failing co-alignment loop, could be evaluated for the Rayleigh and the Mie channel. Finally, with now 7 airborne response calibrations, substantiated statements are possible regarding many parameters (of the A2D system) such as the behaviour of the Mie non-linearity, the stability of the Rayleigh and Mie response curves and others.

All 7 airborne calibrations (2009+2015) show similar intercepts and slopes for Mie channel. However, for unknown reasons the 7th airborne calibration stands out from the others regarding its minimal difference in intercept between Internal Reference and Ground Return.

The non-linearities of Mie Internal Reference and ground return show similar structures and it has been shown that the Mie non-linearity is suitable for a polynomial fit procedure that reduces the random error in the Mie winds. So far the polynomial fit is only performed here as a first test and is not yet implemented in the A2D Mie wind retrieval. Considering the 5 airborne calibrations from 2015, their different properties pass down an unknown wind speed dependent mean bias of 0.5 m/s – 0.7 m/s to the actual wind measurement.

The Rayleigh response calibrations have been evaluated for the Internal Reference, the atmospheric range-gates and the ground return. Slopes, intercepts, non-linearities and residuals have been compared. Regarding the residuals it was shown that the airborne calibrations are of high quality almost comparable to that of four very accurate ground based calibrations from December 2015. Considering only calibrations #3, #4, #5 and #7, their different properties pass down an unknown wind speed dependent mean bias of 0.6 m/s – 1.1 m/s to the actual wind measurement.

For the wind retrieval it was decided to use calibration #7 for the Rayleigh channel and #3 for the Mie channel. The main driver for the selection for the Rayleigh channel in this case was the vertical coverage. Regarding the Mie channel one could have also chosen calibration #4 instead of #3. With frequency drift, CoG outliers and occurrences of emergency triggers both have minor issues (**Table 8-1**). However, these have been accounted for by quality control and by using the knowledge from wavemeter measurements. It is emphasized here that for this study it is non-essential to use the presumably best calibration but to consistently use only a single calibration to process all the wind scenes. Thereby one can exclude the influence of different calibrations as a reason for different performances of the A2D in different wind measurement scenes.

Regarding the Rayleigh channel, calibration #6 is not considered to be of good quality. Its response curve looks more or less accidentally similar to calibrations #3 - #5 because the removed observations occurred at a favourable position for the polynomial fit. If observations would have been removed at other positions within the calibration range, then a different fit would result. As mentioned above, the intercept of the fit can be very sensitive in terms of aggregated missing calibration steps, which has been found to be the weakness of calibration #6. Instead, the parameters of calibration #6 might have likely resembled those of #7 if all frequency steps were available.

After having taken into account all available housekeeping data and having performed the presently implemented quality control steps, the resulting Rayleigh and Mie response curves still differ. These differences are due to unavoidable noise and unknown error sources as well as known effects that have not been corrected for. Regarding the A2D there are only a few parameters left to assess or distinguish the quality of the final response calibrations curves at the moment. One of these parameters is for instance the standard deviation of the residual error (**Figure 8-30**, right). Apart from that mainly the overall flight and instrument conditions during the performance of the calibration are consulted to finally decide about the usage of a specific calibration. Thus, the major remaining difficulty will be to define what constitutes a high quality calibration and to decide which among the selected high quality calibrations is suited best to a specific wind measurement scene. Another approach could be to derive a “mean” calibration from all calibrations that passed the quality control. This could possibly be enhanced by restricting the selection only to calibrations from a certain time window (e.g. the last few weeks for Aeolus) in order to consider potential

	Document Nr. FR.DLR.WindVal.270717	Issue: V1.1	Date: 27.07.2017	Page: 90/146	
	Doc. Title: WindVal Final Report				

long term drifts of the satellite structure or instrument. Also one could look for possibly existing aggregations of certain calibration parameters (intercept, slope, etc.), group these calibrations and maybe derive “mean” calibrations from these groups, which in turn can be compared in terms of their resulting wind retrieval performance. In any case the statistical distribution of calibration parameters for the A2D will very likely differ from those for Aeolus, simply caused by the different instrument set-up (e.g. near vs. far field wind measurements, telescope overlap, etc.) and environments (e.g. vibrations).

It is not clear why the overall shape of the Mie non-linearities of the internal reference (**Figure 8-11**) consistently differs from those of the ground return (**Figure 8-12**). Further investigation, for instance on the WindVal II dataset, is needed to confirm current or create new ideas for an explanation. One reason could be the influence of the molecular background from the remaining atmospheric column of the ground return range-gate due to the non-correction of the ground return signal by a MOUSR procedure. The difference between internal and atmospheric path non-linearities for the MRC should be studied with using the End-to-End Simulator (E2S).

8.7 Recommendations

Considering the profiles of the standard deviation of the residual error (**Figure 8-30** right), an assessment for the Rayleigh atmospheric calibrations as performed for **Figure 8-32** to **Figure 8-34** should better be done with respect to distance from instrument instead of range-gate number (**Figure 8-2**) in future. However, such dependencies are not expected for ADM.

Currently, the non-linearity is not considered in the A2D Mie wind retrieval. Similar to the procedure in the Rayleigh channel it was shown that adequate polynomial fit improve the random error of Mie winds. Consequently, such fits should be implemented for the Mie wind retrieval in the future. The selected order of the polynomial fit for the Mie non-linearity should take into account the evaluation range, meaning: to capture a possible pixilation effect the order of the polynom should be at least equal to the number of pixels contained in the evaluation range. An alternative option could be to use a low order polynomial fit (probably up to 5th order) first to describe the large scale shape of the Mie response curve and subsequently apply a sine-fit to capture the pixilation effect in the residual. The A2D Mie non-linearity should be plotted over pixel on the x-axis to allow for an easier visual comparison with non-linearity shapes already obtained for ALADIN during the IFP tests.

The improved ground return detection scheme that is currently being developed in the framework of a master’s thesis (Weiler 2017) should be applied for the evaluation of Mie and Rayleigh response calibrations after finalization. Some details of this scheme have already been implemented in the L1B processor (V7.0), namely regarding the consideration of ground return signal distributed over several range-gates and use of more than 1 signal derivative.

It is recommended performin an IRC with the A2D (and the 2- μ m DWL) in nadir pointing during an ALADIN IRC underpass for comparison of nadir-pointing observations. The A2D IRC can only be performed in limited regions because the Falcon aircraft needs to circle in order to provide nadir view. For a second ALADIN IRC one could foresee to fly along-track with the DLR Falcon aircraft and characterize the present atmospheric heterogeneity with the A2D (in 20° off-nadir mode) and the 2- μ m DWL (in nadir mode and conical scanning mode). Details for implementation need to be discussed, once the first in-orbit calibrations IRC were performed and analysed.

A lesson learned from the 2009 and 2015 airborne campaign is that a number of 3 response calibrations are considered to be the minimum during an airborne campaign. However, 5 or more airborne calibrations are preferred in order to enable a more founded decision about the quality of the obtained response curves.

	Document Nr. FR.DLR.WindVal.270717	Issue: V1.1	Date: 27.07.2017	Page: 91/146	
	Doc. Title: WindVal Final Report				

9 A2D wind measurements and comparison with 2- μ m winds

This chapter discusses the results of the A2D wind measurements carried out during the WindVal campaign in Iceland in 2015. After an overview of the performed wind measurement scenes and the obtained data, the Rayleigh and Mie wind retrieval algorithms as well as their subsequent validation by statistical comparison with the 2- μ m wind lidar data are exemplarily demonstrated for one selected flight section. Afterwards, additional conclusions that are drawn from the analysis of other wind measurements are outlined. Finally, the results of the statistical comparison of all flight sections are presented, leading to a concluding summary of the findings of the campaign.

9.1 Overview of flights and wind measurements

In the framework of the WindVal campaign, a total number of 14 flights have been performed, including four transfer flights between Oberpfaffenhofen and Keflavík, as shown in **Figure 9-1**. Analysis of the A2D data collected during the 14 flights yielded 21 wind measurement scenes in addition to the 5 calibration scenes discussed in the previous chapter. An overview of the respective flight sections, wind data and quality control is presented in **Table 9-1** and **Table 9-2**. The measurement periods range from only ten minutes to almost one and a half hour, adding up to more than 12 hours of wind measurements over the whole campaign. It should be noted that the end time given in the tables corresponds to the time tag (start time) of the last observation, i.e. the last pulse contributing to each wind measurement section is emitted 14 seconds after that end time. Moreover, it is indicated whether the measurements were obtained during a straight flight or curves are included in the periods. Flight sections with curves require extra analysis during the processing related to ground detection. The four shortest sections took only between 10 and 16 minutes and are marked by red boxes. Due to the large number of observations (184 to 293), the four longest sections with a length of 55 to 88 minutes (green boxes) are preferred for analysis.

The number of Rayleigh and Mie winds that is summarized for each flight section in **Table 9-1** corresponds to wind measurements which have passed the quality control, i.e. after sorting out invalid measurements that showed outliers in the DCO channel, saturation of single pixels on the ACCD or incorrect assignment of range-gates numbers as studied in Marksteiner (2013). The respective DCO ranges for the Rayleigh and Mie channel which were determined for the quality control procedure are indicated in the table as well.

Table 9-2 provides additional information on the range-gate setting for each wind measurement period as well as on the performed measurements for evaluating the Rayleigh background signal on the Mie channel. In particular, different operation modes of the A2D were used to measure the Rayleigh background by tuning the laser such that the Mie fringe is out of the useful spectral range of the Fizeau interferometer (MOUSR).

Due to the different illumination of the field stop for the internal reference and the free path atmospheric and ground signal, the frequency for which the fringe is out of the spectral range of the Fizeau interferometer for the ground and atmospheric layers is a few MHz different from the MOUSR frequency for the internal reference. Therefore, apart from MOUSR measurements, so-called GrOUSR (Ground out of spectral range) or ClOUSR measurements (Clouds out of spectral range, in case of no ground visibility) were performed at slightly different frequency settings with respect to the MOUSR procedure. The colour coding in the respective column of **Table 9-2** indicates the data quality obtained in the single MOUSR, GrOUSR and ClOUSR measurements.

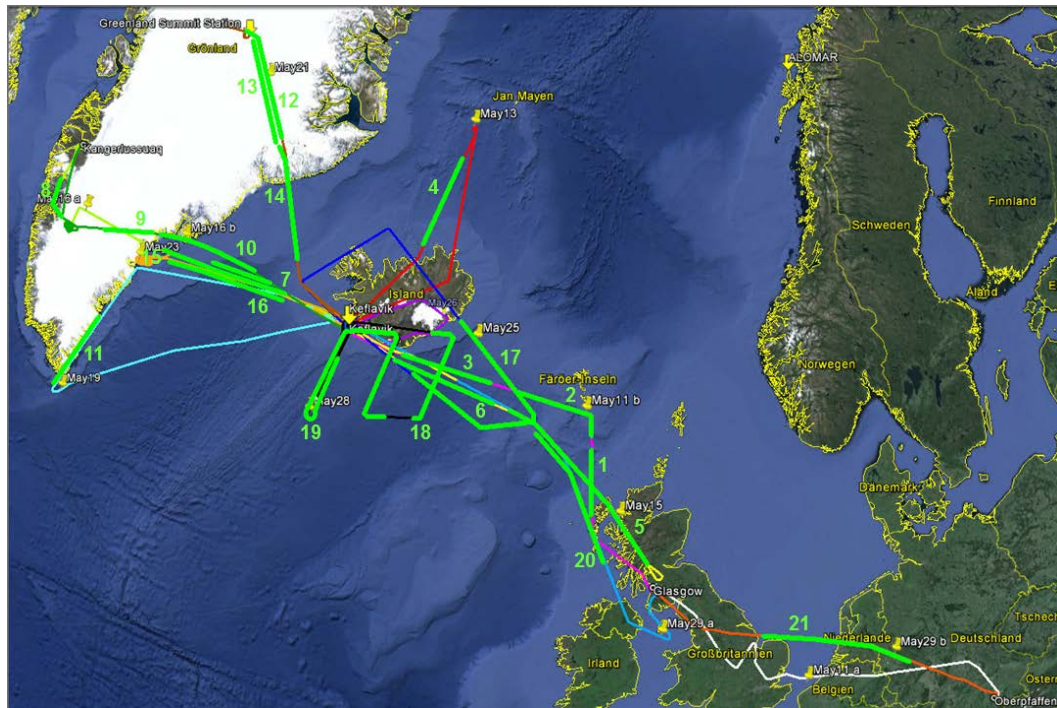


Figure 9-1: Map of the Falcon aircraft flight tracks performed during the WindVal campaign between 11/05/2015 and 29/05/2015. The green sections indicate the 21 wind measurement periods.

Table 9-1: Overview of A2D wind measurement scenes and the collected Rayleigh and Mie wind data as well as determined DCO ranges for Quality Control. The longest periods (>50 min.) are highlighted in green in the “duration” column, while short sections (<20 min.) are indicated in red.

#	DATE of flight	START time	END time	duration (+14 s)	curve(s) included?	# OBS	# meas	invalid meas. RAY	invalid meas. MIE	DCO RAY	DCO MIE
1	11.05.2015	13:03.41	13:18.05	00:14.38	no	49	1715	90	960	399 - 403	308 - 311
2	11.05.2015	13:20.07	13:44.43	00:24.50	YES	83	2905	9	393	398 - 402	307 - 311
3	11.05.2015	13:58.49	14:21.37	00:23.02	no	77	2695	13	10	398 - 402	307 - 311
4	13.05.2015	12:24.58	12:51.40	00:26.56	no	90	3150	4	4	398 - 402	308 - 312
5	15.05.2015	18:09.06	19:09.42	01:00.50	YES	203	7105	7	8	398 - 402	308 - 312
6	15.05.2015	19:14.12	19:44.37	00:30.39	no	101	3535	6	6	398 - 402	308 - 312
7	16.05.2015	14:24.32	14:59.02	00:24.44	YES	116	4060	77	88	399 - 403	307 - 311
8	16.05.2015	16:44.25	16:54.19	00:10.08	YES	34	1190	1	1	399 - 402	307 - 312
9	16.05.2015	19:46.20	20:01.37	00:15.31	YES	52	1820	1	1	398 - 402	307 - 311
10	16.05.2015	20:02.58	20:32.44	00:30.00	YES	100	3500	2	2	397 - 401	307 - 311
11	19.05.2015	13:42.03	14:14.45	00:32.56	no	110	3850	2	2	399 - 403	308 - 312
12	21.05.2015	23:45.23	00:40.53	00:55.44	YES	184	6440	89	88	398 - 402	308 - 312
13	22.05.2015	00:49.53	01:20.47	00:31.07	YES	104	3640	1	1	398 - 402	307 - 311
14	22.05.2015	01:22.14	01:48.02	00:26.02	YES	87	3045	2	2	398 - 402	308 - 312
15	23.05.2015	17:27.08	17:43.02	00:16.08	no	54	1890	6	7	398 - 403	308 - 312
16	23.05.2015	20:08.36	20:39.48	00:31.26	YES	105	3675	0	2	398 - 402	308 - 312
17	25.05.2015	15:24.03	16:47.44	01:23.55	YES	280	9800	7	6	398 - 403	307 - 312
18	28.05.2015	10:50.02	11:17.56	00:28.08	YES	94	3290	138	158	400 - 404	310 - 314
19	28.05.2015	11:25.08	12:52.44	01:27.50	YES	293	10255	81	101	400 - 404	309 - 314
20	29.05.2015	11:09.58	11:45.04	00:35.16	YES	118	4130	17	24	399 - 403	308 - 312
21	29.05.2015	14:37.21	15:16.38	00:39.31	YES	132	4620	24	33	399 - 403	309 - 313

Table 9-2: Overview of A2D wind measurement periods as shown in Table 9-1 together with a list of performed MOUSR/GrOUSR/CIOUSR measurements (MOUSR = Mie fringe out of useful spectral range, GrOUSR = Ground out of useful spectral range, CIOUSR = Clouds out of useful spectral range). The colour coding in the “MOUSR/GrOUSR/CIOUSR” column indicates the quality of the respective data obtained for subtraction of the Rayleigh background in the Mie channel.

#	DATE of flight	START time	END time	duration (+14 s)	curve(s) included?	MOUSR / GROUSR / CIOUSR (green=ok red=bad)	Range-Gate setting
1	11.05.2015	13:03.41	13:18.05	00:14.38	no	L4_9km / Start 10:08	L4_11km
2	11.05.2015	13:20.07	13:44.43	00:24.50	YES	L4_11km / Start 09:21	L4_10km
3	11.05.2015	13:58.49	14:21.37	00:23.02	no	L4_10km / Start 13:48	L4_10km
4	13.05.2015	12:24.58	12:51.40	00:26.56	no	L4_9km_P20 / Start 12:17 L4_9km_P20 / Start 12:54	9km_L4
5	15.05.2015	18:09.06	19:09.42	01:00.50	YES	10km_L4_P20 / Start 19:09	10km_L4
6	15.05.2015	19:14.12	19:44.37	00:30.39	no	no suitable MOUSR available	11km_L4
7	16.05.2015	14:24.32	14:59.02	00:24.44	YES	L4_11km_P20 / Start 15:00	L4_11km
8	16.05.2015	16:44.25	16:54.19	00:10.08	YES	L4_9km_P20 / Start 15:57 L4_9km_P20 / Start 16:32	L4_9km
9	16.05.2015	19:46.20	20:01.37	00:15.31	YES	L4_10km_P20 / Start 20:39	L4_9km
10	16.05.2015	20:02.58	20:32.44	00:30.00	YES	(L4_11km_P20 / Start 19:19)	L4_10km
11	19.05.2015	13:42.03	14:14.45	00:32.56	no	L4_8km_P20 / Start 13:33 L4_8km_P20 / Start 14:24	L4_8km
12	21.05.2015	23:45.23	00:40.53	00:55.44	YES	11km_3km_May21 / Start 23:40	11km_3km_May21
13	22.05.2015	00:49.53	01:20.47	00:31.07	YES	11km_3km_May21 / Start 00:41 GR: 11km_3km_May21 / Start 00:44	11km_3km_May21
14	22.05.2015	01:22.14	01:48.02	00:26.02	YES	11km_3km_May19 / Start 01:47 (11km_May19_P20 / Start 23:02)	11km_3km_May19
15	23.05.2015	17:27.08	17:43.02	00:16.08	no	GR: 11km_May23 / Start 19:15	11km_May19_P20
16	23.05.2015	20:08.36	20:39.48	00:31.26	YES	CL: 11km_May19 / Start 20:40	
17	25.05.2015	15:24.03	16:47.44	01:23.55	YES	GR: 11km_Jet_May25 / Start 16:48	11km_Jet_May25
18	28.05.2015	10:50.02	11:17.56	00:28.08	YES	GR: 8km_May19 / Start 11:19	8km_May19
19	28.05.2015	11:25.08	12:52.44	01:27.50	YES	GR: 8km_May19 / Start 12:53	
20	29.05.2015	11:09.58	11:45.04	00:35.16	YES	GR: 12km_May29 / Start 11:00 GR: 12km_May29 / Start 11:46	12km_May29_P20
21	29.05.2015	14:37.21	15:16.38	00:39.31	YES	GR: 11km_May19 / Start 15:18	11km_May19

9.2 Rayleigh and Mie wind retrieval

The retrieval of the Rayleigh and Mie wind profiles from the raw ACCD data is comprehensively documented in DLR (2010) and DLR (2012b) which deal with the results of the ADM-Aeolus Ground and Airborne Campaigns AGC1 (2006) and AGC2 (2007) as well as AC01 (2007), AC02 (2008) and AC03 (2009). Therefore, the wind processing algorithms will not be described here in full detail. Nevertheless, the single steps from the raw wind profiles (without quality control and the application of masks) up to the statistical comparison of the corrected wind data with the 2- μ m wind lidar will be systematically demonstrated in the following sections. For this purpose, the wind measurement carried out on 19/05/2015 was chosen as an example to explain the procedures which have been developed over the last years to improve the data quality of the A2D wind measurements.

	Document Nr. FR.DLR.WindVal.270717	Issue: V1.1	Date: 27.07.2017	Page: 94/146	
	Doc. Title: WindVal Final Report				

9.2.1 Rayleigh wind retrieval

The processing of the Rayleigh ACCD data to Rayleigh winds is mainly performed as described in TN 5.1., chapter 7.1.1 as well as in TN 5.2, chapter 5 and includes the following steps:

1. subtraction of the DCO and background from Rayleigh ACCD data on measurement level
2. summation over 6 pixels per range-gate to derive the filter A and B signal
3. quality control: removal of invalid Rayleigh measurements (DCO levels out of range, saturation of single pixels on ACCD or incorrect assignment of range-gates numbers)
4. summation of valid Rayleigh measurements to observations
5. determination of the Rayleigh response per observation and layer
6. calculation of the Doppler frequency shift from the Rayleigh response by using the Rayleigh response calibration from 23/05/2015, 18:48 UTC (calibration #7) with a frequency range of 1500 MHz under consideration of the nonlinearity parameters derived from a fifth-order polynomial fit function
7. conversion of the frequency shift to the line-of-sight (LOS) wind speed (in m/s) by use of the Doppler shift equation
8. correction of the Rayleigh wind speed for aircraft LOS velocity per observation

9.2.2 Mie wind retrieval

The processing of the MSP data for Mie winds is mainly performed as described in TN 5.1, chapter 7.2 as well as in TN 5.2, chapter 6 and includes the following steps:

1. subtraction of DCO and background from Mie ACCD data on measurement level
2. quality control: removal of invalid Mie measurements (DCO levels out of range, saturation of single pixels on ACCD or incorrect assignment of range-gates numbers)
3. summation of valid Mie measurements to observations
4. subtraction of telescope image on observation level for each atmospheric range-gate separately using the observations during the MOUSR procedure
5. determination of the Mie response (peak location of the fringe) per observation via the Downhill Simplex Algorithm (DSA)
6. calculation of the Doppler frequency shift from the Mie response by using the Mie response calibration from 16/05/2016, 15:33 UTC (calibration #3) with a frequency range of 1200 MHz and without considering nonlinearities
7. conversion of the frequency shift to the LOS wind speed (in m/s) by use of the Doppler shift equation
8. correction of the Mie wind speed for aircraft LOS velocity per observation
9. determination of the Mie SNR for quality control and application of an SNR-mask to Mie wind profile

The following details of the Mie data processing should be noted:

- The DSA was used for obtaining the Mie responses using a threshold for the FWHM of 1-2 pixels for quality control (these thresholds are relaxed compared to satellite ALADIN processing).
- The Mie nonlinearity-error γ (EMR) was not considered during derivation of the Mie winds.
- The SNR algorithm, which was introduced in TN 5.2, chapter 6.2, was employed for quality control of Mie winds as outlined in section 9.3.6. A more detailed description of the procedure is presented in the following.

9.3 Wind processing exemplarily shown for the flight on 19/05/2015

From the large dataset collected during the WindVal campaign, the wind measurement scene on 19/05/2015 between 13:42 UTC and 14:14 UTC was chosen as an example for presenting the single steps of the A2D wind retrieval summarized in section 0. The selected scenario is especially appropriate for this purpose, as it was characterized by diverse atmospheric conditions with varying cloud cover, thus providing both Rayleigh and Mie winds as well as strong ground return signals required for adequate Zero Wind Correction (ZWC).

The flight track of the Falcon aircraft performed on 19/05/2015 is shown in **Figure 9-2**. Key part of the flight was the section along the east coast of Greenland towards the southern tip. The wind measurement section from 13:42 UTC and 14:14 UTC is indicated as a yellow arrow. A total number of 110 observations (3850 measurements) were conducted in this period (see also measurement period #11 in **Table 9-1** and **Table 9-2**). Prior to the wind measurement, the Rayleigh background signal on the Mie channel was determined by means of a MOUSR measurement carried out from 13:33 to 13:40 UTC, resulting in a telescope image which was later used for Mie signal correction (see section 9.3.6).

The figure also includes a satellite image provided by the Moderate Resolution Imaging Spectroradiometer (MODIS). The picture shows an increasing cloud cover towards the southern tip of the east coast of Greenland which allows for exploiting the complementary design of the A2D Rayleigh and Mie channel in order to measure wind speeds from both molecular and particulate backscatter.

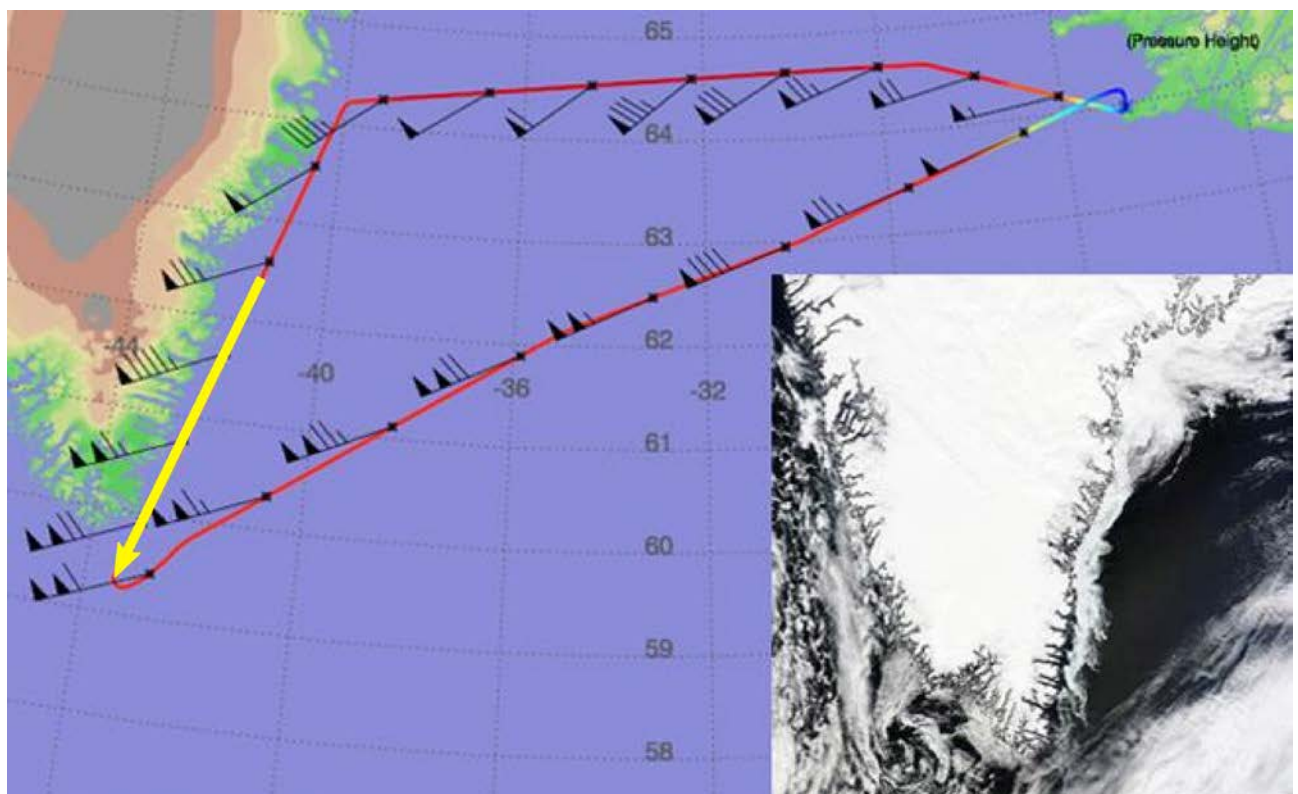


Figure 9-2: Flight track of the Falcon aircraft on 19/05/2015. The wind measurement section along the Greenland east coast between 13:42 and 14:14 UTC is indicated as yellow arrow. The inset shows a composite RGB satellite image provided by MODIS (acquisition period 12:45 to 21:00 UTC).

9.3.1 Flight leg and attitude data

The main parameters of the Falcon flight and attitude data for the regarded flight section are summarized in **Figure 9-3**. The figure includes time series of the aircraft altitude above sea level, groundspeed, pitch and roll angle as well as the resulting off-nadir angle of the A2D instrument and the LOS velocity. As can be seen from the top left plot, the aircraft flew on constant atmospheric pressure levels. Due to a transition from a low pressure area to a high pressure area, the actual height above sea level measured by GPS changed during the flight section from about 8.4 km to 8.6 km (mean altitude: 8.48 km). The roll angle varied by about $\pm 1^\circ$, leading to corresponding variations of the off-nadir angle, while the mean value was determined to be 19.73° . The LOS velocity calculated from the aircraft groundspeed and the attitude data was about -5 to -10 m/s. Furthermore, the following mounting angles were assumed: off-nadir angle: 20° , azimuth angle: 90° , instrument elevation angle: -2° .

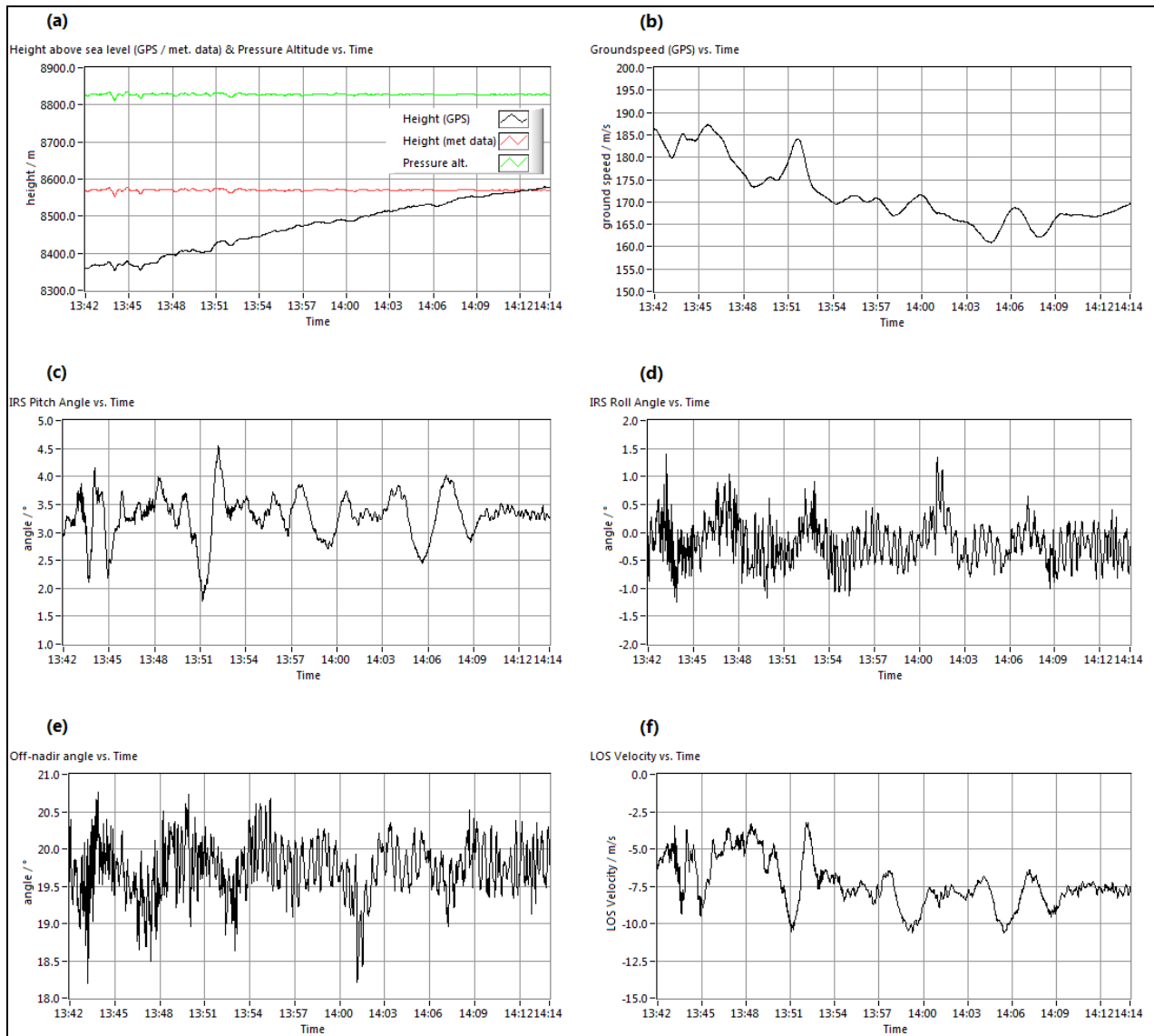


Figure 9-3: Falcon aircraft data for the measurement scene on 19/05/2015 between 13:42 and 14:14 UTC. (a) Falcon altitude above sea level (GPS) and pressure altitude, (b) groundspeed, (c) pitch angle, (d) roll angle without correction of the 0.5° offset angle, (e) off-nadir angle of the A2D instrument after correction of the 0.5° offset angle, (f) LOS velocity.

9.3.2 Range correction and bin size scaling of the intensity distribution

The raw signal intensities measured in the two channels have to be range-corrected, taking into account that the intensity decreases as the inverse square of the range. In addition, the vertical bin scaling, or respectively the range-gate setting, has to be considered. The chosen setting for the regarded measurement period is illustrated in **Figure 9-4**, depicting the altitudes of the bin borders for each range-gate together with the aircraft altitude (bold red line, instrument altitude) and the ground level (black line). The right plot shows the corresponding integration times which were chosen to be 4.2 μs for the atmospheric range-gates #9 to #16 and 2.1 μs for the range-gates at lower altitudes (#17 to #22). Range-gate #4 corresponds to the internal reference. As mentioned before, the aircraft slightly ascended during the measurement period from about 8.4 km to 8.6 km, leading to a corresponding shift in altitude for each range-gate, because the aircraft is flying on constant pressure levels. Due to the ACCD principle for the A2D the timing of the range gates is constant relative to the instrument altitude and thus also all A2D range gates are changing wrt aircraft altitude. This is not the case for the range gates of the 2- μm DWL, although the instrument is also affected by the change in altitude of the aircraft. The 2- μm DWL signals are digitized with 500 MHz corresponding to 0.3 m. This raw signal data is stored for the airborne 2- μm DWL and allows to align the 2- μm range gate borders to constant altitudes wrt ground in the post-processing.

The resulting range-corrected and bin-scaled intensity profiles for the Rayleigh and Mie channel are depicted in **Figure 9-5**. The plots show that the ground echo (from the sea surface) was distributed over multiple range-gates in the course of the flight. In particular, strong ground return signals were detected in range-gates #21 and #22 at the beginning of the measurement section, but shifted to lower range-gates in the second part of the section. Moreover, dense clouds were present towards the end of the flight leg, located in range-gates #17 and #18 (about 1.5 km altitude) as well as in range-gates #8 to #10 (6 to 7 km). The cloud cover resulted in significant reduction of the signal intensities for the range-gates underneath. In contrast, increased signal intensity was observed for the medium-level range-gates during the first part of the section, represented by orange/red colours in the intensity profiles. This can be attributed to aerosols or thin clouds which were distributed over a large horizontal range in about 4 km altitude.

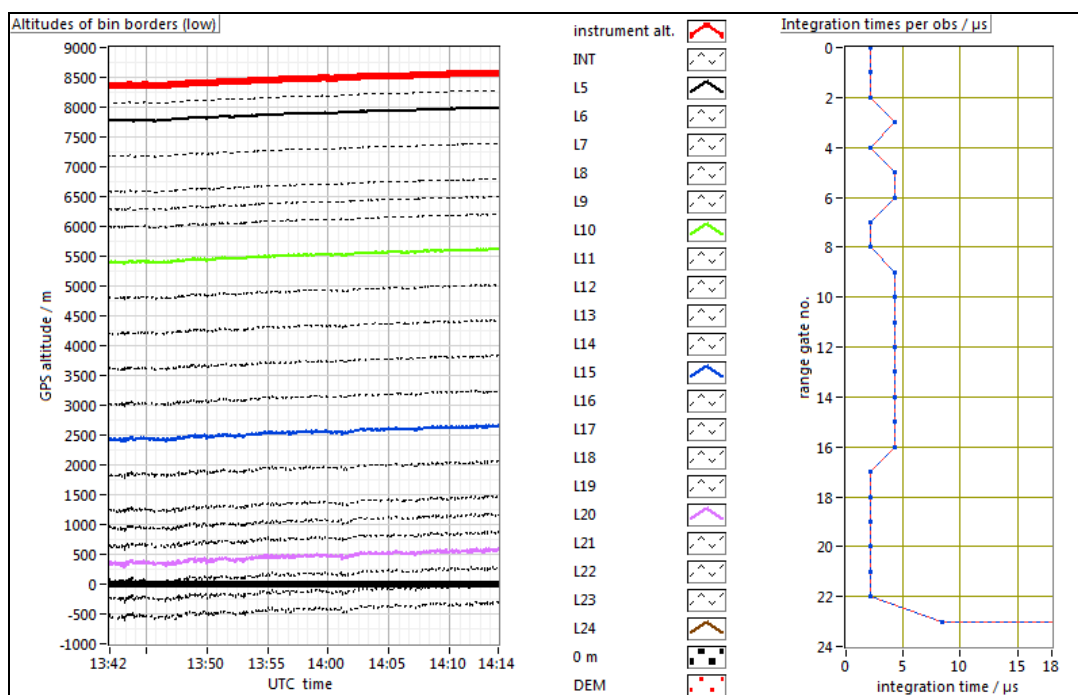


Figure 9-4: Range-gate settings of the A2D during the wind measurement on 19/05/2015 from 13:42 to 14:14 UTC. Left: Altitudes of bin borders for each range-gate (INT = internal reference, DEM = digital elevation model), right: integration times for each range-gate.

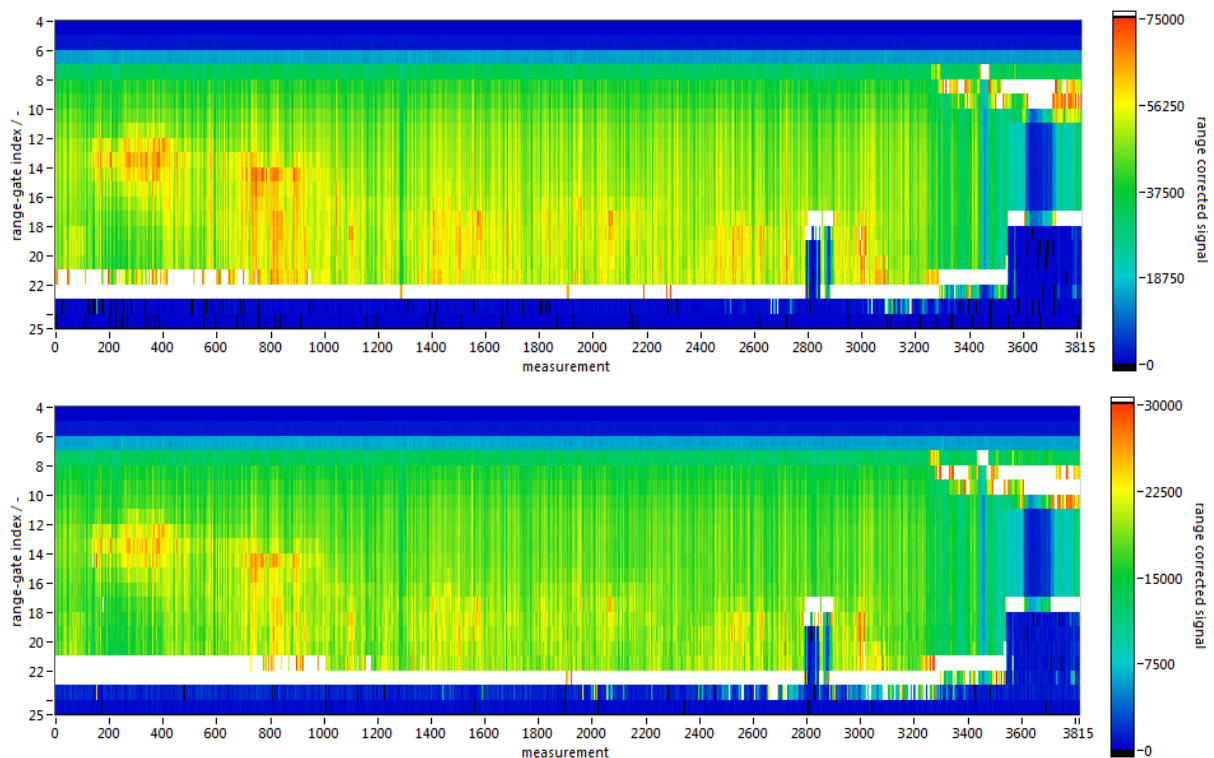


Figure 9-5: Rayleigh (top) and Mie (bottom) signal intensities for the wind measurement on 19/05/2015 from 13:42 to 14:14 UTC after (R^2) range correction and scaling to the bin size of each range-gate according to the range-gate settings depicted in Figure 9-4.

9.3.3 Quality control

An important part of the wind retrieval is the application of quality control (QC) measures which allow distinguishing relevant from invalid data. As described in Marksteiner (2013), chapter 3.6, three main indicators are used for the detection of corrupted measurements which are discarded for the subsequent wind retrieval. Apart from checking whether the detection chain offset (DCO) values are within certain pre-defined margins, QC includes the screening for saturation of single pixels on the ACCD and the incorrect assignment of range-gates numbers. The latter is mostly related to the occurrence of an emergency trigger which entails false data acquisition with the internal reference signal detected in range-gate #3 instead of #4.

The results of the QC carried out for the wind measurement discussed before are depicted in **Figure 9-6**. Here, the DCO margins were set as follows: Rayleigh channel: 399 – 403 LSB, Mie channel: 308 – 312 LSB). Only two measurements were found to have DCO values outside this range, belonging to observations #4 and #5 (see second line from top). False range-gate assignment or saturation of the ACCD pixels did not occur during the regarded flight section (third and fourth line from top). The overall validity plots (bottom line of **Figure 9-6**) therefore only include two outliers for the two channels. The fact that the outliers occur at the same measurements for both the Rayleigh and Mie channel suggests that the underlying reason can be attributed to the same instrumental fault in the detection chain.

An additional parameter which will be implemented in the QC procedure of future wind measurements is the laser pointing which is actively stabilized by means of a co-alignment loop. The latter is realized by imaging a small portion of the backscattered signal passing through the A2D front optics onto a UV camera in order to monitor the horizontal and vertical position of the centre of gravity (CoG) of the beam. A reference position (CoG_x / CoG_y) is defined and a feedback loop involving three piezo-actuators mounted on the last laser transmit mirror is applied to actively stabilize the co-alignment of the transmitted and received laser beam. In this way, the variations in the incidence angle of the atmospheric return signals on the Rayleigh and Mie spectrometers are reduced.

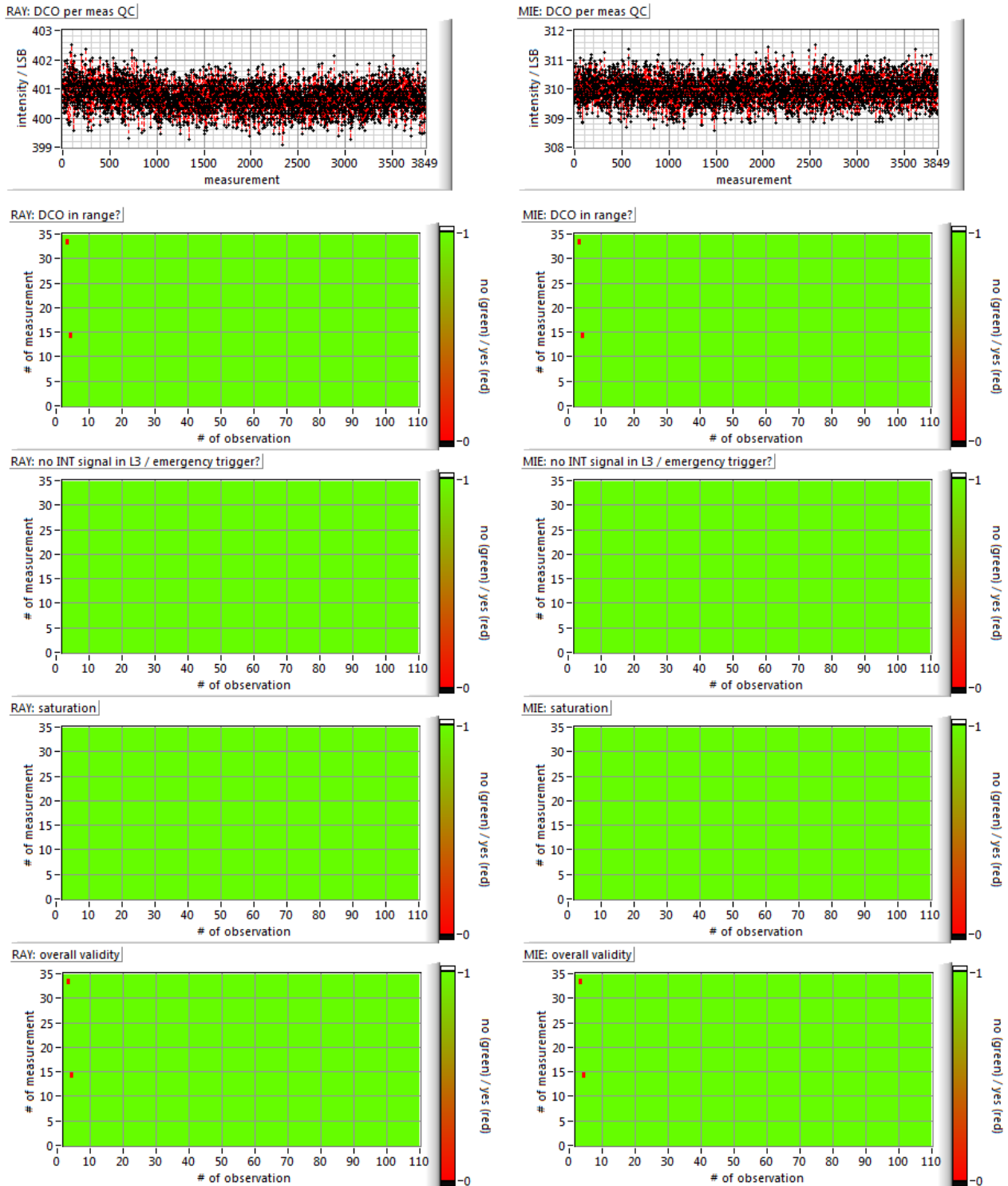


Figure 9-6: Quality control of the Rayleigh (left) and Mie (right) signal for the measurement section on 19/05/2015 from 13:42 to 14:14 UTC. The two plots on top show the detector chain offset (DCO) signal for both channels within the valid ranges (Rayleigh: 399 – 403 LSB, Mie: 308 – 312 LSB). The plots below illustrate the occurrence of DCO outliers, emergency triggers (i.e. false assignment of range-gates numbers) or pixel saturation in the respective channels. The two bottom plots represent a combination of the three QC measures, depicting the discarded measurements from the dataset (red dots).

The fluctuations of the horizontal and vertical CoG coordinate measured during the scene on 19/05/2015 from 13:42 to 14:14 UTC are shown in **Figure 9-7**. The reference position was set to $CoG_x = 385$ pixels (on the UV camera) and $CoG_y = 153$ pixels, respectively. Despite the active stabilization, the CoG position fluctuates by more than one pixel in both spatial directions, e.g. in observation #21. According to TN 5.3, this corresponds to variations in the incidence angle on the Rayleigh spectrometer of about $13 \mu\text{rad}$ vertically and about $6.75 \mu\text{rad}$ horizontally which, in turn, introduces large wind errors of up to 0.4 m/s. Therefore, for future wind retrieval, it is intended to remove those observations in which the measured CoG position shows large deviations from the reference position.

However, it should also be noted that the variations in the CoG position not only result from the laser pointing instability, but also from the uncertainty of the CoG determination itself. As the beam profile of the registered spot as well as the SNR of the camera signal are affected by atmospheric disturbances and multiple scattering as well as by the optical depth of the atmosphere, the calculation of the CoG position yields different values depending on the atmospheric conditions, thus leading to fluctuations of the measured spatial coordinates of the CoG.

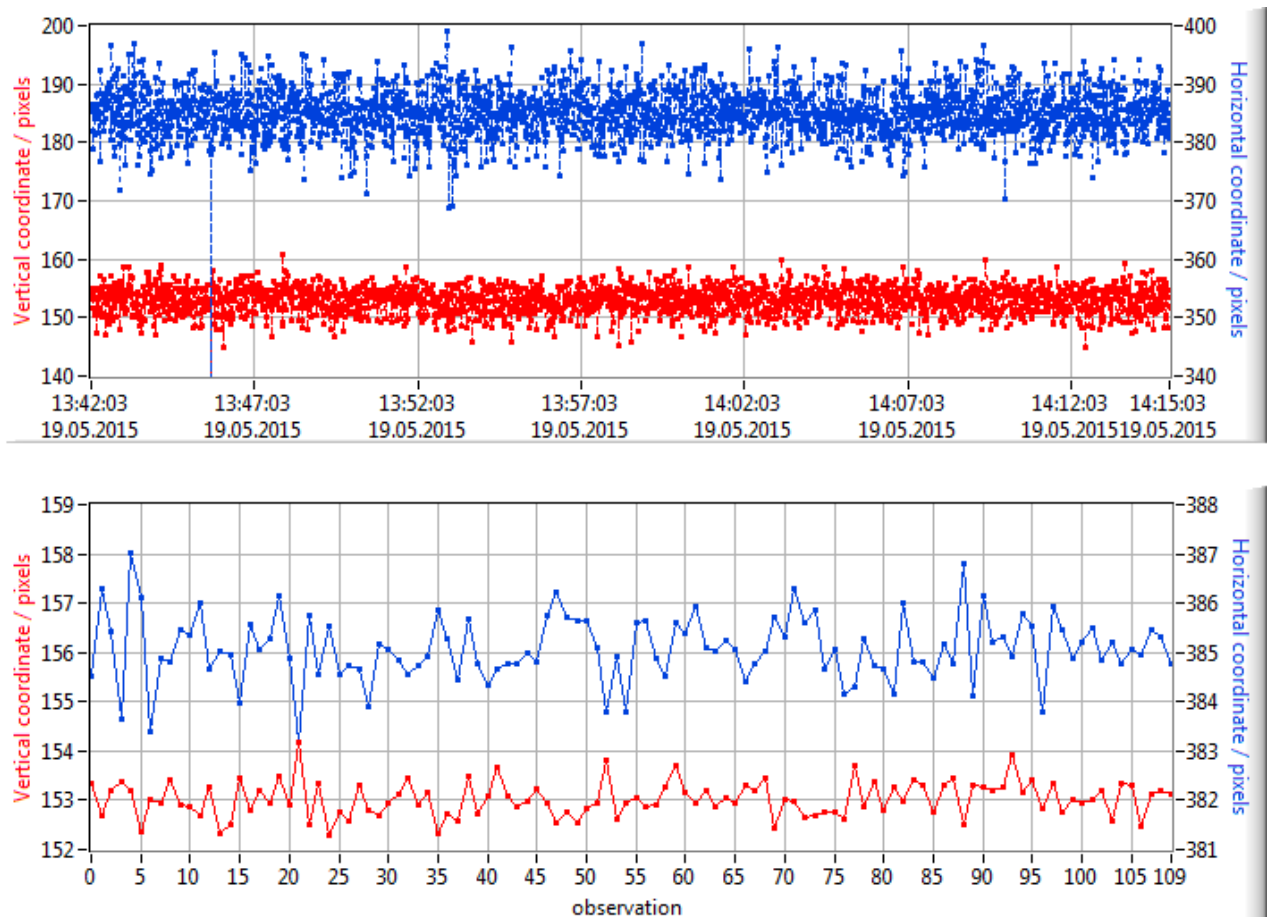


Figure 9-7: Variations of the horizontal (blue) and vertical (red) component of the centre of gravity (CoG) position measured on 19/05/2015 from 13:42 to 14:14 UTC. The plot on top shows the detected position in periods of 1 s, while the bottom plot depicts the variations on observation level (18 s).

9.3.4 Raw wind profiles

The Rayleigh and Mie wind retrieval algorithms were performed as explained in Marksteiner (2013), chapter 3.5. For the calculation of the Doppler frequency shift, and in turn the Rayleigh wind speeds, the Rayleigh response calibration from 23/05/2015, 18:48 UTC (calibration #7) with a frequency range of 1500 MHz was used, while considering the Rayleigh nonlinearities. Retrieval of the Mie wind profiles was performed using the downhill simplex algorithm and by employing the Mie response calibration from 16/05/2016, 15:33 UTC (calibration #3) with a frequency range of 1200 MHz. Here, the Mie nonlinearity error was not considered.

The coefficients resulting from the linear and subsequent fifth-order polynomial fit of the Rayleigh response calibration data for the internal reference (INT), for one selected atmospheric range-gate (ATM), namely range-gate #15, and for the summed ground return (GR) are summarized in **Table 9-3**, while the slope and intercept values obtained from the linear fit of the Mie response calibration data for the internal reference and the summed ground are listed in **Table 9-4**.

Table 9-3: Slope (sensitivity) and intercept (offset) values obtained from the linear fit of the Rayleigh response calibration #7 data as well as fit coefficients of the Rayleigh nonlinearity error derived from the fifth-order polynomial fit for the internal reference (INT), atmospheric range-gate #15 (ATM) and the summed ground return (GR).

Parameter	Unit	INT	ATM	GR
Slope	10^{-4} MHz ⁻¹	4.56	5.77	4.57
Intercept	-	-0.0008	-0.0601	0.0095
0 th order	10^{-3}	3.74	-13.3	5.04
1 st order	10^{-6} MHz ⁻¹	7.35	35.5	10.8
2 nd order	10^{-8} MHz ⁻²	-1.39	6.38	-2.75
3 rd order	10^{-11} MHz ⁻³	-0.930	-9.99	-3.87
4 th order	10^{-14} MHz ⁻⁴	-1.55	0.937	0.450
5 th order	10^{-17} MHz ⁻⁵	-2.94	0.361	1.77

Table 9-4: Slope (sensitivity) and intercept (offset) values obtained from the linear fit of the Mie response calibration #3 data for the internal reference (INT) and the summed ground return (GR).

Parameter	Unit	INT	GR
Slope	MHz/pixel	-99.57	-97.26
Intercept	pixel ⁻¹	7.26	7.14

The Rayleigh and Mie response values per observation and range-gate are plotted in **Figure 9-8**. By using the calibration fit coefficients and the Doppler shift equation the wind speed can be calculated for each bin, resulting in the raw wind profiles depicted in **Figure 9-9**. The Mie wind can be processed with or without subtraction of the Rayleigh background obtained from the MOUSR procedure (see section 9.3.6). Note that wind velocities below -5 m/s and above 21 m/s are shown as white and black bins, respectively. In order to distinguish between valid and invalid winds, several techniques are applied which will be presented in the following sections.

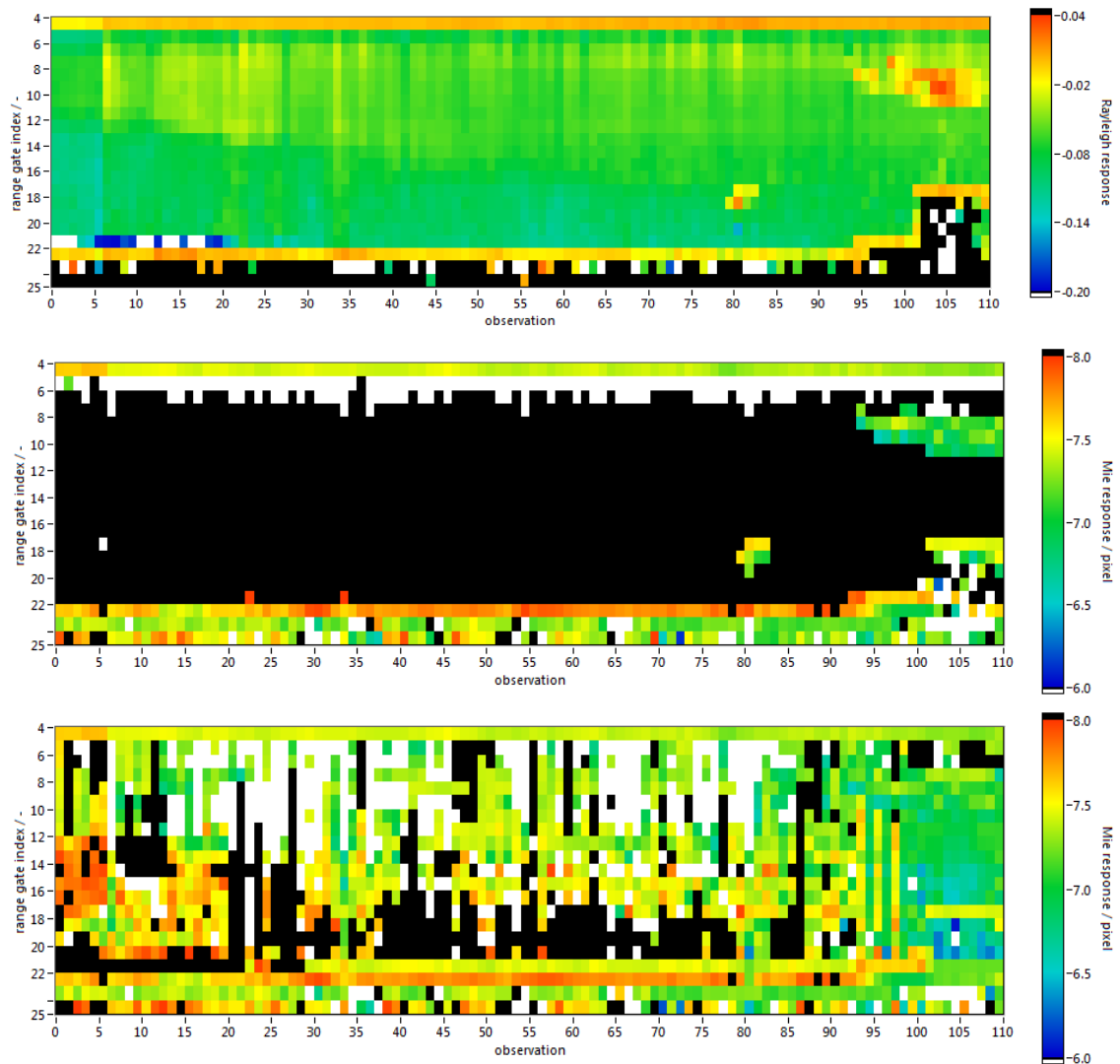


Figure 9-8: Rayleigh response (top) and Mie response without (middle) and with Rayleigh background subtraction (bottom) measured during the scene on 19/05/2015 from 13:42 to 14:14 UTC.

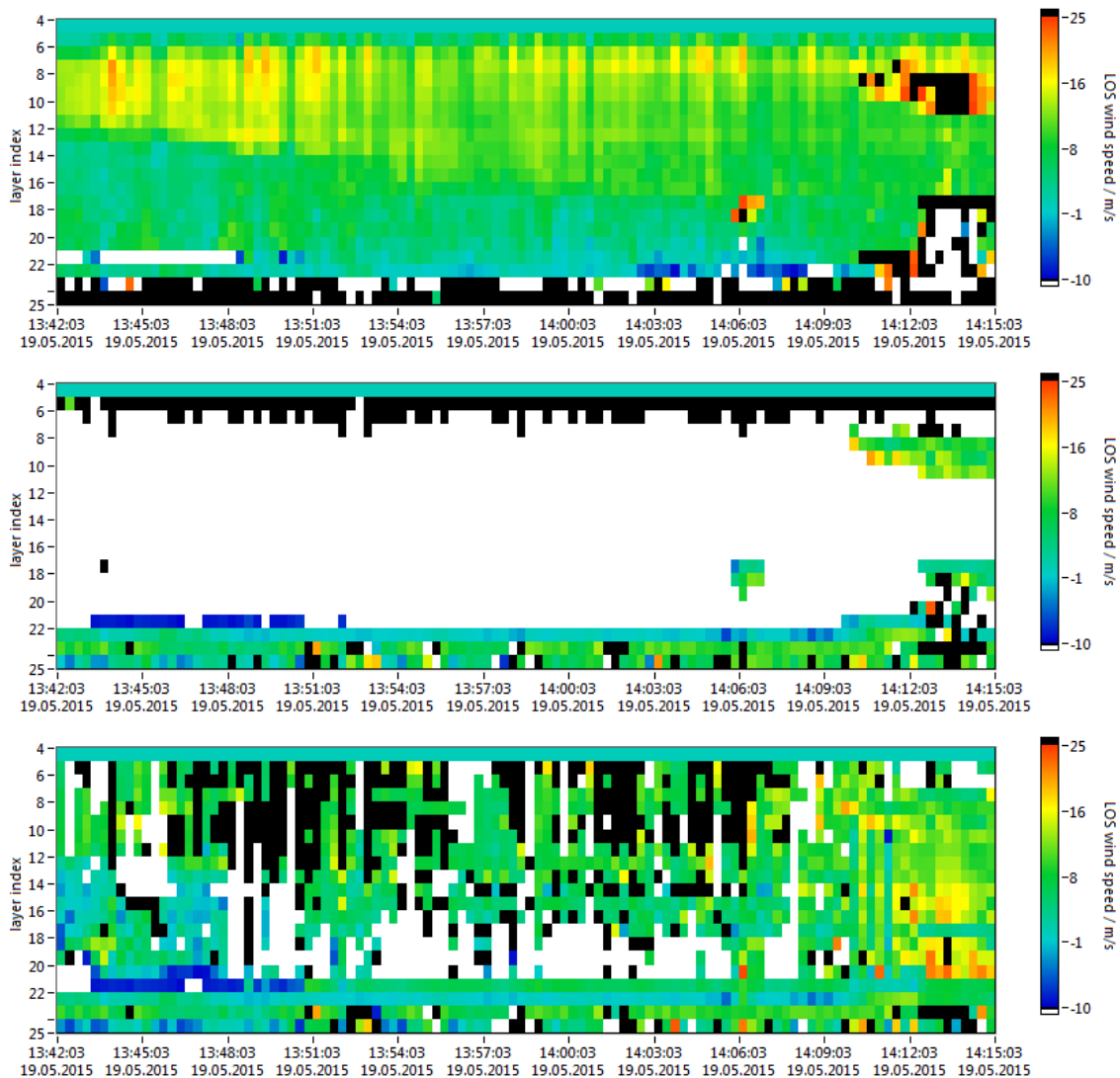


Figure 9-9: Raw LOS wind profiles obtained for the Rayleigh (top) and Mie channel without (middle) and with Rayleigh background subtraction (bottom) during the scene on 19/05/2015

9.3.5 Cloud and ground mask for Rayleigh winds

The identification of invalid winds retrieved from the Rayleigh channel involves the detection of bins which were affected by particulate backscatter from clouds or aerosols, since this Mie contamination introduces systematic errors of the measured Rayleigh response. Therefore, bins showing signal intensities that are unusually high for pure molecular backscatter are excluded from further analysis. The same approach is taken for the removal of bins that contain ground return signals. For the processing of all wind measurements carried out in the WindVal campaign, a minimum intensity of 75000 LSB was chosen as threshold for identifying a bin as a cloud or ground bin. Due to the attenuation of the laser beam during propagation through the clouds, the wind information obtained from the range-gates below clouds is very likely to be also derogated. Consequently, not only the cloud bins themselves are flagged invalid but also all the bins in the range-gates below. The resulting cloud and ground masked (**Figure 9-10**, top) is finally combined with the mask resulting from the quality control described in 9.3.3, where all the observations including invalid measurements (here observations #4 and #5) are discarded. The threshold amount of invalid measurements leading to a removal of a complete observation is an adjustable parameter and was set to 1 in the present case. The combined Rayleigh mask and the Rayleigh wind profile after its application are shown in **Figure 9-10**.

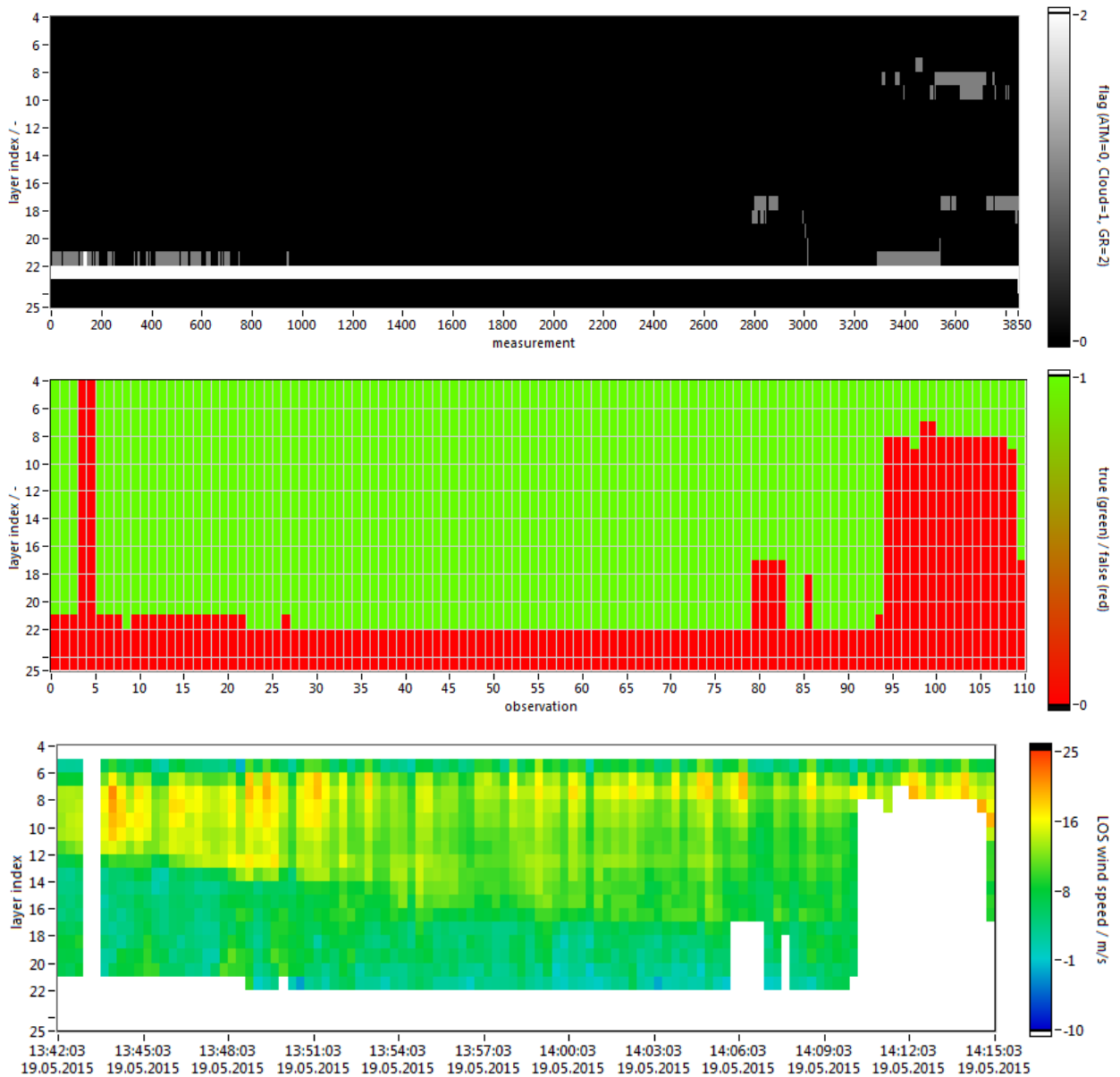


Figure 9-10: Top: Cloud and ground mask (atmosphere: black, cloud: grey, ground: white) obtained by applying an intensity threshold for the Rayleigh signal (here: 75000 LSB). The cloud and ground bins as well as all the bins below are flagged invalid, resulting in the combined Rayleigh mask depicted in the middle plot which also considers the invalid measurements (red boxes) identified during the QC. The masked Rayleigh wind profile is shown on the bottom (see for comparison Figure 9-9, top).

The fact that all the bins below clouds are excluded from the dataset represents a very stringent quality guideline which is likely to involve the removal of valid Rayleigh winds. An alternative approach for discriminating the Rayleigh winds based on the Mie SNR mask is discussed at end of the next section.

9.3.6 Rayleigh background subtraction and Mie SNR mask

In contrast to the Rayleigh wind retrieval, an additional step is taken for the correction of the Mie winds prior to the application of a mask: the Rayleigh background correction. For this purpose, the Rayleigh background signal on the Mie channel, also referred to as telescope image (TIm), is subtracted from the Mie signal on observation level for each range-gate. For the present case, the TIm was determined by a MOUSR (Mie Out of Useful Spectral Range) measurement which was carried out from 13:33 to 13:40 UTC, i.e. directly before the wind measurement period on 19/05/2015. The MOUSR was particularly adequate for the correction of the Mie signal, as it was performed at the same range-gate settings as the subsequent wind measurement. Furthermore, the aircraft attitude and altitude varied only slightly during the procedure. The resulting telescope image is shown in **Figure 9-11**.

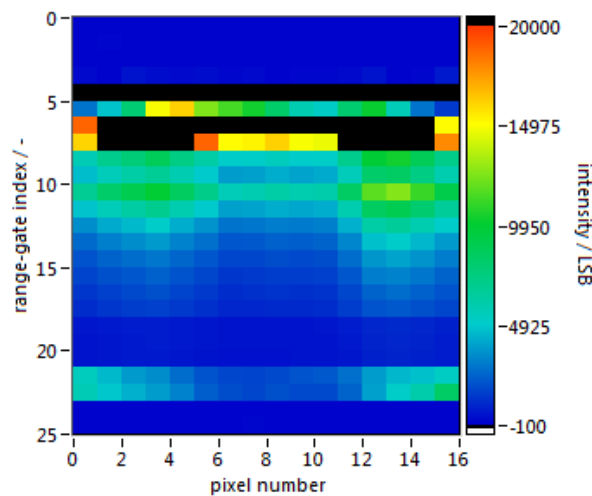


Figure 9-11: Telescope image (mean per observation) obtained from the MOUSR procedure on 19/05/2015 between 13:33 and 13:40 UTC.

As can be seen from the telescope image, the ground return is distributed in range-gates #21 and #22. Due to the aforementioned shift of the ground return to lower range-gates in the course of the wind measurement section, a mismatch occurs between the MOUSR and the wind measurement in terms of the ground and atmospheric range-gates. Consequently, the subtraction of the telescope image from the original Mie signal which is performed uniformly for all observations leads to erroneous (negative) intensities in the affected range-gates #21 and #22 for observations in which the ground return is located in lower range-gates. The subtraction of too much signal also occurs for the atmospheric bins below clouds where the original signal intensities are reduced.

The subtraction of the Rayleigh background also affects the signal to noise ratio (SNR) of the Mie signal. This becomes obvious when comparing the SNR profiles before and after subtraction of the telescope image which are shown in **Figure 9-12**. The bins with SNR values ≥ 10 are marked in white and will later pass the QC that involves a rejection of bins with SNR values below a threshold of 10.

The SNR value, which is plotted in **Figure 9-12** and which is relevant for the quality control of the retrieved Mie winds, is based on a definition that was introduced in TN 5.2, chapter 6.1 as follows:

$$SNR(i) = \frac{I_s(i, j_{max})}{\frac{1}{11} \left(\sum_{j=0}^{15} I_s(i, j) - \sum_{j=j_{max}-2}^{j_{max}+2} I_s(i, j) \right)}$$

Here, I_s is the Mie signal per layer i and pixel j after subtraction of the DCO, background, telescope image and minimum value. The index j_{max} is independent from the index i and corresponds to the pixel index where the maximum intensity pixel of the internal reference is found for the respective observation.

In contrast to the SNR definition used for the Mie wind retrieval in the 2009 campaign (see Eq. 7.15 in TN 5.1), where the numerator was the sum of the signal over the 5 pixels around the internal maximum pixel index, here the numerator is simply the single maximum intensity value within this range of 5 pixels. Moreover, instead of taking the sum of the intensity of the remaining pixels noise in the denominator, now the mean over this sum is used. That leads to a division by 11 instead of 16, referring to the definition of the noise on the remaining pixels only.

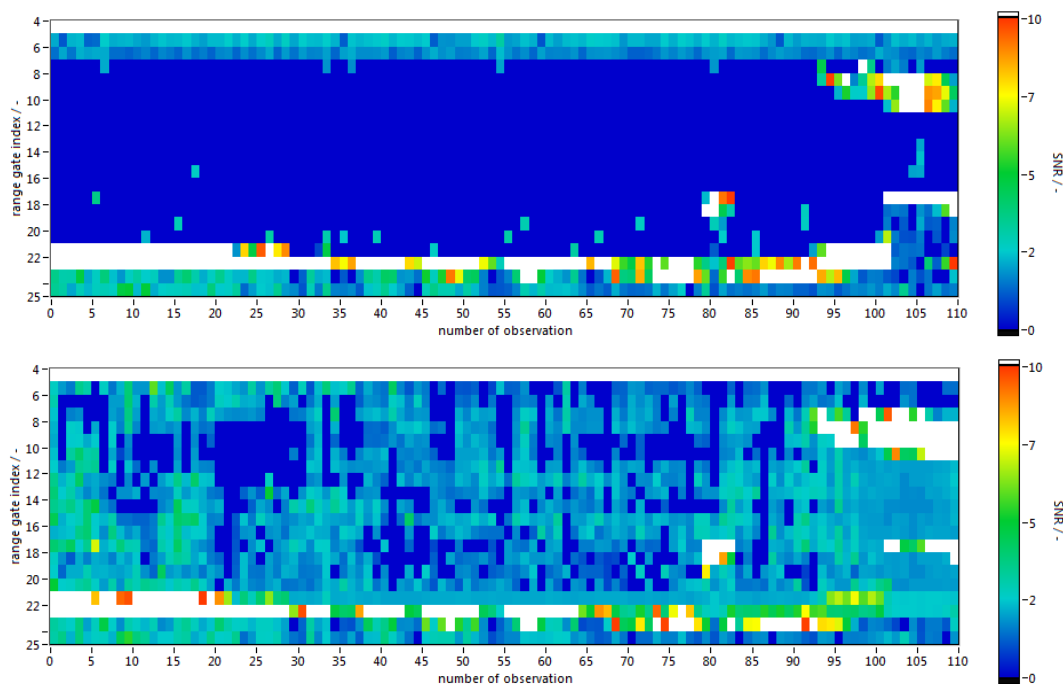


Figure 9-12: Mie SNR without (top) and with subtraction of the Rayleigh background (bottom). The telescope image used for Rayleigh background correction is shown in Figure 9-11. All bins with SNR values above 10 (used threshold for Mie SNR mask) are indicated in white. The white line on top (range-gate #4) corresponds to the internal reference.

Hence, the given SNR is a comparison of the intensity of the maximum pixel *signal* level to the mean signal level (*noise*) of the remaining pixel intensities outside the region of the 5 pixels around the maximum. This SNR definition allows sorting out wind measurement bins that show obviously inconsistent values. However, it is not applicable to potential Mie scattering ratio calculations for the retrieval of aerosol products, especially due to problems related to the elimination of the dominating telescope image effect for lower Mie signal intensities. It should also be noted that the search for the maximum intensity pixel of the internal reference with its restriction to a 5-pixel range and the resulting index will lead to incorrect determination of the SNR for higher absolute wind speeds, i. e. higher than ≈ 44 m/s ($100 \text{ MHz/pixel} \cdot 5/2 \text{ pixel} / 5.6 \text{ MHz/(m/s)}$).

The application of the SNR threshold on the Mie wind profile measured on 19/05/2015 is depicted in **Figure 9-13**. The plot on top shows the Mie SNR mask based on the SNR distribution after Rayleigh background subtraction shown in **Figure 9-12** (bottom) for a threshold value of 10. The resulting Mie wind profile is displayed below. As can be seen, the ground return is distributed over two range-gates at the beginning of the flight section. Although this wind measurement period yielded only a small amount of valid Mie winds, the wind speeds match well with those of adjacent bins obtained from the Rayleigh channel (**Figure 9-10**, bottom). Nevertheless, the 2- μm wind lidar shows a better coverage with valid winds (see **Figure 9-17**, top), which clearly indicates that the coherent-detection system is more sensitive to particulate backscatter.

Since only the Mie SNR mask is applied in the Mie wind processing algorithm, ground bins with sufficiently high SNR are not removed from the wind profiles. However, these bins do not enter the statistical comparison with the 2- μm reference wind lidar system, as 1) there is no reference data available for the ground and 2) the ground layers are cut from the A2D profiles used for the comparison.

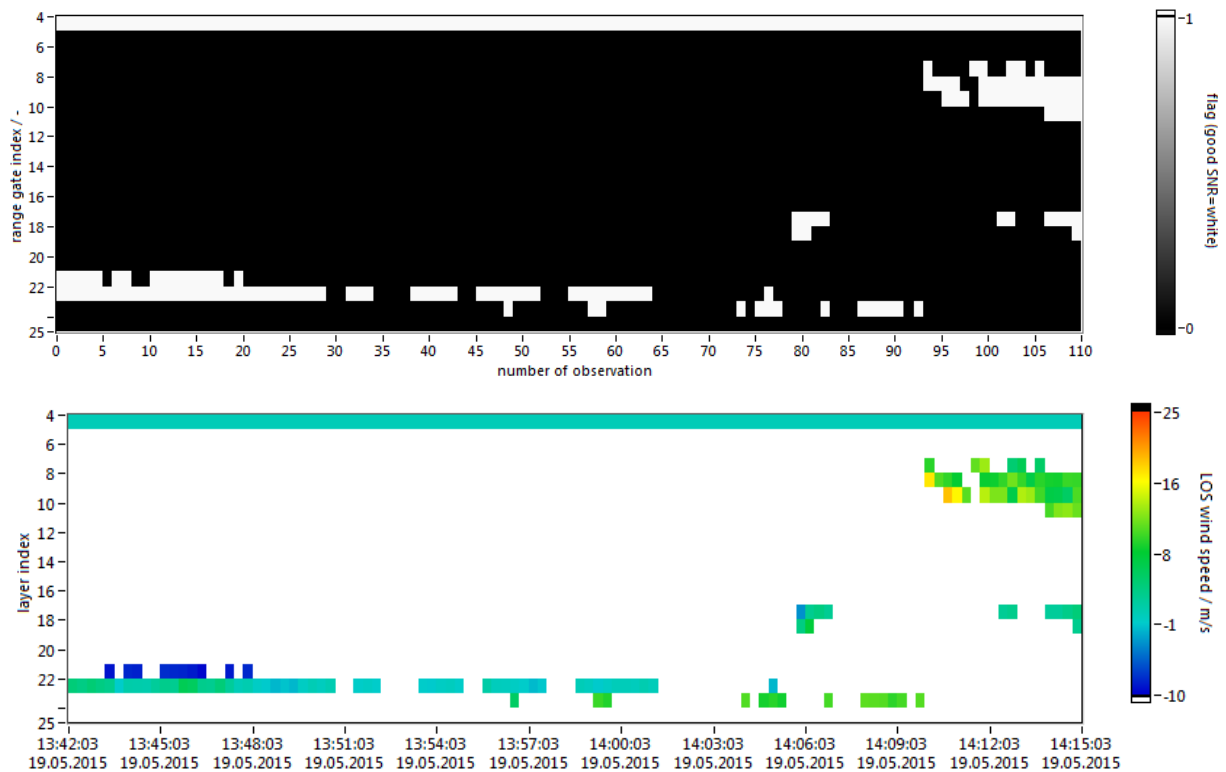


Figure 9-13: Top: Mie SNR mask obtained by setting the Mie SNR threshold to 10. The resulting Mie wind profile is depicted on the bottom (see for comparison Figure 9-9, bottom).

The Mie SNR mask can also be applied to the Rayleigh wind profile, thus offering an alternative to the cloud and ground mask described in section 9.3.5. For this purpose, the Mie SNR mask is inverted so that all bins which show a low Mie SNR, i.e. bins with low cloud or aerosol loads, are flagged valid. Application of the inverted Mie SNR mask to the Rayleigh wind profile for the flight section on 19/05/2015 is depicted in **Figure 9-14**. Comparison with the cloud and ground masked wind profile in **Figure 9-10** (bottom) reveals that the alternative approach represents a less stringent QC, leaving a large number of invalid winds. In particular, many invalid winds below clouds as well as below the ground are not filtered by this method. However, this mask also retains a significant amount of valid Rayleigh winds (e.g. in range-gates #11 to #17 at the end of the section) which were rejected by the cloud mask. It is intended to extend the function of the inverted Mie SNR mask and to develop an adequate combination with the cloud and ground mask in order to exploit the advantages of both approaches.

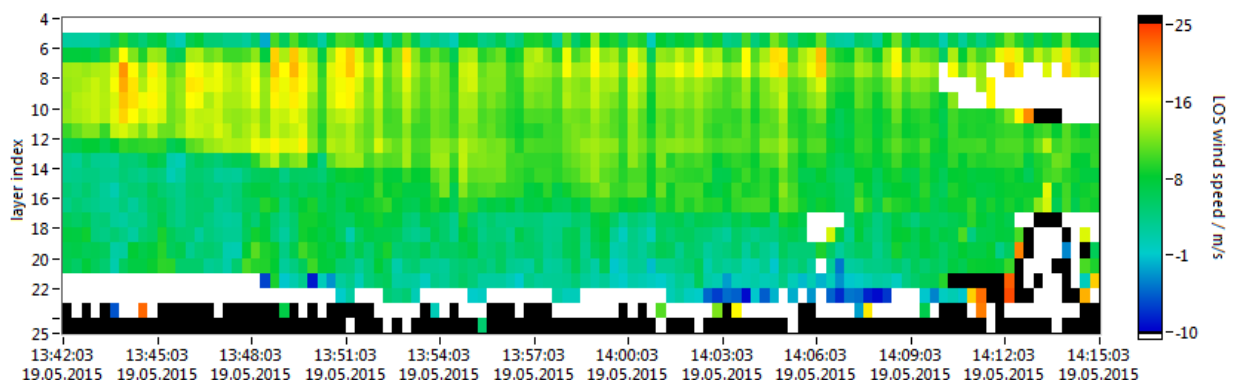


Figure 9-14: Rayleigh wind profile after when applying the inverted Mie SNR mask instead of the cloud and ground mask as shown in Figure 9-10.

9.3.7 Zero wind correction (ZWC)

The acquisition of ground return signals can be used for the correction of the Rayleigh and Mie wind speeds, as the LOS speed determined for the range-gate which contains the ground return should be 0 m/s after subtraction of the aircraft induced velocity, thus providing a reference for the wind speeds measured in the atmospheric range-gates (see Marksteiner (2013), chapter 3.5.3) In this way, unknown contributions to the measured LOS wind velocity can be compensated. This includes first of all contributions from an imperfect determination of the aircraft attitude data. In particular, improper knowledge of the yaw angle will result in an error of the retrieved wind speed, as the measured Doppler shift from the aircraft ground speed is most sensitive to a rotation around the yaw axis. Moreover, it is assumed that an offset in A2D wind speed is introduced by slight changes in the co-alignment of the transmit-receive path which differs between calibration and wind measurement.

For the present wind measurement scene, the ground return signal was obtained from the sea surface. Due to the low cloud and aerosol loads, especially during the first part of the flight section, sufficiently high signal intensities were detected in the ground range-gate #22. The observations that were considered for the determination of the ZWC value are indicated in **Figure 9-15**. The diagram on top depicts a mask which flags all observations that contribute to the ZWC value for the Rayleigh and Mie channel. As a precondition, the respective ground bin must contain at least 80% of the ground signal (on measurement level) in order to be considered valid for ZWC. For this purpose, a mask based on a digital elevation model (DEM) was applied in combination with a predefined threshold intensity, yielding 66 valid ZWC values for the measurement period on 19/05/2015, 13:42 to 14:14 UTC. The values are plotted in **Figure 9-15**, showing a similar variation for both channels. The mean values were calculated to be 0.09 m/s and -0.76 m/s for the Rayleigh and Mie channel, respectively. Here, a threshold standard deviation of 1σ was applied in order to exclude outliers from the set of ZWC values. An alternative approach for analysing the ZWC data is to calculate the median of all valid ZWC values, yielding -0.40 m/s for Rayleigh and -0.67 m/s for the Mie channel.

The large discrepancy between the determined values depending on the statistical method is rather unsatisfactory. Therefore, a more detailed analysis of ground return signals and their applicability for Zero Wind Correction on observation level is currently being undertaken by a master student at DLR (Weiler 2017). The focus of the study is on the refinement of the ground detection procedure on measurement level for improving the quality of the calibration and wind data.

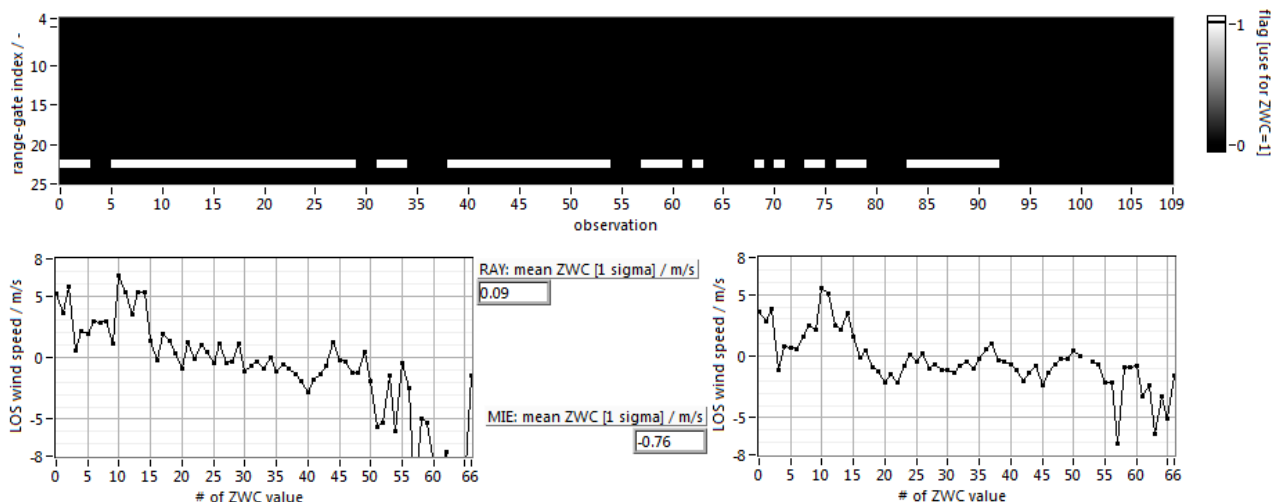


Figure 9-15: Zero wind correction of the Rayleigh and Mie winds. The plot on top shows the ground bins that were considered for ZWC, while the two plots below depict the determined LOS wind speeds for the corresponding observations derived for the Rayleigh and Mie channel.

9.3.8 Statistical comparison with 2- μ m winds

In contrast to the A2D which measures LOS wind velocities at a constant off-nadir angle of 20°, the 2- μ m lidar performs a conical VAD (Velocity Azimuth Display) scan with an opening angle of 20°. The scan is performed in a so called “step & stare” mode. Here, the information from 21 azimuthal positions, which corresponds to one observation, is used to calculate a three dimensional wind vector. On each azimuthal position the signal from 500 laser pulses is analysed and averaged to obtain one LOS profile. The total time for positioning the laser to its scan starting position varies around 21 s. Thus, in total one 2- μ m observation of the wind vector profile takes around 42 s, whereas an A2D observation lasts 18 s.

For adequate comparison of the winds measured with the 2- μ m and the A2D lidar, the 2- μ m 3D-winds have to be projected onto the A2D LOS axis. This is carried out for each 2- μ m observation by the calculating the scalar product of the measured 2- μ m wind vector and the mean A2D-LOS unit vector, while the latter is calculated from the Falcon attitude data (recorded per second) for the period of the respective 2- μ m observation (≈ 42 s). The procedure is explained in detail in TN 5.2, chapter 5.2.1.

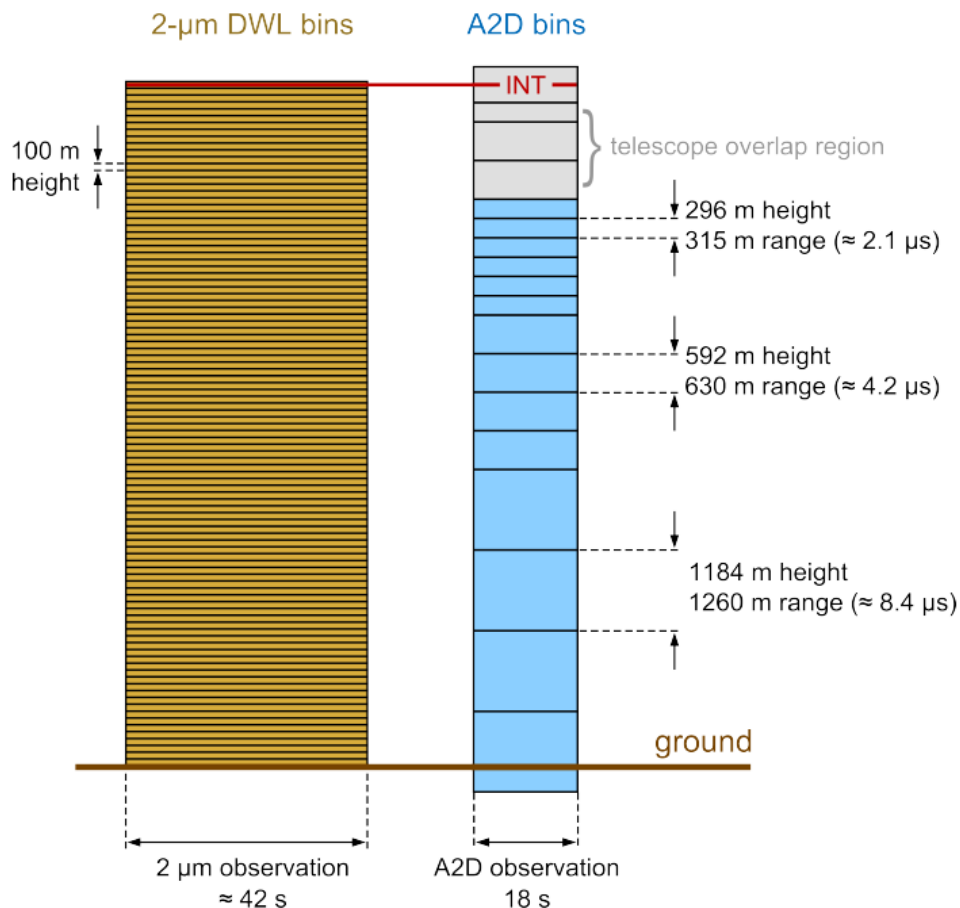


Figure 9-16: Comparison of the different temporal and spatial resolution grids of the 2- μ m DWL (left) and A2D (right). The schematic is true to scale regarding the respective axes. The 2- μ m grid (orange) consists of bins of 100 m vertical thickness reaching from the aircraft to right above the earth surface, whereas the A2D grid (blue) extends from below the aircraft to the ground with a minimum bin thickness of 296 m (corresponding to 315 m in range due to the 20° off-nadir pointing). One 2- μ m DWL observation lasts ≈ 42 s, while one A2D observation takes 18 s. The flight altitude is indicated as red line and corresponds to the height of the internal reference bin (INT) of the A2D.

	Document Nr. FR.DLR.WindVal.270717	Issue: V1.1	Date: 27.07.2017	Page: 110/146	
	Doc. Title: WindVal Final Report				

Another aspect that has to be taken into account regarding the comparison of the two wind data fields is the different temporal and spatial resolution of the two lidar instruments. **Figure 9-16** depicts the measurements grids of the two instruments. The schematic is true to scale with respect to the horizontal and vertical extension of the respective bins. For the 2- μ m lidar, the distance from the aircraft to the ground is subdivided into bins of 100 m vertical thickness. The vertical bin thickness of the A2D data depends on the ACCD integration times as well as on the off nadir angle of the laser LOS. The minimum integration time per bin of 2.1 μ s translates into 315 m in range and, considering the off nadir angle of 20°, into 296 m in height. Based on the flight altitude of the aircraft which is indicated as red line and used as the definition for the middle of the internal reference bin, the upper and lower boundary of each A2D bin are calculated considering the off nadir angle. The A2D range-gate setting illustrated in the sketch is only exemplary and can be changed depending on the scientific objective of the measurement section (see e.g. **Figure 9-4**).

The spatial and temporal differences of the two lidar instruments necessitate an aerial interpolation as comprehensively explained in TN 5.2, 5.2.2 and Marksteiner (2013), chapter 4.1.1. Here, one considers the whole two-dimensional A2D measurement scene grid overlaid by the 2- μ m grid. In this way, a single A2D bin can be covered by multiple 2- μ m bins horizontally and vertically. The contributions of the single 2- μ m bins to the wind data comparison are weighted by their horizontal and vertical overlap with the regarded A2D bin. The weighting of the total aerial contribution of a 2- μ m bin to the coverage of the selected A2D bin is the product of the respective horizontal and vertical weighting values, where the weighting values are chosen such that the product-weightings of all the contributing 2- μ m bins sum up to 1. Finally, the wind value of every contributing 2- μ m bin is multiplied by the corresponding weighting and the resulting sum is allocated as a 2- μ m wind value to the respective bin on the A2D grid. The 2- μ m wind data obtained during the measurement period on 19/05/2015 between 13:42 and 14:14 UTC is depicted in **Figure 9-17**. While the plot on top shows the profile after projection onto the A2D-LOS axis, the bottom plot represents the 2- μ m wind data after aerial interpolation to the A2D grid.

It often occurs that the whole area of an A2D range-bin is not entirely covered by 2- μ m bins, so that the 2- μ m wind speed value used for comparison with the A2D wind speed value must be determined from the remaining contributions. In order to calculate a correct interpolated wind speed for the composite 2- μ m bins, the wind speed obtained from the valid contributions has to be divided (scaled) by the percentage of their area on the whole area of the A2D range-bin. This procedure holds the risk of large discrepancies between the interpolated 2- μ m wind and the compared A2D wind in case of a too low coverage, especially for strong vertical or horizontal wind shear on spatial scales comparable to the size of an A2D range-gate.

Therefore, the percentage of coverage has been introduced as a quality control parameter. In this way, an interpolated 2- μ m bin is only considered representative and thus used for statistical comparison with an A2D bin if the coverage ratio exceeds a certain adjustable threshold. For most of the statistical comparisons performed in the frame of the WindVal campaign, an empirically determined minimum threshold of 80%-85% was chosen (see **Table 9-7**, except for 1 flight with 50%). This value was found to provide an optimal trade-off between comparability and quantity of the 2- μ m bins, thus yielding an acceptable number of representative composite 2- μ m bins that were used for comparison. The relatively large values of 80% was chosen for the WindVal campaign in order to minimize the risk of large discrepancies between the interpolated 2- μ m winds and the compared A2D winds in case of strong vertical or horizontal wind shear on spatial scales comparable to the size of an A2D range-gate. The 80% coverage ratio was investigated for the 2009 campaign dataset (DLR 2012b) and in the thesis by Marksteiner (2013). Lower values would certainly increase the bias and standard deviation in case of large wind gradients. In addition it should be mentioned that the atmospheric range-gates which were within the telescope overlap region (range-gates #5 to #7) were excluded from the statistical comparison.

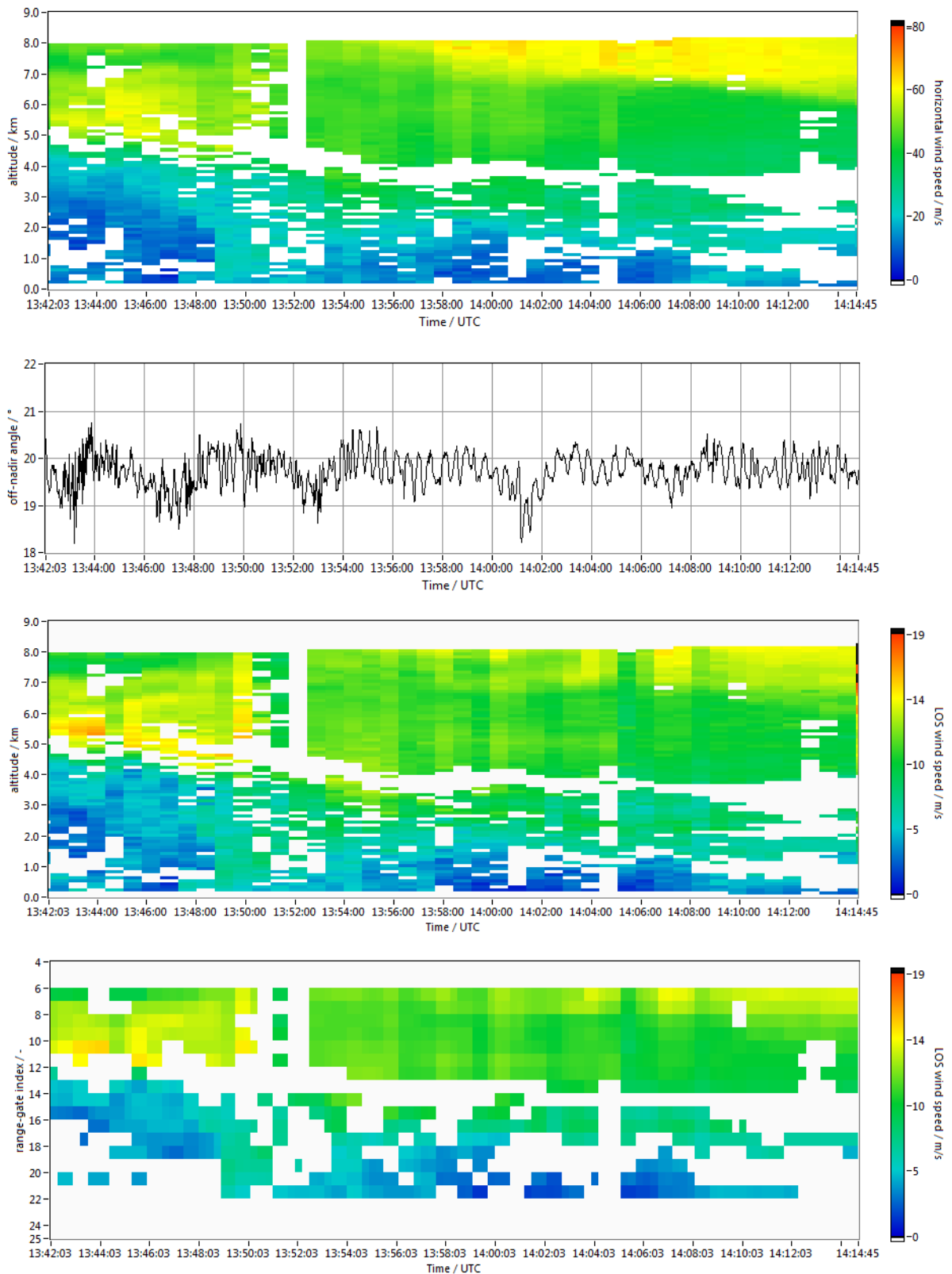


Figure 9-17: 2- μ m coherent wind lidar profiles measured on 19/05/2015 from 13:42 to 14:14 UTC. The plot on top shows the original horizontal wind profile. After projection onto the A2D-LOS axis considering the off-nadir angle variations (second plot from top), the LOS wind speed profile is obtained (third plot). Subsequent interpolation of the wind data onto the A2D measurement grid yields the profile on the bottom.

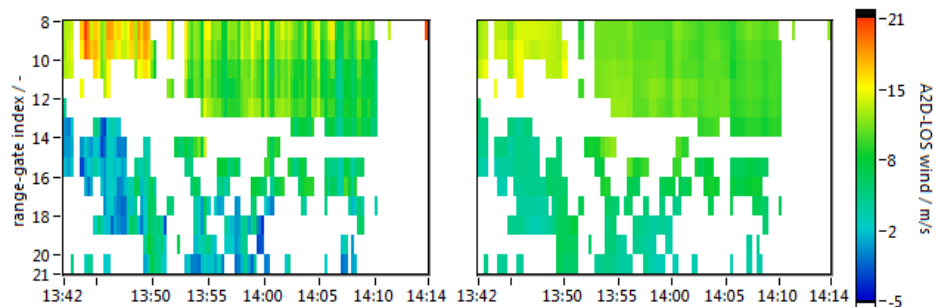


Figure 9-18: Wind profiles from 19/05/2015, 13:42 to 14:14 UTC measured with the A2D Rayleigh channel (left) and with the 2- μm coherent wind lidar (right). The 2- μm wind data was adapted to the A2D measurement grid. The plots shows only wind data for bins which contain both valid A2D Rayleigh and 2- μm winds (coverage ratio threshold: 85%). In addition, wind data inside the telescope overlap region (range-gates #5 to #7) are disregarded.

The A2D Rayleigh and 2- μm wind profiles used for comparison of the wind measurements on 19/05/2015 are shown in **Figure 9-18**. Here, the coverage ratio threshold was set to 85%. Due to the cloud and ground mask applied to the Rayleigh profile (see **Figure 9-10**) and the fact that the range-gates in the telescope region are disregarded, only very few winds measured after 14:10 UTC enter the statistical comparison. The results of the latter are best illustrated by means of a scatterplot as shown in **Figure 9-19**. Here, the A2D Rayleigh winds are plotted versus the corresponding interpolated 2- μm winds, resulting in a cloud of data points which ideally lie on the black dotted line representing $y = x$. The systematic error of the A2D winds is expressed in terms of the mean bias, i.e. the mean of the wind speed differences $v_{\text{A2D}} - v_{2-\mu\text{m}}$. Concerning the evaluation of the random wind error, the *median absolute deviation* (MAD) was determined in addition to the well-known *standard deviation* (STD). The MAD is defined as the median of the absolute variations of the measured wind speeds from the median of the wind speed differences:

$$\text{MAD} = \text{median} \left[\left| v_{\text{A2D},i} - \text{median} \left(v_{\text{A2D},i} - v_{2-\mu\text{m},i} \right) \right| \right]$$

The MAD represents a robust measure of the variability of the measured wind speeds and is more immune to outliers compared to the standard deviation. If the random wind error is normally (Gaussian) distributed, the MAD value is related to the standard deviation as $\text{STD} \approx 1.4826 \cdot \text{MAD}$. Hence, the value of $1.4826 \cdot \text{MAD}$ is calculated as well for comparison to the STD. The difference of both values indicates the probability and magnitude of outliers and deviation from a Gaussian normal distribution.

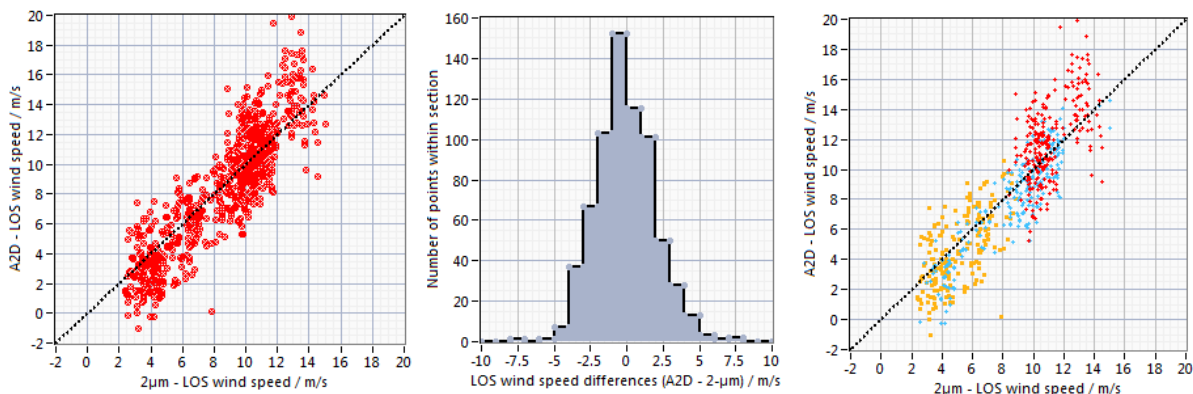


Figure 9-19: (Left) Scatterplot comparing the A2D Rayleigh and 2- μm wind speeds for all bins with valid wind measurements between range-gates #8 to #20 (as shown in Figure 9-18). (Middle) Corresponding probability density function of the wind speed differences (A2D – 2- μm). (Right) Scatterplot with the scatters divided into three groups according to the atmospheric range-gates. Data points for range-gates #8 to #10, #11 to #15 and #16 to #20 are shown in red, blue and yellow, respectively.

	Document Nr. FR.DLR.WindVal.270717	Issue: V1.1	Date: 27.07.2017	Page: 113/146	
	Doc. Title: WindVal Final Report				

The histogram in the middle of shows the number of data points per as a function of the wind speed difference $V_{A2D} - V_{2-\mu m}$ (in bins of 1 m/s) The distribution is close to a Gaussian-distributed and can be interpreted as the probability density function (PDF) of the wind error. The scatterplot on the right gives more insight into the range-dependence of the A2D wind measurement, as it shows the data points grouped into three clusters according to the atmospheric range-gates. The red data points belong to range-gates #8 to #10 (top regime close to the aircraft), the blue data points represent the middle range (#11 to #15) and the yellow group is associated to range-gates #16 to #20 (bottom regime close to the ground).

The results of the statistical comparison derived from the scatterplot are summarized in Table 9-5. Apart from the results obtained for the Rayleigh winds that were processed with the consistently used response calibration #7, the table also provides the respective comparison values for Rayleigh winds that were processed with another response calibration (Cal. #3). As outlined in section 8, calibration #3 was affected by a small anomaly supposedly in the transmit-receive path co-alignment loop which introduced an outlier in the response curve. As a result, the retrieved Rayleigh wind profile shows larger deviations to the 2- μm winds compared to the profile that was processed with calibration #7. While the mean bias and standard deviation are 0.22 m/s and 2.15 m/s, respectively for the winds processed with calibration #3, the values account for -0.06 m/s and 2.00 m/s for calibration #7.

Table 9-5: Results of the statistical comparison between the A2D Rayleigh winds and the 2- μm winds for the measurement section on 19/05/2015 from 13:42 to 14:14 UTC. The A2D winds were processed with two different Rayleigh response calibrations. The results given in the right column correspond to the left scatterplot shown in Figure 9-19.

	Calibration #3 16/05/2015, 15:33 UTC	Calibration #7 23/05/2015, 18:48 UTC
Number of compared bins	759	681
Correlation coefficient r	0.90	0.88
Mean bias (m/s)	0.22	-0.06
Standard deviation (m/s)	2.15	2.00
1.4826 · MAD (m/s)	2.10	1.95

The right plot in **Figure 9-19** reveals that the mean bias varies for winds obtained from different groups of range-gates. In particular, the bias is larger for the data points belonging to the range-gates close to the aircraft (range-gates #8 to #10, red points). This could be due to differences in the temperature profile along the LOS between the calibration and wind measurement, which inevitably causes range-dependent errors in the Rayleigh winds. Since the wind speeds are correlated with the altitude (higher wind speeds at higher levels, see right plot in **Figure 9-19**), the bias increases towards higher wind speeds. The maximum temperature difference between calibration #7 performed on 23/05/2015, between 18:48 and 19:12 UTC and the wind measurement on 19/05/2015 can be determined from temperature profiles that were measured by dropsondes released from the DC-8 aircraft in the vicinity of the respective measurement area of the A2D. The profiles obtained from multiple dropsondes released on the two days are shown in **Figure 9-20**. Comparison of the temperature profiles shows that differences up to 9 K were present at altitudes around 4 km between the calibration and the wind scene. According to DLR (2015a, section 5.2.4), a temperature drop by 15 K, however, leads to an increase in sensitivity of the measurement of only $\approx 0.1 \cdot 10^{-4} \text{ MHz}^{-1}$ (see also DLR 2010, Fig. 5.66 with a maximum temperature sensitivity of $6.4 \cdot 10^{-7} \text{ MHz}^{-1} \cdot \text{K}^{-1}$) Taking into account the Rayleigh sensitivity of about $5.8 \cdot 10^{-4} \text{ MHz}^{-1}$ in the atmospheric range-gates (see table **Table 9-3**), this corresponds to a relative (wind) error of only 1.7% for 15 K. This temperature dependency of the Rayleigh response slope is depending on the actual Fabry-Perot interferometer filter parameter (spacing, FWHM) and to some small extent also to atmospheric pressure. A value of $\approx 2\%/10 \text{ K}$ is reported by Dabas et al. (2008) and DLR (2017a) for the satellite instrument parameters of ALADIN. Thus the observed temperature difference of 9 K between calibration and wind measurement would result in Rayleigh slope errors of only 1-2%, which can not explain the observed slope errors in the wind measurements. Also the large differences

in statistical parameters using 2 different calibrations can not be explained by temperature differences between the 2 calibrations. The temperature differences derived from DC-8 dropsonde observations on 16/05/2015 (cal. #3) and 23/05/2015 (cal. #7) were about 5 K in the troposphere, and temperature differences between 2 different calibrations from one day were less than 2-3 K.

Another aspect that has an impact on the mean bias is the aircraft altitude which is generally different between the response calibration procedure and the wind measurement, leading to a deviating distribution of the range-gates over the altitude range from the aircraft to the ground. Consequently, the temperature and pressure conditions which affect the shape of the response curve in each range-gate do not exactly match those of the respective range-gates in the wind measurements.

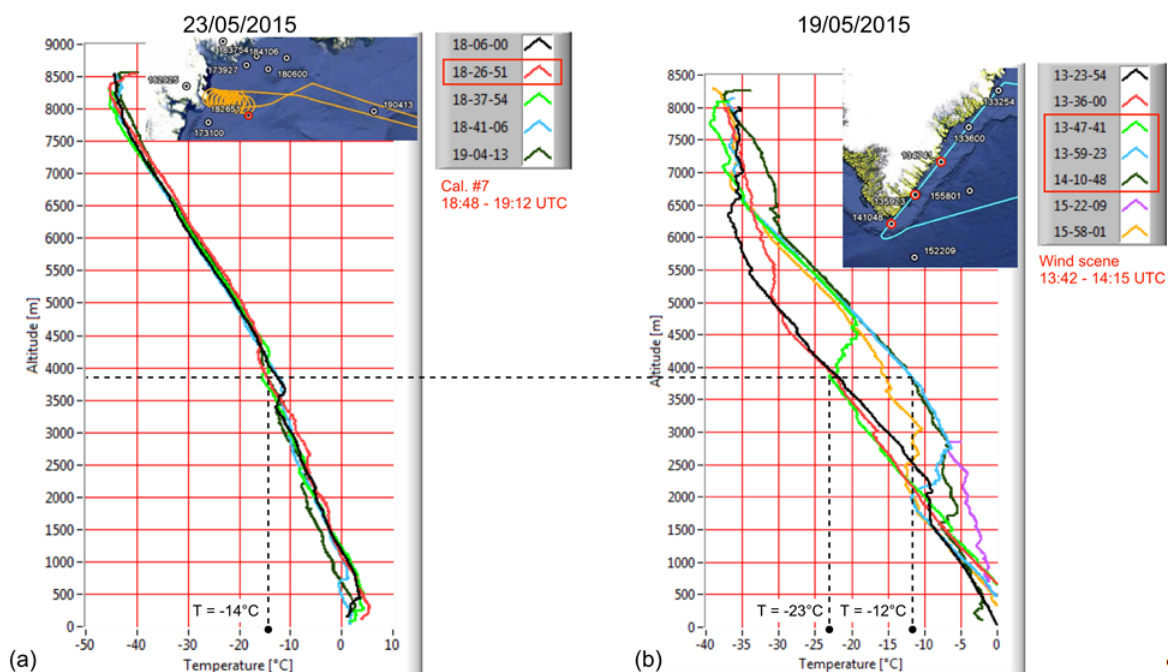


Figure 9-20: Temperature profiles measured by dropsondes that were released from the DC-8 aircraft (a) on 23/05/2015 and (b) on 19/05/2015. The red circles in the insets indicate the location of the dropsonde release. The red profile in the left diagram is representative for the Rayleigh response calibration #7, while the green, blue and dark green profiles in the right diagram were measured along the Falcon flight track during the wind scene on 19/05/2015.

In previous studies, e.g. for the airborne campaign in 2009, non-weighted linear fits $v_{A2D} = A \cdot v_{2\mu m} + B$ were performed for each wind scene in order to derive slope and intercept values which were used for evaluating the degree of accordance between the A2D and 2- μm wind data. However, it was found that the slope and intercept values crucially depend on the wind speed range that is considered for the statistical comparison. Since the random error (standard deviation) of the Rayleigh wind speeds is typically in the order of 2 to 3 m/s, a small span of wind speed values (<10 m/s) results in a rather vertically extended distribution of data points in the scatterplot. Consequently, the accuracy of the fit parameters obtained from linear regression is reduced and the slope is more likely to deviate from 1.0. In addition, not only the width of the wind speed range, but also its position has an effect on the linear fit and especially the intercept value. As the measured 2- μm wind speeds range from 2 to 15 m/s, i.e. are all positive, the intercept value is determined from an extrapolation to $v_{2\mu m} = 0$ m/s which has larger uncertainty compared to a linear fit performed for a dataset containing both positive and negative wind speeds. Hence, the slope and intercept do not represent useful statistical parameters, unless the dataset contains a broad range of positive and negative wind speed values. A more detailed assessment of the slope value is provided in the summarising discussion of the statistical analysis of the Rayleigh and Mie winds in section 9.5.

The scarce coverage of Mie winds in the discussed measurement scene prevents a statistical comparison with the 2- μm wind data, as only 25 bins fulfil the coverage ratio requirement (85%). A selected wind

	Document Nr. FR.DLR.WindVal.270717	Issue: V1.1	Date: 27.07.2017	Page: 115/146	
	Doc. Title: WindVal Final Report				

measurement which allowed for an evaluation of Mie winds is presented in section 9.4.2, while the next section highlights the results of the wind measurement carried out on 25/05/2015.

9.4 Results from selected flights

This section collects some of the highlights of the campaign and picks out particular wind measurements which are of interest for the evaluation of the wind retrieval algorithms. First, a long wind measurement performed on 25/05/2015 is presented which is characterized by a broad coverage of Rayleigh wind data and is thus appropriate for a meaningful statistical comparison with the 2- μ m reference wind lidar data. Second, the influence of the Rayleigh background correction on the quality of the Mie winds is demonstrated on the example of the flight on 28/05/2015. Finally, the characteristics of the wind data obtained in the WindVal campaign is compared to that of the AC03 campaign in 2009.

9.4.1 Rayleigh wind results from 25/05/2015 – broad data coverage

The goal of the measurement flight conducted on 25/05/2015 was to sample the North Atlantic jet stream which was located south of Iceland. For this purpose, the Falcon aircraft flew a rectangular box pattern in order to transect the jet stream two times, as shown in **Figure 9-21** (a) and (b), thus offering a broad range of wind speeds as well as large wind gradients to be measured with the A2D and the 2- μ m reference lidar.

The wind measurement scene from 15:24:03 to 16:48:02 UTC was one of the longest of the entire campaign, yielding 280 consecutive observations (9800 measurements, see also measurement period #11 in Table 1.1 and Table 1.2). It spanned over three flight legs, two of which were conducted whilst crossing the jet stream region. During the first section (orange track in **Figure 9-21**(a)), the horizontal component of the A2D LOS unit vector was nearly parallel to the horizontal wind vector, resulting in positive LOS wind velocities, whereas negative wind speeds were measured on the way back to Iceland (blue track). The section in between showed very low wind speeds, as the A2D LOS unit vector pointed perpendicularly to the wind vector. The wind profiles measured with the A2D Rayleigh and Mie channel are depicted in **Figure 9-21**(c) and (d), while the projected wind data obtained with the 2- μ m coherent wind lidar is shown in subfigure (e). The latter was not operational after 16:31 UTC, leading to a data gap in the last part of the flight section.

The retrieved Rayleigh wind profile shows a notably high data coverage. Even though the cloud and ground mask was applied with an intensity threshold as low as 75000 LSB, a total number of 3986 valid Rayleigh winds was obtained. A thick cloud layer at about 2 to 4 km altitude prevented the acquisition of valid Rayleigh wind data in lower range-gates. In this layer, 711 Mie winds passed the SNR quality control whose threshold was set to 5.0. The small number of Mie winds is especially remarkable since the 2- μ m wind data coverage was very broad, underlining the higher sensitivity of the coherent system for detecting particulate backscatter.

Evaluation of the Rayleigh winds was made by comparison with the 2- μ m wind data which were interpolated onto the A2D measurements grid as explained in section 9.3.8. A minimum coverage ratio of 80% was set, resulting in the overlapping Rayleigh and 2- μ m profiles shown in **Figure 9-22**. Despite to the aforementioned data gap of the 2- μ m lidar and the lack of available 2- μ m winds at the beginning of the middle flight section at altitudes around 8 km, the number of bins entering the statistical comparison was as high as 1996.

The scatterplot in **Figure 9-23** demonstrates the excellent agreement of the A2D Rayleigh wind data with that of the reference lidar system. The mean bias (A2D – 2- μ m wind speeds) was determined to be 0.70 m/s, while the standard deviation (random error) was calculated to be 1.80 m/s. These results verify the good performance of the A2D system during the investigated flight section and the good applicability of the Rayleigh response calibration (#7 from 23/05/2015) used for the Rayleigh wind processing. The scatterplot also indicated the broad range of detected wind speeds which can be classified into three groups according to the three flight sections with different orientation of the LOS unit vector with respect to the wind vector as explained above. The histogram plotted on the right of **Figure 9-23** exhibits only slight deviations from a Gaussian distribution. Consequently, the value $1.4826 \cdot \text{MAD} = 1.67 \text{ m/s}$ is very similar to the standard deviation.

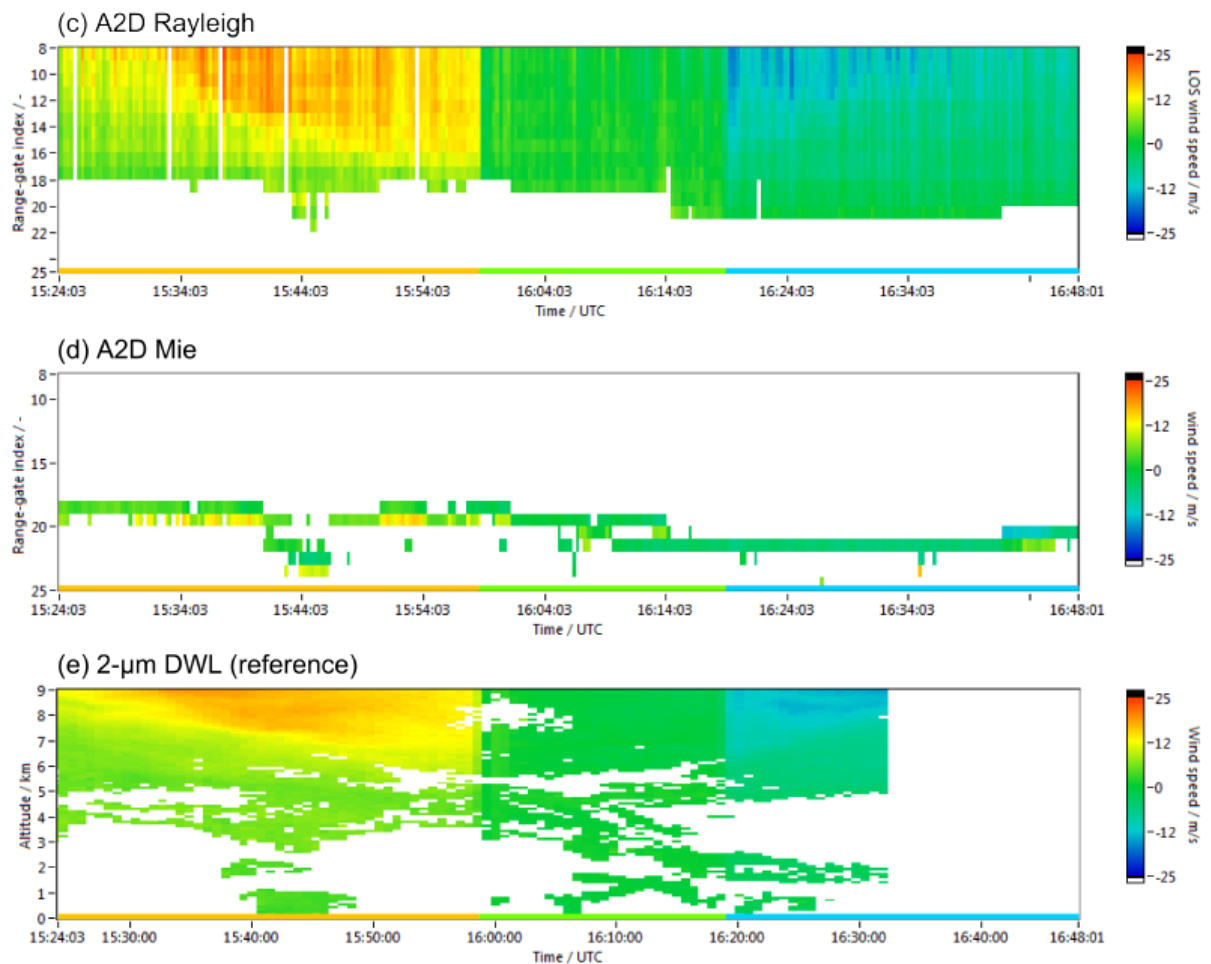
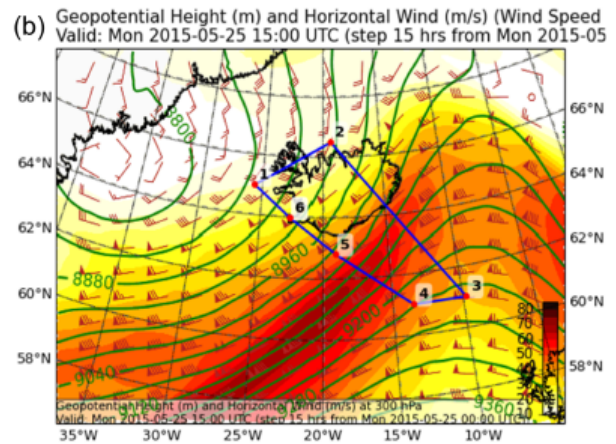
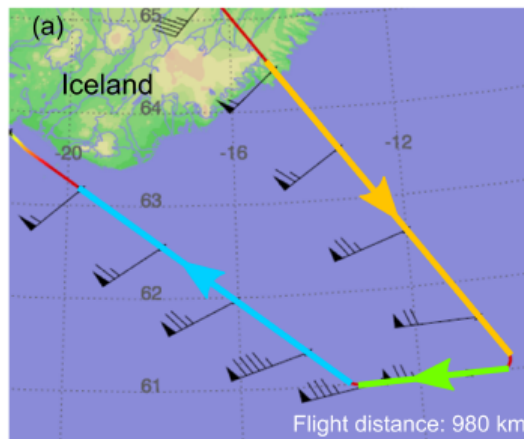


Figure 9-21: Wind measurement scene performed on 25/05/2015 between 15:24:03 and 16:48:02 UTC: (a) Flight track of the Falcon aircraft south of Iceland with three separate legs, (b) horizontal wind speed on 25/05/2015, 15:00 UTC according to a ECMWF forecast from 25/05/2015, 0:00 UTC, (c) - (e) depict the A2D Rayleigh, A2D Mie and the 2- μ m DWL LOS wind profiles obtained for the respective flight section. The 2- μ m DWL was not operational after 16:31 UTC.

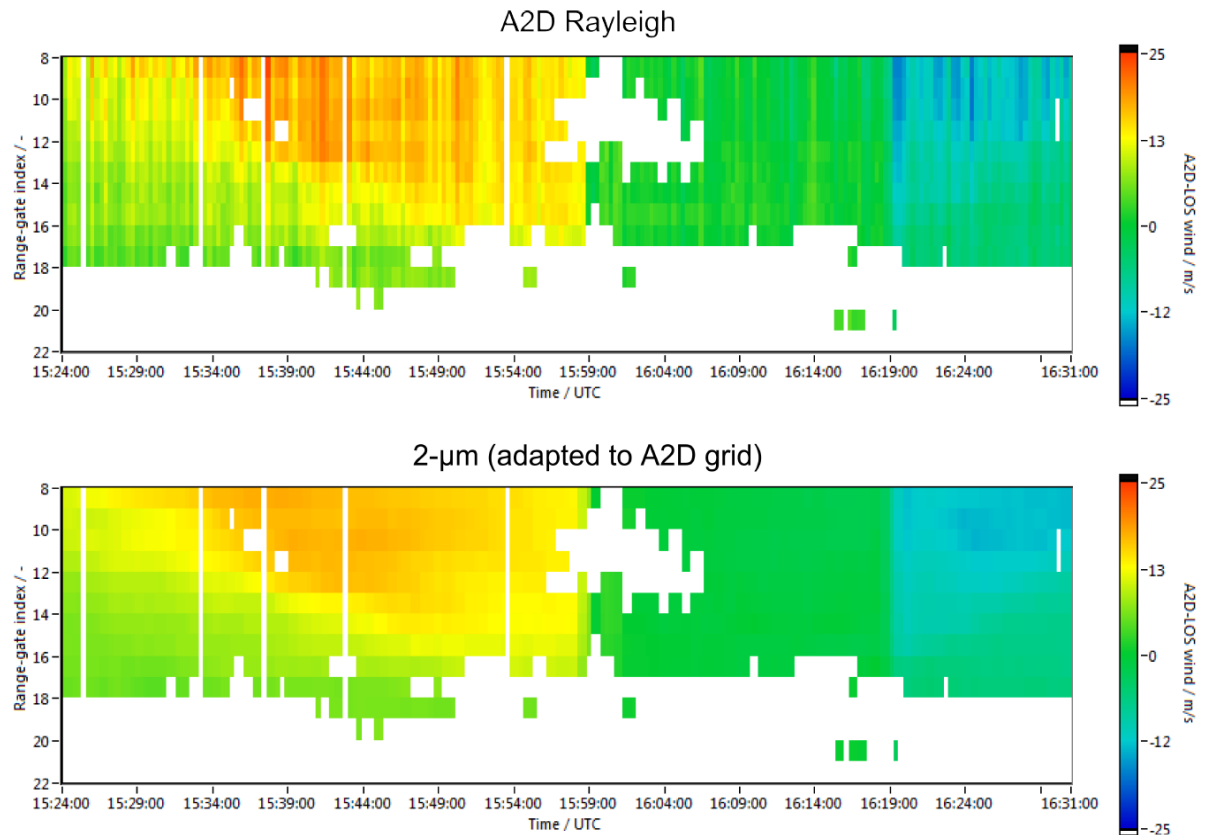


Figure 9-22: Wind profiles from 25/05/2015, 15:24 to 16:31 UTC measured with the A2D Rayleigh channel (top) and with the 2- μ m coherent wind lidar (bottom). The 2- μ m wind data was adapted to the A2D measurement grid. The plots shows only wind data for bins which contain both valid A2D Rayleigh and 2- μ m winds (coverage ratio threshold: 80%).

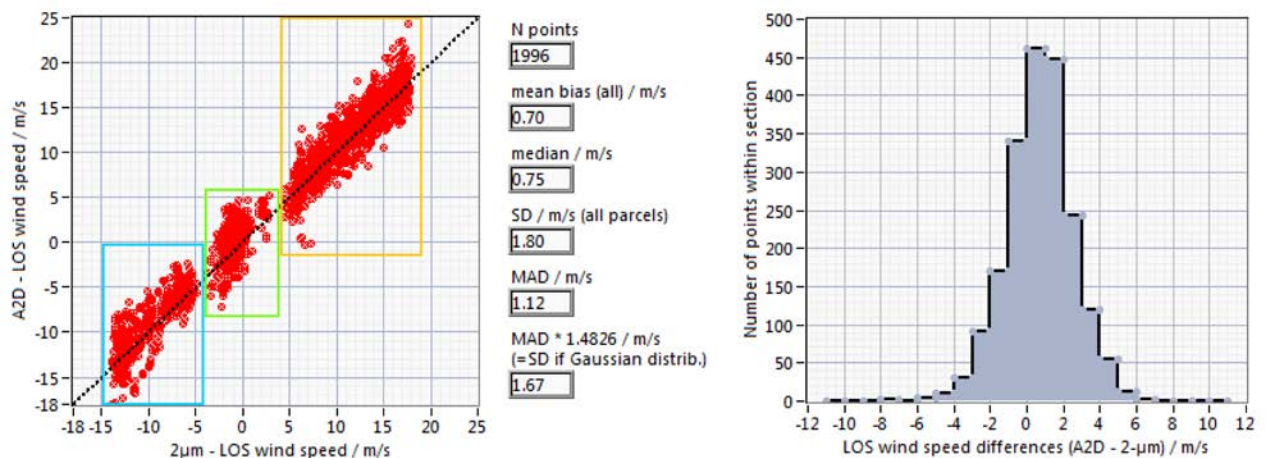


Figure 9-23: (Left) Scatterplot comparing the A2D Rayleigh and 2- μ m wind speeds for all bins with valid wind measurements between range-gates #8 to #22 (as shown in Figure 9-22). The three portions of data points indicated by coloured boxes can be attributed to the three separate flight legs within the measurement period (see Figure 9-21), since each flight section (aircraft orientation) provided different ranges of LOS wind speeds. (Right) Corresponding probability density function of the wind speed differences (A2D – 2- μ m).

Grouping of the data points according to the atmospheric range-gates, as introduced in 9.3.8, leads to the plot shown in **Figure 9-24**. The diagram illustrates that the highest (absolute) wind speeds (± 15 m/s) were measured in the range-gates close to the aircraft (red points), i.e. in the altitudes where the jet stream resides. In contrast, rather low wind velocities (± 7 m/s) were detected close to the ground (yellow points). Although the span in wind speed is different for the three groups, the corresponding linear fits are very similar and agree well with the ideal case $x = y$.

In general, the availability of both positive and negative winds in the three “range groups” of data points increases the significance of the linear regression for the three groups. Furthermore, it facilitates the decoupling of range-dependent errors, e.g. related to the co-alignment loop, from the actual slope error, which is caused by an imperfect response calibration. Due to the correlation between wind speed and altitude, data points belonging to a specific group of range-gates are typically clustered in a specific region of the scatterplot, as observed for the flight on 19/05/2015 (see **Figure 9-19**), so that it is impossible to separate the range-dependent from the wind speed-dependent error sources. Hence, the statistical comparison only allows unambiguous conclusions to be drawn regarding the range-dependence, if the dataset contains LOS winds with both signs in all range-gates. This can be accomplished by performing flight legs back and forth along the same track in order to collect wind data with similar absolute values but opposite sign, thus enabling the differentiation between positive and negative bias from the different error sources.

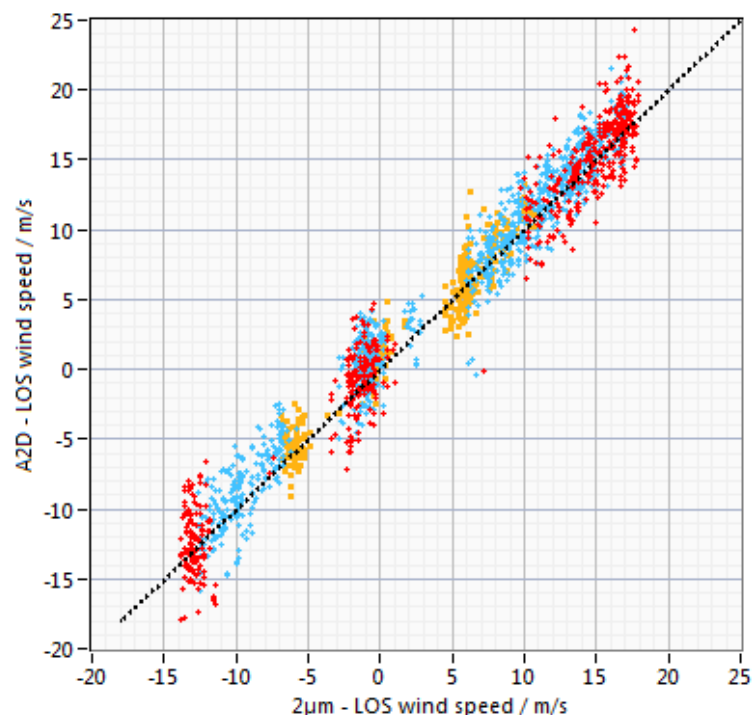


Figure 9-24: The same scatterplot as shown in Figure 9-23, but the data points are divided into three groups according to the atmospheric range-gates. Data points for range-gates #8 to #10, #11 to #15 and #16 to #20 are shown in red, blue and yellow, respectively.

Finally, it is worthwhile to analyse the range-dependence of the mean bias which is illustrated as the black graph in **Figure 9-25**. The plot reveals that mean bias increases with increasing distance from the aircraft, whereby the values for range-gates #18 to #21 are of minor significance due to the small amount of observations in this regime. Nevertheless, the values for the LOS wind speed bias especially those for the range-gates near the aircraft (0.4 m/s) are very promising with a view to the ADM-Aeolus mission where HLOS mean bias values of 0.7 m/s are required, corresponding to LOS bias values of 0.24 m/s.

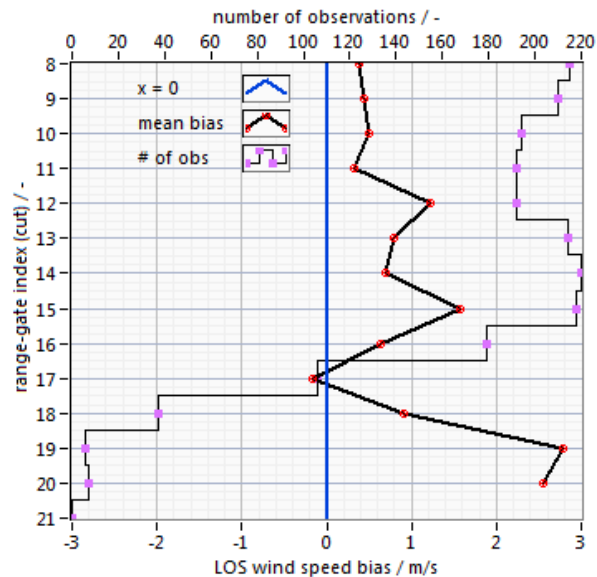


Figure 9-25: Mean bias between A2D Rayleigh and 2- μ m winds (red dots, black line) in dependence on the range-gate for the measurement scene on 25/05/2015 from 15:24 to 16:31 UTC. The pink dots indicate the number of observations available for each range-gate.

9.4.2 Mie winds from 28/05/2015 – Influence of Rayleigh background subtraction

After discussion of several Rayleigh wind profiles, the focus of this section is on the investigation of Mie winds. For this purpose, the Mie wind measurement performed on 28/05/2015 between 11:25:08 and 12:53:02 UTC (line #19 in Table 1.1 and Table 1.2) will be presented in the following. Here, 293 observations (10255 measurements) were performed, making it the longest measurement period of the whole campaign. The Falcon performed an Ω -shaped flight pattern south of Iceland as depicted in **Figure 9-26(a)**. The weather forecast predicted a mixture of low-, middle- and high-level clouds in the sampled region so that the measurement of Mie winds in all range-gates was expected.

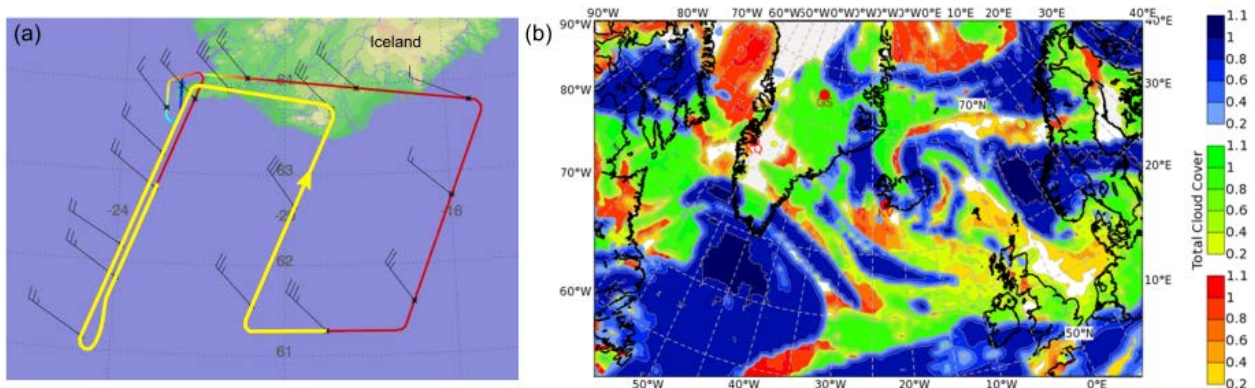


Figure 9-26: (a) Flight track of the Falcon on 28/05/2015. The wind measurement period between 11:25 and 12:53 UTC is indicated in yellow. (b) Total cloud cover on 28/05/2015, 12:00 UTC according to the ECMWF forecast from 26/05/2015, 0:00 UTC. Low-, middle- and high-level clouds are shown in orange/red, green and blue colour, respectively.

Indeed, for an SNR threshold of 4, more than 1200 Mie winds passed the quality control, resulting in the masked Mie wind profile depicted in **Figure 9-27** (bottom). The plot on top shows the SNR values for each bin during the measurement period from 11:25 to 12:53 UTC. High SNR values were especially obtained in the upper range-gates between 11:40 and 12:10 UTC when the Falcon flew close to the Icelandic coast and encountered dense high-level clouds, as predicted by the forecast (see blue region in **Figure 9-26(b)**.)

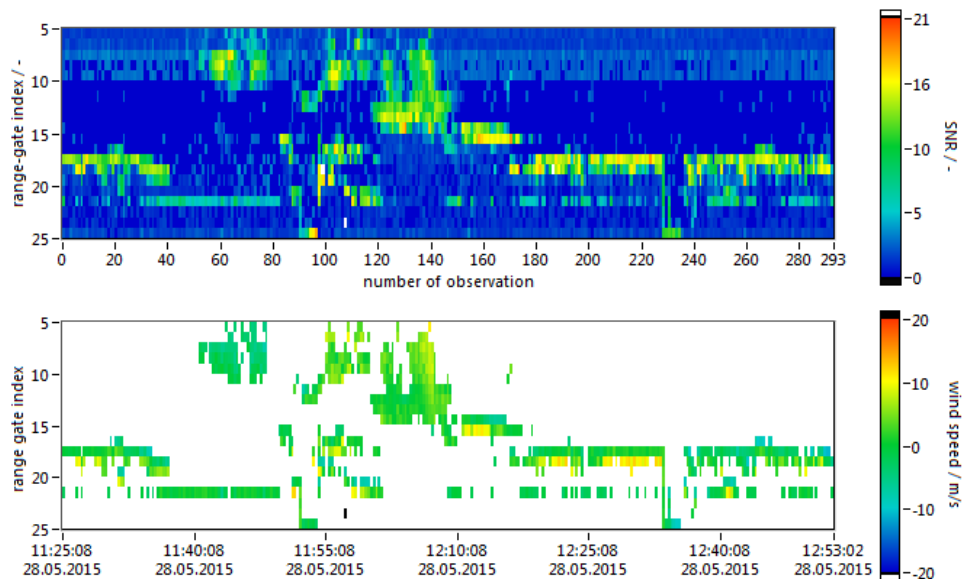


Figure 9-27: (Top) Mie signal-to-noise ratio depending on range-gate for the flight on 28/05/2015 from 11:25 to 12:53 UTC and resulting masked Mie LOS wind profile (bottom).

Next, the influence of the Rayleigh background subtraction on the data quality of the Mie wind will be presented. The telescope image used for the Rayleigh background correction was produced from the GrOUSR measurement performed between 11:19 and 11:24 UTC. It is displayed in **Figure 9-28** together with the resulting Mie SNR and Mie wind profile after Rayleigh background correction. Since the SNR distribution is affected by the background correction, a larger number of valid Mie winds were obtained (1360) which were subsequently evaluated by comparison with the 2- μ m wind data.

The scatterplots illustrating the correlation between the 2- μ m winds and the Mie winds without and with Rayleigh background correction are shown in **Figure 9-29**, while the resulting statistical values are summarized in **Table 9-6**. As can be seen, the correction of the Mie signal provides a significant improvement in the agreement of the A2D and 2- μ m wind data. The LOS mean bias is reduced by 33% from 0.83 to 0.56 m/s, while the standard deviation decreased from 3.31 to 2.89 m/s (13%).

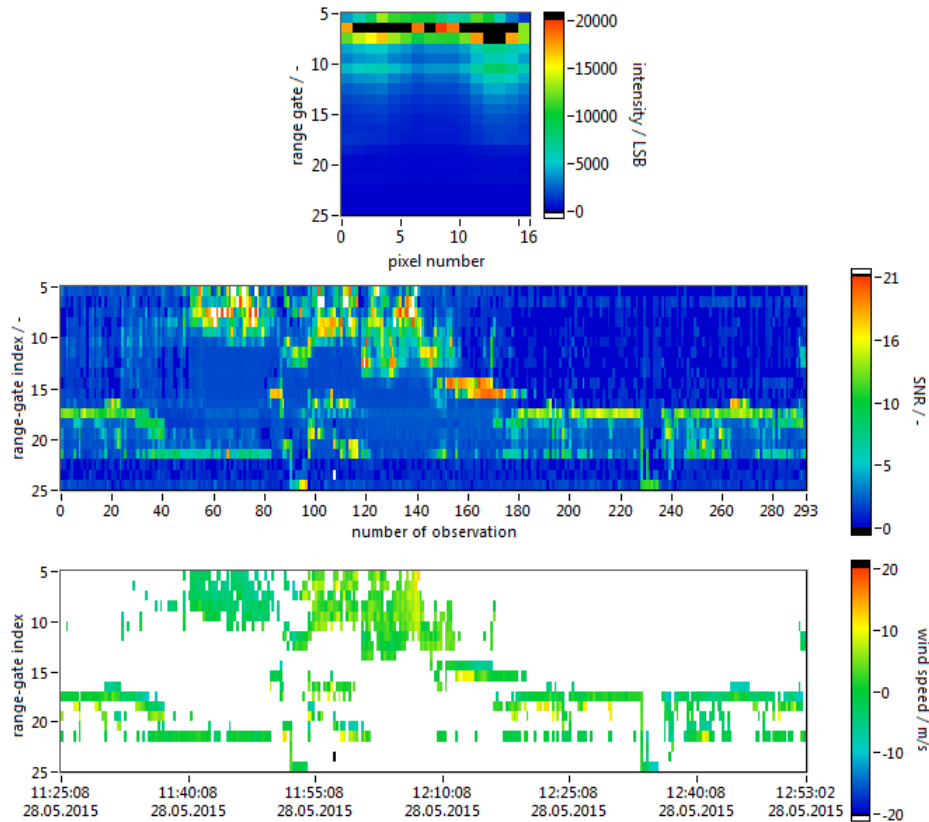


Figure 9-28: (Top) Telescope image obtained from the GROUSR procedure on 28/05/2015 between 11:19 and 11:24 UTC, (middle) Mie SNR profile and (bottom) Mie LOS wind profile after Rayleigh background subtraction.

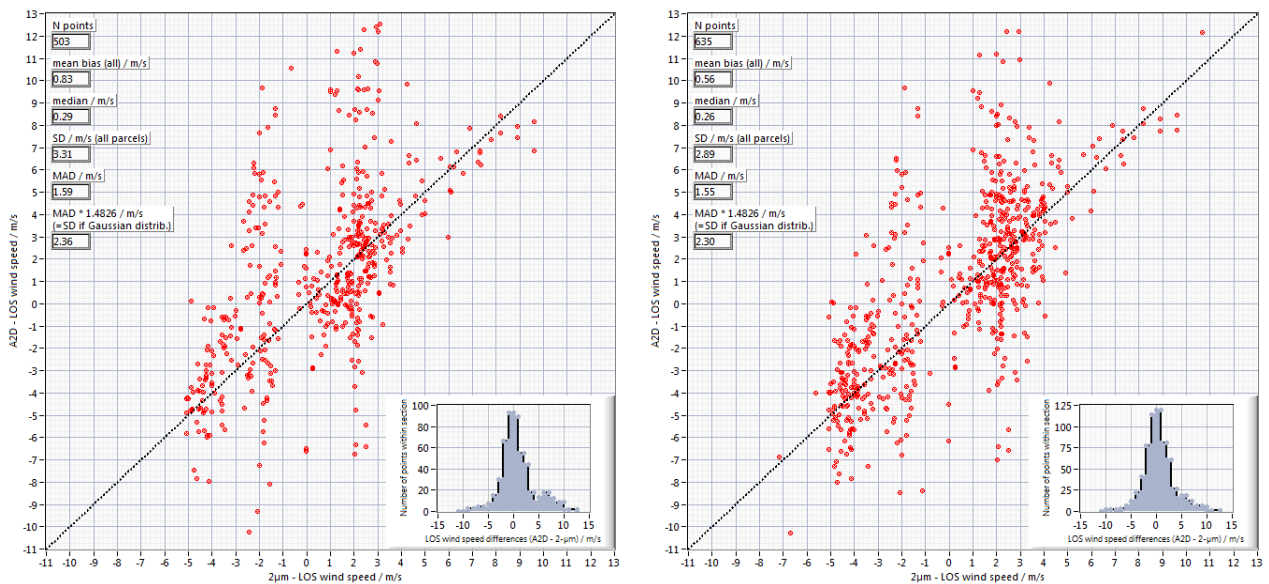


Figure 9-29: Scatterplot comparing the A2D Mie and 2- μ m wind speeds for all bins with valid wind measurements between range-gates #7 and #22 obtained during the flight section on 28/05/2015 from 11:25 to 12:53 UTC. The diagrams show the comparison for Mie winds without (left) and with (right) Rayleigh background subtraction, respectively (see corresponding wind profiles in Figure 9-27 and Figure 9-28). The insets show the corresponding probability density function of the wind speed differences (A2D – 2- μ m).

Table 9-6: Results of the statistical comparison between the A2D Mie winds and the 2- μ m winds for the measurement section on 28/05/2015 from 11:25 to 12:53 UTC. Better agreement is achieved after Rayleigh background correction.

	Without Rayleigh background correction	With Rayleigh background correction
Number of compared bins	503	635
Correlation coefficient r	0.60	0.71
Mean bias (m/s)	0.83	0.56
Median (m/s)	0.29	0.26
Standard deviation (m/s)	3.31	2.89
1.48 · MAD (m/s)	2.36	2.30

Nevertheless, large differences are present between the A2D Mie and the 2- μ m wind profiles that entered the statistical comparison, as shown in **Figure 9-30** (third and fourth diagram from top). The largest discrepancies in wind speed of up to ± 10 m/s are observed in the lower range-gates #14 to #19 which is visualized by the plot on the bottom of **Figure 9-30** illustrating the wind speed difference between the 2- μ m DWL and A2D data. In addition, the figure provides the 2- μ m DWL range-corrected signal intensity and the wind profile obtained after projection onto the A2D-LOS axis (first two plots from the top).

For investigating the origin of the large wind errors, some of the affected bins were further analysed with respect to the Mie SNR and 2- μ m DWL signal intensity. **Figure 9-31** shows a portion (range-gates #12 to #19) of the Mie SNR data and wind profiles discussed before. The group of bins exhibiting the largest wind errors are indicated by a black frame (see also the corresponding areas in **Figure 9-30**). While the 2- μ m wind speeds (third plot from top) are nearly identical and close to 0 m/s within this spatiotemporal region, the A2D Mie winds exhibit large differences in the order of ± 10 m/s between adjacent range-gates and at a time difference of less than two minutes. Interestingly, the corresponding Mie SNR shows large variations within the selected region ranging from 5 (close to the threshold) to 21.

Hence, it can be assumed that this scene was characterized by a high heterogeneity of the atmosphere with a highly variable cloud and aerosol content within the regarded altitude range and measurement period. This is supported by the variable range-corrected 2- μ m DWL signal intensity in this region (see blue frame in **Figure 9-30**, plot on top). Obviously, large gradients in backscatter coefficient from clouds cause erroneous wind speed gradients. The wind speed error is especially large for bins with coverage ratios below 1 (range-gate #14) as well as for bins with low SNR (range-gate #15).

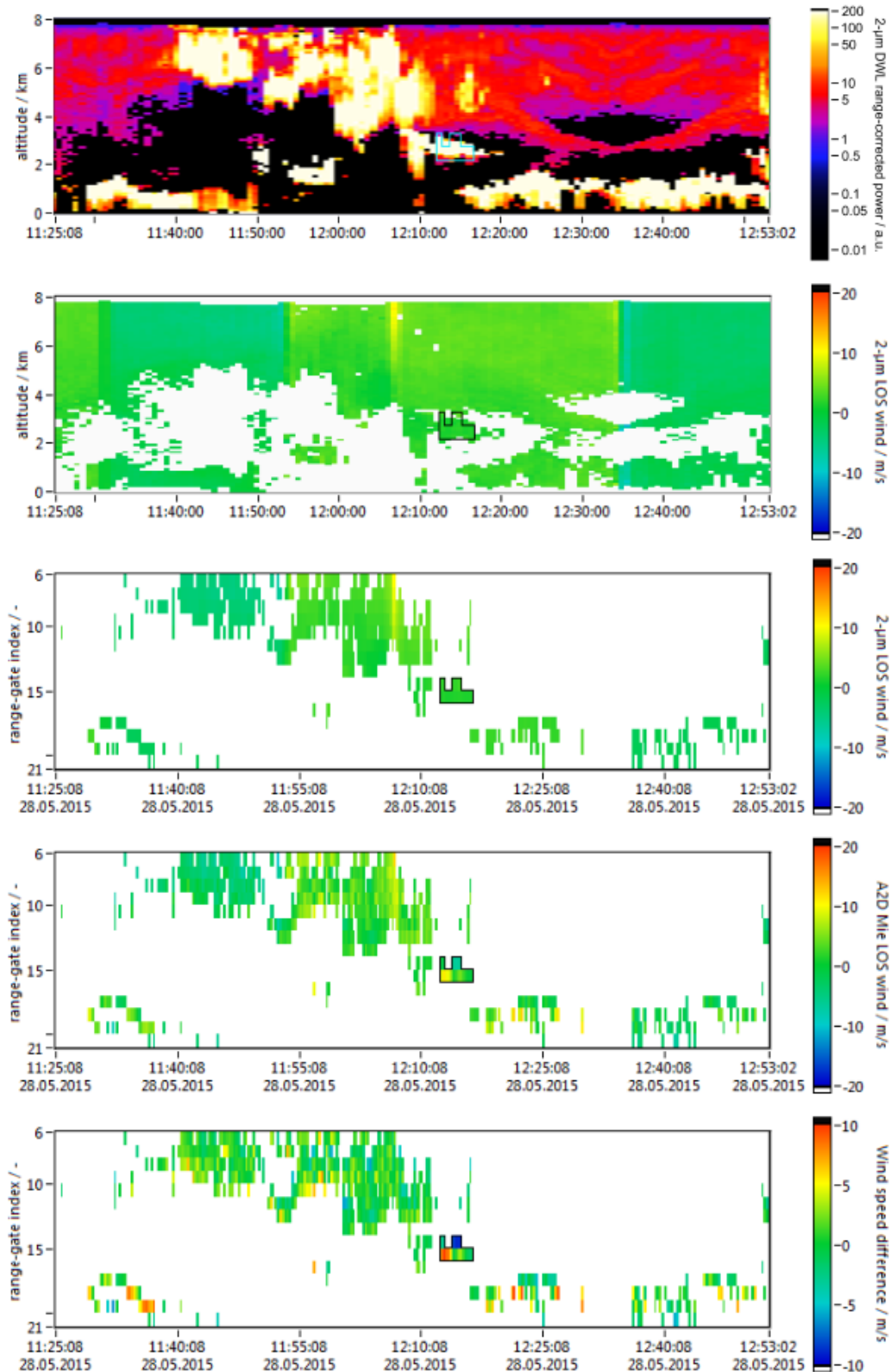


Figure 9-30: Comparison of 2-µm DWL and A2D Mie data measured on 28/05/2015, 11:25 to 12:53 UTC. The 2-µm range-corrected signal intensity (power) and LOS wind profile without adaptation to the A2D measurement grid are shown on top. The third and fourth diagram depict the 2-µm and A2D wind profiles used for the statistical comparison, respectively, while the bottom plot displays the wind speed difference A2D – 2-µm. The region with the largest wind error is indicated in all plots.

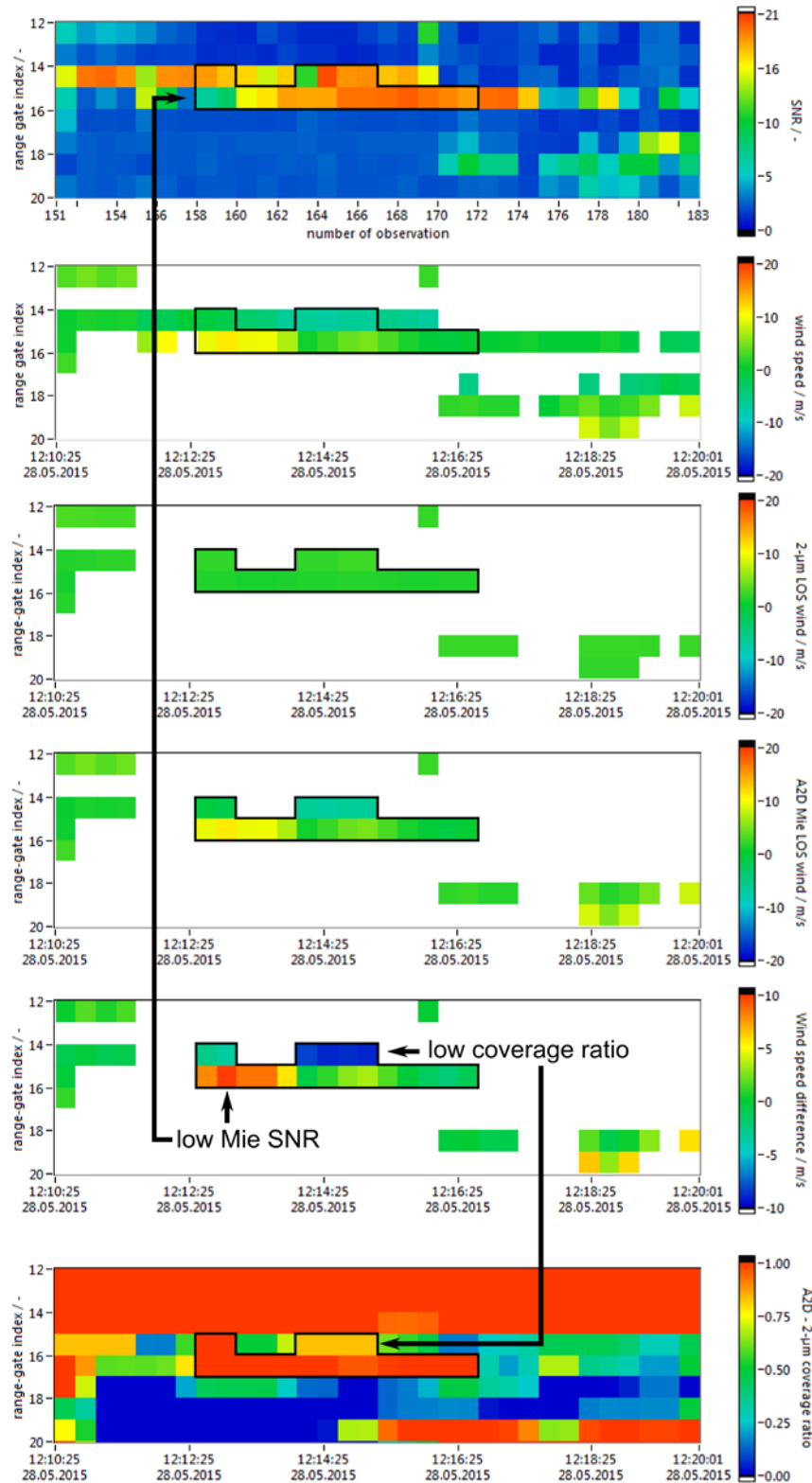


Figure 9-31: Portion of the Mie SNR, 2- μm and A2D Mie wind profiles from Figure 9-28 and Figure 9-30. The diagrams show from top to bottom: the Mie SNR profile, the Mie wind profile after Rayleigh background subtraction, the 2- μm DWL wind profile after aerial interpolation onto the A2D grid, the Mie wind profile containing only bins which are available from both the 2- μm and the A2D Mie wind data, the wind speed difference A2D – 2- μm and the coverage of 2- μm DWL data on the respective A2D bin.

9.4.3 Increased Mie standard deviation compared to the campaign in 2009

Despite the improvement of the Mie wind accuracy and precision by means of the Rayleigh background correction, the random error of almost 3 m/s is still too large regarding the mission requirements of ADM-Aeolus. Taking a look at a similar scenario studied during the AC03 campaign in 2009, it becomes obvious that the random error of the Mie winds has increased from 2009 to the particular wind measurement scene in 2015 presented before. **Figure 9-32** shows the scatterplot resulting from the statistical comparison of the 2- μm and Mie winds measured on 01/10/2009 from 9:35 to 10:39 UTC. In contrast to the right plot in **Figure 9-29**, the correlation is much higher (0.97 compared to 0.71) and the standard deviation is only 1.49 m/s. However, the mean bias is lower in the 2015 case due to the fact that the A2D winds are nearly symmetrically distributed about the reference 2- μm winds, leading to positive and negative deviations of similar magnitude which compensate each other.

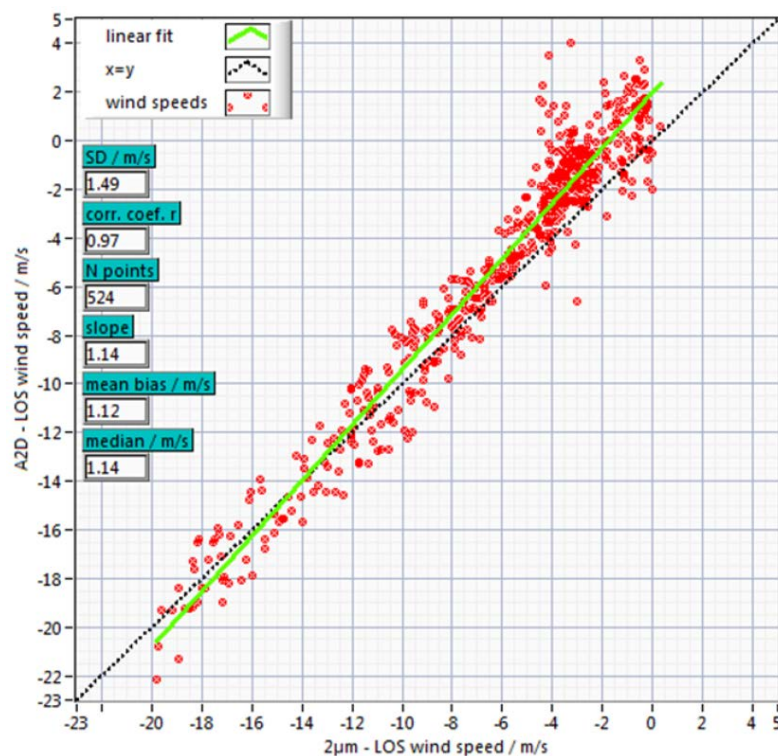


Figure 9-32: Scatterplot comparing the A2D Mie and 2- μm wind speeds for the flight section on 01/10/2009 from 9:35 to 10:39 UTC.

One possible explanation for the increased random error encountered for the flight on 28/05/2015 is the occurrence of a special cloud structure and an exceptionally heterogeneous atmosphere as discussed above. In particular, the position of the top edges of optically thick clouds within the range-gates has a significant influence on the wind data. According to Sun et al. (2014) who investigated the performance of ADM-Aeolus in heterogeneous atmospheric conditions using high-resolution radiosonde data, a non-uniform distribution of clouds and/or aerosols within a range bin introduces biases in the Mie winds exceeding 0.4 m/s and random errors of more than 2 m/s.

Simulations revealed that the bias for Rayleigh winds is largest for optically thick and geometrical thin particle layers within a range bin, whereas the bias for Mie winds is largest for optically thick and geometrical thick particle layers (Sun et al. 2014). Furthermore, it was concluded that, in case of a vertical bin size of 1 km and a (typical) wind shear of 0.01 s^{-1} , the Mie winds show large height assignment errors of several hundred meters and corresponding wind errors of 1.5 to 2.9 m/s, depending on the cloud conditions. Also, it was found that the random wind error increases linearly with the vertical bin size.

The diagram in **Figure 9-33** shows the scatterplot from **Figure 9-29** after grouping of the data points according to the atmospheric range-gates, as introduced in 9.3.8. It illustrates that the largest deviations between the A2D Mie and 2- μm winds occurred in the lower range-gates close to the ground (yellow data points). However, the fact that the resolution of these range-gates ($2.1\ \mu\text{s}$, 315 m bin size) was set to be higher than that of the medium range-gates ($4.2\ \mu\text{s}$, 630 m bin size), suggests that the origin of the increased error is not entirely due to the heterogeneous atmospheric conditions as elaborated above.

However, another aspect that has to be considered in this context is the range-gate overlap. Like for the ground return signals, the return signal from clouds can be contained in two neighboring range-gates owing to the operation principle of the ACCD. Unlike for the ground echos, the return signals from clouds covering multiple range-gates are not added which introduces a bias to the Mie winds. This effect is especially pronounced in smaller range-gates, as the relative size of the overlap region is larger compared to range-gates with longer integration time. As discussed in TN 5.2, section 3.2.5, the signal summation over two adjacent range-gates containing cloud signals results in better agreement between the Mie winds and the 2- μm DWL wind data.

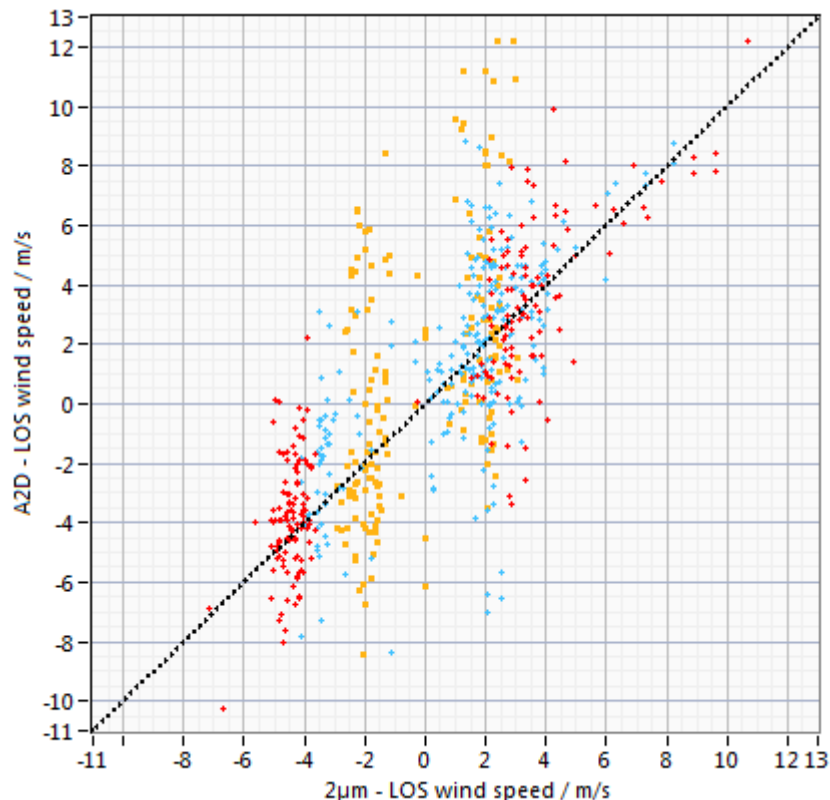


Figure 9-33: The same scatterplot as shown in Figure 9-29, but the data points are divided into three groups according to the atmospheric range-gates. Data points for range-gates #6 to #8, #9 to #14 and #16 to #20 are shown in red, blue and yellow, respectively.

	Document Nr. FR.DLR.WindVal.270717	Issue: V1.1	Date: 27.07.2017	Page: 127/146	
	Doc. Title: WindVal Final Report				

9.5 Statistical comparison of all wind measurement scenes

After presentation of selected wind measurements, an overall summary of the results obtained from all flights is provided in this section. From the 21 wind measurements carried out in the scope of the WindVal campaign, 18 Rayleigh wind scenes and 5 Mie wind scenes have been compared to the corresponding 2- μm wind profiles. An overview of the outcomes of the statistical comparison is given in **Table 9-7** and **Table 9-8** for the Rayleigh and Mie winds, respectively and will be discussed in the following.

9.5.1 Statistical comparison of Rayleigh winds with 2- μm winds

Apart from 18 Rayleigh wind measurements conducted in the WindVal campaign, **Table 9-7** also provides information on the accuracy and precision of the wind data obtained for two flights in 2009 (first two lines). The asterisked values given in the “ N ” column indicate the number of compared winds after outlier removal, i.e. after sorting out bins for which the wind speed differences between the Rayleigh and 2- μm winds is larger than ± 10 m/s. For the sake of completeness, the table also presents the slope value calculated from a linear fit through the A2D - 2- μm scatterplot. Results showing good agreement between the two lidar systems (slope near 1.0, low mean bias, small standard deviation, etc.) are highlighted in green, while large discrepancies are shown in red.

The table reveals that a total number of more than 12000 Rayleigh winds were analysed by comparison with 2- μm winds. The best agreement was found for the flight on 25/05 which was discussed in section 9.4.1. Here, the deviation from the ideal slope is below 1% and the mean bias is 0.60 m/s, while the standard deviation is 1.80 m/s. These results are especially remarkable since this flight section was also the longest one yielding the largest dataset for statistical comparison. Even lower mean bias was determined for the flight section on 15/05 from 18:09 to 19:09 UTC, yielding -0.13 m/s, while the standard deviation was moderate (2.16 m/s). In contrast, the measurement period on 16/05, starting at 20:02 UTC produced only 126 valid Rayleigh winds to be compared to the 2- μm data. Consequently, a very poor correlation was obtained (correlation coefficient: 0.32), so that the slope and mean bias values of 0.43 and 3.69 m/s lack statistical significance.

In order to assess the uncertainty of the slope A , the *standard error* s_A was calculated according to

$$s_A = \sqrt{\frac{\frac{1}{N-2} \sum_{i=1}^N \hat{\varepsilon}_i^2}{\sum_{i=1}^N (v_{2-\mu\text{m},i} - \overline{v_{2-\mu\text{m}}})^2}}$$

Here, the numerator in the square root represents the mean square error which is determined by the residuals of the linear regression $\hat{\varepsilon}_i = v_{\text{A2D},i} - (A \cdot v_{2-\mu\text{m},i} + B)$, while the denominator is the variance of the 2- μm wind speeds, i.e. a measure of the wind speed range. Hence, the smaller the wind speed range, the larger the standard error of the fitted slope. Based on the standard error, confidence intervals can be calculated for the slope values of the respective measurement scenes. Assuming a Student's t-distribution, the (two-sided) 95%-confidence intervals (CIs, probability level $\alpha = 1 - 0.95 = 0.05$) for the slope values are given as

$$\left[A - t_{1-\alpha/2, N-2} \cdot s_A; A + t_{1-\alpha/2, N-2} \cdot s_A \right],$$

where $t_{1-\alpha/2, N-2}$ is the so-called critical value, while N is the number of samples (compared bins). The precise critical values are listed in tables or can be computed on interactive calculating web pages, e.g. on <http://www.danielsooper.com/statcalc/calculator.aspx?id=10>. For typical sample sizes used in the statistical analysis of the A2D winds with several hundreds of compared winds, the critical value is $t_{0.975, N-2} \approx 2.0$.

Hence, the 95%-confidence intervals are approximately $A \pm 2s_A$. The confidence intervals are given in **Table 9-7** and **Table 9-8** together with the respective slope values for each measurement scene.

	Document Nr. FR.DLR.WindVal.270717	Issue: V1.1	Date: 27.07.2017	Page: 128/146	
	Doc. Title: WindVal Final Report				

Comparison of the scenes reveals that the slope not only shows large uncertainty in case of a small number of data points, but also crucially depends on the range of wind speeds within the dataset according to the above definition of the standard error. The same holds for the correlation coefficient. This becomes obvious for the scene on 13/05, where the wind speed span was only 4 m/s, resulting in a very broad confidence interval of 0.40 and low correlation coefficient of 0.27, despite a relatively large number of compared bins (536). In contrast, the interval for the outstanding flight on 25/05 is as narrow as 0.016.

In a next step, the confidence interval can be used to test the statistical significance of the linear fit. As the true slope has to be 1.0 (assuming negligible wind error of the 2- μm reference lidar), the slope value can be considered meaningless if the 95%-confidence interval does not include this true value. This is the case for 7 of the 18 scenes used for the statistical comparison of the Rayleigh winds. Thus, the respective slope values are given in parentheses in **Table 9-7**. The quantity 1.4826-MAD is provided in the two tables as well. The fact that STD and 1.4826-MAD show large discrepancies for several scenes, e.g. for the flight on 16/05, 20:02 UTC indicates that the wind speed error is far from a normal Gaussian distribution in these cases.

Taking a look at the variation of the statistical parameters in the course of the campaign, one notices that the quality of the Rayleigh winds changes from flight to flight. For instance, very low random error was obtained in the measurement periods on 23/05, whereas the results from the flight on 28/05 showed large mean bias and random errors (see also **Figure 12-5** and **Figure 12-6** in the appendix). Large statistical differences are also observed between subsequent measurements performed during the same flight. On 16/05, the Rayleigh winds retrieved during the period from 19:46 to 20:01 UTC showed negative mean bias (-1.53 m/s, see **Figure 12-7**), while the profiles measured shortly afterwards (20:02 to 20:32 UTC) have a positive bias (3.69 m/s) and much larger random error (3.58 m/s, see **Figure 12-8**). This is especially striking since the number of compared bins is comparable in both scenes. Moreover, the wind speed range is even larger in the second case so that a better correlation between the 2- μm and Rayleigh winds would be expected. In contrast, the correlation coefficient is only 0.32.

The reasons for this drastic change in data quality are not clarified, yet. One possible explanation is the presence of clouds which introduce large errors due to Mie contamination of the Rayleigh channel as explained above. Additionally, clouds (especially in the vicinity of the aircraft) deteriorate the performance of the transmit-receive path co-alignment loop due as they influence the beam propagation, thus affecting the incidence angle of the backscatter signals on the Fabry-Pérot interferometer. According to TN 5.3 which discusses the Rayleigh spectrometer alignment sensitivity, an unconsidered vertical incidence angle change of 1 μrad causes an error in wind speed determination of 0.39 m/s.

Table 9-7: Results of the statistical comparison between the A2D Rayleigh winds and the 2- μ m winds for two flights performed in 2009 (first two lines) and all wind measurement scenes in 2015 (excluding the transfer flights on 11/05/2015). The Rayleigh response calibration #7 from 23/05/2016, 18:48 UTC was used for Rayleigh wind processing of the data obtained in the frame of the WindVal campaign. The asterisked values indicate the number of compared winds after outlier removal (wind speed differences larger than 10 m/s). Results showing good agreement between the A2D and 2- μ m winds (slope near 1.0, low mean bias, small standard deviation, etc.) are highlighted in green, while large discrepancies are shown in red. The last row provides the parameters obtained from the statistical comparison of all winds (see the corresponding scatterplot on the left side of Figure 9-34).

Measurement section	<i>N</i>	Corr. coeff. <i>r</i>	Slope (95% CI)	Mean bias (m/s)	Median (m/s)	STD (m/s)	1.48-MAD (m/s)	RRC	Range-gate start	Cov. ratio (%)
26/09/2009 11:50 – 12:19	511	0.85	0.97	-0.57	-0.89	2.34	2.11	Cal.2	7	85
01/10/2009 09:35 – 10:39	565	0.89	1.03	0.78 (ZWC)	0.40 (ZWC)	3.12	-	Cal.2	8	80
13/05/2015 12:24 – 12:51	536	0.27	[0.63 ±0.20]	1.62	1.58	2.13	2.10	Cal.7	8	50
15/05/2015 18:09 – 19:09	1572	0.70	[1.11 ±0.06]	-0.13	-0.13	2.16	2.01	Cal.7	8 (to 18)	80
15/05/2015 19:15 – 19:44	613	0.38	0.85 ±0.16	0.86	0.77	2.01	1.89	Cal.7	8	80
16/05/2015 14:24 – 14:59	621	0.52	[0.72 ±0.10]	1.65	1.26	4.02	4.03	Cal.7	8	80
16/05/2015 16:44 – 16:54	364	0.75	0.95 ±0.10	2.08	1.92	1.98	1.75	Cal.7	8	80
16/05/2015 19:46 – 20:01	123	0.41	1.0 ±0.4	-1.53	-1.68	1.81	1.79	Cal.7	8	80
16/05/2015 20:02 – 20:32	126*	0.32	[0.43 ±0.22]	3.69	3.83	3.58	4.22	Cal.7	8	80
19/05/2015 13:42 – 14:15	842	0.88	[1.18 ±0.04]	-0.16	-0.24	2.04	1.94	Cal.7	8	85
21/05/2015 23:45 – 00:40	882	0.44	1.09 ±0.16	-0.48	-0.53	1.62	1.44	Cal.7	8	80
22/05/2015 00:49 – 01:20	652	0.21	[0.70 ±0.26]	-0.64	-0.66	1.56	1.49	Cal.7	8 (to 19)	80
22/05/2015 01:22 – 01:48	395	0.79	0.92 ±0.08	0.69	0.51	1.79	1.69	Cal.7	8	80
23/05/2015 17:27 – 17:43	251	0.69	1.07 ±0.14	-0.56	-0.55	1.23	0.99	Cal.7	8	80
23/05/2015 20:08 – 20:39	736*	0.70	[1.11 ±0.08]	1.26	1.23	1.52	1.44	Cal.7	8	80
25/05/2015 15:24 – 16:47	1996	0.98	0.994 ±0.008	0.70	0.75	1.80	1.67	Cal.7	8	80
28/05/2015 10:50 – 11:17	322*	0.40	0.79 ±0.20	2.31	2.01	2.37	2.17	Cal.7	8	80
28/05/2015 11:25 – 12:52	1532*	0.76	1.05 ±0.05	2.37	2.11	2.70	2.44	Cal.7	8 (to 20)	80
29/05/2015 11:09 – 11:45	781	0.56	0.94 ±0.10	-0.02	-0.23	1.80	1.65	Cal.7	8	80
29/05/2015 14:37 – 15:16	303*	0.71	1.04 ±0.12	-1.01	-1.16	2.53	2.13	Cal.7	8	80
ALL	12647	0.94	1.001 ±0.006	0.68	0.50	2.44	2.08			

Accumulation of all the bins which were used for the statistical comparisons between the A2D Rayleigh and the 2- μm winds from the entire WindVal campaign yields the scatterplot depicted in **Figure 9-34** (top) together with the corresponding probability density functions (PDFs). The plot contains 12647 data points demonstrating the good data coverage of the 2- μm lidar even at low aerosol and cloud content, where the A2D Mie SNR is below the threshold and only Rayleigh winds are obtained. A linear regression fit results in statistical parameters that slightly differ from the mean values calculated in **Table 9-7**. Here, a nearly “perfect” slope of 1.001 (95% confidence interval [0.995;1.007]) and an intercept of 0.68 m/s are computed.

The latter value is identical with the mean bias $v_{\text{A2D}} - v_{2\mu}$, while the STD was determined to be 2.44 m/s ($1.4826 \cdot \text{MAD} = 2.08$ m/s). The discrepancy between the STD and the $1.4826 \cdot \text{MAD}$ value results from the fact that the wind error is not normally distributed about the mean, which is also visible in the PDF plots. In particular, the PDF exhibits a pedestal of uniformly distributed gross errors. Here, it should be noted that bins showing wind speed differences $v_{\text{A2D}} - v_{2\mu}$ larger than ± 10 m/s were removed from the dataset. The scenes for which this outlier removal was performed are indicated by an asterisk in **Table 9-7**.

The results of the statistical comparison of all Rayleigh winds are very promising with respect to the upcoming ADM-Aeolus mission, although the LOS random error is still too high and additional analysis is required to reduce this value. Nevertheless, the good agreement of the A2D Rayleigh wind data with the 2- μm reference lidar data over a large wind speed range from about -15 m/s to +18 m/s underlines the excellent performance of the A2D Rayleigh channel during the WindVal campaign and its high relevance for future Cal/Val activities after the launch of ADM-Aeolus.

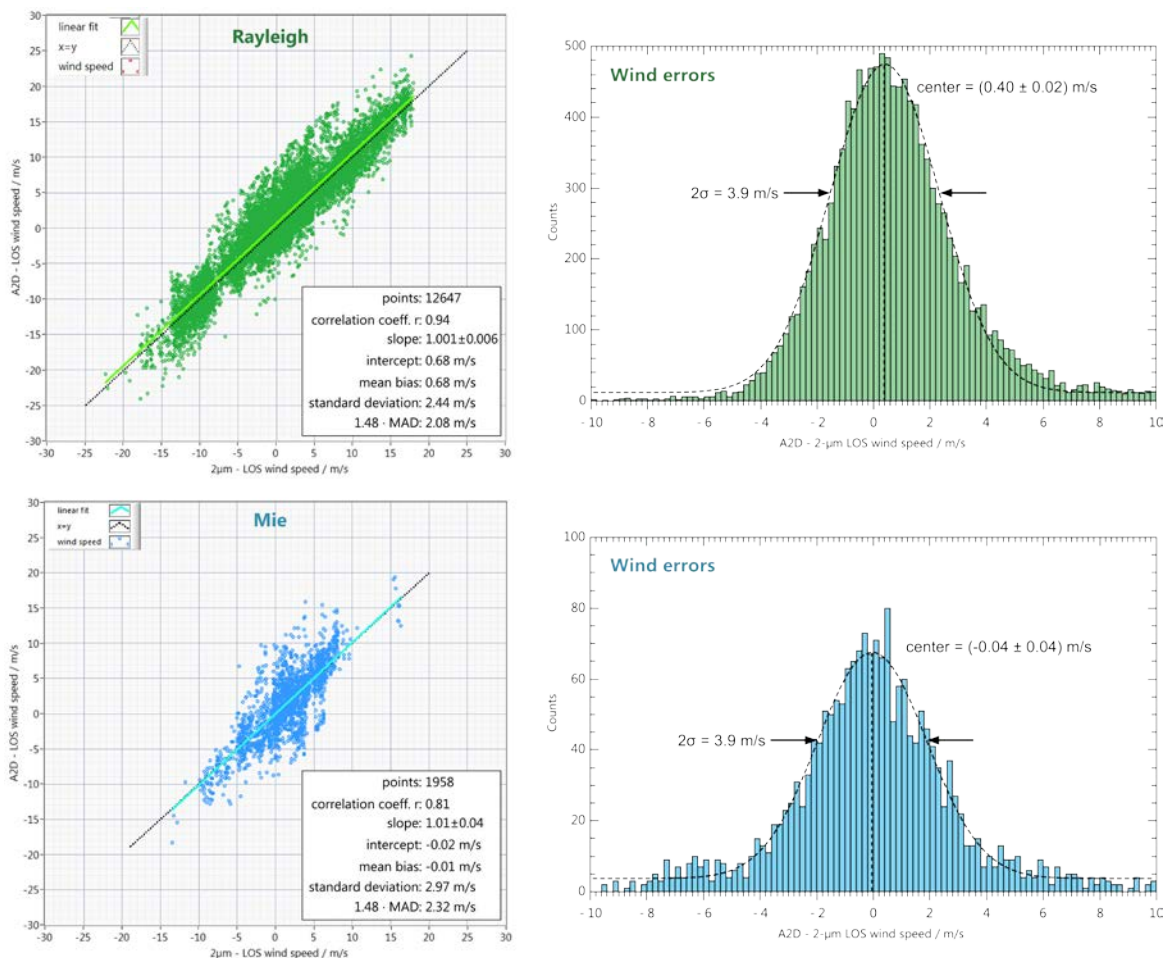


Figure 9-34: (Left) Scatterplots showing the statistical comparison between the 2- μm winds and all A2D Rayleigh winds (top) and Mie winds (bottom) measured during WindVal campaign. (Right) Corresponding probability density functions (PDFs) for the wind differences (A2D – 2- μm) for the Rayleigh (top) and Mie channel (bottom).

9.5.2 Statistical comparison of Mie winds with 2- μ m winds

Proper evaluation of the performance of the A2D Mie channel is hindered by the fact that the number of adequate winds which were obtained during the WindVal campaign is relatively small compared to the Rayleigh channel. This is primarily due to the circumstance that most of the flights carried out in the frame of the campaign were planned to be performed under clear-air conditions in order to achieve broad data coverage for the Rayleigh channel. As a result, only five Mie scenes out of 21 wind measurement periods were appropriate for statistical comparison with the 2- μ m reference lidar. The resulting statistical parameters are summarized in **Table 9-8** together with the values determined for two flights in 2009. Apart from the flight on 25/05, the mean bias is below 0.6 m/s for the 2015 flights, while the standard deviation ranges from 2.7 m/s to 3.2 m/s. The linear fits performed in the scatterplots yielded large deviations from the ideal slope of up to 60% (slope = 1.6) for the first scene on 28/05/2015. However, this value is of low significance, as it resulted from a comparison of only 175 winds ranging over only 3 m/s, resulting in a standard error of 0.3.

Interestingly, despite the poor slope values and large confidence intervals determined for the single wind measurement periods, the linear fit in the scatterplot containing all valid Mie winds measured during the entire campaign yields excellent slope and intercept values, as shown in **Figure 9-34** (bottom). The slope is 1.01 ± 0.04 and the mean bias almost vanishes, as the positive and negative biases calculated for the single flights compensate each other. However, the standard deviation of 2.97 m/s is quite high and even exceeds that obtained for the Rayleigh channel (2.43 m/s). Reduction of the mean bias (per measurement scene) and random error is expected from the consideration of the Mie nonlinearity error. Following the approach taken for the Rayleigh channel as introduced in Marksteiner (2013), the Mie response calibration data should be fitted by a fifth-order polynomial instead of a linear function to decrease the systematic and random errors.

Another aspect that becomes clear when comparing the two scatterplots in **Figure 9-34** is the fact that the range of wind speeds measured with the Mie channel (± 10 m/s when disregarding the few data points outside this range) is much smaller compared to the Rayleigh channel. This can be explained with the higher wind speeds usually occurring at high altitudes close to the aircraft. Owing to the intended low cloud and aerosol content especially at higher altitudes throughout the campaign, the range of wind speeds detected with the Mie channel was much narrower compared to the Rayleigh channel.

Table 9-8: Results of the statistical comparison between the A2D Mie winds and the 2- μ m winds for two flights performed in 2009 (first two lines) and selected wind measurement sections in 2015. The data obtained in the section on 16/05/2015 was processed with two different telescope images for Rayleigh background subtraction. The Mie response calibration #3 from 16/05/2016, 15:33 UTC was used for Mie wind processing of the data obtained in the scope of the WindVal campaign. The coverage ratio was 80% in all cases. The last row gives the parameters obtained from the statistical comparison of all winds (see the corresponding scatterplot on the right side of Figure 9-34).

Measurement section	N	Corr. coeff. <i>r</i>	Slope (95% CI)	Mean bias (m/s)	Median (m/s)	STD (m/s)	1.48-MAD (m/s)	Telescope Image	MRC	Range-gate start
26.09.2009 11:50 – 12:19	451	0.95	1.05 ± 0.08	0.64	0.66	1.30	1.16	MOUSR 1	Cal.1	5
01.10.2009 09:35 – 10:39	524	0.97	1.14	1.12	1.14	1.49		MOUSR 1	Cal.1	5
16.05.2015 20:02 – 20:32	678	0.78	[1.28 ± 0.08]	0.09	0.32	2.72	2.10	MOUSR 15:00 UTC	Cal.3	6
16.05.2015 20:02 – 20:32	227	0.81	[1.17 ± 0.12]	-0.29	-0.30	2.68	2.11	MOUSR 20:39 UTC	Cal.3	6
25.05.2015 15:24 – 16:47	243	0.82	1.04 ± 0.10	-2.13	-2.00	3.15	2.10	GrOUSR 11:19 UTC	Cal.3	9
28.05.2015 10:50 – 11:17	175	0.40	1.6 ± 0.6	0.91	0.57	2.86	2.67	GrOUSR 11:19 UTC	Cal.3	6
28.05.2015 11:25 – 12:52	635	0.71	[0.91 ± 0.08]	0.56	0.26	2.89	2.30	GrOUSR 11:19 UTC	Cal.3	5
ALL	1958	0.81	1.01 ± 0.04	-0.01	-0.02	2.97	2.32			

	Document Nr. FR.DLR.WindVal.270717	Issue: V1.1	Date: 27.07.2017	Page: 132/146	
	Doc. Title: WindVal Final Report				

9.6 Summary

- 18 wind measurement scenes from 14 research flights were analysed within the scope of the WindVal campaign. The measurement periods range from 10 to 88 minutes, adding up to more than 12 hours of wind measurements over the whole campaign. The longest section was conducted on 28/05/2015 between 11:25:08 and 12:53:02 UTC, yielding 293 observations (10255 measurements).
- The Rayleigh winds were processed by using the Rayleigh response calibration from 23/05/2015, 18:48 UTC (calibration #7) with a frequency range of 1500 MHz. The Mie winds were processed by using the Mie response calibration from 16/05/2016, 15:33 UTC (calibration #3) with a frequency range of 1200 MHz.
- Quality Control was performed separately for the Rayleigh and Mie channel and included the screening for three indicators of data corruption: outliers in the detection chain offset (DCO) signals, saturation of the ACCD and incorrect assignment of range-gates numbers.
- A filter mask was applied to the Rayleigh winds to sort out clouds and ground bins as well as all the bins below these affected bins. The cloud and ground mask is a very strong filter which potentially removes valid data. Alternatively, the inverted Mie SNR mask can be applied and represents a less stringent filter which retains a significant amount of (valid) Rayleigh winds. However, it may leave a large number of invalid winds, especially below clouds.
- Rayleigh background subtraction was performed for correcting the Mie wind data. For the measurement period on 28/05/2015 between 11:25:08 and 12:53:02 UTC, the subtraction of the telescope image provided an improvement in Mie wind accuracy and precision. The LOS mean bias was reduced by 33% from 0.83 to 0.56 m/s, while the standard deviation decreased from 3.31 to 2.89 m/s (13%).
- In addition, Rayleigh background correction facilitates the discrimination between valid and invalid Mie winds, as the contrast between bins with high SNR and those with too low SNR is increased. Hence, filtering of invalid Mie winds by means of an SNR (threshold) mask is more effective.
- Zero Wind Correction values derived from ground signals vary strongly (± 5 m/s) from observation to observation. Consequently, the value taken for the correction of the wind data depends on the statistical method of determination (mean, median, mean after outlier removal, etc.). The Zero Wind Correction procedure is currently being studied, refined and applied by a master student at DLR who investigates ground return signals and their applicability for improving the quality of both the calibration and wind data.
- The accuracy and precision of the Rayleigh and Mie wind profiles were evaluated by statistical comparison with data from a coherent 2- μ m wind lidar. Analysis of the Rayleigh winds from 19/05/2015 revealed that the best agreement between A2D and 2- μ m winds is obtained when using the Rayleigh response calibration from 23/05/2015 (Cal. #7).
- The parameters resulting from a linear fit in the scatterplot (A2D winds vs. 2- μ m winds) are only meaningful if, firstly, the dataset contains a sufficient number of compared bins (>250), and secondly, the dataset contains a broad range (>10 m/s) of both positive and negative wind speed values. The significance of the slope can be assessed by calculating the standard error and, from this, the 95%-confidence intervals based on a Student's t-test. If the true value 1.0 is not within the interval, the linear regression, and hence, the fitting parameters are not useful.
- The median absolute deviation (MAD) was introduced as an additional parameter for evaluating the random wind error, as it represents a more robust measure compared to the standard deviation with respect to outliers.
- The Rayleigh winds measured on 23/05/2015 showed high accuracy (mean bias: 0.60 m/s) and low random error (1.80 m/s) over a large range of wind speeds from -15 m/s to +20 m/s. The accuracy of the LOS wind speeds determined for the range-gates near the aircraft (0.4 m/s) is very promising with a view to the Aeolus mission.
- The Mie winds measured during the campaign showed large random errors of about 3 m/s. In contrast, typical values in the order of 2 m/s were obtained in the airborne campaign 2009. One possible explanation is strong wind gradients within one bin in combination with the presence of a special cloud structure which leads to a non-uniform distribution of particles inside the bin.

	Document Nr. FR.DLR.WindVal.270717	Issue: V1.1	Date: 27.07.2017	Page: 133/146	
	Doc. Title: WindVal Final Report				

- The impact of the heterogeneity of the atmosphere on the wind error is especially pronounced in case of low coverage of the 2- μm wind data on the A2D bin as well as for bins with low SNR.
- Large deviations in Rayleigh accuracy and precision were observed from flight to flight and even between subsequent measurement periods during one flight. This may be explained with varying atmospheric conditions which affect the transmit-receive path co-alignment and, in turn, the incidence angle of the backscatter signals on the Rayleigh spectrometer.
- Overall accuracy and precision of the Rayleigh and Mie winds (comparison over whole campaign):

<i>Rayleigh:</i>	+0.68 m/s (accuracy)	2.44 m/s (precision)	2.08 m/s (1.4826 · MAD)	<1% slope error
<i>Mie:</i>	-0.01 m/s (accuracy)	2.97 m/s (precision)	2.32 m/s (1.4826 · MAD)	1% slope error

The A2D and the 2- μm reference wind lidar are highly appropriate and relevant for future Cal/Val activities after the launch of ADM-Aeolus.

9.7 Recommendations and open points

Recommendations with respect to A2D:

- Additional QC measures should be implemented in the wind retrieval algorithm to improve the discrimination between relevant and invalid wind measurements and observations. For instance, observations in which the measured CoG position of the laser spot on the UV camera shows large deviations from the CoG reference position should be removed, as this points to a poor co-alignment between the transmit and receive path of the laser, thus resulting in large Rayleigh wind errors.
- The ZWC procedure should be refined, preferably by using a polynomial fit on observation level instead of using the mean or median over the whole scene. In this context, accurate detection of the ground return under consideration of the range-gate overlap should be performed.
- The mounting angles of the A2D instrument should be determined with higher accuracy using ground return data.
- The Rayleigh background correction procedure (telescope image subtraction) has to be modified. In case of a mismatch of the ground range-gates between MOUSR and wind measurement, the subtraction of the telescope image from the original Mie signal which is performed uniformly for all observations leads to erroneous (negative) intensities in atmospheric range-gates which contained ground return during the MOUSR.
- An adequate combination of the inverted Mie SNR mask and the cloud/ground mask should be developed in order to exploit the advantages of both approaches for the identification of valid Rayleigh winds.
- The ground mask used for the Rayleigh channel should also be applied to the Mie channel (in combination with the Mie SNR mask) in order to remove the ground bins from the Mie wind profiles.
- The influence of the Rayleigh background subtraction on the Mie SNR should be further analysed. In a next step, the adjustment of the Mie SNR threshold depending on the atmospheric conditions (heterogeneity, cloud structure) should be optimized, e.g. higher threshold for highly variable cloud and aerosol content between adjacent bins.

Recommendations with respect to ALADIN algorithms:

- The Mie nonlinearity error using a (fifth or higher-order) polynomial fit should be implemented in the Mie wind retrieval in order to reduce both the systematic and the random error of the Mie winds.

Recommendations with respect to the Cal/Val activities:

- Heterogeneity was found to be a significant contributor to Mie wind errors due to the coarse vertical resolution of the A2D (and ALADIN). Therefore, homogeneous scenes (wrt. cloudiness and wind gradient) are preferred for analyzing the instrument performance in a first step, as large error sources can be excluded. High-level cirrus clouds might provide a good Mie target, but are often associated with strong wind gradients in the upper troposphere leading to large height assignment and resulting wind errors.

	Document Nr. FR.DLR.WindVal.270717	Issue: V1.1	Date: 27.07.2017	Page: 134/146	
	Doc. Title: WindVal Final Report				

Higher resolution validation measurements are needed for that purpose. In a next step, heterogeneous scenes (e.g. cloud layers with strongly varying optical thickness along the flight track) should be sampled for quantifying the influence of the atmospheric heterogeneity on the wind error and for developing algorithms which compensate for these effects.

- The 2- μm wind data with higher resolution should be investigated with regard to the identification of clouds and their localization within a certain bin in order to better understand the impact of the cloud location within the bin and its vertical extension on the Mie wind error.
- During validation flights in coordination with satellite overpasses, it is desired to have most range-gates of ALADIN (except for two) at altitudes below the Falcon aircraft. The respective range-gate settings of ALADIN and A2D (high resolution directly below the aircraft or closer to the ground) could be varied for the purpose of quantifying the impact of the atmospheric heterogeneity on the respective winds. It is preferred to have high-resolution ALADIN range-gate settings (250 m/500 m) in case of wind gradients (e.g. North Atlantic validation) and then perform post-processing. Triple collocation with the 2- μm DWL (or model) could then provide information on the influence of the bin size on the wind error.
- In order to separate range-dependent from wind speed-dependent, i.e. calibration-related error sources, flight legs back and forth along the same track shall be performed. In this way, LOS wind data can be collected with similar absolute values but opposite sign, thus enabling the differentiation between positive and negative bias of different error sources.
- The 95%-confidence intervals of the slope and the median absolute deviation (MAD) should be derived from the statistical comparison of the A2D and 2- μm winds in order to evaluate the significance of the linear regression and to obtain a more robust measure of the random wind error, respectively.

10 Summary and recommendations

The achievements wrt the objectives are summarized in chapter 4. All major objectives (no. 1-5) and the secondary objectives (no. 8/9) were achieved; two of the secondary objectives (no. 6/7) could not be achieved due to the prevailing weather conditions during the campaign. These objectives were successfully implemented for the WindVal II campaign in September-October 2016. Each sub-chapter contains a summary of the corresponding results and recommendations.

The main achievements for WindVAL 2015 are summarized below:

- DLR Falcon was deployed in Iceland with the A2D and 2- μm DWL from May 11-29, 2015 during 3 weeks. A total of 47.5 flight hours (including transfer) were performed with the following achievements
 - 3 calibrations over Greenland ice + 2 calibrations over sea ice (only 2 calibrations in 2009)
 - high wind-speed + gradients during 2 Jet Stream flights and Greenland Tip Jet flight
 - inhomogeneous, cloudy conditions were sampled during several flights with more cloudy scenes than in 2009
 - satellite underpasses: Aeolus-like tracks, ASCAT and TDS-1
 - 1 flight over the Greenland summit station equipped additionally with a ground-based wind lidar for 2 months
- The NASA DC-8 aircraft was deployed during May 2015 with 2 wind lidars on board; the coherent detection wind lidar DAWN and the direct-detection wind lidar TWiLiTE; all flights from the DLR Falcon were coordinated with the NASA DC-8, except Greenland summit (May 21) and ASCAT underpass (May 28); 84 dropsondes are available during coordinated flights. This was the first campaign with 4 wind lidars operated on 2 aircrafts in parallel.
- Large increase in statistical evidence for comparison A2D and 2- μm from 2 scenes in 2009 ($N_{\text{Ray}}=1076$, $N_{\text{Mie}}=975$) to 18 scenes ($N_{\text{Ray}}=12647$) for Rayleigh and 5 scenes ($N_{\text{Mie}}=1958$) for Mie with the following result (all values in LOS with 20°):

A2D vs. 2- μm	Rayleigh	Mie
Bias	0.7 m/s	< 0.1 m/s
Random error	2.4 m/s	3.0 m/s
1.4826 · MAD	2.1 m/s	2.3 m/s
Slope (95% confidence interval)	1.001 (± 0.006)	1.01 (± 0.04)
correlation r	0.94	0.81
Number of compared winds N	12647	1958

	Document Nr. FR.DLR.WindVal.270717	Issue: V1.1	Date: 27.07.2017	Page: 136/146	
	Doc. Title: WindVal Final Report				

Recommendations

Here the recommendations from the WindVAL campaign wrt Cal/Val phase (incl. orbit predictions) and A2D and Aeolus operations and algorithms are discussed.

Recommendations wrt satellite orbit predictions and flight planning:

During WindVAL 2015 publically available web-sites for satellite orbit predictions from NASA and N2YO were used. CALIPSO orbit predictions were obtained directly from the CALIPSO team at NASA Langley via S. Greco (SWA). In addition an orbit prediction for Aeolus was available from ESA (T. Kanitz) for one orbit repeat cycle of 1 week. No ESA websites or tools were available during WindVAL 2015, which could be tested for orbit predictions. Different orbit prediction tools were available for testing before the Aeolus Cal/Val workshop in March 2017, which were tested by DLR. Details of the ALADIN instrument operation during IOCV (In Orbit Commissioning and Validation) phase, including the vertical sample settings wrt. specific cal/val activities are found in ESA (2017).

It is recommended to operate Aeolus with specific modes (calibration) and settings during the period of airborne campaigns and provide the following information

- Measurement track location (latitude, longitude for ground intersection point) and time is needed 4 days in advance for each day and a specific geographical region; flight planning is performed using location of 2 waypoints; updates on the flight track should be provided in case of any changes, e.g. orbital manoeuvre
- the EOMER tool was tested for orbit predictions; it was recognized that the information on the time of the overpass was missing in the graphical output (for an overview); the orbit prediction tool should allow easy download of track location and time in text format
- information on operation status (on, stand-by) and mode (wind, calibration, orbital manoeuvre); this information is needed 4 days in advance with latest updates on the day of flight up to 1 hour before take-off
- information on vertical range-gate settings; this would allow to adapt the A2D vertical sampling
- most ALADIN vertical range-gates should be aligned below flight level of Falcon aircraft (e.g. 11 km); 2 range-gates should be placed in altitudes above the flight level; it is preferred to operate ALADIN with a number of accumulated pulses $P=20$ (see ESA (2017), Fig. 9).
- time and location of Instrument Response Calibration (IRC) mode several days in advance and positioned within range of Falcon aircraft; preferably several IRC's per week, because weather conditions will not be favourable for aircraft underpasses.

Recommendations wrt A2D, 2- μ m DWL and ground-based wind lidar operation

- a minimum of 3-weeks with 50 flight hours (incl. 10 h transfer) should be foreseen for an airborne campaign, including 2-3 response calibration flights (10 h)
- morning (5-7 UTC) and evening (17-19 UTC) overpass of Aeolus in Iceland is feasible; evening overpass is preferred for operational reasons, due to the preparation time of the instruments (3-4 hours) before take-off. Also some airports have only limited operation times (e.g. DLR Oberpfaffenhofen), which needs to be considered. In principle it would be possible to consider also morning overpasses (e.g. at the airport in Keflavik), if other criteria (weather conditions, limited number of overpasses) are predominant
- it was demonstrated that DLR's 2- μ m DWL can be used as reference (no bias, random error < 1m/s) and provides sufficient coverage for Rayleigh and Mie winds
- remarkable good vertical data coverage for 2- μ m DWL despite low aerosol content in the North Atlantic region => 60-80 % relative humidity forecast correlates well with 2- μ m coverage. This RH criterion is one among several criterias; for post-launch validation the aircraft flight tracks need to be aligned to the satellite track independent of the RH or cloudiness. But the selection of a specific underpass day and time or region (within the aircraft range) should include RH and cloudiness as criteria.

	Document Nr. FR.DLR.WindVal.270717	Issue: V1.1	Date: 27.07.2017	Page: 137/146	
	Doc. Title: WindVal Final Report				

- minimum of 2 calibration flights (local Iceland, Greenland double flight) needed with 3-5 response calibrations (10 flight hours) for each campaign
 - sea ice calibrations with extended range (compared to Greenland with 2 to 3 km); sea ice was present in May 2015 (but not October 2016)
 - perform “micro”-calibrations (5 frequency steps) during each flight in curves
 - need for response calibrations over ice, land and sea
 - sea ice or ice calibrations are preferred to calibrations over land; but calibrations over land with lower albedo were performed also during WindVAI II in 2016
- A2D flight level either >2 km above cloud or below cirrus cloud; no constraints for flight level from 2- μ m DWL
- Need for ground-returns over land/ice for each flight for A2D (also beneficial for 2- μ m DWL)
- 45 minutes needed after take-off for A2D switch-on and temperature stabilisation (+3 hours pre-heating in hangar); temperature controlled hangar with 18-25 °C is needed for ensuring stability of A2D laser alignment
- In order to separate range-dependent from wind speed-dependent, i.e. calibration-related error sources, flight legs back and forth along the same track shall be performed. In this way, LOS wind data can be collected with similar absolute values but opposite sign, thus enabling the differentiation between positive and negative bias of different error sources.
- It is recommended performing an IRC with the A2D (and the 2- μ m DWL) in nadir pointing during an ALADIN IRC underpass for comparison of nadir-pointing observations. The A2D IRC can only be performed in limited regions because the Falcon aircraft needs to circle in order to provide nadir view. For a second ALADIN IRC one could foresee to fly along-track with the DLR Falcon aircraft and characterize the present atmospheric heterogeneity with the A2D (in 20° off-nadir mode) and the 2- μ m DWL (in nadir mode and conical scanning mode). Details for implementation need to be discussed, once the first in-orbit calibrations IRC were performed and analysed.
- It is recommended to provide summary information of the instrument performance for A2D and 2- μ m DWL close to the data acquisition period. This type of information was provided to ESA in form of flight reports for each flight, which were released about 1 day after each flight (or earlier) during WindVal II in 2016. The flight reports contain both aircraft flight tracks, time period, instrument status and anomaly reporting. That type of information should be provided by all instrument teams close to the acquisition period of the Aeolus overpass times, and provided to all teams including satellite and ALADIN performance to all teams. This eases planning of next acquisition periods.
- The vertical coverage of ground-based coherent wind lidars is limited to the atmospheric boundary layer, clouds and elevated aerosol layers (e.g. desert dust). Most commercial ground-based coherent wind lidars operate with low pulse energy (μ J) and high pulse repetition rate (kHz), which further limits the vertical range. Ground-based wind lidars are typically not sensitive to low aerosol backscatter of the free troposphere above the boundary layer, which could be sensed by airborne coherent wind lidars. The use of ground-based coherent wind lidars for validation of Aeolus is limited, because of the coarse range gate resolution of ALADIN (250 m - 500 m) in combination with the presence of ground-return signal over the long horizontal averaging length in the lowest range bin. Thus the lowest 250-500 m range gate from ALADIN close to the ground could be potentially contaminated by ground returns. This limits the vertical range of collocation from 500 m to typically 1.5 km - 2.5 km, which corresponds to 4-8 range gates (500 m resp. 250 m). But the coherent wind lidars typically provide high accuracy wind vector profiles without need for a wind-speed calibration. But a manual QC and analysis is needed during post-processing of the data, which are usually obtained with proprietary software from the manufacturers. Nevertheless the validation of Aeolus could benefit from ground-based coherent wind lidars for the following reasons:
 - Continuous validation of boundary layer winds from the ALADIN Mie channel on several sites with the use of commercially available wind lidars.
 - Ground-based sites, where elevated aerosol layers are observed regularly, e.g. desert dust (e.g. Sahara, Southern Europe, Islands at the west coast of Africa, China, Middle East) would allow collocations also for higher altitudes above the boundary layer.

	Document Nr. FR.DLR.WindVal.270717	Issue: V1.1	Date: 27.07.2017	Page: 138/146	
	Doc. Title: WindVal Final Report				

- Ground-based sites on the ice sheet (e.g. Greenland, Antarctica) would be beneficial to assess the atmospheric contamination of the ALADIN ground-returns during response calibration and for zero-wind calibration, although the vertical range on these sites might be limited to a few hundred meters.

Recommendations wrt Cal/Val data analysis

- A significant contribution of cloud height assignment errors (heterogeneity of backscatter in combination with wind gradients) in statistical comparison of A2D Mie and 2- μm winds was present, which could be more dominant for ALADIN due to coarser range-gate resolution. This error source should be further investigated
 - this error source should be further investigated by use of high-resolution 2- μm data (signal intensity, cloud winds from 2- μm from 0.3 m raw data resolution) to identify A2D (or ALADIN) range-gates, which could be affected
 - this issue will be also present for ALADIN validation and will be different for airborne (cloud top) and ground-based observations (cloud bottom)
- The calculation of a bias is misleading for some cases due to compensation of negative and positive values for same flight tracks with opposite direction, this will be also the case for Aeolus with ascending and descending orbits; another option would be to use the sum of the absolute deviation
- The 95%-confidence intervals of the slope and the median absolute deviation (MAD) should be derived from the statistical comparison of the A2D and 2- μm winds in order to evaluate the significance of the linear regression and to obtain a more robust measure of the random wind error, respectively.
- The 2- μm ground return range, derived from the digitized raw signals with 0.3 m resolution can be used to determine the location of the ground-return within the A2D ground bin (Weiler (2017)). This can be used to assess the atmospheric contamination.

Recommendations wrt A2D and L1B/L2B algorithms

- Use of ground returns from A2D for zero-wind correction ZWC was more challenging than expected:
 - trade-off within ground-detection (on measurement level) between summation over several bins (due to range-gate overlap) and minimization of atmospheric contribution
 - strong variability of Rayleigh ground return results from calibration RRC, which results in large difference for ZWC when different calibrations are used
 - Atmospheric contribution (aerosol+wind), molecular contribution (even without wind), atmospheric height above ground and surface albedo
 - Use of different calibrations for different surfaces (ice, land, and sea)
 - most of ground-returns around Iceland are from sea surface (low albedo due to 20° off-nadir angle, moving sea surface)
 - use of polynomial fit with ZWC values instead of mean/median (as done in 2009), which is similar to HBE approach
 - refinement of ground-detection scheme using thresholds with more than 1 signal derivative as investigated in Weiler (2017) and implemented in L1B V7.0.
- optimisation of A2D mounting angles with use of ground return range should be performed
- Perform polynomial fit (5th order or higher) in Mie response calibration non-linearity (internal and atmosphere) and use these fits for wind retrieval (as for Rayleigh); in addition perform a combination of polynomial (5th order) and sinusoidal fit for ALADIN MRC non-linearity (as seen in ALADIN instrument full performance test from April 2016)
- The difference in MRC non-linearity for the internal and atmospheric path should be investigated by use of E2S. A non-expected difference was observed with the A2D, which could be related to a non-correction of ground-returns from Rayleigh background (using MOUSR) for MRC data, which would then be A2D specific.

	Document Nr. FR.DLR.WindVal.270717	Issue: V1.1	Date: 27.07.2017	Page: 139/146	
	Doc. Title: WindVal Final Report				

Recommendations for TV test and IOCV

- Perform an analysis of the absolute frequency drifts of both flight lasers during the Thermal Vacuum test (TRG-11) according to **Figure 8-8**
- Perform a MOUSR (Mie Out of Useful Spectral Range) procedure in orbit in order to verify the assumed TOBS correction array (ESA 2017)

	Document Nr. FR.DLR.WindVal.270717	Issue: V1.1	Date: 27.07.2017	Page: 140/146	
	Doc. Title: WindVal Final Report				

11 References

- Chouza, F., Reitebuch, O., Jähn, M., Rahm, S., Weinzierl, B. (2016a). Vertical wind retrieved by airborne lidar and analysis of island induced gravity waves in combination with numerical models and in situ particle measurements. *Atmospheric Chemistry and Physics*, 16, 4675-4692.
- Chouza, F., Reitebuch, O., Benedetti, A., Weinzierl, B. (2016b). Saharan dust long-range transport across the Atlantic studied by an airborne Doppler wind lidar and the MACC model. *Atmospheric Chemistry and Physics*, 16, 11581-11600.
- Dabas, A., M. L. Denneulin, P. Flamant, C. Loth, A. Garnier, and A. Dolfi-Bouteyre (2008): Correcting winds measured with a Rayleigh Doppler lidar from pressure and temperature effects. *Tellus*, 60A, 206-215.
- DLR: Reitebuch (2005): ADM-Aeolus Campaigns – A2D Data Content Level 0, V1.0, July 2005, 19 pages.
- DLR: Reitebuch, O., Paffrath, U. Nikolaus, I. (2010): TN 5.1 ADM-Aeolus Ground Campaigns Results, V 1.1, 26.02.2010, 309 pages.
- DLR: Reitebuch, O., et al. (2012a): Final Report ADM-Aeolus Airborne Campaigns Results, V 1.0, 15.06.2012, 34 pages.
- DLR: Reitebuch, O., U. Marksteiner, Ch. Lemmerz (2012b): TN 5.2 ADM-Aeolus Airborne Campaigns Results, V 3.0, 24.02.2012, 202 pages.
- DLR: Witschas, B., Nikolaus, I., Reitebuch, O., Lemmerz C. (2014): TN 5.3 A2D Rayleigh spectrometer alignment sensitivity, V 3.0, 21.08.2014, 64 pages.
- DLR: Lemmerz, Ch., U. Marksteiner, O. Reitebuch, B. Witschas (2015a): WindVal Instrument Test Plan and Report ITPR. V 1.0, 06.05.2015, 16 pages.
- DLR: Reitebuch, O. (2015b): WindVal: Campaign Implementation Plan CIP Joint DLR-ESA-NASA Wind Validation for Aeolus. V1.1, 28.05.2015, 42 pages.
- DLR: (2015c): Handouts and Minutes of Meeting MoM from Progress Meeting 1 on November 2, 2015 at AOML, Miami, USA.
- DLR: Reitebuch, O. (2016a): WindVal: Data Acquisition Report DAR Joint DLR-ESA-NASA Wind Validation for Aeolus. V1.0, 28.01.2016, 39 pages.
- DLR: (2016b): Handouts and Minutes of Meeting MoM from Progress Meeting 2 on June 9, 2016 at DLR Oberpfaffenhofen, Germany.
- DLR: (2016c): Handouts and Minutes of Meeting MoM from Progress Meeting 3 on November 22, 2016 at DLR Oberpfaffenhofen, Germany.
- DLR: Witschas B., U. Marksteiner, O. Reitebuch, Ch. Lemmerz, O. Lux (2016d): Final Report Analysis of enhanced noise in A2D observations. AE.FR.DLR.A2D.CN11.110716, V2.0, 11 July 2016, 110 pages.
- DLR: Schmidt, K., O. Reitebuch, D. Huber (2017a): Technical Note 51.2 Mie and Rayleigh Algorithm Performance Assessment (WP5100, Phase 2). AE.TN.DLR.5100.2.20170207, V1.3, 7 Feb 2017, 179 pages +appendix.
- DLR: (2017b): Handouts and Minutes of Meeting MoM from Final Meeting on May 30, 2016 at ESA-ESTEC, Noordwijk, The Netherlands.
- ESA: Schüttemeyer D. (2015): Statement of Work on “Technical Assistance for the Deployment of the ALADIN Airborne Demonstrator (A2D) lidar during the 2015 ESA/NASA Joint Wind Validation (WindVal) Campaign”. EOP-SM/2722/DS-ds from 16 March 2015, Contract No. ESA 4000114053/15/NL/FF/gp.
- ESA: Kanitz Th. (2017): ESA Instrument and Processor activities during IOCV. Issue 1.0, 24 April 2017, AE-PL-ESA-SY-021, 39 pages.
- Frehlich, R., and R. Sharman, 2004: Estimates of turbulence from numerical weather prediction model output with applications to turbulence diagnosis and data assimilation. *Mon. Wea. Rev.*, 132, 2308–2324.

	Document Nr. FR.DLR.WindVal.270717	Issue: V1.1	Date: 27.07.2017	Page: 141/146	
	Doc. Title: WindVal Final Report				

- Frehlich, R., Hannon, S. M., Henderson, S. W. (1997). Coherent Doppler lidar measurements of winds in the weak signal regime. *Applied optics*, 36(15), 3491-3499.
- Gentry, B., H. Chen, J. Cervantes, S. Mitchell, R. Machan, D. Reed (2014): Status of the TWiLiTE-GH Direct Detection Doppler Lidar. Presentation at Space Based Lidar Winds Working Group Meeting, May 13, 2014.
- Kavaya, M. J., J. Y. Beyon, G. J. Koch, M. Petros, P. J. Petzar, U. N. Singh, B. C. Trieu, and J. Yu (2014): The Doppler Aerosol Wind (DAWN) Airborne, Wind-Profiling Coherent-Detection Lidar System: Overview and Preliminary Flight Results. *J. Atmos. Oceanic Tech.*, 31, 826-842.
- Marksteiner, U. (2013): Airborne Wind-Lidar Observations for the Validation of the ADM-Aeolus Mission. Ph. D Thesis at Technical University Munich, DLR FB 2013-25, 176 pages.
- Päschke, E., R. Leinweber, V. Lehmann (2015): An assessment of the performance of a 1.5 μm Doppler lidar for operational vertical wind profiling based on a 1-year trial. *Atmos. Meas. Tech.*, 8, 2251-2266.
- Paffrath, U., Lemmerz, Ch., Reitebuch, O., Witschas, B., I. Nikolaus, V. Freudenthaler (2009): The airborne demonstrator for the direct-detection Doppler wind lidar ALADIN on ADM-Aeolus: II. Simulations and Rayleigh receiver radiometric performance. *J. Atmos. Ocean. Tech.*, 26, 2516-2530.
- Reitebuch, O., Lemmerz, Ch., Nagel, E., Paffrath, U., Durand, Y., Endemann, M., Fabre, F., Chaloupy, M. (2009): The airborne demonstrator for the direct-detection Doppler wind lidar ALADIN on ADM-Aeolus: I. Instrument design and comparison to satellite instrument. *J. Atmos. Ocean. Tech.*, 26, 2501-2515.
- Smalikhov, I., 2003: Techniques of wind vector estimation from data measured with a scanning coherent Doppler lidar. *J. Atmos. Oceanic Technol.*, 20, 276–291.
- Shupe M. D., D. D. Turner, Von P. Walden, R. Bennartz, M. P. Cadeddu, B. B. Castellani, Ch. J. Cox, D. R. Hudak, M. S. Kulie, N. B. Miller, R. R. Neely III, W. D. Neff, and P. M. Rowe (2013): High and Dry: New Observations of Tropospheric and Cloud Properties above the Greenland Ice Sheet. *Bull. Am. Meteor. Soc.*, 169-186.
- Sun, X. J., Zhang, R. W., Marseille, G. J., Stoffelen, A., Donovan, D., Liu, L., Zhao, J. (2014): The performance of Aeolus in heterogeneous atmospheric conditions using high-resolution radiosonde data. *Atmos. Meas. Tech.*, 7, 2695–2717.
- Weiler, F., (2017): Bias correction using ground echoes for the airborne demonstrator of the wind lidar on the ADM-Aeolus mission. Master's thesis at Faculty of Geo- and Atmospheric Sciences of the University of Innsbruck, 96 pages.
- Weissmann, M., Busen, R., Dörnbrack, A., Rahm, S., Reitebuch, O. (2005): Targeted Observations with an Airborne Wind Lidar. *J. Atmos. Ocean. Tech.*, 22, 1706-1719.
- Witschas, B., Rahm, S., Dörnbrack, A., Wagner, J., Rapp, M. (2017). Airborne Wind Lidar measurements of vertical and horizontal winds for the investigation of orographically induced gravity waves. *Journal of Atmospheric and Oceanic Technology*, 34, 1371-1386.

12 Appendix A: Additional plots from selected wind measurements

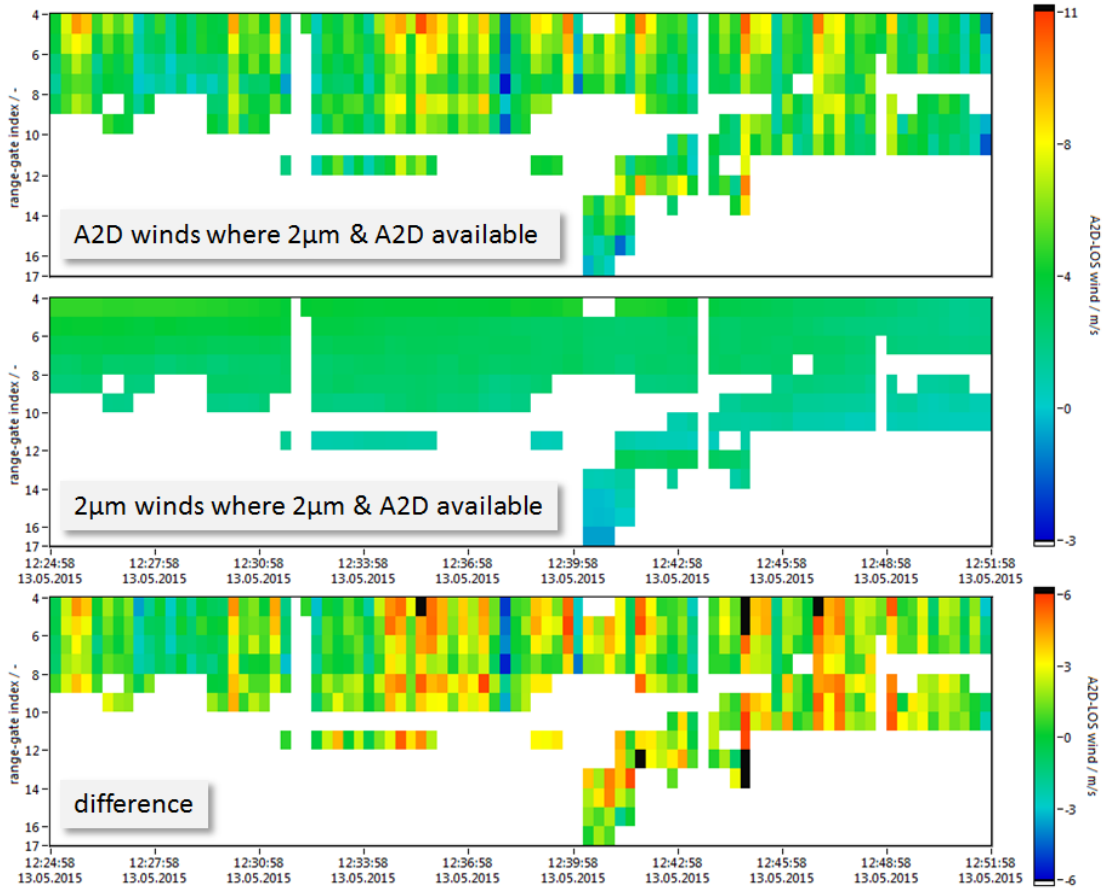


Figure 12-1: A2D Rayleigh wind profile (top) and 2- μ m wind profile (middle) obtained in the measurement period on 13/05/2015 from 12:24:58 to 12:51:58 UTC. Only bins that are available from both instruments are shown (coverage ratio: 80%). The bottom plot shows the difference in wind speeds.

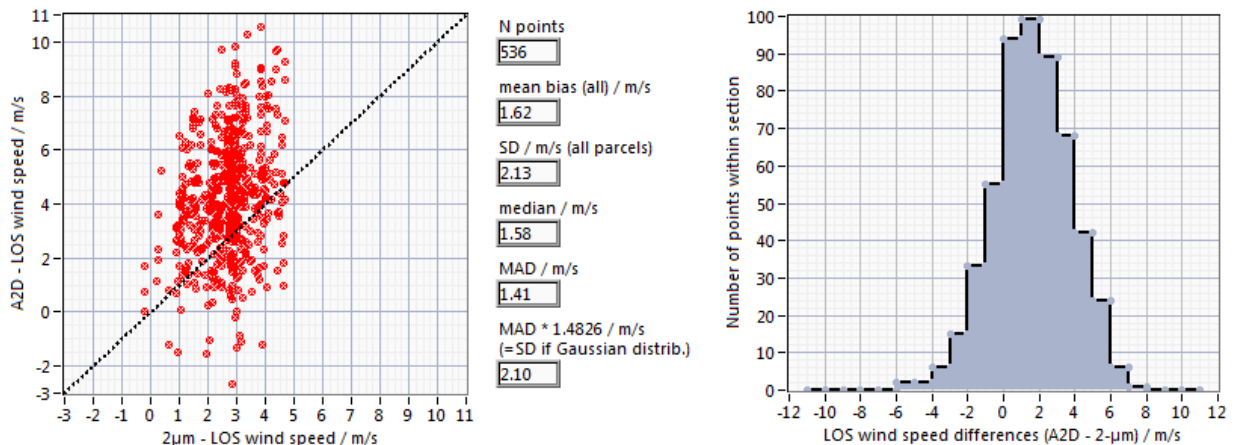


Figure 12-2: (Left) Scatterplot comparing the A2D Rayleigh and 2- μ m wind speeds for the flight section on 13/05/2015 from 12:24:58 to 12:51:58 UTC. (Right) Corresponding probability density function of the wind speed differences (A2D – 2- μ m).

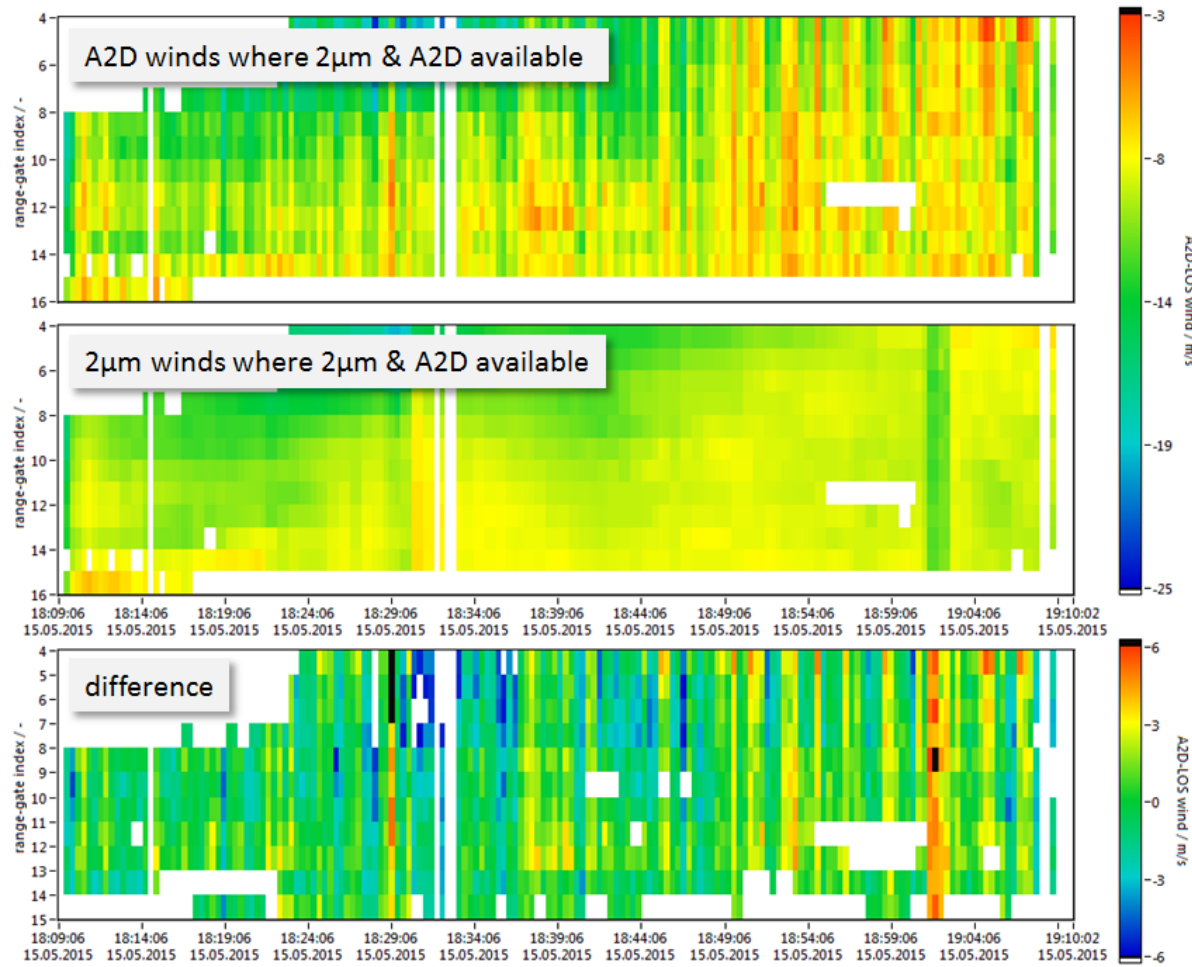


Figure 12-3: A2D Rayleigh wind profile (top) and 2- μ m wind profile (middle) obtained in the measurement period on 15/05/2015 from 18:09:06 to 19:10:02 UTC. Only bins that are available from both instruments are shown (coverage ratio: 80%). The bottom plot shows the difference in wind speeds.

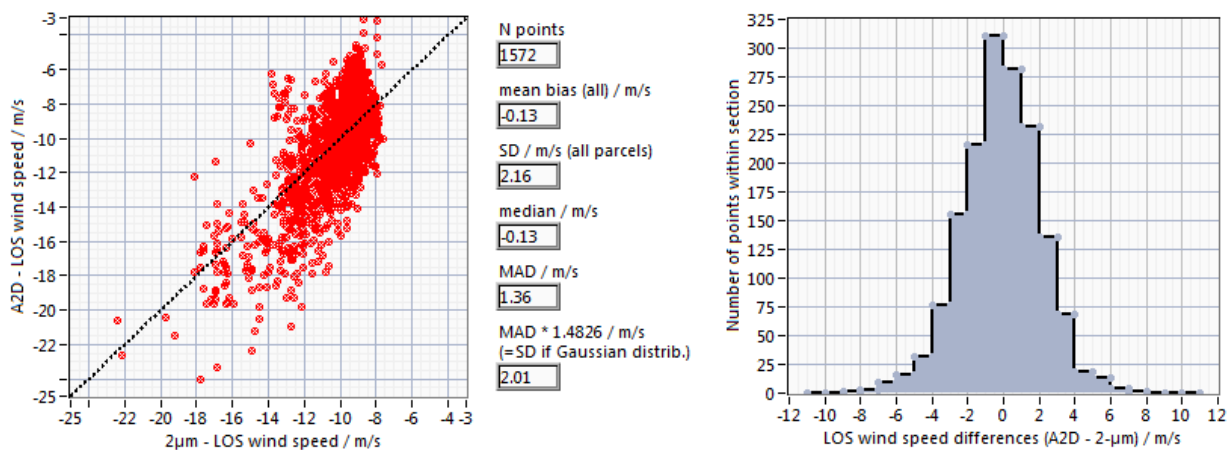


Figure 12-4: (Left) Scatterplot comparing the A2D Rayleigh and 2- μ m wind speeds for the flight section on 15/05/2015 from 18:09:06 to 19:10:02 UTC. (Right) Corresponding probability density function of the wind speed differences (A2D – 2- μ m).

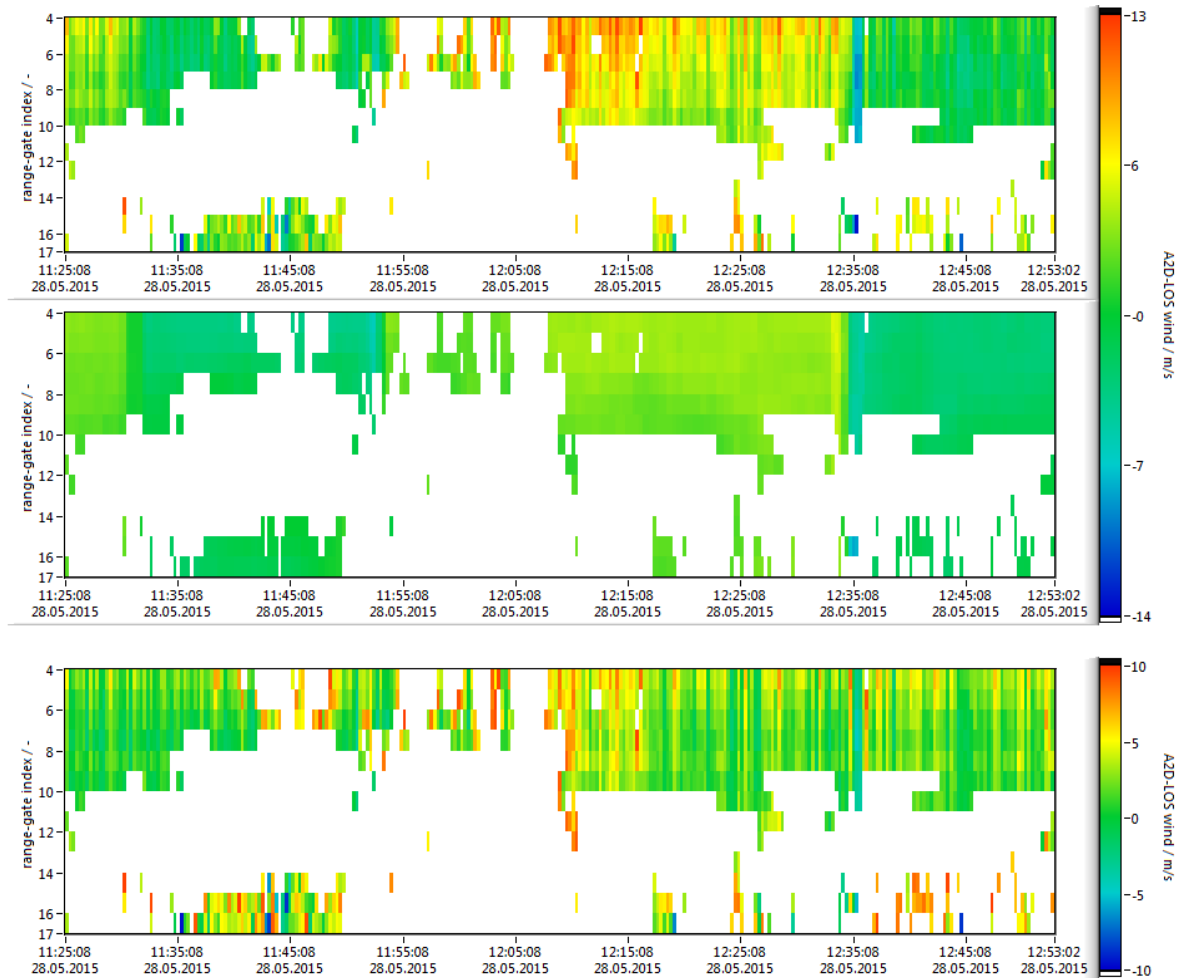


Figure 12-5: A2D Rayleigh wind profile (top) and 2- μm wind profile (middle) obtained in the measurement period on 28/05/2015 from 11:25:08 to 12:53:02 UTC. Only bins that are available from both instruments are shown (coverage ratio: 80%). The bottom plot shows the difference in wind speeds.

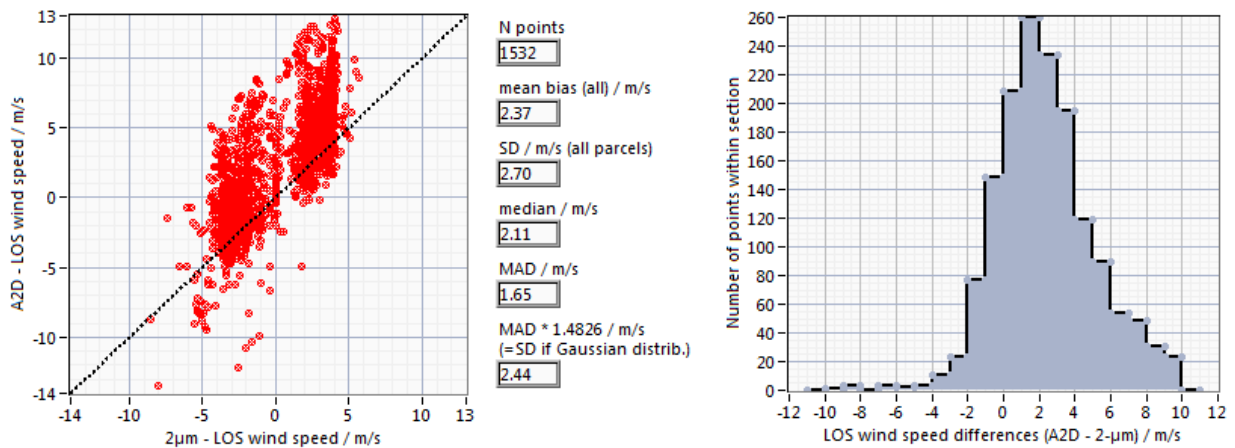
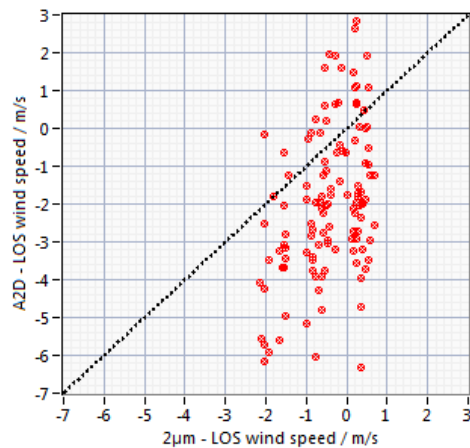


Figure 12-6: (Left) Scatterplot comparing the A2D Rayleigh and 2- μm wind speeds for the flight section on 28/05/2015 from 11:25:08 to 12:53:02 UTC. (Right) Corresponding probability density function of the wind speed differences (A2D – 2- μm).



N points
 123
 mean bias (all) / m/s
 -1.53
 SD / m/s (all parcels)
 1.81
 median / m/s
 -1.68
 MAD / m/s
 1.21
 MAD * 1.4826 / m/s
 (=SD if Gaussian distrib.)
 1.79

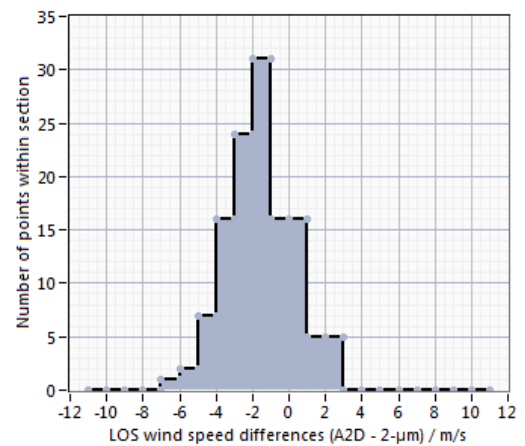
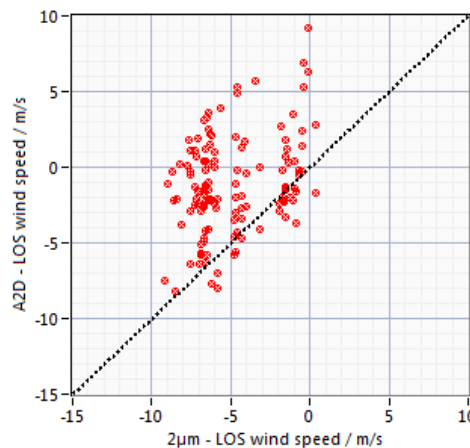


Figure 12-7: (Left) Scatterplot comparing the A2D Rayleigh and 2- μ m wind speeds for the flight section on 16/05/2015 from 19:46:20 to 20:01:54 UTC. (Right) Corresponding probability density function of the wind speed differences (A2D – 2- μ m).



N points
 126
 mean bias (all) / m/s
 3.69
 SD / m/s (all parcels)
 3.58
 median / m/s
 3.83
 MAD / m/s
 2.85
 MAD * 1.4826 / m/s
 (=SD if Gaussian distrib.)
 4.22

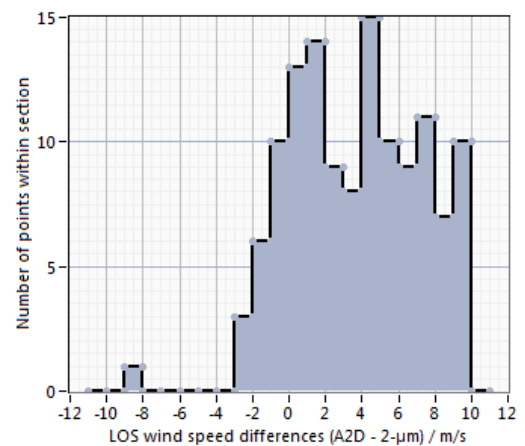


Figure 12-8: (Left) Scatterplot comparing the A2D Rayleigh and 2- μ m wind speeds for the flight section on 16/05/2015 from 20:02:58 to 20:32:02 UTC. (Right) Corresponding probability density function of the wind speed differences (A2D – 2- μ m).

	Document Nr. FR.DLR.WindVal.270717	Issue: V1.1	Date: 27.07.2017	Page: 146/146	
	Doc. Title: WindVal Final Report				

13 Appendix B: Data Acquisition Report

	Document Nr. DAR.DLR.WindVal. 28.01.16	Issue: V1.0	Date: 28.01.2016	Page: 1/39	
	Doc. Title: WindVal Data Acquisition Report				

<u>Doc.-Nr.:</u>	DAR.DLR.WindVal.28012016
<u>Doc.-Title:</u>	WindVal Data Acquisition Report DAR Joint DLR-ESA-NASA Wind Validation for Aeolus
<u>Contract Number:</u>	ESA 4000114053/15/NL/FF/gp
<u>Number of pages:</u>	39 pages
<u>Prepared by:</u>	Oliver Reitebuch (DLR, Oberpfaffenhofen, Germany)

	Document Nr. DAR.DLR.WindVal. 28.01.16	Issue: V1.0	Date: 28.01.2016	Page: 2/39	
	Doc. Title: WindVal Data Acquisition Report				

0.1 Document Change Log

Issue.	Date	New pages	Modified pages (after introducing new pages)	Observations	Name
V0.9	18.12.2015	1-35	--	draft prepared by Reitebuch with input from Marksteiner for A2D data and SWA for dropsondes	Reitebuch
V1.0	28.01.2016	5, 35-36, appendix A 39 ff	4, 17, 38	Review comments by Ch. Lemmerz (DLR) and D. Schüttemeyer (ESA) included, input from R. Neely (Uni Leeds) included for ch. 3.3. and 5.7.	Reitebuch

	Document Nr. DAR.DLR.WindVal. 28.01.16	Issue: V1.0	Date: 28.01.2016	Page: 3/39	
	Doc. Title: WindVal Data Acquisition Report				

0.2 Table of Contents

0.1	Document Change Log	2
0.2	Table of Contents	3
1	Introduction, purpose of document and objectives of campaign	4
2	Airborne instrumentation and flights	6
2.1	Payload of the DLR Falcon aircraft	6
2.2	Payload of the NASA DC-8	7
2.3	Flight Tracks during airborne campaign 2015	10
2.4	Coordination with NASA DC-8	13
3	Ground Instrumentation	14
3.1	Ground Instrumentation in Europe	14
3.2	Radiosondes around Greenland and Iceland	15
3.3	Greenland Summit Station	17
4	Satellite underpasses	18
5	Datasets from WindVal 2015	19
5.1	A2D from DLR Falcon	19
5.2	2- μ m DWL from DLR Falcon	25
5.3	In-situ data from the DLR Falcon	29
5.4	DAWN data from NASA DC-8	31
5.5	TWILITE data from NASA DC-8	31
5.6	Dropsonde data from NASA DC-8	32
5.7	Greenland Summit Data	35
5.8	Radiosonde data	37
5.9	Mission summaries	37
6	References	38
	Appendix A with Mission Summaries	39

	Document Nr. DAR.DLR.WindVal. 28.01.16	Issue: V1.0	Date: 28.01.2016	Page: 4/39	
	Doc. Title: WindVal Data Acquisition Report				

1 Introduction, purpose of document and objectives of campaign

This document describes the data acquired during the joint DLR-ESA-NASA wind validation campaign (WindVal) in preparation of the ADM-Aeolus validation. It covers tasks in response to the Statement of Work (SoW) from ESA with reference EOP-SM/2722/DS-ds from 16 March 2015 with title "Technical Assistance for the Deployment of the ALADIN Airborne Demonstrator (A2D) lidar during the 2015 ESA/NASA Joint Wind Validation (WindVal) Campaign" (ESA 2015, Contract Number ESA 4000114053/15/NL/FF/gp). The Data Acquisition Report (DAR) was prepared by Oliver Reitebuch (DLR) with support from Uwe Marksteiner (DLR) for the A2D data, Simpson Weather Associates (SWA) for the NASA DC-8 dropsondes, and Ryan Neely (Uni Leeds) for the Greenland Summit data.

This DAR is output from WP 200 from DLR's proposal to ESA's SoW as Deliverable Item D3. It is based on the Campaign Implementation Plan CIP (DLR 2015b) with updates on the instrument chapters based on the actual performance and operation (Ch. 2, 3, 4). Within chapter 5 the datasets and its formats are described.

The main objectives of the campaign as discussed in the CIP (DLR 2015b) with highest priority are:

1. Confirm and document the technical performance of the ALADIN Airborne Demonstrator (A2D) lidar and its suitability for the foreseen calibration/validation of ADM-Aeolus.
2. Extend existing datasets on response calibrations over favourable areas for Aeolus calibrations, e.g. ice or land with high surface albedo in nadir-pointing mode.
3. Extend existing datasets on Rayleigh and Mie wind observations. This shall include measurements in highly variable atmospheric conditions (vert./hor.) w.r.t. wind and clouds
4. Rehearsal for airborne Cal/Val activity after launch with focus on
 - a. Test Aeolus satellite measurement-track predictions and airborne flight planning
 - b. Enhance and test capabilities for quick-look data processing
 - c. Coordination with other aircrafts and ground validation sites
 - d. Demonstrate complementarities and synergies between different measurement techniques utilized aboard the same platform, from co-located platforms and on-ground during the campaign.
 - e. Demonstrate the performance and adequacy of the A2D data processing chain for the foreseen Aeolus CAL/VAL campaigns
 - f. Provide feedback on measurement strategies and procedures of data collection for future campaigns
 - g. Extend lessons learnt from previous campaigns
5. Perform at least one flight under the satellite track of TDS-1 to achieve co-located satellite measurements of wind vectors with airborne wind lidars.

The following objectives were targeted with lower priority on a best-effort basis:

6. Extend existing datasets on Rayleigh and Mie wind observations for variable aerosol conditions, e.g. low to high backscatter and different depolarization's characteristics from the aerosol.
7. Extend existing datasets on response calibration during less favourable conditions (cloud contamination or strongly varying ground albedo conditions, PBL snow drift conditions).
8. Demonstrate the ADM-Aeolus capabilities in resolving the vertical structure of the atmosphere and compare measurements to output from numerical weather prediction models.
9. Perform satellite underpasses for CALIPSO, ASCAT, or other existing satellite sensors of interest.

No.	Objective	Achievement
1	Confirm A2D performance	All flights incl. test flight, 47.5 flight hours
2	Extend Response Calibrations	5 response calibrations over ice (May 16) + 2 over sea ice (May 23)
3	Wind observations in variable atmospheric conditions	All flights with clear and cloudy conditions, strong wind gradients for Jet Streams (May 15, 25), Tip Jet (May 19)
4	Rehearsal	Overall Campaign implementation
4a	Aeolus sat track predictions	Similar to other satellite underpass flights exercises, Aeolus-like track on May 13, 19, 28.
4b	Quick-Lock processing	Falcon in-situ (few hours), 2- μ m DWL (1-2 days), A2D (1-2 days) data processing on-site in Iceland
4c	Coordination with other a/c and ground sites	Coordinated flights with DC-8, Greenland summit station, and transfer flights over Netherlands (Cabauw), UK (windprofiler); no flight to ALOMAR (Norway) due to weather
4d	Show complementarities of different sensors	4 wind lidars on 2 aircrafts, dropsondes and ground-site instrumentation
4e	A2D data processing chain	Re-format A2D data for use in L1B-L2B-chain will be performed
4f	Provide feedback for Cal/Val campaigns	after campaign data analysis and lessons learnt
4g	Extend lessons learnt	campaign on-site experience and data analysis
5	TDS-1 Satellite underpass	Flight on May 13
6	A2D observations of aerosol	low amount of aerosol during all flights; no long-range transport (e.g. biomass burning)
7	Response Calibration during less favourable conditions	all response calibrations during no/low cloud conditions
8	Resolve vertical structures and compare to NWP analysis	comparison to ECWMF analysis will be performed
9	Satellite underpass of CALIPSO, ASCAT and others	Metop-B (ASCAT) underpass on May 28

Table 1-1: Objectives of the WindVAL campaign and its assessment of achievement

2 Airborne instrumentation and flights

2.1 Payload of the DLR Falcon aircraft

The payload of the DLR Falcon aircraft consisted of the A2D (Reitebuch et al. 2009, Paffrath et al. 2009) and the 2- μm Doppler wind lidar (DWL, Weissmann et al. 2005).

The A2D and the 2- μm DWL were pointing in the same line-of-sight LOS direction to the right side of the aircraft (in flight direction) with a nadir angle of 20°.

The nominal operation of the 2- μm DWL was the measurement of the LOS wind and conical step-stare scans (21 LOS directions, 20° off-nadir angle) were performed in order to measure the horizontal wind vector during flight. Different off-nadir angles of both instruments, e.g. 0-3° were achieved by rolling the aircraft while flying curves (May 16 and 23). The vertical sampling of the A2D was similar as during the airborne campaign in 2009 (Fig. 2-1). The vertical sampling was set such, that the ground layers are sampled with highest vertical resolution (2.1 μs , 315 m range).

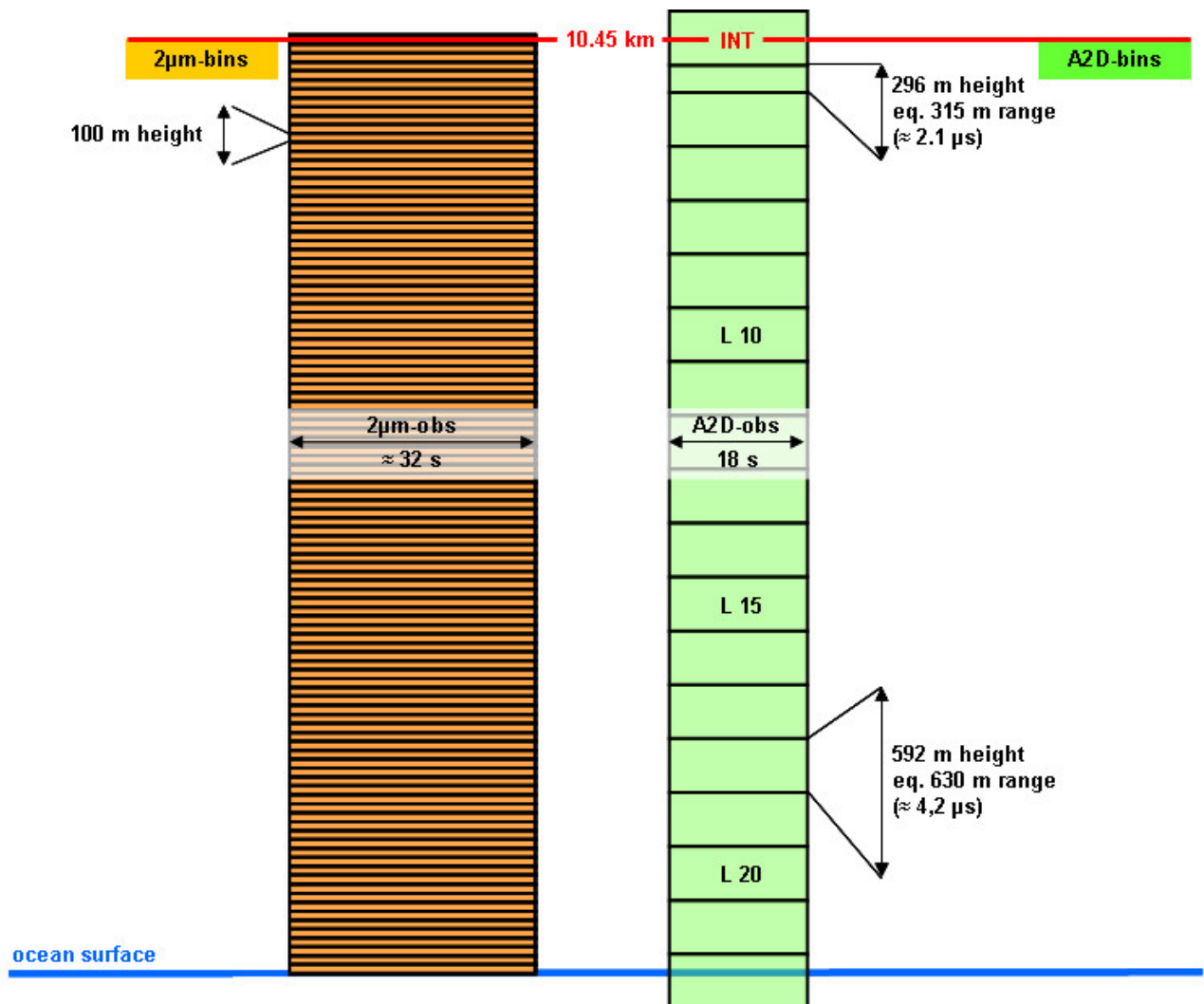


Figure 2-1: Principle of vertical and horizontal sampling for the 2- μm wind lidar with 100 m range gates and a duration of 32 s for 1 scan and A2D with vertical sampling of 592 m, which will be adapted for each flight; horizontal distance of each A2D profile is 18 s and averaging time is 14 s; 4 s are needed for data transfer (note that the figure needs to be updated, because 2- μm scanning duration was 44 s during WindVAL campaign 2015).

	Document Nr. DAR.DLR.WindVal. 28.01.16	Issue: V1.0	Date: 28.01.2016	Page: 7/39	
	Doc. Title: WindVal Data Acquisition Report				

The 2- μm DWL measures time series of raw signal with a sampling rate of 500 MHz, which corresponds to a range resolution of 0.3 m for each emitted laser shot with a repetition rate of 500 Hz. This amounts to rather high raw-data rates of up to 60 GByte/hour depending on maximum range. The data will be processed on-ground to range-gates of 100 m resolution and temporal resolution of 1 s (500 shots).

An extensive and detailed description on the data analysis methods for deriving results from A2D calibrations and wind mode can be found in DLR (2012b, ch. 4., ch. 5, ch. 6) and Marksteiner (2013, ch. 3). The methods for validation and comparison of A2D data with 2- μm DWL and other observations (e.g. ECMWF model) are discussed in DLR (2012b ch. 5.2., ch. 6.2) and Marksteiner (2013, ch. 4).

Standard meteorological parameters (pressure, horizontal wind vector, vertical wind speed, temperature, humidity (relative humidity, mixing ratio)) were measured by in-situ sensors inside the Falcon nose-boom with a temporal resolution of up to 100 Hz and processed with resolution of 1 Hz. Thus vertical profile data are available for ascent and descent and flight-level data from cruising altitude.

2.2 Payload of the NASA DC-8

The NASA DC-8 was equipped with the 2- μm DWL DAWN (Doppler Aerosol Wind) from NASA (Langley), the 355-nm DWL TWiLiTE from NASA (Goddard) and a Yankee dropsonde unit. The 2- μm DWL from NASA is equipped with a single, conical wedge-scanner, which allows pointing with fixed 30.1 ° off-nadir angle (Kavaya et al. 2014). The control of the scanner allows step-stare pointing in forward direction (not full 360°) with a difference in azimuthal position of 22.5° and a maximum number of 5 LOS directions. The DAWN laser transmitted 100 mJ/pulse (nominal 250 mJ/pulse) with a repetition rate of 5 Hz (nominal 10 Hz) and uses a 15 cm telescope, compared to the DLR 2- μm DWL with 1-2 mJ/pulse, a repetition rate of 500 Hz, and a 10.8 cm telescope. The DAWN laser operated only with 1 amplifier due to stability issues, which resulted in lower pulse energy and repetition rate. A 4 s duration for signal acquisition is used for each LOS direction and a total of 25 s is needed for all 5 directions. The DAWN data are processed to 156 m range gate lengths (non-overlapping).

Instead the DLR 2- μm DWL is equipped with a double wedge-scanner, which allows also vertical pointing, and full 360° scanning capability. The Figure-of-Merit FOM for comparison of coherent wind lidars ($\text{energy} \cdot \text{aperture} \cdot \sqrt{\text{PRF}}$) is a factor of 13 higher for DAWN compared to the DLR 2- μm DWL. After the campaign a signal loss in the receiver part of DAWN was encountered, which could result in a degradation of 20 dB for the DAWN performance (see PM1 presentation by D. Emmitt (DLR 2015c)). The main properties of the 4 different wind lidars A2D, DLR 2- μm DWL, DAWN and TWiLiTE are summarized in Table 2-1 and 2-2.

The direct-detection wind lidar TWiLiTE from NASA-GSFC (<http://twilite.gsfc.nasa.gov/>) is a direct detection wind lidar at 355 nm using the double-edge technique for the molecular return (Gentry et al. 2014). It is equipped with a conical, step-stare, holographical scanner with an off-nadir angle of 45 ° and thus measures LOS winds and horizontal wind vector. A LOS wind is obtained within 30 s averaging per LOS and 192 s for a full conical scan with 6 LOS directions at 45° azimuthal difference (except 0°/180°). The laser transmits 200 pulses per second with 25 mJ/pulse. In combination with the larger telescope, this leads to a factor of 5 higher power-aperture product for TWiLiTE compared to the A2D (this factor does not include any optical efficiencies or transmission losses, which are different for TWiLiTE and A2D). TWiLiTE operates autonomously and was deployed on the ER-2, WB-57 and the Global Hawk before. The optical receiver for TWiLiTE uses a Fabry-Perot Interferometer FPI for the detection of the Doppler shift of the molecular return with slightly different FPI parameters (FWHM, FSR) than the A2D or ALADIN. A photomultiplier tube PMT is used as a detector. The FPI calibration is performed by varying the FPI distance, in contrast to A2D and ALADIN where the laser frequency is tuned. A FPI calibration scan is performed every 15 minutes during flight. A significant FPI frequency drift was observed during WindVAL due to thermal drifts, which are caused by the DC-8 operating environment. Procedures to correct for FPI drifts have to be developed. The laser frequency is monitored via an additional FPI locking channel with different FWHM than used for the atmospheric signal. 6 PMT's (photomultiplier tubes) are used for both FPI filters as high (90%), medium (9%) and low (1%) intensity channels. A 7th PMT is used as a pure backscatter channel without transmitting the signal through the FPI. A 1s temporal and 21 m vertical resolution is obtained for the raw data, which is processed to 30 s and 100 m resolution for the LOS product.

A number of 101 dropsondes from Yankee Environmental Systems (<http://www.yesinc.com/news/research.html>) were deployed during the campaign. The dropsondes measure pressure, horizontal wind vector, temperature, and relative humidity and can be deployed every 4 s. 17 dropsondes provided no data, so a total of 84 dropsondes are available. The dropsondes do not have a parachute as the NCAR AVAPS dropsondes (AVAPS: Airborne Vertical Atmospheric Profiling System). Thus different descent modes (wobbling, spiral) with different fall speeds (10-15 minutes, 5-6 minutes) could be observed. This results in different quality and noise on the wind speed of the dropsondes, e.g. oscillations of the wind speed.

Parameter	DLR A2D	NASA TWiLiTE
Wavelength	354.89 nm	354.7 nm
Laser energy	50-60 mJ	25 mJ
Pulse repetition rate	50 Hz	200 Hz
Pulse length	20 ns (FWHM)	15 ns (FWHM)
Telescope diameter	20 cm	32 cm (eff.)
Vertical resolution	300 m – 2.4 km	100 m (21 m raw data)
Temporal averaging raw data (horizontal)	20 laser shots = 0.4 s	200 laser shots = 1 s
Temporal averaging product (horizontal)	14 s (+4 s data gap)	30 s for each LOS 192 s for 6 LOS scan
Horizontal resolution @ 200 m/s=720 km/h = 12 km/min.	3.6 km (18 s)	6.0 km for LOS 38 km wind vector
Scanning capabilities	No, fixed 20° off nadir	Yes, step-stare conical scan with 45 ° off nadir
Precision (random error)	1.5 m/s Mie wind 2.5 m/s Rayleigh wind	2 m/s

Table 2-1: Main specifications and products from the 2 different direct-detection wind lidars (updated after PM 1 (DLR 2015c)).

Parameter	DLR 2- μ m DWL	NASA 2- μ m DAWN
Wavelength	2022.54 nm	2053.472 nm
Laser energy	1-2 mJ	100 mJ (nominal 250 mJ)
Pulse repetition rate	500 Hz	5 Hz (nominal 10 Hz)
Pulse length	400-500 ns (FWHM)	180 ns
Telescope diameter	10.8 cm	15 cm
Vertical resolution	100 m	156 m (78 m with 50% overlap)
Temporal averaging raw data (horizontal)	single shot = 2 ms	single shot = 200 ms
Temporal averaging product (horizontal)	1 s per LOS (500 shots), 44 s scan (21 LOS)	4 s per LOS (20 shots) 25 s per scan; 5 LOS
Horizontal resolution @ 200 m/s=720 km/h = 12 km/min.	0.2 km LOS, 8.8 km scan	0.8 km LOS 5 km scan
Scanning capabilities	Yes, double wedge, conical scan, fixed LOS and vertical	Yes, single wedge, conical scan, only fixed 30.12° off nadir with 5 LOS in forward direction
Precision (random error)	< 1 m/s wind speed	< 1 m/s wind speed

Table 2-2: Main specifications and products from the 2 different coherent-detection wind lidars (updated after PM 1 (DLR 2015c)).

2.3 Flight Tracks during airborne campaign 2015

The flight tracks from the airborne campaign 2015 are shown in Fig. 2-2 and 2-3. The duration and time of flight is summarized in Table 2-3. A total of 47.5 flight hours was performed on the Falcon aircraft including the test flight. The flight track, data sets and results from the test flight are reported in DLR (2015a).

Date	Time (UTC)	route	Objective
30.04.	12:51 – 15:47	OBF-OBF	Test flight
11.05.	08:12 - 10:46	OBF-PIK	Transfer 1
	12:29 - 14:49	PIK-KEF	Transfer 2
13.05.	10:56 - 13:39	KEF-KEF	TDS-1 underpass
15.05.	16:02 - 20:11	KEF-KEF	Jet Stream
16.05.	13:54 -17:19	KEF-SFJ	Ice Calibration
	18:12 - 21:12	SFJ-KEF	Ice Calibration
19.05.	11:58 - 15:54	KEF-KEF	Greenland Tip Jet Aeolus Track
21.05.	22:28 - 02:25	KEF-KEF	Greenland Summit
23.05.	16:54 - 21:09	KEF-KEF	Sea ice calibration
25.05.	14:04 – 17:20	KEF-KEF	Jet Stream
28.05.	10:23 - 13:24	KEF-KEF	ASCAT underpass Aeolus Track
29.05.	10:08 - 12:39	KEF-PIK	Transfer 1
	13:54 - 15:54	PIK-OBF	Transfer 2

Table 2-3: List of all flights from the airborne campaign WindVal in 2015 with the following IATA codes: OBF: Oberpfaffenhofen, PIK: Glasgow Prestwick, KEF: Keflavik, SFJ: Kangerlussuaq.

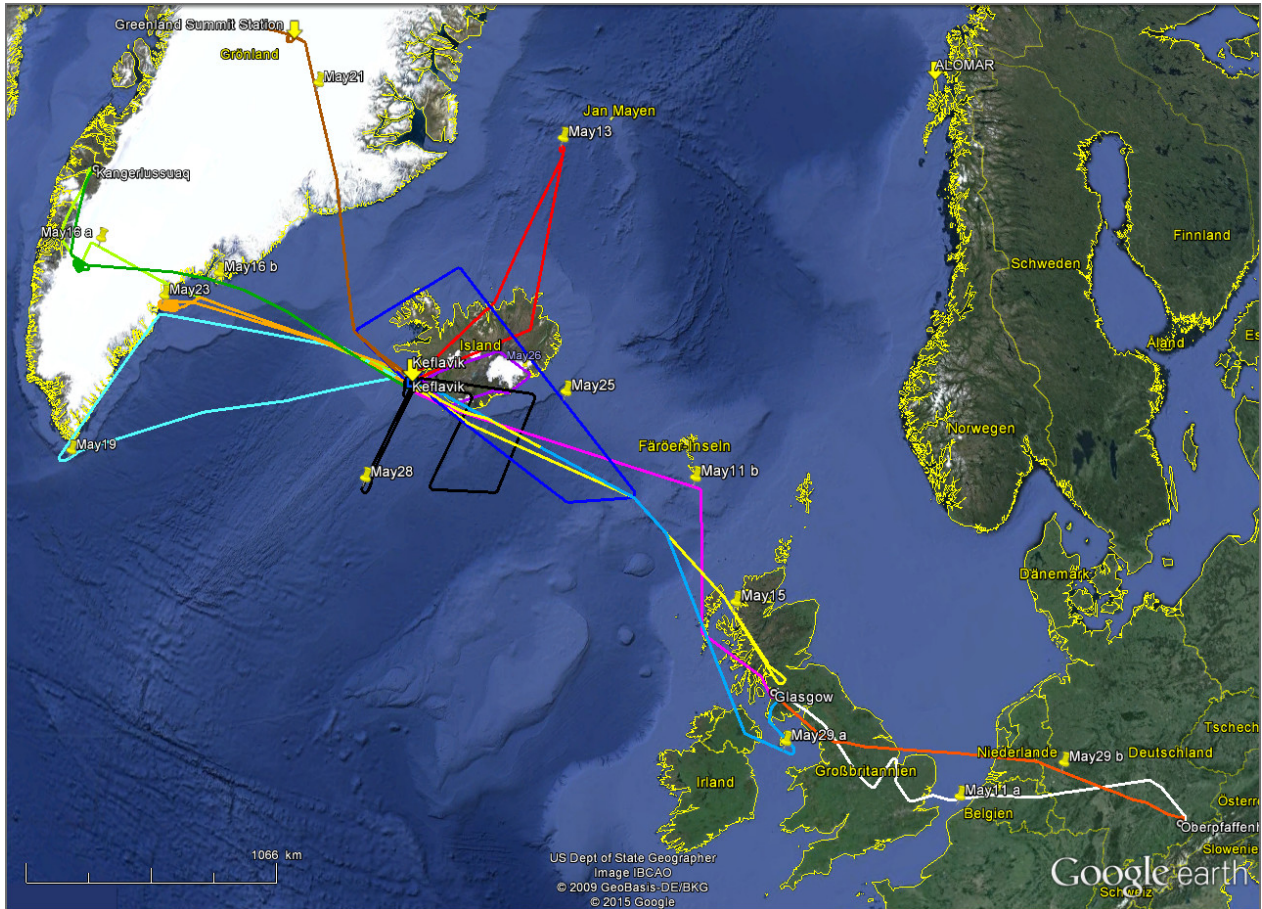


Figure 2-2: Map with flight tracks of the Falcon aircraft during the WindVal campaign in 2015 from May 11 to 29 (w/o test flight on April 30); deployment in Iceland from May 11 to May 29; each colour represents a single flight; transfer from OBF to Keflavik on May 11 (white, magenta flight) via Prestwick; transfer flight from Keflavik to OP on May 29 (blue, orange flight) via Prestwick.

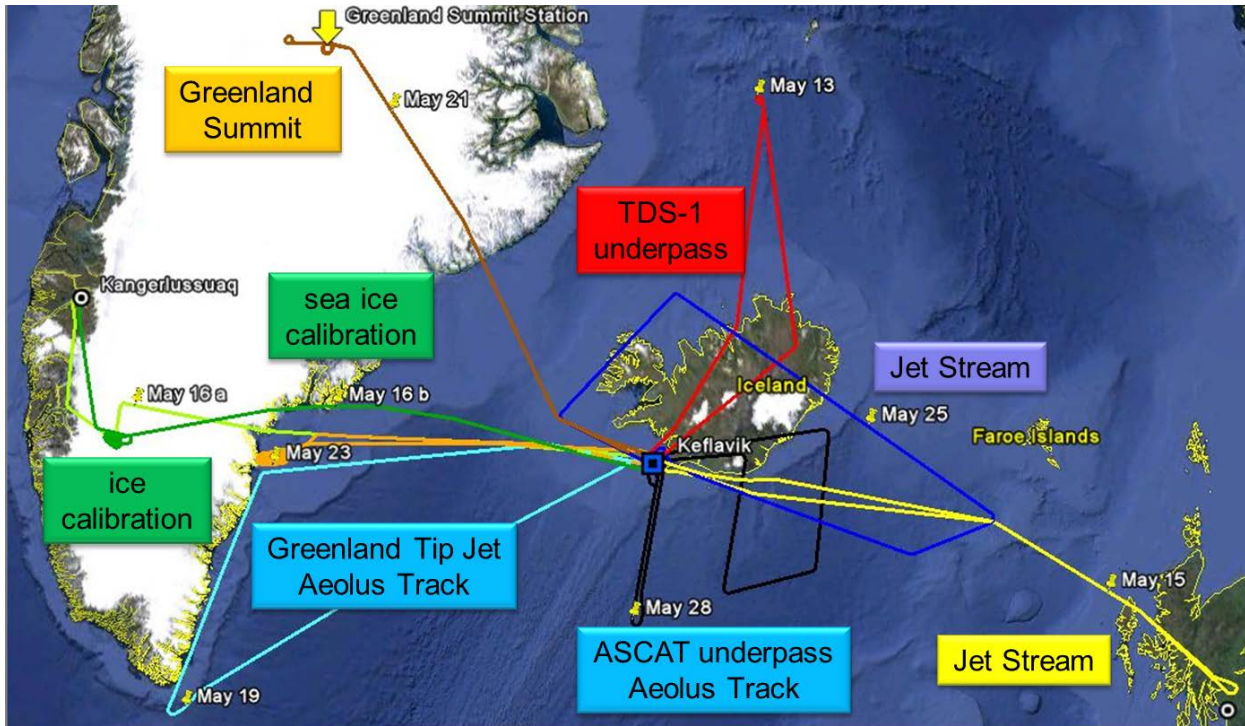


Figure 2-3: Map with flight tracks of the Falcon aircraft from Keflavik from May 13 to May 28 with the corresponding objectives of the flight.

2.4 Coordination with NASA DC-8

The NASA DC-8 aircraft transferred to Iceland from California on May 9 and back on May 28, 2015. The DLR Falcon aircraft and the NASA DC-8 aircraft performed coordinated flights, except for the Greenland Summit flight on May 21 and the ASCAT underpass on May 28 with only the Falcon aircraft. Due to the extended duration and range of the DC-8 compared to the Falcon, the DC-8 could extend the flight tracks after the Falcon had to fly back to Keflavik. A total number of 51 flight hours (excluding transfer flights) were performed by the DC-8. The flight tracks of the DC-8 are shown in Figure 2-4. The DC-8 was flying mainly behind the Falcon in a distance of several km. For the calibration flights on May 16 and May 23 the DC-8 was flying in the vicinity of the circles of the Falcon.

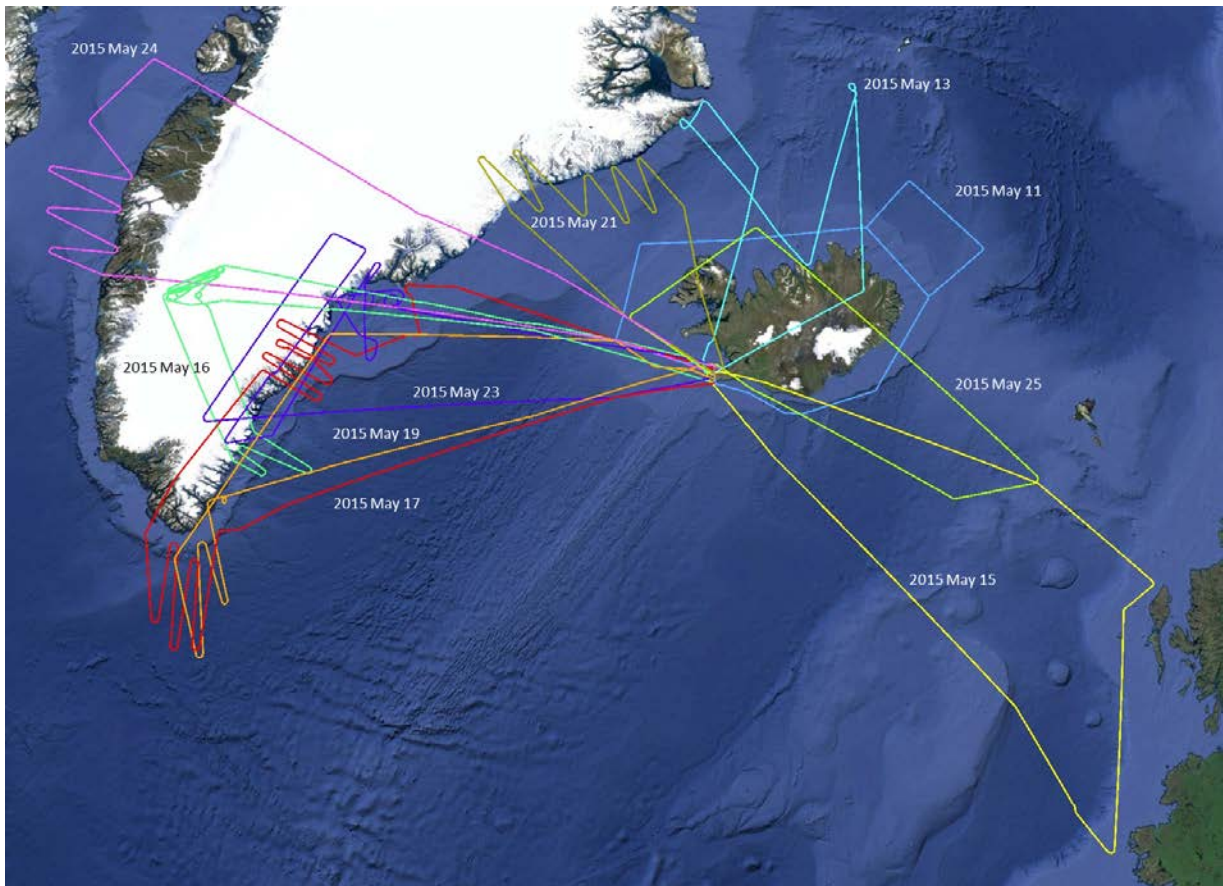


Figure 2-4: Map with flight tracks of the NASA DC-8 aircraft from Keflavik from May 11 to May 28 (courtesy D. Emmitt) with a total of 51 hours.

3 Ground Instrumentation

3.1 Ground Instrumentation in Europe

During the transfer flight on May 11 the Cabauw site (Netherlands) with its ground-based Raman lidar CAELI and the windprofiler sites in UK (Wattisham, South Uist) were passed (Table 3-1 and Figure 3-1). Due to the actual air-traffic it was not possible to fly directly above the Cabauw site on May 11 as planned; the aircraft had to pass south of Cabauw. Also due to heavy air-traffic around London it was not possible to fly over other windprofiler sites in UK (e.g. Aberystwyth, Chilbolton, Isle of Man). During the transfer flight on May 29 the UK windprofiler sites (South Uist, Isle of Man) were overflown.

The windprofilers with frequency of 915 MHz and 1290 MHz in the UHF (ultra-high frequency) band are boundary layer profilers, which provide wind profiles up to 3-4 km typically (Wattisham, Isle of Man, Cabauw). The windprofiler in Cabauw was not operating in May 2015 due to maintenance. The profilers operating at 40-65 MHz in the VHF (very-high frequency) band can reach up to the stratosphere (South Uist).

Site	Location	Instruments
Cabauw, Netherlands	51.96791 °N 4.92947 °E -0.5 m ASL	1290 MHz windprofiler, RASS (not operating) ; RAMAN lidar CAELI 355 nm, 532 nm, 1064 nm
Wattisham, UK	52.7 °N 0.058°E 87 m	1290 MHz windprofiler
Isle of Man, UK	54.06 °N 4.37 °W 55 m ASL	915 MHz windprofiler
South Uist, UK	57.353 °N 7.375 °W 4 m ASL	64 MHz windprofiler

Table 3-1: Coordinates of ground sites Cabauw and windprofilers from E-WINDPROF which were passed during the transfer flight on May 11 and May 29, 2015.

No ground sites with windprofilers are available in the region of Iceland and Greenland. Radiosondes are launched at 0 UTC and 12 UTC from Keflavik (Iceland) and sites in Greenland (Fig. 5 and Tab. 5).



Figure 3-1: E-WINDPROF Wind Profiler Profiler Network 2015; access on 20/02/2015 (<http://www.metoffice.gov.uk/science/specialist/cwind/profiler/>).

3.2 Radiosondes around Greenland and Iceland

The following radiosonde stations are available around Greenland and Iceland (Figure 3-2, Table 3-2).



Figure 3-2: Radiosonde network around Greenland and Iceland in 2015; access on 20/02/2015 for map (<http://weather.uwyo.edu/upperair/sounding.html>).

Name	Identifier	WMO station nr.	Lat.	Long.	Elev.	Location
Lerwick	3005	3005	60.13 °	-1.18 °	84 m	Shetland Islands
Thorshavn	6011	6011	62.02 °	-6.77 °	56 m	Faroer Islands
Keflavik	BIKF	4018	63.96 °	-22.60 °	54 m	Iceland
Jan Mayen	ENJA	1001	70.93 °	- 8.66 °	9 m	north of Iceland
Ittoqqortoormiit	BGSC	4339	70.48 °	- 21.95 °	69 m	Greenland east coast, north
Tasiilaq, Ammassalik	BGAM	4360	65.50 °	- 37.63 °	52 m	Greenland east coast, central
Narsarsuaq	BGBW	4270	61.15 °	-45.43 °	5 m	Greenland east coast, south
Aasiaat, Egedesminde	BGEM	4220	68.70 °	-52.85 °	41 m	Greenland west coast, central
Greenland Summit		4417	72.58 °	-38.48 °	3216 m	Greenland summit station

Table 3-2: Location of radiosonde around Iceland and Greenland, all stations have 0/12 UTC soundings, 1001 ENJA (Jan Mayen) has in addition 6/18 UTC soundings.

3.3 Greenland Summit Station

The Greenland Summit Station (72.58°N, 38.48 W, 3216 m ASL) releases 2 radiosondes per day and is equipped with an aerosol lidar from the MPL (micro-pulse lidar) network (contact Ralf Bennartz, Uni Vanderbilt, Wisconsin, Shupe et al. 2013). Online quicklooks of the data from an on-going campaign at Summit are available at <http://www.esrl.noaa.gov/psd/arctic/observatories/summit/browser/>.

The NCAS (National Centre for Atmospheric Science) Atmospheric Measurement Facility (AMF) Doppler Aerosol lidar (Halo Photonics) collected data continuously at Summit, Greenland from May 1, 2015 to June 27, 2015 (contact Ryan Neely, University Leeds). The lidar specifications are summarized in Table 3-3 and at <https://www.ncas.ac.uk/index.php/en/data-products/campaign-products/251-amf-main-category/amf-doppler-lidar/1093-doppler-lidar-overview>.

The instrument operated continuously throughout the period with varying success. During periods of low clouds (<5km) and deep layers blowing snow at the surface (also referred to as diamond dust) excellent observations of vertical and horizontal wind were obtained. During periods of clear sky and low blowing snow, the low aerosol loading and relatively weak signal of the NCAS Halo Photonics lidar hindered accurate wind profiles (even with ~10 min integration periods).

During the deployment lidar scans were specifically scheduled to observe the aerosol layers lowest to the ground and the horizontal wind speed with respect to blowing snow conditions. The scan parameters were following a set pattern of measuring vertical wind and depolarization profiles for 30 minutes followed by a 8 point PPI at 0 degrees, a 8 point PPI at 30 degrees, a 8 point PPI at 70 degrees, a RHI scan from East to West (i.e. from 0 degrees to 180 degrees), a RHI scan from North to South and a standard 3 point DBS wind profile at 70 degrees (PPI: Plan Position Indicator, RHI: Range Height Indicator, DBS: Doppler Beam Swinging). This will provide 3D wind observations at several different heights and a detailed look at the boundary layer every 30 minutes.

The precision of the horizontal wind vector from the HALO Photonics Doppler Wind Lidar was assessed by a 1-year comparison (2012-2013) with a radar wind profiler at 482 MHz and the Vaisala RS92 radiosonde at DWD Lindenberg observatory (Päschke et al. 2015). The root-mean square error RMSE of the comparison was 0.6 to 0.9 m/s for horizontal wind speed and 5-10° for direction with negligible systematic differences of 0.06 m/s.

Parameter	NCAS Doppler Wind Lidar
Wavelength	1.55 µm
Pulse repetition rate	15 kHz
Vertical resolution	18 m
Temporal averaging raw data (horizontal)	15 000 laser shots = 1 s
Scanning capabilities	Hemispheric scanning
Precision (RMSE) horizontal wind vector	0.6 m/s – 0.9 m/s 5° – 10 °

Table 3-3: Main specifications of the NCAS Wind Lidar.

	Document Nr. DAR.DLR.WindVal. 28.01.16	Issue: V1.0	Date: 28.01.2016	Page: 18/39	
	Doc. Title: WindVal Data Acquisition Report				

4 Satellite underpasses

The planned underpasses with the following satellite instruments were achieved.

- CALIPSO lidar from NASA providing attenuated backscatter, cloud and aerosol location (16 days repeat cycle, 233 orbits): no direct underpass performed with Falcon aircraft, but CALIPSO passes were in the vicinity of the Falcon flight tracks on May 11, 16, 19, and 25.
- Scatterometer ASCAT on Metop A and Metop B from EUMETSAT providing sea surface winds at 10 m with two swaths of 500 km width on each side of the satellite ground track (29 day repeat cycle); an underpass was performed on May 28; some passes were in the vicinity of the Falcon flight tracks on May 15, 16, and 19.
- Rotational Fan-Beam scatterometer on HY2A with a 6:00 Local Time of Ascending Node (LTAN) and a 1800 km wide nadir swath: no underpass was performed
- TechDemoSat 1 (TDS-1) with GNSS reflection technique to derive sea-surface winds; a direct underpass was performed on May 13, but the GNSS instrument was not operating during the underpass time.
- ALADIN lidar from ESA (7 day repeat cycle, 109 orbits); similar flight tracks than ALADIN were flown on May 19 and 21.

The satellite data products (plot, quicklook) of the specific days are found in the "Mission Summaries" (see chapter 5.9)

The satellite track predictions were obtained from: <http://www-angler.larc.nasa.gov/predict/> and <http://www.n2yo.com/>

The publically available CALIPSO track predictions are not accurate enough for flight track planning. Thus the correct predictions were provided by NASA LaRC (via SWA). A specific DLR tool was prepared during the campaign to visualize the satellite tracks for the specific days and regions from the CALIPSO tracks and the information provided on the n2yo-Website. It should be noted here that this website provides numerous satellite track predictions, but is maintained by amateur astronomers. An ESA website for satellite track predictions was not available during the campaign, but is considered as necessary for Aeolus Cal/Val activities.

Trial runs were performed with predicted Aeolus tracks (geographical location and time) provided by ESTEC (Thomas Kanitz) on May 19 (along Greenland Coast) and May 21 (south of Iceland). It is expected that actual track predictions for Aeolus will be available daily from ESOC or ECMWF after launch, because this track information is needed for providing meteorological fields (AUX_MET data based on predicted orbits). In addition to track predictions the actual instrument settings for ALADIN, e.g. calibration or wind mode, vertical sampling, on-board pulse accumulation should be provided. It is expected that the ALADIN time of overpasses are around 5-7 UTC and 19-21 UTC in the North-Atlantic Region; thus it was only considered to collocate with the evening overpass during the WindVal Campaign.

The TechDemoSat 1 mission was launched in July 2014, and has the capability to derive sea-surface winds by use of an enhanced GPS receiver to monitor reflected signals to determine the ocean roughness. This is equivalent to the 10 m sea-surface wind speed (equivalent to sea surface winds from scatterometer).

<http://noc.ac.uk/conference/ocean-observation-workshop>

www.MERRByS.co.uk

The satellite track predictions for TDS-1 were available on the n2yo-Website. It was encountered during the campaign the GPS receiver instrument is not switched on all the time due to power constraints. Thus, in addition to the track predictions, the specific operating times for the instruments should be provided by ESA in the future.

	Document Nr. DAR.DLR.WindVal. 28.01.16	Issue: V1.0	Date: 28.01.2016	Page: 19/39	
	Doc. Title: WindVal Data Acquisition Report				

5 Datasets from WindVal 2015

5.1 A2D from DLR Falcon

Generally, the A2D was operating without major technical problems and yielded a large amount of wind and calibration measurements, particularly more than during the 3rd airborne campaign in 2009. However, as Table shows, the fuse of the Reference Laser (RL) stabilization broke during the flight on May 15th which will constrain the analysis of the affected A2D data and will impose several algorithm modifications. Further limitations on the evaluation of A2D wind measurements might be posed by sporadic interruptions of the co-alignment loop and frequency instabilities during the IRC's (Instrument Response Calibration). Additionally, a few minor incidences occurred during the campaign such as an increased laser frequency jitter, icing on the lidar window of the Falcon and missing laser housekeeping data. Unforeseen data gaps were caused e.g. by software issues, jammed acquisition, a DEU (Detection Electronics Unit) error and occasional crashes of the co-alignment loop (COG: center of gravity).

Flight Date	Mission	A2D operation	Limitations	Comments
May 11 a/b	Transfer to Island, refuel in Prestwick	Nominal	a: 5 min interruption from crashed co-alignment loop (COG). Slight icing on lidar window.	Laser 2.8 W at start, 2.6 W before landing for refuel. Automatic reboot problem after refueling.
May 13	TDS-1 underpass	Nominal	Interruptions from jammed acq. during first half of the flight. Higher timing jitter for 2 nd half. WM data gap 5 min.	Detection electronics (DEU) unstable trigger. Original trigger scheme set for 2 nd half. WM-notebook power interruption. Cloudy 2 nd half. Laser 2.9 - 2.7 W.
May 15	Jet-stream flight Scotland	Nominal (Wind measurements available for flight back from Scotland)	2 nd half of the fight needs to be analyzed using WM-frequency measurement. Interruptions from Cavity control (CC) - error and DEU. WM recording interruptions.	Broken fuse of RL stabilization unit. Manual frequency stabilization during second half of the flight using WM-observations
May 16 a/b	Calibration over Greenland ice	Nominal and Imaging 2 Calibrations (IRC) a, 1 IRC b	a: laser frequency instability sporadic during start of 2 nd IRC. b: 10 min missing Laser HK at end	Alignment verification in imaging mode Laser 2.9 W. SL fiber splitter by-passed in Kangerlussuaq. Receiver background 2 min.
May 19	Greenland Tip-Jet, Aeolus-track	Nominal and Imaging	Data gaps in last third of flight back to Island due to jammed acq. and in-flight alignment activities	Laser 2.9 W FM4 realignment after hitting it on the way back to Island
May 21	Greenland summit	Imaging Nominal, 0 ^o and nominal over summit	Wind data gap first 30 min. due to imaging mode for alignment verification. 3 min. gap (COG jammed)	Laser 2.8 W COG variation alignment checked confirmed original setting
May 23	Sea-ice calibration	Nominal 2 Calibrations (IRC)	Data gap 20 min. on way to sea-ice (CC- and DEU error). 2 min. COG-gap @1 st IRC. Turns start 1.5 min after start of 2 nd IRC.	Laser 2.9 W; different MOUSR settings tested on way back to Island.

May 25	Jet-stream south of Island	Nominal	Declined frequency stability (PLL-SL locking instability) especially during northern leg. Sporadic frequency jumps and slow drifts during rest of flight. 3 min. COG-gap	Laser 2.9 W
May 28	ASCAT underpass/ Aeolus-track	Nominal	WM-data gap 4 min. due to software crash. sporadic turbulence and clouds	Laser 2.7 W
May 29 a/b	Transfer to OBF, refuel in Prestwick	Nominal	a: Frequency slow drifts b: Sporadic frequency jumps and slow drifts	Laser 2.9 W

Table 5-1: Mission objectives and A2D operation modes for all flights along with related information about the laser performance and causes for data gaps; nominal operation is referring to wind measurements in comparison to other instrument modes, e.g. imaging mode, response calibrations, WM: wavemeter, SL: seed-laser; FM4: Flight Mirror no. 4; MOUSR: Mie out of Useful Spectral Range; PLL: Phased-Locked Loop; OBF: Oberpfaffenhofen.

#	DATE of flight	START time	END time	duration (+14 s)	curve(s) included?	# OBS	# meas	invalid meas. RAY	invalid meas. MIE
1	11.05.2015	13:03.41	13:18.05	00:14.38	no	49	1715	90	960
2	11.05.2015	13:20.07	13:44.43	00:24.50	YES	83	2905	9	393
3	11.05.2015	13:58.49	14:21.37	00:23.02	no	77	2695	13	10
4	13.05.2015	12:24.58	12:51.40	00:26.56	no	90	3150	4	4
5	15.05.2015	18:09.06	19:09.42	01:00.50	YES	203	7105	7	8
6	15.05.2015	19:14.12	19:44.37	00:30.39	no	101	3535	6	6
7	16.05.2015	14:24.32	14:59.02	00:24.44	YES	116	4060	77	88
8	16.05.2015	16:44.25	16:54.19	00:10.08	YES	34	1190	1	1
9	16.05.2015	19:46.20	20:01.37	00:15.31	YES	52	1820	1	1
10	16.05.2015	20:02.58	20:32.44	00:30.00	YES	100	3500	2	2
11	19.05.2015	13:42.03	14:14.45	00:32.56	no	110	3850	2	2
12	21.05.2015	23:45.23	00:40.53	00:55.44	YES	184	6440	89	88
13	22.05.2015	00:49.53	01:20.47	00:31.07	YES	104	3640	1	1
14	22.05.2015	01:22.14	01:48.02	00:26.02	YES	87	3045	2	2
15	23.05.2015	17:27.08	17:43.02	00:16.08	no	54	1890	6	7
16	23.05.2015	20:08.36	20:39.48	00:31.26	YES	105	3675	0	2
17	25.05.2015	15:24.03	16:47.44	01:23.55	YES	280	9800	7	6
18	28.05.2015	10:50.02	11:17.56	00:28.08	YES	94	3290	138	158
19	28.05.2015	11:25.08	12:52.44	01:27.50	YES	293	10255	81	101
20	29.05.2015	11:09.58	11:45.04	00:35.16	YES	118	4130	17	24
21	29.05.2015	14:37.21	15:16.38	00:39.31	YES	132	4620	24	33

Table 5-2: Overview of main wind measurement sections including information about the A2D performance.

	Document Nr. DAR.DLR.WindVal. 28.01.16	Issue: V1.0	Date: 28.01.2016	Page: 21/39	
	Doc. Title: WindVal Data Acquisition Report				

After first analyses of the available A2D data, 21 wind measurement sections longer than 10 minutes were selected and are presented in Table 5-2 together with their date, start and end time. The end time corresponds to the time tag (start time) of the last observation, i.e. the last pulse contributing to each wind measurement section is emitted 14 s after that end time. The four shortest sections marked by red boxes last between 10 and 16 min. Due to their length of 55 min to 88 min (including 184 – 293 observations) the four longest sections marked by green boxes are preferred for analysis. The occurrences of invalid measurements on the Rayleigh and Mie channel in Table 5-2 are highly correlated and the invalidity is mainly caused by signal on the DCO channel, saturation of single pixels on the ACCD, saturation of signal or incorrect assignment of range-gates numbers as studied in Marksteiner (2013). Additionally, it is indicated for each flight leg whether or not the measurements were obtained during a straight flight or in curves. Flight sections with curves require extra analysis during the processing related to ground detection.

After processing the resulting A2D LOS winds, a subset of Table 5-2, will be delivered per observation, sorted by Rayleigh & Mie channel according to Table 5-3. The subset depends on the quality of the derived LOS winds, e.g. it is not clear today, if LOS winds can be processed with sufficient quality from all flight legs of Table 5-2. The A2D LOS winds will be compared to the 2- μ m DWL and visualized. Comparable graphs can be found in DLR (2012b, ch. 4., ch. 5, ch. 6) and in ch.4 of Marksteiner (2013) which also contains the relevant information about the wind retrieval (ch.3.5), the applied quality control (ch.3.6) and the handling of the instrument response calibrations (ch.3.4). All 5 response calibrations (IRC) will be analysed and a subset of wind mode data will be processed using two different response calibrations results.

	Parameter	Comments
Main Header	Date	---
	Calibration info	Date & time; important settings
	No. of profiles / observations	---
	Delimiter	Default: tabulator
	Default	-999
Specific Header (i)	Start time of observation	Milliseconds from 00:00 UTC
	Geolocation: latitude / longitude	---
	Ground bin	---
Profile info (i)	Bin number	---
	Altitude	Top of bin; above MSL
	Range from instrument	Top of bin
	Rayleigh LOS wind	m/s
	Mie LOS wind	m/s
	Rayleigh signal	LSB; channel A+B
	Mie SNR	According to Marksteiner (2013)

Table 5-3: Format of A2D Level 1 LOS winds with one main header as well as one specific header and profile information per observation.

It is envisaged to use selected A2D measurements (wind+calibration) as input to the E2S-L1B chain. Therefore pre-processed data from different sources (A2D raw binary product, A2D housekeeping data, Falcon IRS, etc.) are compiled in an ASCII file according to the example shown in Figure 5-1. This format has already been used for deliveries of the 2009 airborne campaign data. These files contain information about the UV laser frequency, time, flight altitude, off-nadir angle and P-N setting (all in the header; P: number of pulses, N: number of measurements) as well as per observation the location and size of the single bins and the measured LSB (least significant bit) per pixel on the ACCD.

```

freq. offset (UV) / MHz:          2228.333400
obs. time stamp / s: 3336806605
flight altitude / m: 10452.66
internal reference: 4
off-nadir angle / °: 20.24
# of measurements: 35
# of pulses per meas.:          20

| bin # | altitude upper edge / m | latitude / ° | longitude / ° | LOS azimuth / ° | int_time_Ray / µs | int_time_Mie / µs ||| Ray0_dco Ray1_dco Ray2 ... Mie17 Mie18_dco Mie19_dco |||
0
20090926_124325
0 -1679.50 64.224 -38.410 26.530 3750.000 3750.000 397.250 397.250 422 ... 346 316.187 316.187
1 10452.66 64.224 -38.410 26.530 2.104 2.104 397.250 397.250 393 ... 316 316.187 316.187
2 10452.66 64.224 -38.410 26.530 2.104 2.104 397.250 397.250 398 ... 315 316.187 316.187
3 10452.66 64.224 -38.410 26.530 2.104 2.104 397.250 397.250 399 ... 319 316.187 316.187
4 10452.66 64.224 -38.410 26.530 4.208 4.208 397.250 397.250 2211 ... 622 316.187 316.187
5 10156.76 64.224 -38.410 26.530 2.104 2.104 397.250 397.250 477 ... 344 316.187 316.187
6 9860.85 64.224 -38.410 26.530 8.416 8.416 397.250 397.250 834 ... 598 316.187 316.187
7 8677.23 64.224 -38.410 26.530 8.416 8.416 397.250 397.250 560 ... 559 316.187 316.187
8 7493.60 64.224 -38.410 26.530 8.416 8.416 397.250 397.250 478 ... 463 316.187 316.187
9 6309.97 64.224 -38.410 26.530 8.416 8.416 397.250 397.250 435 ... 416 316.187 316.187
10 5126.35 64.224 -38.410 26.530 8.416 8.416 397.250 397.250 419 ... 379 316.187 316.187
11 3942.72 64.224 -38.410 26.530 4.208 4.208 397.250 397.250 409 ... 346 316.187 316.187
12 3350.91 64.224 -38.410 26.530 4.208 4.208 397.250 397.250 404 ... 341 316.187 316.187
13 2759.10 64.224 -38.410 26.530 2.104 2.104 397.250 397.250 404 ... 326 316.187 316.187
14 2463.19 64.224 -38.410 26.530 2.104 2.104 397.250 397.250 401 ... 332 316.187 316.187
15 2167.28 64.224 -38.410 26.530 2.104 2.104 397.250 397.250 406 ... 331 316.187 316.187
16 1871.38 64.224 -38.410 26.530 2.104 2.104 397.250 397.250 400 ... 328 316.187 316.187
17 1575.47 64.224 -38.410 26.530 2.104 2.104 397.250 397.250 401 ... 329 316.187 316.187
18 1279.56 64.224 -38.410 26.530 2.104 2.104 397.250 397.250 405 ... 326 316.187 316.187
19 983.66 64.224 -38.410 26.530 2.104 2.104 397.250 397.250 404 ... 327 316.187 316.187
20 687.75 64.224 -38.410 26.530 2.104 2.104 397.250 397.250 398 ... 320 316.187 316.187
21 391.84 64.224 -38.410 26.530 2.104 2.104 397.250 397.250 401 ... 320 316.187 316.187
22 95.94 64.224 -38.410 26.530 2.104 2.104 397.250 397.250 402 ... 318 316.187 316.187
23 -199.97 64.224 -38.410 26.530 2.104 2.104 397.250 397.250 397 ... 317 316.187 316.187
24 -495.88 64.224 -38.410 26.530 8.416 8.416 397.250 397.250 399 ... 320 317 319

1
20090926_124325
0 -1679.50 64.224 -38.410 26.530 3750.000 3750.000 397.937 397.937 416 ... 345 315.687 315.687
1 10452.66 64.224 -38.410 26.530 2.104 2.104 397.937 397.937 400 ... 317 315.687 315.687
:
:

```

Figure 5-1: Example visualising the format in the A2D data will be delivered as input to the E2S-L1B

	Document Nr. DAR.DLR.WindVal. 28.01.16	Issue: V1.0	Date: 28.01.2016	Page: 23/39	
	Doc. Title: WindVal Data Acquisition Report				

The structure of the delivered A2D data and results of the WindVal campaign is organised under three main directories as follows:

1. DATA

1.1. Day of flight

1.1.1. Data recording session

- Raw data
 - A2D binary products (*.deu)
 - Housekeeping and telemetry data (*.tle)
 - Logbook (*logbook.csv)
 - Thermal data of receiver (*thermal.csv)
 - UV camera data, i.e. CoG information (*uvcam.csv)
 - Configuration file for the A2D system (*acu_conf.csv)
 - Folders containing copies of the raw data of selected sections for easier access
 - sorted e.g. by wind measurement
 - calibration
 - MOUSR (Mie Out of Useful Spectral Range)
 - imaging mode, etc.
- 1.2. ALMEMO (contains pressure, temperature and humidity on-board the Falcon)
- 1.3. UVcam (contains information about the laser pointing and hence the CoG)
- 1.4. WAVEMETER (contains frequency measured by the wavemeter)
- 1.5. 2mu Lidar (contains Level 2 scanning data for comparison against A2D winds)
- 1.6. ... (additional data sets, e.g. radiosondes, DC-8 dropsondes)

2. RESULTS

(contains VIs with the results of the comparison of all calibrations)

2.1. Day of flight

2.1.1. Data recording session

- Overview VI presenting the main results in a fixed arrangement
 - Overview Powerpoint showing contents of the VI and additional info
- 2.2. FALCON (contains the Falcon flight tracks plotted in Google Earth)
- 2.3. ... (additional Powerpoint presentations, drafts and overview tables)

3. LabView

3.1. ALADIN_PROC

3.2. TOOLS

- 3.2.1. 2mu-Plotting LOS
- 3.2.2. 2mu-Plotting Scan
- 3.2.3. CMET_data plots
- 3.2.4. Comparison A2D – 2mu
- 3.2.5. Comparison A2D – DEM
- 3.2.6. Comparison A2D – ECMWF
- 3.2.7. Comparison A2D – MieRay
- 3.2.8. Comparison A2D – RaSo_WPR
- 3.2.9. Comparison ECMWF – RaSo
- 3.2.10. GoogleEarth_Stuff
- 3.2.11. Plot_Tracks_CMET_and_DEM_Intersection
- 3.2.12. Zero_Wind

	Document Nr. DAR.DLR.WindVal. 28.01.16	Issue: V1.0	Date: 28.01.2016	Page: 24/39	
	Doc. Title: WindVal Data Acquisition Report				

The placeholders “*Day of flight*” and “*Data recording session*” stand for the directories dedicated to each of the:

- 10 scientific flights, e.g. “*2015-05-19 - Greenland Tip Jet*”
- Recording sessions performed on the actual day of flight, e.g. “*20150515s4 - Scotland Jet Stream*” (here 4th session on May 15th in 2015)

The content of part of the files contained in “RAW DATA” (*.tle, *uvcam.csv, *.deu) is described in DLR (2005).

The directory “WAVEMETER” contains the measurements of the A2D laser frequency by a High Finesse WSU-2. The data is available in long-term recording format (*.lta) and as pre-processed version in *.txt format. The latter can be converted by the VI “*Wavemeter - mean freq per obs.vi*” in “*LabView\ALADIN_PROC\Wavemeter - mean freq per obs - BW*” to mean frequencies per observation which are an optional input to the processing of the A2D response calibrations.

The directory LabView/TOOLS contains LabView processors that can be used for a more detailed analysis of A2D winds and related data, mainly for comparisons against wind speeds from other wind sources such as ECMWF and the 2- μ m lidar. The VIs in the directory CMET_data_plots with the main VI “*MAIN_Plot_cmet_data.vi*” is mainly used to derive the additional LOS speed induced by the attitude and speed of the Falcon aircraft which is input to the corresponding correction in the A2D calibration and wind processing.

The directory LabView/ALADIN_PROC contains all LabView VIs used for processing the delivered results. The main VI to be used is “*START_Cal_Wind.VI*” from which the different processors can be called.

	Document Nr. DAR.DLR.WindVal. 28.01.16	Issue: V1.0	Date: 28.01.2016	Page: 25/39	
	Doc. Title: WindVal Data Acquisition Report				

5.2 2- μ m DWL from DLR Falcon

The 2- μ m DWL was operating w/o technical problems, except for some GPS receiver problems on May 19 and 21, which resulted in some small data gaps of a few profiles during these flights. The 2- μ m DWL data are processed using 2 different algorithms for retrieving the 3-dimensional horizontal wind vector from the LOS directions. An inversion algorithm (using a sinusoidal fit-function) and a signal accumulation algorithm recently adapted for airborne DWL measurements (Smalikho 2003). The baseline for the accumulation algorithm can be found in Smalikho (2003) and an earlier comparison between the inversion and accumulation algorithm in Weissmann et al. (2005). The final 2- μ m DWL data product combines the output of the inversion and the accumulation algorithm.

First the wind vector is derived from a number of 21 LOS winds using the inversion algorithm, based on 3 LOS wind values separated by 120°. Thus a maximum number of $21/3 = 7$ wind vectors are obtained for each scan, which are averaged to 1 wind vector. An averaged wind vector is reported as valid, if a minimum number of wind vectors (default 4) were obtained from the 7 inversion results. The accumulation algorithm is used for those altitude levels, where no results from the inversion algorithm are obtained. Several QC criteria are used within the accumulation algorithm. As a final step a median filter is applied to each range bin. The neighbouring range bins in a box of N by N range bins (default N=5) is investigated. The range bin is considered as valid, if a fraction (default value is 20 %) of all horizontal wind speed values surrounding this range bin is within a certain range of wind speeds (default is ± 4 m/s).

The 2- μ m DWL data are provided for wind vector profiles (Level 2; filename *_L2.txt) from conical scans and as LOS wind profiles from conical scans and in case of non-scanning mode (Level 1, filename *_L1.txt). For the Level 2 wind vector profiles only altitude levels from aerosol backscatter are reported. No level 2 wind vector profiles are derived from high SNR targets as clouds or ground. Cloud backscatter is not reported in Level 2 product, because the cloud backscatter is often not uniform within 1 scan, e.g. clouds are present only for some LOS pointing directions. In contrast the information for aerosol, clouds and ground LOS winds is obtained in the Level 1 product.

It must be mentioned here that the times provided in the Level 1 and Level 2 files are based on GPS time, which is not corrected for leap seconds. Thus, the following correction needs to be applied to obtain time in UTC (before 1 July 2015): UTC = GPS -16 s.

The 2- μ m DWL Level 2 wind vector data are provided as TXT file per flight with the following information:

- 1 general header with information according to Table 5-4
- a number of wind vector profiles with
 - specific header according to Table 5-5
 - altitude profile for each wind vector (u,v,w) according to Table 5-6

The 2- μ m DWL Level 1 LOS data are provided as TXT file per flight with the following information:

- 1 general header with information according to Table 5-7
- a number of LOS profiles with
 - specific header according to Table 5-8
 - specific header indicating, if LOS is obtained from aerosol ("Aerosol"), cloud ("Wolke") or ground ("Boden") with the corresponding number of range gates; for a ground return it is indicated if it is a "sea" or a "land" surface return
 - altitude profile (in m) for each LOS wind (in m/s) and power (a. u.)

The 2- μ m DWL is switched on after take-off and it takes about 15-20 minutes to reach stable laser and instrument operation, which is usually during ascent to the flight level of 10-11 km. The 2- μ m DWL is usually switched-off during descent when an altitude of 3 km is reached, which is about 10-15 minutes before landing. Thus 2- μ m DWL measurements are available for about 30 minutes less than the flight duration.

Some flights show strong vertical updrafts (e.g. May 16), even though those are retrieved from a conical scan over a large horizontal distance of about 8 km. These strong vertical updrafts are not considered as instrumental or retrieval artefacts. For resolution of smaller-scales gravity waves, the 2- μ m DWL needs to be pointed vertically and not used in conical scanning mode.

	Document Nr. DAR.DLR.WindVal. 28.01.16	Issue: V1.0	Date: 28.01.2016	Page: 26/39	
	Doc. Title: WindVal Data Acquisition Report				

Parameter	Default	Comment
Observation data		Day of flight
Vertical resolution	100 m	
No. of profiles		no. of wind vector profiles in file
No. of vertical levels	120	No. of altitude levels per profile
Default value	-999.00	Unvalid data value
Delimiter	Tabulator	Delimiter used to separate columns
Time	milliseconds from 00:00 GPS	
Qualitätskriterien Median	Same parameters for each flight	Quality criteria for median filter
Qualitätskriterien Accumulation	Same parameters for each flight	Quality criteria for accumulation algorithm
Qualitätskriterien Inversion	Same parameters for each flight	Quality criteria for Inversion algorithm

Table 5-4: General Header for 2- μ m DWL Level 2 data for each flight; although the unit for time is labelled as “ms UTC” in the file it is “ms GPS” w/o correction of leap seconds

Parameter	Unit
Time since midnight	ms GPS
Latitude	°N
Longitude	°E
Altitude	m ASL
Horizontal velocity	m/s
Vertical velocity	m/s
Heading angle	°N
Roll angle	°
Number of scan	
Number of LOS per scan	21

Table 5-5: Specific header for 2- μ m DWL Level 2 data for each wind vector profile with aircraft parameters.

Parameter	Unit	Comment
Altitude	m	ASL
North velocity v	m/s	Positive towards North
East velocity u	m/s	Positive towards east
Downward velocity -w	m/s	Positive downward

Table 5-6: Content of 2- μ m DWL Level 2 data for each profile; although the vertical velocity w is usually positive for upward direction, the file reports “downward” direction for positive values.

Parameter	Default	Comment
Datum		date
Kommentar	1 s LOS	Content 1 s LOS
Anzahl_LOS		Number of LOS profiles
Quality parameters		Quality criteria for LOS winds
Korrektur Power	R-Quadrat	Power is multiplied with R^2 in a.u. linear scale

Table 5-7: General header for 2- μ m DWL Level 1 data for each LOS profile with aircraft parameters, a.u. arbitrary units.

Parameter	Unit
Time since midnight	ms GPS
Latitude	°N
Longitude	°E
Altitude	m ASL
North-South velocity	m/s
East-West velocity	m/s
Vertical velocity	m/s
North direction LOS	unit vector
East direction LOS	unit vector
Down direction LOS	unit vector
x-scanner	°
y-scanner	°
LOS aircraft	m/s
Laser offset	MHz

Table 5-8: Specific header for 2- μ m DWL Level 1 data for each LOS profile with aircraft parameters with time in GPS in ms w/o correction of leap seconds.

	Document Nr. DAR.DLR.WindVal. 28.01.16	Issue: V1.0	Date: 28.01.2016	Page: 29/39	
	Doc. Title: WindVal Data Acquisition Report				

5.3 In-situ data from the DLR Falcon

The in-situ data from the DLR Falcon aircraft are provided for each flight containing:

- a kml-file for displaying the flight track in Google Earth
- a nas-file including all the data in TXT-format
- a folder for each flight including figures of flight tracks, height profiles of parameters during ascent/descent and time series of parameters during flight
- a PDF-file including all figures

The content of the in-situ data from the Falcon is described in the header of each file. It contains the parameters according to Table 5-9 from different sensors with a time resolution of 1 s. The raw data of the different sensors are stored with 10-100 Hz.

The altitude of the aircraft can be derived from different sources of the aircraft data. The meteorological height is derived from the pressure and temperature measurements during ascent and descent. As the flight tracks are performed along a pressure gradient within the atmosphere, and the aircraft is flying on constant pressure altitudes, the actual flight height is changing. Thus the meteorological height cannot account for that gradient and is systematically incorrect. Thus the more accurate height information is derived from the GPS altitude (ASL).

The Falcon in-situ data from the IRS (pitch, roll, heading angle) and the GPS (lat, lon, altitude, aircraft ground speed) are used within the A2D processing for the derivation of the line-of-sight LOS pointing direction and the aircraft ground speed. The 2- μ m DWL uses its own GPS antenna and receiver and interfaces to the aircraft ARINC-429 bus to access IRS data with high frequency up to 100 Hz.

Sensor	Parameter	Comment
Flight Management Computer FMC	Lat, Lon	composite of several sources
Global Positioning System GPS	Height (ASL), Lat, Lon, EWV, NSV	
Inertial Reference System IRS	track angles, accelerations, ground speed, heading, roll, pitch angle and rates	
Aircraft Ground speed	EWV, NSV Vertical velocity	Composite from IRS+GPS from IRS
Time	UTC time	Manually set at start of flight
Humidity	absolute, relative humidity, mixing ratio	Composite of 3 instruments (source is indicated); no values are reported within clouds (100% RH) and for very low humidity ($<10^{-4}$ kg/kg)
Noseboom pressure sensors	Angle of attack, angle of sideslip, pressure altitude, Mach number, static and dynamic pressure, TAS	
Temperature	Total air temperature, dewpoint temperature, potential temperature, virtual potential temperature, static air temperature, virtual temperature	
Wind Vector	East Component (u), North component (v), vertical component (w), horizontal wind speed and direction	No vertical wind during ascent / descent and other conditions, e.g. curves.
Altitude	GPS altitude (ASL) Height (ASL) calculated from meteorological sensors Pressure altitude	

Table 5-9: Content of DLR Falcon in-situ dataset; Lat: Latitude, Lon: Longitude, EWV: East-West Velocity, NSV: North-South Velocity, TAS True Airspeed, ASL: above sea level (geoid)

	Document Nr. DAR.DLR.WindVal. 28.01.16	Issue: V1.0	Date: 28.01.2016	Page: 31/39	
	Doc. Title: WindVal Data Acquisition Report				

5.4 DAWN data from NASA DC-8

The 2- μm lidar from DAWN are not available yet.

5.5 TWILITE data from NASA DC-8

The TWILITE lidar data are not available yet.

5.6 Dropsonde data from NASA DC-8

The DC-8 dropsondes were provided in 2 versions by SWA in August 2015 (Version 1) and December 2015 (version 2). Both versions are described below

1) Dropsonde Version 1 (August 2015)

The DC-8 dropsonde data were provided for collocated flights with the Falcon aircraft for the 10 days in May 2015 (May 11, 13, 15, 16, 17, 19, 21, 23, 24, 25). For each dropsonde one file is provided. It contains the following data as text files (Table 5-10). Two different format styles are used with fixed position (format 1) and comma-separated values (CSV, Format 2), e.g.

Format 1: 13:46:51.00 490.5 -27.57 26.4 4 ...
 Format 2: "16:22:18.00",264.5,-44.85,"nan",19.9,

Column (Format 2)	Position Format 1	Length Format1	Parameter	Unit
1	1	11	Time	UTC (tbd)
2	16	10	Pressure	hPa
3	30	10	Temperature	°C
4	41	10	Relative Humidity	%
5	53	10	v-component	m/s
6	65	10	u-component	m/s
7	73	6	fall velocity	m/s
15	137	10	Wind Speed	m/s
16	147	10	Wind Direction	°
17	158	10	GPS-Altitude	m not used
18	169	10	Geoheight	m ASL (tbd)
19	179	10	Latitude	°N
20	190	11	Longitude	°E

Table 5-10: File content of dropsonde files with two different formats (Version 1)

It is assumed that the time information is provided in UTC (column 1). Several different altitude columns are provided, including column 17 with GPS-Altitude (in m) and column 18 Geoheight (in m ASL tbd). It is assumed that the Geoheight altitude is referenced wrt the geoid and thus ASL (above sea level).

The qualities of the dropsondes, which are close to the DLR Falcon flight track, were assessed manually according to several criteria (Table 5-11):

- Noise on wind speed: 0: random noise < 1 m/s, 1: noise ~ 1m/s, 2: noise > 1 m/s
- Δ -time: Time difference in seconds between dropsonde and the closest wind profile from the DLR 2- μ m DWL
- Δ -distance: Difference in kilometers between dropsonde and the closest wind profile from the DLR 2- μ m DWL

The dropsondes marked with "x" (column quality) fulfill the quality criterions: noise < 1 m/s, Δ -time < 120s and Δ -distance < 5 km and are therefore reference dropsondes for the comparison to the DLR 2- μ m DWL.

The dropsondes show different noise characteristics on the wind speed profiles, which is due to different descent modes. These could be either slow descents (with wobbling behaviour) or fast descents (with spiral behaviour). These different modes could be also observed within 1 dropsonde descent. The noise can be filtered in post-processing by vertically averaging the data.

Date	Time	Quality	Noise[0/1/2]	Δ -time[s]	Δ -distance [km]
13.05.	11:50:07		1	9	2.04
	12:28:33	x	0	4	0.47
	12:40:22	x	0	26	2.25
15.05.	16:59:07	x	0	14	1.99
	17:14:05	x	0	80	4.28
	17:19:32	x	0	59	2.68
	17:24:42	x	0	61	1.98
	17:29:44	x	0	56	3.32
16.05.	15:24:15		2	27	2.16
	18:50:20		0	286	39.00
19.05.	13:23:54	x	0	7	1.46
	13:36:00	x	0	16	2.82
	13:47:41	x	0	4	0.24
	13:59:23		1	7	1.01
	14:10:48	x	0	24	3.52
23.05.	18:06:00		0	119	45.36
	18:26:51		2	1091	10.09
25.05.	16:21:29	x	0	25	3.57
	16:27:42	x	0	1	0.47

Table 5-11: Quality assessment of NASA DC-8 dropsondes (version 1), which were used for comparison with DLR 2- μ m DWL indicated by "x".

2) Dropsonde Version 2 (December 2015)

A re-processed version of the dropsondes was provided by SWA in December 2015. Some initially reported variables such as internal temperature, battery voltage, RH_sensor, IR_Sensor, GPS_altitude, GPS_Lock_Age, etc. are not included in this version, but can be provided upon request.

A new height – called hydrostatic height (column 17) – was computed, which is considered by SWA as the most accurate height information. This height is referenced to mean sea level (msl).

Each dropsonde information is contained in one file with the filename indicating data and time of sounding and the following information within the TXT file in CSV format (Table 5-12). A “nan” indicates a non-valid value after QC (nan: not a number). The first line contains date (YYYY/MM/DD), start time (in UTC) and geolocation with latitude (°N) and longitude (°E). The other lines contain the data with the following columns:

Column	Parameter	Unit
1	Elapsed Time	s
2	Pressure	hPa / mbar
3	Temperature	°C
4	Relative Humidity	%
5	fall velocity	m/s
6	Surface Temperature	°C
7	Accel. Temperature	°C
8	Accel. RH	%
9	Dew Point Temperature	°C
10	Potential Temperature	K
11	Eq. pot. Temperature	K
12	U-component	m/s
13	V-component	m/s
14	Wind Speed	m/s
15	Wind Direction	°
16	GPS-Altitude	m ASL
17	Hydrostatic height	m ASL
18	Latitude	°N
19	Longitude	°E

Table 5-12: File content of NASA DC-8 dropsonde files (Version 2); accel. accelerometer

A total number of 84 dropsonde files are provided from flights on May 11, 13, 15, 16, 17, 19, 21, 23, 24, and 25. The quality of the dropsonde from version 2 has not been assessed yet. It should be noted here, that non-valid data are excluded by a QC (“nan”), but no additional averaging or filtering was applied to the original data.

	Document Nr. DAR.DLR.WindVal. 28.01.16	Issue: V1.0	Date: 28.01.2016	Page: 35/39	
	Doc. Title: WindVal Data Acquisition Report				

5.7 Greenland Summit Data

The NCAS (National Centre for Atmospheric Science) Atmospheric Measurement Facility (AMF) Doppler Aerosol lidar (Halo Photonics) collected data continuously at Summit, Greenland from May 1, 2015 to June 27, 2015. The instrument operated continuously throughout the period with varying success. During periods of low clouds (<5km) and deep layers blowing snow at the surface (also referred to as diamond dust) excellent observations of vertical and horizontal wind were obtained. During periods of clear sky and low blowing snow, the low aerosol loading and relatively weak signal of the NCAS Halo Photonics lidar hindered accurate wind profiles (even with ~10 min integration periods).

Observations

During the deployment the following scan types were made (name in parentheses corresponds to the top level directory name of the data): 1) Wind Profiles (WP), 2) PPIs (ppi), 3) RHIs (rhi) 4) Vertical Stare ('fix_co' and 'fix_cr') and 5) 4 user specified patterns ('user 1', 'user 2', 'user 3', 'user 4') which changed over the deployment depending on the science question being addressed.

For all line of sight data (designated by LoS in the file name) collected, the observations separated into files that contain the backscatter ('beta') and files containing the radial velocity ('rv'). The individual data files follow the naming convention 'Scan_Type_18_YYYYMMDD_HHMMSSLoS_Variable.nc'. The derived WP data files are just labelled with a simple 'YYYYMMDD.nc'.

Data File Descriptions

As per NCAS AMF protocol, upon completion of the deployment the data was processed by the NCAS AMF Instrument Scientist. The processing included application of quality controls, transformation of the raw instrument files into netCDF and archival of the data on to the Centre for Environmental Data Analysis (CEDA) archive. Data is provided to ESA and CEDA in netCDF format and follows the AMF protocol for file naming and structure. Each data files contain no more than 24 hours' worth of data. Detailed information about the data format may be found at <https://www.ncas.ac.uk/index.php/en/the-facility-amf/251-amf-main-category/amf-doppler-lidar/1126-doppler-aerosol-lidar-data>.

Data Collected During Falcon Over-Flight of Summit on May 22, 2015

During the flyover of Summit on May 22, 2015 the lidar collected 14-minute average 3-point wind profiles (each ray took 1/3 of the total average time) at 60 degrees in elevation. The WP was followed by a 4 point PPI (spaced equally at 90 degree intervals from true N). Each ray of the PPI was averaged for 2.5 minutes. Both scans were repeated every 30 minutes. The long averages were needed due to the extremely clear conditions during the overpass.

Two example measurements of wind profiles and backscatter from May 2015 are shown below.

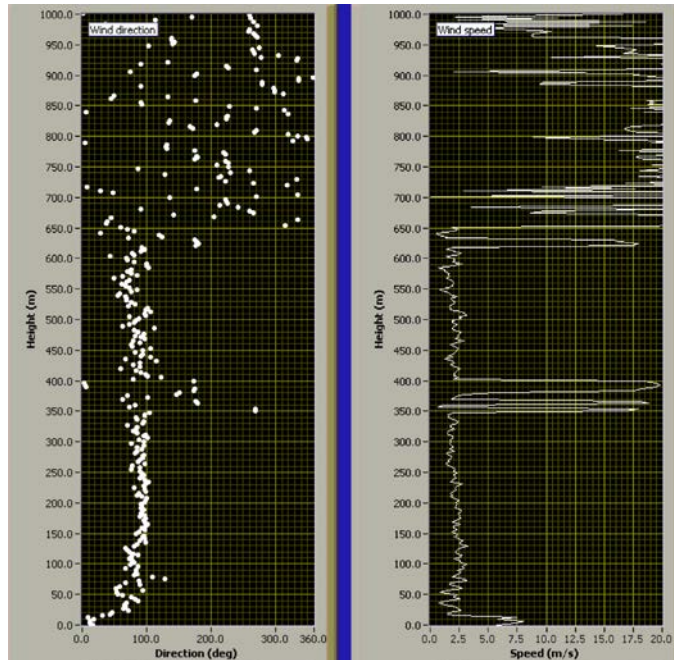


Figure 5-2: Wind Profile from the period of the Falcon overpass on 25/05/2015. Example shows the relatively short profile due to the low SNR in clear conditions.

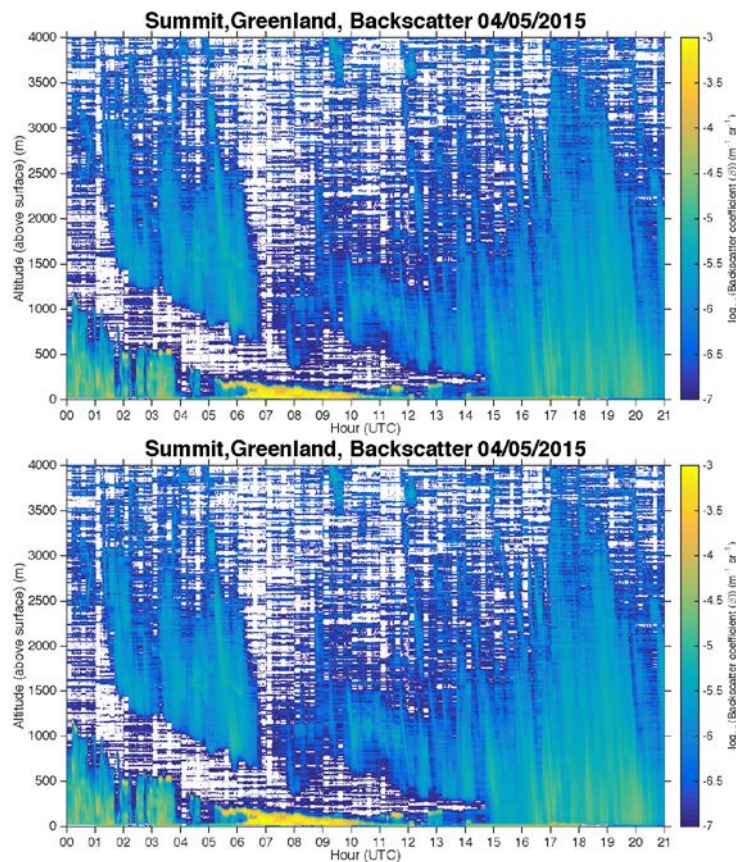


Figure 5-3: Typical observations collected from vertical stare scans collected in 30 minute segments (separated by WP and other scans) over 24-hour period. Top panel contains backscatter profiles and the bottom panel depicts the corresponding vertical velocities.

	Document Nr. DAR.DLR.WindVal. 28.01.16	Issue: V1.0	Date: 28.01.2016	Page: 37/39	
	Doc. Title: WindVal Data Acquisition Report				

5.8 Radiosonde data

The radiosonde data are provided for each flight. All radiosondes in the proximity of the flight track were obtained from the University of Wyoming Website (<http://weather.uwyo.edu/upperair/sounding.html>). The data are provided as single files per radiosonde in TXT format. The files contain pressure, altitude, temperature, relative humidity, mixing ratio, wind direction, wind speed, potential (THTA), equivalent potential (THTE) and virtual potential (THTV) temperature.

5.9 Mission summaries

For each flight a summary file as PPT is provided, which includes the following figures.

- Flight track including horizontal wind vector in flight level
- Horizontal wind speed, direction, vertical wind speed, and signal power from the DLR 2- μ m DWL processed with 2 algorithms (inversion, accumulation) showing different vertical coverages
- Horizontal wind speed and direction during ascent and descent from Falcon in-situ data
- Satellite imagery (when available) including Falcon flight track and web-source of image, e.g. MODIS VIS, MODIS IR, CALIPSO, ASCAT
- Radiosonde data
- Dropsonde data from NASA DC-8
- Other relevant data, e.g. Summit station data for flight on May 21, 2015.

The CALIPSO lidar products including “lidar browse images” were downloaded from <http://www-calipso.larc.nasa.gov/> and http://www-calipso.larc.nasa.gov/tools/data_avail/

The ASCAT products (12.5 km, 25 km and coastal winds) were downloaded from <http://manati.star.nesdis.noaa.gov/datasets/ASCATData.php>

The ASCAT products (12.5 km, 25 km and coastal winds) are also available at: <http://www.osi-saf.org/> and <http://www.knmi.nl/scatterometer/>.

The mission summaries are included in Appendix A.

	Document Nr. DAR.DLR.WindVal. 28.01.16	Issue: V1.0	Date: 28.01.2016	Page: 38/39	
	Doc. Title: WindVal Data Acquisition Report				

6 References

- DLR: Reitebuch (2005): ADM-Aeolus Campaigns – A2D Data Content Level 0, V1.0, July 2005, 19 pages.
- DLR: Reitebuch, O, et al. (2012a): Final Report ADM-Aeolus Airborne Campaigns Results, V 1.0, 15.06.2012, 34 pages.
- DLR: Reitebuch, O, U. Marksteiner, Ch. Lemmerz (2012b): TN 5.2 ADM-Aeolus Airborne Campaigns Results, V 3.0, 24.02.2012, 202 pages.
- DLR: Lemmerz, Ch., U. Marksteiner, O. Reitebuch, B. Witschas (2015a): WindVal Instrument Test Plan and Report ITPR. V 1.0, 06.05.2015, 16 pages.
- DLR: Reitebuch, O. (2015b): WindVal: Campaign Implementation Plan CIP Joint DLR-ESA-NASA Wind Validation for Aeolus. V1.1, 28.05.2015, 42 pages.
- DLR: (2015c): Handouts and Minutes of Meeting MoM from Progress Meeting 1 on November 2, 2015 at AOML, Miami.
- ESA: Schüttemeyer D. (2015): Statement of Work on “Technical Assistance for the Deployment of the ALADIN Airborne Demonstrator (A2D) lidar during the 2015 ESA/NASA Joint Wind Validation (WindVal) Campaign”. EOP-SM/2722/DS-ds from 16 March 2015, Contract No. ESA 4000114053/15/NL/FF/gp.
- Gentry, B., H. Chen, J. Cervantes, S. Mitchell, R. Machan, D. Reed (2014): Status of the TWiLiTE-GH Direct Detection Doppler Lidar. Presentation at Space Based Lidar Winds Working Group Meeting, May 13, 2014.
- Kavaya, M. J., J. Y. Beyon, G. J. Koch, M. Petros, P. J. Petzar, U. N. Singh, B. C. Trieu, and J. Yu (2014): The Doppler Aerosol Wind (DAWN) Airborne, Wind-Profiling Coherent-Detection Lidar System: Overview and Preliminary Flight Results. *J. Atmos. Oceanic Tech.*, 31, 826-842.
- Marksteiner, U. (2013): Airborne Wind-Lidar Observations for the Validation of the ADM-Aeolus Mission. Ph. D Thesis at Technical University Munich, DLR FB 2013-25, 176 pages.
- Päschke, E., R. Leinweber, V. Lehmann (2015): An assessment of the performance of a 1.5 μm Doppler lidar for operational vertical wind profiling based on a 1-year trial. *Atmos. Meas. Tech.*, 8, 2251-2266.
- Paffrath, U., Lemmerz, Ch., Reitebuch, O., Witschas, B., I. Nikolaus, V. Freudenthaler (2009): The airborne demonstrator for the direct-detection Doppler wind lidar ALADIN on ADM-Aeolus: II. Simulations and Rayleigh receiver radiometric performance. *J. Atmos. Ocean. Tech.*, 26, 2516-2530.
- Reitebuch, O. (2005): ADM-Aeolus Campaigns A2D Data Content Level 0. V.1.0, 08.07.2015, 19 pages.
- Reitebuch, O., Lemmerz, Ch., Nagel, E., Paffrath, U., Durand, Y., Endemann, M., Fabre, F., Chaloupy, M. (2009): The airborne demonstrator for the direct-detection Doppler wind lidar ALADIN on ADM-Aeolus: I. Instrument design and comparison to satellite instrument. *J. Atmos. Ocean. Tech.*, 26, 2501-2515.
- Smalikho, I., 2003: Techniques of wind vector estimation from data measured with a scanning coherent Doppler lidar. *J. Atmos. Oceanic Technol.*, 20, 276–291.
- Shupe M. D., D. D. Turner, Von P. Walden, R. Bennartz, M. P. Cadetdu, B. B. Castellani, Ch. J. Cox, D. R. Hudak, M. S. Kulie, N. B. Miller, R. R. Neely III, W. D. Neff, and P. M. Rowe (2013): High and Dry: New Observations of Tropospheric and Cloud Properties above the Greenland Ice Sheet. *Bull. Am. Meteor. Soc.*, 169-186.
- Weissmann, M., Busen, R., Dörnbrack, A., Rahm, S., Reitebuch, O. (2005): Targeted Observations with an Airborne Wind Lidar. *J. Atmos. Ocean. Tech.*, 22, 1706-1719.

	Document Nr. DAR.DLR.WindVal. 28.01.16	Issue: V1.0	Date: 28.01.2016	Page: 39/39	
	Doc. Title: WindVal Data Acquisition Report				

Appendix A with Mission Summaries

This appendix includes the summaries of each flight mission (see chapter 5.9).